Synthetic Polymer and Microbubble Systems for Gene Delivery to the Brain

James-Kevin Young Tan

A dissertation

submitted in partial fulfillment of the

requirements for the degree of

Doctor of Philosophy

University of Washington

2016

Reading Committee:

Suzie H. Pun, Chair

Michalakis Averkiou

Patrick S. Stayton

Program Authorized to Offer Degree:

Bioengineering

University of Washington

Abstract

Synthetic Polymer and Microbubble Systems for Gene Delivery to the Brain

James-Kevin Tan

Chair of the Supervisory Committee:
Suzie H. Pun, Professor
Bioengineering

The natural neurogenesis after neuron death in cases like traumatic brain injury and neurological diseases is sparse. Increasing the replenishment of functional neurons can improve patient outcome and prognosis. One way to encourage neurogenesis is by selective differentiation of neural progenitor cells and neural stem cells in the brain. Gene delivery has emerged as a promising strategy to accomplish this due to the development of effective gene transfer vehicles and the identification of factors that can modulate neural differentiation.

The first half of this thesis focuses on improving the efficacy of synthetic gene delivery vehicles. Typically, negative-charged DNA is condensed and protected from degradation by complexing it with positively charged materials. These cationic materials improve gene transfection efficiency by enabling for endosomal uptake and escape from the lysosomal

degradation pathway. However, the cationic nature of the materials also brings about deleterious effects such as cell cytotoxicity. Therefore, a there is a balance between transfection efficiency and cytotoxicity with cationic vectors. Strategies to reduce cytotoxicity and improve upon transfection efficiency are explored in this section.

Even with the most effective transfection agents, a major hurdle is reaching the neural progenitor cells and neural stem cells in the subventricular zone of the brain. The blood-brain barrier and the blood-cerebrospinal fluid barrier effectively block substances from reaching the brain parenchyma after systemic and intraventricular injection. Recently, the use of microbubbles and ultrasound have been shown to transiently disrupt the blood-brain barrier and allow the permeation of larger molecular drugs into the brain parenchyma. Microbubbles and ultrasound will be investigated as a way to disrupt the brain-cerebrospinal fluid barrier and increase the permeation of our gene delivery vehicles into the brain in the second half of this thesis.

TABLE OF CONTENTS

LIST OF FIGURES

Part 3: Synthetic Polymers for Gene Delivery to the Brain

Part 4: Microbubbles and Ultrasound for the Transient Disruption of the Choroid Plexus

LIST OF TABLES

ACKNOWLEDGEMENTS

This thesis would not have been possible without the help, encouragement, and support of a wide variety of people. I would like to thank everyone including the people not listed below who helped me finish this long and arduous process

First, I would like to thank Suzie for the opportunity to work in her lab and for all the guidance she provided. Without her support and training, this would not be possible. I deeply thank Suzie for her talents and her ability to provide the resources, wisdom, intellectual challenge, and mentorship to bring students through the winding road of graduate school and prepare them for their next journey. Her dedication to her students and her ability to adapt to the needs of each student is truly mesmerizing.

To the other members of my Supervisory and Reading Committee, including Shaoyi Jiang, Patrick Stayton, Anthony Convertine, and Michalakis Averkiou, thank you all for your insight, guidance, and help with both scientific problems and figuring out what lies ahead beyond graduate school.

To my family, thanks for the guidance, support, and love throughout all of these twenty-something years. My mother always wanted what is best for me and would push me to do better and be better. When I would come to her to vent during graduate school, the Tiger Mom in her told me to stop complaining and hurry up and finish. Haha. Thanks, Dad, for being the more lenient parent and letting us get away with more things, especially dough. I would especially like to thank both of them for the financial stability to let me retire after graduate school (if only!). Thanks, Steven, for your friendship and understanding all these years. I wish you the best of luck in finishing up your graduate studies.

To Susan and John, my apartment mates for the last four and three years, respectively, but really four years. Graduate school would not have been the same without both of you. All the eating, board games, television shows, shopping, fashion shows, and chatting will not be forgotten. We have shared in the ups, downs, happiness, frustration, and panic of graduate school but we will all be done shortly. I appreciate all the memories and support throughout everything.

To Dave (Dabe), my first mentor, your teachings, help, and friendship have been invaluable in graduate school and life throughout these years. I wish I had actually known you while we were both in the Kamei Lab at UCLA. The food, alcohol, night life, games, shopping, and random craziness will always be cherished.

To Christine, my lab mate of the same cohort, thanks for your friendship and laughs as we pushed through graduate school. Together we tackled all sorts of problems and kept the lab and other people in check. I believe the lab is in better shape than when we entered.

To Chayanon, your non-stop work ethic was inspiring and also demoralizing. I have to thank you for your endless amount of suggestions and tips even when I was not actively looking for help. The laughter and camaraderie were also a great comic relief even if you didn't understand everything.

To Bob, you will always be my little mentee in undergraduate school, graduate school, and in life. Your upbeat and happy-go-lucky personality brings joy to everyone. Thanks for always being a ray of sunshine even when you had to fake it.

To two great undergraduate students, Jen and Binhan, thanks for your assistance and help with a wide variety of experiments and lab tasks. Jevin will always complete us and will live on forever. Really, without both of your work, this thesis would not have been possible. Best of luck in both of your medical endeavors.

To other mentors of the lab, Drew, Joan, Hua, and Yilong, thank you for your scientific guidance and instruction. I have learned a lot from each of you and would not be able to complete this without your help.

To Leslie, Ida, and Jasmin, thanks for your friendship, laughter, food, boba runs, and discussions about graduate school and life.

To my great list of retail therapists: David, Jane, Wilson, Asuka, Oi-ling, Eric, Christian, Nataly, Lyndi, and Evelyn, my closet would not be the same without all of you. I feel like I have a closet that doesn't belong to a graduate student. All of the chats about new inventory, fashion houses, discounts, gossip, and co-workers were such fun entertainment and a great stress relief.

To undergraduate friends, Chris and Shivani, thanks for the continued memories and crazy antics that followed into graduate school. Who knew we would all end up at UW after leaving UCLA?

To the high school “K-Squad” of Ashley, Dat, and Vanessa, thanks for the support and discussions about life. It was great catching up on all of our struggles in graduate school, gossiping about ourselves and other people, and figuring out how we will all be together again in the future.

Lastly, I would like to thank the people I did not have the chance to mention for their encouragement, strength, and support – you know who you are.

DEDICATION

To my parents, John & Sally,
my brother, Steven,
and my other brothers, Smokey & Lucky

Part 1: Introduction

Chapter 1. Diseases and Injuries that Result in Neuron Death

Many neurological diseases and injuries result in the loss of neuronal function and neuronal death. Currently, the only standard of care is to mitigate the damage; there is no established treatment to remedy these neurons or resurrect new ones. However, the adult brain has a natural mechanism to cope with the damage and regenerate new neurons. In the subventricular zone (SVZ) lining the lateral ventricles and the subgranular zone (SGZ) of the hippocampal dentate gyrus, lie populations of new neurons, neural progenitor cells (NPCs), and neural stem cells (NSCs) that are capable of neuron regeneration.[1–3] After neuron loss, these cells rapidly proliferate, migrate towards the site of neuron death, and differentiate into region-appropriate neuronal phenotypes.[3,4] Nevertheless, only a very miniscule fraction of these cells differentiate into functional neurons that can reverse the damage.[5] Thus, an improved prognosis can be achieved by augmenting the natural neurogenesis response and increasing the number of replacement neurons. This introduction explores the different types of ailments that result in neuron loss, current treatments and strategies, and ways to deliver these therapeutics to pertinent areas of the brain.

1.1 Neurodegenerative Diseases

As the general population reaches older and older ages, the likelihood of suffering from a neurodegenerative disease rises sharply.[6] New cases of diseases such as Parkinson's disease (PD), Huntington's disease (HD), Alzheimer's disease (AD), and amyotrophic lateral sclerosis (ALS) are on the rise and only continue to climb as scientists struggle to identify the causes and pathogenesis of each one. Current understanding suggests that each disease affects specific parts of the brain. For instance, AD primarily affects the hippocampus, while PD the substantia nigra, and ALS the spinal cord and primary motor cortex as shown in **Figure 1.1**. However, as each disease progresses, they all culminate in the loss of function and death of neurons, usually a specific phenotype, and serious neurological disabilities.[7,8] AD involves degeneration of the cholinergic neurons and cells in the forebrain and results in memory loss and dementia. HD progresses in degeneration of the basal ganglia and forebrain structures, resulting in movement

and cognitive impairments. PD entails the progressive degeneration of dopamine neurons and is associated with the disruption of normal motor functions like walking. Current therapies involve replenishing different factors to maintain neuron health and function, cell transplantation to restore specific neuron phenotypes, and gene therapy to augment the natural neurogenesis.[7,9]

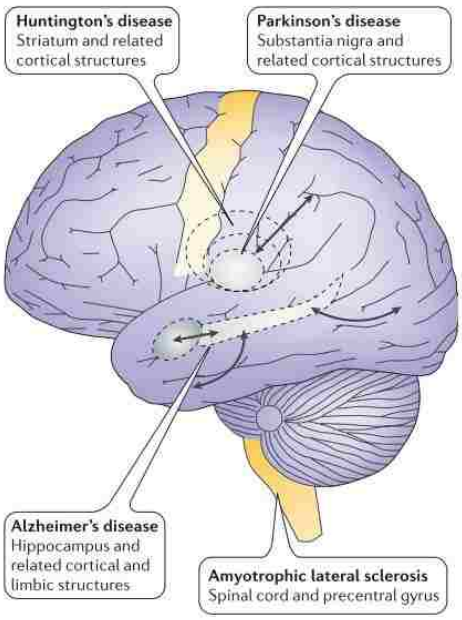

Figure 1.1 Different neurodegenerative diseases affect specific areas of the adult brain and eventually lead to neuron loss. Adapted from Mattson, *et al*. *Nature Reviews Neuroscience*. (2006) **7**:278-294.

1.2 TRAUMATIC BRAIN INJURY

Traumatic brain injury (TBI) is a leading cause of death and disability in the United States and affects over 1.5 million individuals each year.[10] The initial primary injury can cause the death of a variety of neuron phenotypes, loss of local and long distance neuron circuitry, hemorrhage, and concussions.[11] Even after the initial injury, more damage can occur through secondary injury where the brain swells as a coping mechanism. To ameliorate the damage, the body naturally undergoes changes at the injury site and at the primary neuro-regenerative parts of the adult brain – the SVZ and the hippocampus. At the site of injury, astrocytes and microglia activate as well proliferate to remove debris from damaged cells as well as establish a barrier around the damaged tissue.[10] To replace the lost neurons, cells in the SVZ and the hippocampus rapidly proliferate, migrate towards the damage, and differentiate into new neurons.[10,12–15] Nevertheless, the outcome

from these responses are far from returning an individual back to the pre-TBI state and result in paralysis, memory loss, and comas. Currently, medical treatments rely on mitigating the secondary damage and include oxygenating the patient, lowering the intracranial pressure, and neurosurgical surgery.[11] There are no medical treatments that have shown to be effective in improving mortality or limiting disability following injury;[16] therefore, new treatment strategies are needed to augment the natural neurogenesis and restore neuron function.

1.3 ISCHEMIC STROKE

Ischemic stroke is an occlusion of a cerebral artery resulting in the lack of nutrients and oxygen to the surrounding tissues. This causes cell and neuron death in the affected area and a subsequent natural neurogenesis stemming from the SVZ and hippocampus[4,17] as shown in **Figure 1.2**.

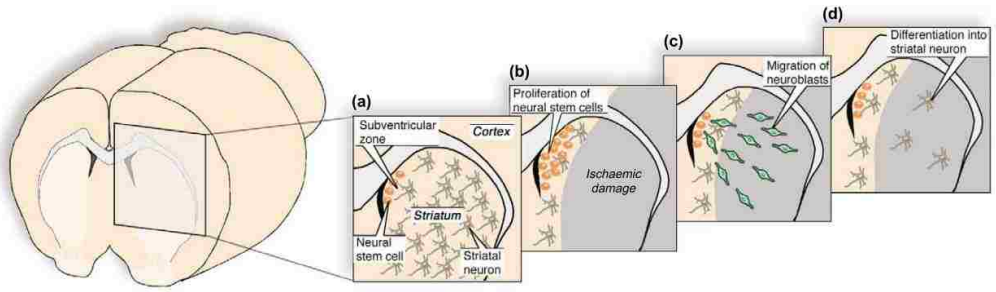

Figure 1.2 Stroke-induced neurogenesis in the striatum. **(a)** Neural stem or progenitor cells reside in the SVZ. **(b)** Ischemic stroke results in pronounced loss of striatal and cortical neurons and causes increases proliferation of neural progenitors. **(c)** Neuroblasts and other cells migrate into the injury site. **(d)** A small fragment of these cells different into neurons to replace the ones lost from damage. Adapted from Kokaia, *et al*. *Current Opinion in Neurobiology*. (2003) **13**:127-132.

Again, only a miniscule number of these progenitors effectively differentiate into functional neurons capable of enervating the damaged site. In one study of ischemic stroke in adult rats, it was estimated that only 0.2% of the dead neurons had been replaced with new, functional neurons after 6 weeks.[5] Currently, there are no therapies that can prevent stroke-induced neurological dysfunction in humans. New treatment strategies that effectively augment the natural neurogenesis or introduce new neurons into damaged tissues are in dire need.

Chapter 2. Current Treatments to Restore Neurons

Even with the natural neurogenesis in the adult brain to repopulate lost neurons, it is not enough to fully restore neuron function. Improving prognosis focuses on repopulating the lost neuron population through the administration of factors to stimulate neuron regrowth, gene delivery to drive neuron differentiation, and cell transplantation to provide new sources of neurons.

2.1 Factors for Neuroprotection and Regeneration

A number of different factors have shown to increase neuronal protection and regeneration including: brain-derived neurotrophic factor (BDNF), glial-derived neurotrophic factor (GDNF), erythropoietin (EPO), Noggin, fibroblast growth factor-2 (FGF-2), epithermal growth factor (EGF), vascular endothelial growth factor (VEGF), and insulin-like growth factor-I (IGF-1).[2,18–25] These factors have shown to have a range effects such as rapid proliferation in the SVZ, directed neuron differentiation, angiogenesis, and prolonging neuron life. These are usually administered by intracerebroventricular or intraventricular injection and are only efficacious for as long as the factor is present in the brain or damaged area. Thus this treatment strategy is best suited for cases where the brain is already exposed such as after TBI or neurological surgery and is not a viable strategy for long-term treatments for neurological disorders.

2.2 Gene Therapy

Gene therapy involves transfecting a cell with exogenous DNA so it can be transcribed and translated into a therapeutic factor or protein. Naked DNA is highly unstable in the body and gets rapidly degraded; thus, a carrier is used to condense and protect the DNA. There are two types of carriers: viral and non-viral. With viral vectors, viruses such as adenovirus and adeno-associated virus are used as transfection agents and they are highly efficient. However, a number of safety concerns have emerged due to their ability to permanently alter the genome (retrovirus and lentivirus) and activate the immune system.[26] Conversely, non-viral vectors utilize synthetic materials such as liposomes and polymers to protect DNA. These materials are often less efficient than their viral counterparts but do offer advantages of safety and being more easily customizable.

Gene therapy has already entered clinical trials for the treatment of neurodegenerative

disorders and has shown promise in animal models for the treatment of TBI and ALS.[27] Gene transfer of genes encoding VEGF, Neurogenin-2, FGF-2, and IGF-1 have already shown to be neuroprotective and neuro-restorative in a number of ischemic stroke and ALS animal models.[28–31] Thus, gene therapy directed at the regeneration of neurons could realize its full potential upon the development of safe and effective delivery methods.

2.3 Cell Transplantation

NSCs and NPCs have emerged as an area of high interest due to their ability to self-renew and be multipotent for the different neuronal lineages of the central nervous system (CNS) even in the adult brain.[2] In *in vitro* settings, stem cells can be differentiated into a variety of neuronal cells such as striatal neurons, oligodendrocyte progenitor cells, and astroglia.[32] When stem cells or neural precursors are transplanted into the brain, they can differentiate into apropos neurons based on their surrounding region and environmental cues.[2] For example, when SVZ precursor cells are transplanted in the hippocampus, they generate into hippocampal neurons, and SGZ precursors generate into olfactory interneurons in the rostral migratory stream.[33] Currently, there are three strategies that are especially attractive for clinical translation: (1) transplantation of oligodendrocyte progenitor cells as a means of treating the disorders of myelin; (2) transplantation of phenotypically restricted NPCs to treat diseases of discrete loss of a single neuronal phenotype, such as Parkinson disease; and (3) implantation of mixed progenitor pools to treat diseases characterized by the loss of several discrete phenotypes.[34] While NSC strategies are promising, the application of stem cells is at an early stage and the goal of *in vivo* neuron regeneration is an ambitious one with many milestones to be accomplished. Many basic issues still need to be resolved such as: an ethical and limitless source of NSCs and NPCs, a reliable method of identifying and isolating stem cells, a full understanding of the specific cues for each type of neuron differentiation, and the stable integration of transplanted cells into the host body.[35,36]

Chapter 3. Synthetic Polymer Vectors for Neuron Regeneration

Of the three strategies discussed above, gene therapy is the most readily applicable treatment since it has a longer effect than a bolus administration of factors and is more clinically ready than cell transplantation strategies. Therefore, our lab focuses developing synthetic polymers for gene delivery.

3.1 Controlled Radical Polymerization

Advances in polymer synthesis and chemistry have resulted in the ability to synthesize controlled polymers of various chemical compositions, desired molecular weight, and low polydispersity.[37,38] The most common polymer techniques for controlled radical polymerization are stable free-radical polymerization (SFRP), atom-transfer radical polymerization (ATRP), and reversible addition-fragmentation chain transfer (RAFT) (**Figure 3.1**).

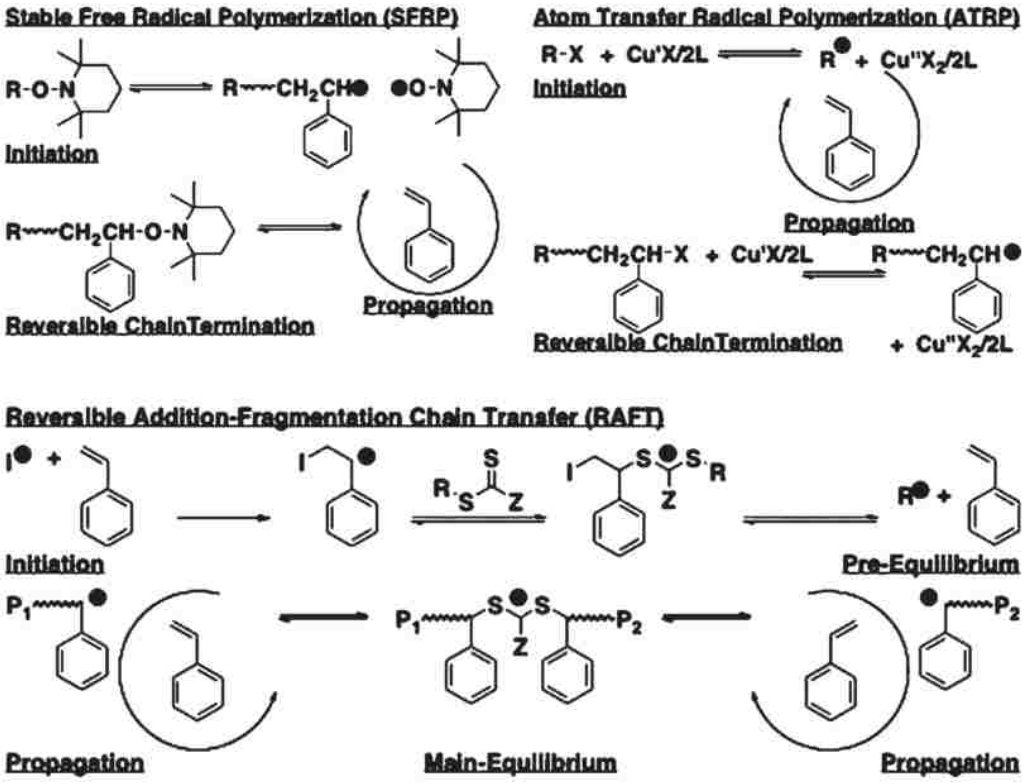

Figure 3.1 Controlled radical polymerization of styrene by SFRP, ATRP, and RAFT. Adapted from Chu, *et al. Accounts of Chemical Research*. (2012) **45**:1089-1099.

Each polymerization technique has its own advantages and disadvantages and the method of polymerization can be tailored to best provide control of a specific set of monomers.

The ease and reproducibility of polymer synthesis has allowed for the creation of a wide variety of chemical functionalities and polymer architectures. Functional groups and different moieties such as alcohols, amines, carboxylic acids, and poly(ethylene glycol)[37,38] have been polymerized and this has allowed for the creation of more complex architectures such as grafted, star, and multivalent polymer shapes (**Figure 3.2**).

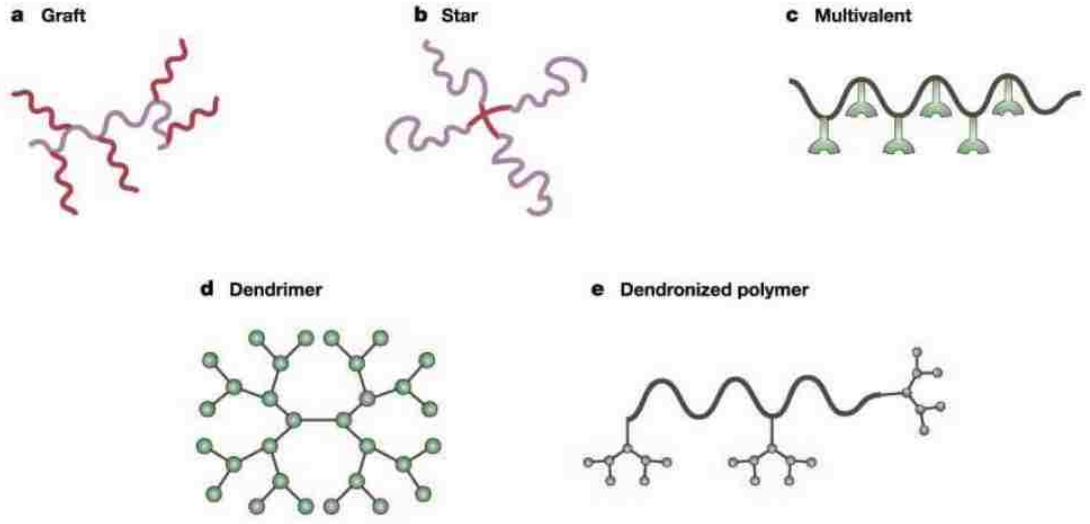

Figure 3.2 Advances in polymer synthesis have allowed for the creation of a variety of complex architectures such as **(a)** graft, **(b)** star, **(c)** multivalent, **(d)** dendrimer, and **(e)** dendronized polymers. Adapted from Duncan. *Nature Reviews. Drug Discovery*. (2003) **2**:347-360.

In turn, the variety of polymeric architectures have allowed for the development of diverse therapeutic and drug delivery platforms. Polymers can stand alone as a therapeutic or can be conjugated to moieties to form polymer-protein conjugates or polymer-drug conjugates (**Figure 3.3**). In addition, polymers can form nanoparticles such as micelles, microspheres, and vesicles to be used for drug delivery. Polymer chemistry allows for the synthesis of customizable polymers with distinct functionalities and chemistries that can be applied to a variety of drug delivery constructs and applications.

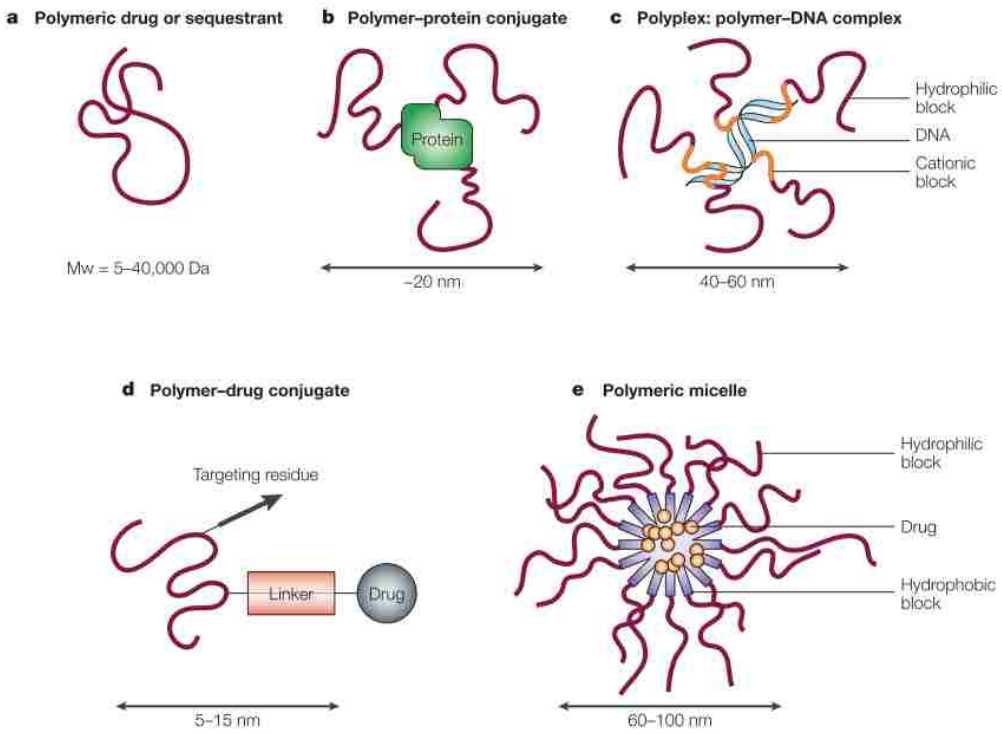

Figure 3.3 Schematic representations of the diverse drug delivery platforms that can be synthesized with polymers including **(a)** polymer alone, **(b)** polymer-protein conjugates, **(c)** polyplexes, **(d)** polymer-drug conjugates, and **(e)** polymeric micelles. Adapted from Duncan. *Nature Reviews. Drug Discovery*. (2003) **2**:347-360.

3.2 Polymer Criteria for Gene Delivery

Synthetic gene delivery has benefited greatly from the advent of customizable polymers and architectures. The transfection of cells with exogenous DNA involves a number of hurdles that must be overcome in order to ensure that DNA is protected from being degraded, endocytosed into the cell, and trafficked into the nucleus for transcription as shown in **Figure 3.4** The pathway of DNA from the cell surface to the nucleus for effective transfection. The DNA must be endocytosed into the cell, escape lysosomal degradation, and traffic into the nucleus for DNA transcription. Adapted from Pack, *et al*. *Nature Reviews. Drug Discovery*. (2005) **4**:581-593.**Figure 3.4**.[39] In polymeric gene delivery systems, negatively charged DNA is typically condensed and protected from extracellular degradation by the complexation with positively charged polymers to form "polyplexes."

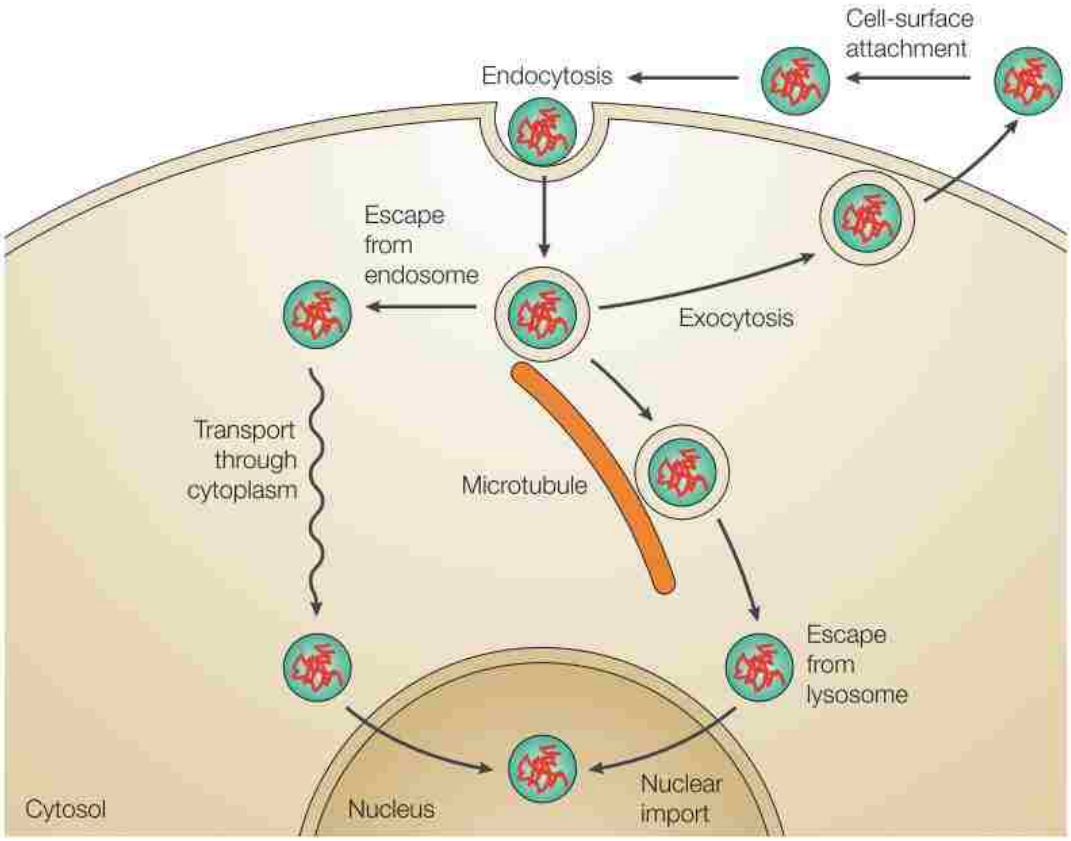

Figure 3.4 The pathway of DNA from the cell surface to the nucleus for effective transfection. The DNA must be endocytosed into the cell, escape lysosomal degradation, and traffic into the nucleus for DNA transcription. Adapted from Pack, *et al*. *Nature Reviews. Drug Discovery*. (2005) **4**:581-593.

Common examples are polyethyleneimine and poly-*L*-lysine.[39–41] These materials can facilitate DNA endocytosis, endosomal escape, and DNA unpackaging. Synthetic vectors can mask the electrostatic repulsions between DNA and the cell surface and can even be functionalized with targeting moieties like peptides or antibodies for cell specificity.[42,43] Membrane lytic groups can disrupt endosomal vesicles or the cationic nature of the material can trigger endosomal release by the proton sponge effect.[41,44–46] Sometime during this process, the DNA must unpack and separate from the carrier so that it can be successfully transcribed. One way of ensuring the release of the DNA cargo is by including degradable linkages that can break up with triggers such as the more acidic environment of the endosomes or the reducing environment of the cell cytoplasm.[39,47,48] Overall, polymers provide a facile way to bring together different chemistries and designs that can overcome each of the hurdles involved in gene delivery.

Chapter 4. Accessing the Central Nervous System

Even with the most successful transfection agents, neuron regeneration by gene therapy is still a feat due to the hurdle of reaching the neuronal precursors in the SVZ and SGZ. The CNS is integral to the function of an organism and any damage to it could have severe, long-lasting impacts to the life of the individual. Thus, there are formidable barriers that separate the CNS from the rest of an organism: the blood-brain barrier (BBB) and the blood-cerebrospinal fluid (CSF) barrier.

4.1 Brain Barriers

The BBB separates blood from the interstitial fluid of the brain and is comprised of endothelial cells that line the brain capillaries and are linked together by tight junctions.[49] This tight network of cells, together with a high expression of efflux pumps and transporter proteins, prevents almost all molecules from entering the brain parenchyma except those that are necessary for cell survival and function.[50] Nearly 100% of large-molecule therapeutics and more than 98% of all small-molecule drugs are excluded from the brain. Even molecules as small as histidine cannot pass the BBB as shown in **Figure 4.1**. By filtering out most molecules, the BBB provides the optimal environment for the CNS to function and is a major hurdle in the delivery of therapeutics to the brain.[51]

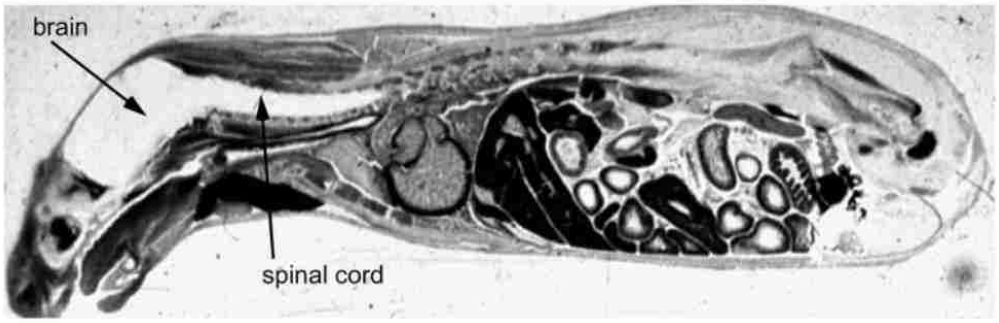

Figure 4.1 The BBB prevents small molecules such as radioactive histidine form entering the murine CNS. Adapted from Pardridge, *et al*. *NeuroRx*. (2005) **2**:3-14.

The separate blood-CSF barrier consists of choroid plexus epithelium cells that line the cavities of the ventricles and the cranial and spinal sub-arachnoid space.[52,53] This ependymal layer filters substances out of the blood before entering the CSF and is responsible for secreting CSF

and other peptides and factors.[52] The blood-CSF barrier is not as stringent as the BBB and virtually all non-cellular substances in the blood partition into the CSF.[54] However, penetration into the brain parenchyma is extremely difficult due to low diffusion and the constant movement of CSF fluid through the CNS and back into the bloodstream. Small molecules and peptides directly administered into the CSF diffuse only 0.3 mm into the choroid plexus and only about 1% leaves the CSF compartment.[54] Even though the choroid plexus epithelium is easier to penetrate than the BBB, it still is a formidable barrier to much larger platforms such as gene delivery vehicles.

4.2 Methods of Bypassing and Permeabilizing the Blood-Brain Barrier

Despite the difficulty in reaching the CNS, there are different strategies in crossing the BBB. The least complicated method is by direct injection intraventricularly or intrathecally into the subarachnoid space of the brain.[50] However, safety concerns arise as too quick of an administration or too large of an administered volume can easily cause damage to surrounding tissues.[55] In addition, substances injected into the CSF will have a limited half-life and poor partitioning into the parenchyma due to the bulk flow of the CSF and the limited diffusion past the choroid plexus epithelium.[49,54]

With chemical permeabilization methods, the aim is to either increase the permeability of a substance through the brain barrier or to temporarily open the barrier with chemicals. For example, increasing the lipophilicity of peptides by methylation or dimethylation has shown to provide some success in partitioning peptides across the BBB.[56] Other chemical modulators focus on opening the BBB by destabilizing the membranes of endothelial cells. Chemicals like ethanol and dimethylsulfoxide or detergents like sodium dodecyl sulfate and Tween-80 have allowed for the efficacy of drugs in the brain that otherwise would have no effect.[57]

Another group of permeabilization techniques focuses on mechanical ways to open the BBB. The use of an osmotic pump to deliver a hypertonic solution of mannitol into the carotid artery has shown to open the BBB by shrinking the endothelial cells and disrupting tight junctions.[49] More recently, the use of microbubbles (MBs) and ultrasound (US) has safely and temporarily opened the BBB in mice and monkeys.[58–60] MBs, or gas-filled bubbles, vibrate or cavitate under US and are capable of permeabilizing membranes and disrupting tight junctions to allow the enhanced permeation of larger molecules.[61,62]

References

1. Gage, F. H. Mammalian Neural Stem Cells. *Science (80-.).* **287,** 1433–8 (2000).

2. Emsley, J. G., Mitchell, B. D., Kempermann, G. & Macklis, J. D. Adult neurogenesis and repair of the adult CNS with neural progenitors, precursors, and stem cells. *Prog. Neurobiol.* **75,** 321–341 (2005).

3. Sawada, M. & Sawamoto, K. Mechanisms of Neurogenesis in the Normal and Injured Adult Brain. *Keio J. Med.* **62,** 13–28 (2013).

4. Parent, J. M., Vexler, Z. S., Gong, C., Derugin, N. & Ferriero, D. M. Rat forebrain neurogenesis and striatal neuron replacement after focal stroke. *Ann. Neurol.* **52,** 802–13 (2002).

5. Arvidsson, A., Collin, T., Kirik, D., Kokaia, Z. & Lindvall, O. Neuronal replacement from endogenous precursors in the adult brain after stroke. *Nat. Med.* **8,** 963–70 (2002).

6. Mattson, M. P. & Magnus, T. Ageing and neuronal vulnerability. *Nat. Rev. Neurosci.* **7,** 278–294 (2006).

7. Geraerts, M., Krylyshkina, O., Debyser, Z. & Baekelandt, V. Concise review: therapeutic strategies for Parkinson disease based on the modulation of adult neurogenesis. *Stem Cells* **25,** 263–270 (2007).

8. Shihabuddin, L. S., Palmer, T. D. & Gage, F. H. The search for neural progenitor cells: Prospects for the therapy of neurodegenerative disease. *Mol. Med. Today* **5,** 474–480 (1999).

9. Kim, M., Lee, S.-T., Chu, K. & Kim, S. U. Stem cell-based cell therapy for Huntington disease: a review. *Neuropathology* **28,** 1–9 (2008).

10. Chirumamilla, S., Sun, D., Bullock, M. R. & Colello, R. J. Traumatic brain injury induced cell proliferation in the adult mammalian central nervous system. *J. Neurotrauma* **19,** 693–703 (2002).

11. Ghajar, J. Traumatic brain injury. *Lancet* **356,** 923–929 (2000).

12. Zhang, R., Zheng, N., Song, Z., Yin, L. & Cheng, J. The effect of side-chain functionality and hydrophobicity on the gene delivery capabilities of cationic helical polypeptides. *Biomaterials* **35,** 3443–3454 (2014).

13. Dash, P. K., Mach, S. a & Moore, a N. Enhanced neurogenesis in the rodent hippocampus following traumatic brain injury. *J. Neurosci. Res.* **63,** 313–319 (2001).

14. Ramaswamy, S., Goings, G. E., Soderstrom, K. E., Szele, F. G. & Kozlowski, D. a. Cellular proliferation and migration following a controlled cortical impact in the mouse.

Brain Res. **1053,** 38–53 (2005).

15. Saha, B., Peron, S., Murray, K., Jaber, M. & Gaillard, A. Cortical lesion stimulates adult subventricular zone neural progenitor cell proliferation and migration to the site of injury. *Stem Cell Res.* **11,** 965–77 (2013).

16. Zheng, W. *et al.* Neurogenesis in adult human brain after traumatic brain injury. *J. Neurotrauma* **30,** 1872–80 (2013).

17. Wiltrout, C., Lang, B., Yan, Y., Dempsey, R. J. & Vemuganti, R. Repairing brain after stroke: A review on post-ischemic neurogenesis. *Neurochem. Int.* **50,** 1028–1041 (2007).

18. Lim, D. a. *et al.* Noggin antagonizes BMP signaling to create a niche for adult neurogenesis. *Neuron* **28,** 713–726 (2000).

19. Jin, K. *et al.* Vascular endothelial growth factor (VEGF) stimulates neurogenesis in vitro and in vivo. *Proc. Natl. Acad. Sci. U. S. A.* **99,** 11946–11950 (2002).

20. Zigova, T., Pencea, V., Wiegand, S. J. & Luskin, M. B. Intracentricular Administration of BDNF Increases the Number of Newly Generated Neurons in the Adult Olfactory Bulb. *Mol. Cell. Neurosci.* **245,** 234–245 (1998).

21. Gritti, A., Cova, L., Parati, E. a., Galli, R. & Vescovi, A. L. Basic fibroblast growth factor supports the proliferation of epidermal growth factor-generated neuronal precursor cells of the adult mouse CNS. *Neurosci. Lett.* **185,** 151–154 (1995).

22. Whittemore, S. R., Morassutti, D. J., Walters, W. M., Liu, R. H. & Magnuson, D. S. Mitogen and substrate differentially affect the lineage restriction of adult rat subventricular zone neural precursor cell populations. *Exp. Cell Res.* **252,** 75–95 (1999).

23. Arsenijevic, Y. & Weiss, S. Insulin-like growth factor-I is a differentiation factor for postmitotic CNS stem cell-derived neuronal precursors: distinct actions from those of brain-derived neurotrophic factor. *J. Neurosci.* **18,** 2118–2128 (1998).

24. Traynor, B. J. *et al.* Neuroprotective agents for clinical trials in ALS: a systematic assessment. *Neurology* **67,** 20–7 (2006).

25. Dodge, J. C. *et al.* AAV4-mediated expression of IGF-1 and VEGF within cellular components of the ventricular system improves survival outcome in familial ALS mice. *Mol. Ther.* **18,** 2075–84 (2010).

26. Thomas, C. E., Ehrhardt, A. & Kay, M. a. Progress and problems with the use of viral vectors for gene therapy. *Nat. Rev. Genet.* **4,** 346–58 (2003).

27. Weber-Adrian, D. *et al.* Gene delivery to the spinal cord using MRI-guided focused ultrasound. *Gene Ther.* 1–10 (2015). doi:10.1038/gt.2015.25

28. Masserdotti, G. *et al.* Transcriptional Mechanisms of Proneural Factors and REST in

Regulating Neuronal Reprogramming of Astrocytes. *Cell Stem Cell* 74–88 (2015). doi:10.1016/j.stem.2015.05.014

29. Matsuoka, N. *et al.* Adenovirus-mediated gene transfer of fibroblast growth factor-2 increases BrdU-positive cells after forebrain ischemia in gerbils. *Stroke.* **34,** 1519–25 (2003).

30. Zhang, Y., Pak, C., Han, Y. & Ahlenius, H. Rapid single-step induction of functional neurons from human pluripotent stem cells. *Neuron* **78,** 785–798 (2013).

31. Jin, K. *et al.* Neurogenesis and aging: FGF-2 and HB-EGF restore neurogenesis in hippocampus and subventricular zone of aged mice. *Aging Cell* **2,** 175–83 (2003).

32. Tabar, V. & Studer, L. Pluripotent stem cells in regenerative medicine: challenges and recent progress. *Nat. Rev. Genet.* **15,** 82–92 (2014).

33. Suhonen, J. O., Peterson, D. a, Ray, J. & Gage, F. H. Differentiation of adult hippocampus-derived progenitors into olfactory neurons in vivo. *Nature* **383,** 624–627 (1996).

34. Goldman, S. Stem and progenitor cell-based therapy of the human central nervous system. *Nat. Biotechnol.* **23,** 862–71 (2005).

35. Lindvall, O., Kokaia, Z. & Martinez-Serrano, A. Stem cell therapy for human neurodegenerative disorders-how to make it work. *Nat. Med.* **10 Suppl,** S42–S50 (2004).

36. Rossi, F. & Cattaneo, E. Opinion: neural stem cell therapy for neurological diseases: dreams and reality. *Nat. Rev. Neurosci.* **3,** 401–409 (2002).

37. Chu, D. S. H. *et al.* Application of living free radical polymerization for nucleic acid delivery. *Acc. Chem. Res.* **45,** 1089–99 (2012).

38. Moad, G., Rizzardo, E. & Thang, S. H. Living Radical Polymerization by the RAFT Process. *Aust. J. Chem.* **58,** 379 (2005).

39. Pack, D. W., Hoffman, A. S., Pun, S. & Stayton, P. S. Design and development of polymers for gene delivery. *Nat. Rev. Drug Discov.* **4,** 581–93 (2005).

40. Burke, R. S. & Pun, S. H. Extracellular barriers to in vivo PEI and PEGylated PEI polyplex-mediated gene delivery to the liver. *Bioconjug. Chem.* **19,** 693–704 (2008).

41. Schellinger, J. G. *et al.* Melittin-grafted HPMA-oligolysine based copolymers for gene delivery. *Biomaterials* **34,** 2318–26 (2013).

42. Chu, D. S. H., Schellinger, J. G., Bocek, M. J., Johnson, R. N. & Pun, S. H. Optimization of Tet1 ligand density in HPMA-co-oligolysine copolymers for targeted neuronal gene delivery. *Biomaterials* **34,** 9632–7 (2013).

43. Wei, H., Schellinger, J. G., Chu, D. S. H. & Pun, S. H. Neuron-targeted copolymers with sheddable shielding blocks synthesized using a reducible, RAFT-ATRP double-head agent. *J. Am. Chem. Soc.* **134,** 16554–7 (2012).

44. ur Rehman, Z., Hoekstra, D. & Zuhorn, I. S. Mechanism of polyplex- and lipoplex-mediated delivery of nucleic acids: real-time visualization of transient membrane destabilization without endosomal lysis. *ACS Nano* **7,** 3767–77 (2013).

45. Al-Dosari, M. S. & Gao, X. Nonviral gene delivery: principle, limitations, and recent progress. *AAPS J.* **11,** 671–81 (2009).

46. Kwon, E. J., Liong, S. & Pun, S. H. A truncated HGP peptide sequence that retains endosomolytic activity and improves gene delivery efficiencies. *Mol. Pharm.* **7,** 1260–5 (2010).

47. Wei, H. *et al.* Dual responsive, stabilized nanoparticles for efficient in vivo plasmid delivery. *Angew. Chem. Int. Ed. Engl.* **52,** 5377–81 (2013).

48. Tan, J.-K. Y., Choi, J. L., Wei, H., Schellinger, J. G. & Pun, S. H. Reducible, dibromomaleimide-linked polymers for gene delivery. *Biomater. Sci.* **3,** 112–120 (2015).

49. Begley, D. Understanding and circumventing the blood- brain barrier. *Acta Paediatr.* **443,** 83–91 (2003).

50. Gabathuler, R. Development of new peptide vectors for the transport of therapeutic across the blood-brain barrier. *Ther. Deliv.* **1,** 571–586 (2010).

51. Abbott, N. J. Blood-brain barrier structure and function and the challenges for CNS drug delivery. *J. Inherit. Metab. Dis.* **36,** 437–449 (2013).

52. Mortazavi, M. M. *et al.* The choroid plexus: A comprehensive review of its history, anatomy, function, histology, embryology, and surgical considerations. *Child's Nerv. Syst.* **30,** 205–214 (2014).

53. Dohrmann, G. J. The choroid plexus: a historical review. *Brain Res.* **18,** 197–218 (1970).

54. Pardridge, W. M. Drug transport in brain via the cerebrospinal fluid. *Fluids Barriers CNS* **8,** 7 (2011).

55. Begley, D. J. Delivery of therapeutic agents to the central nervous system: the problems and the possibilities. *Pharmacol. Ther.* **104,** 29–45 (2004).

56. Witt, K. a & Davis, T. P. CNS drug delivery: opioid peptides and the blood-brain barrier. *AAPS J.* **8,** E76–88 (2006).

57. Pardridge, W. The blood-brain barrier: bottleneck in brain drug development. *NeuroRx* **2,** 3–14 (2005).

58. Aryal, M., Arvanitis, C. D., Alexander, P. M. & McDannold, N. Ultrasound-mediated blood–brain barrier disruption for targeted drug delivery in the central nervous system. *Adv. Drug Deliv. Rev.* (2014). doi:10.1016/j.addr.2014.01.008

59. McDannold, N., Arvanitis, C. D., Vykhodtseva, N. & Livingstone, M. S. Temporary disruption of the blood-brain barrier by use of ultrasound and microbubbles: safety and efficacy evaluation in rhesus macaques. *Cancer Res.* **72,** 3652–63 (2012).

60. Marquet, F. *et al.* Real-time, transcranial monitoring of safe blood-brain barrier opening in non-human primates. *PLoS One* **9,** e84310 (2014).

61. Panje, C. M., Wang, D. S. & Willmann, J. K. Ultrasound and microbubble-mediated gene delivery in cancer: progress and perspectives. *Invest. Radiol.* **48,** 755–69 (2013).

62. Meairs, S., Alonso, A., Fatar, M., Kern, R. & Hennerici, M. Microbubbles traversing the blood-brain barrier for imaging and therapy. *Med. Biol. Eng. Comput.* **47,** 839–49 (2009).

Part 2: Non-viral Nucleic Acid Delivery Strategies to the Central Nervous System

James-Kevin Y. Tan, Drew L. Sellers, Binhan Pham, Suzie H. Pun, Philip J. Horner

This work has been submitted for publication in *Frontiers in Neuroscience*.

Synopsis:

With an increased prevalence and understanding of central nervous system injuries and neurological disorders, nucleic acid therapies are gaining promise as a way to regenerate lost neurons or halt disease progression. While more viral vectors have been used clinically as tools for gene delivery, non-viral vectors are gaining interest due to lower safety concerns and the ability to deliver all types of nucleic acids. Nevertheless, there are still a number of barriers to nucleic acid delivery. In this focused review, we explore the *in vivo* challenges hindering non-viral nucleic acid delivery to the central nervous system and the strategies and vehicles used to overcome them. Advantages and disadvantages of different routes of administration including: systemic injection, cerebrospinal fluid injection, intraparenchymal injection, and peripheral administration are discussed. Non-viral vehicles and treatment strategies that have overcome delivery barriers and demonstrated in vivo gene transfer to the central nervous system are presented. These approaches can be used as guidelines in developing synthetic gene delivery vectors for central nervous system applications and will ultimately bring non-viral vectors closer to clinical application.

Keywords: central nervous system, delivery, *in vivo*, non-viral, nucleic acid

Chapter 1. Introduction

The incidence of neurological diseases and injuries is increasing with the rising life expectancy.[6] Nucleic acid therapeutics, such as genes and small interfering RNA (siRNA) oligonucleotides have emerged as a promising treatment strategy to preserve neuron function, enhance neurogenesis, and prevent the progression of neurological diseases. The delivery of nucleic acids encoding brain-derived neurotrophic factor,[63] epidermal growth factor,[64] fibroblast growth factor-2,[29] Huntingtin,[65] neurogenin-2,[28,30] insulin growth factor-1,[66] and vascular endothelial growth factor[25] have been shown to increase neuron regeneration or delay the progression of neurological diseases in mice, rats, and gerbils. Targeting gene delivery vehicles to the appropriate cells and proper protein regulation remain the primary challenges to making these pathways feasible. While viral vectors such as the adeno-associated virus have typically been used clinically, interest in non-viral nucleic acid delivery remains high due to lower safety concerns, greater customizability, and an ease in manufacturing.[39]

With neurological diseases specifically affecting different parts of the brain and even sub-phenotyes of neural cells, the route of administration is a crucial aspect of nucleic acid delivery. Intraventricular injection places therapeutics closer to the subventricular zone, one of the stem cell niches of the brain, whereas localized intraparenchymal injections may be used to target a specific part of the brain where neurodegeneration occurs or at the location of disease (e.g. brain tumor). In this focused review, we explore the barriers to *in vivo* nucleic acid delivery and highlight the recent synthetic vehicles and different strategies that have overcome these challenges to deliver nucleic acids to the central nervous system (CNS).

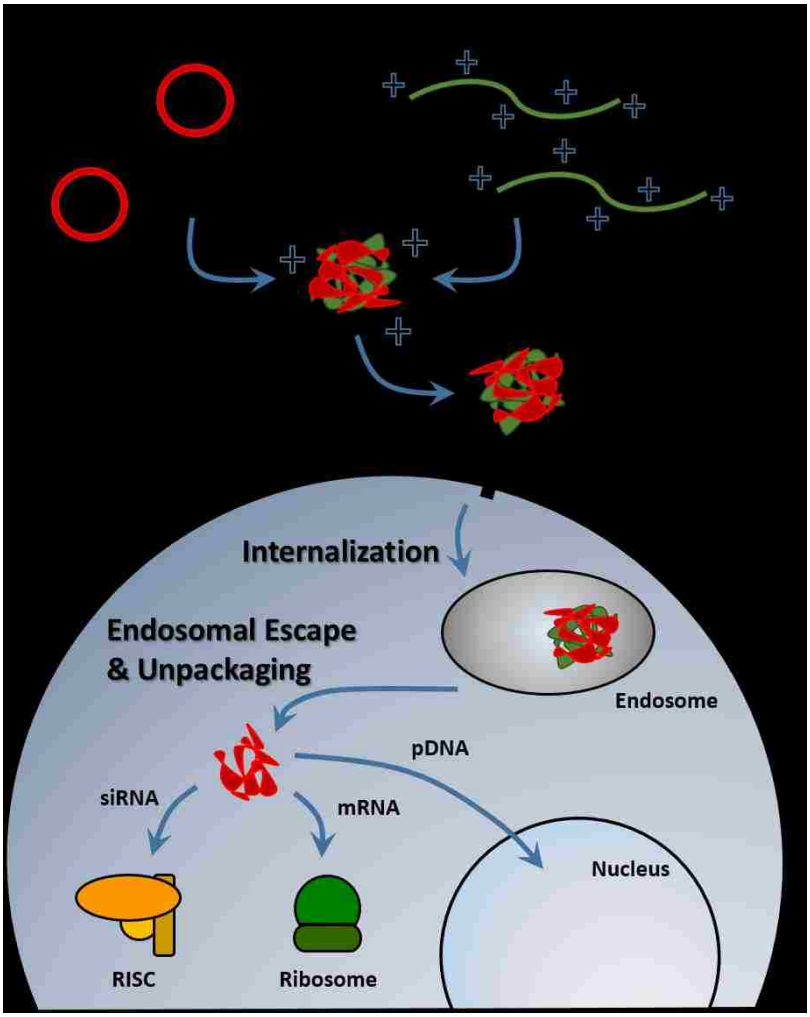

Figure 1.1 Stages of nucleic acid delivery into a cell. Nucleic acids are typically condensed and complexed with a cationic material. This complex must be recognized by a cell, be internalized, and escape the endosomal-lysosomal degradation pathway. Once in the cell cytoplasm, the nucleic acid can separate from its vehicle and traffic to its intended target based on its type.

1.1 Nucleic Acid Protection

Nucleic acids are susceptible to chemical degradation and clearance from the body due to the presence of extracellular nucleases and the immune system. To overcome this challenge, negatively charged nucleic acids are typically complexed with cationic, synthetic materials.[39] This significantly condensed and compact form allows the nucleic acids to remain hidden and avoid degradation. Common complexation agents used for *in vitro* gene transfer include cationic polymers, such as polyethylenimine (PEI), which electrostatically bind to nucleic acids to form

"polyplexes," or polymer-nucleic acid complexes. Similarly, cationic lipids can also be used to complex nucleic acids to form "lipoplexes." Another method of enhancing stability is by modifying the nucleic acid itself so that it avoids recognition and degradation. For example, altering the ribose moiety and introducing 2'-fluoro and phosphorothioate near the terminal region of siRNA duplexes enhances stability and prolonged siRNA half-life *in vivo*.[67]

Despite the protection afforded to nucleic acids by electrostatic complexation, these cationic complexes are still subject to challenges such as aggregation, toxicity, premature sequestration by phagocytic cells, and non-specific interaction with cell membranes and serum proteins.[68] When intravenously administered, PEI, one of the most effective transfection agents *in vitro*, causes severe toxic side effects due to polyplex aggregation and strong electrostatic interactions with cell membranes, proteins, and the extracellular matrix.[45] To overcome these challenges, shielding strategies have been developed to hide nucleic acid delivery vehicle by moieties like poly(ethylene glycol) (PEG) and albumin.[69,70]

PEG, a biocompatible, hydrophilic polymer, is commonly used as a shielding agent for nanoparticles.[71] By creating a barrier around the complex, it was previously believed that PEG prevents the adsorption of proteins.[72] However, recent studies suggest that PEGylation of nanoparticles results in preferential binding of clusterin, a chaperone protein that binds to hydrophobic domains of unfolded proteins and prevents non-specific binding.[73] When conjugated to delivery vehicles, PEG has been shown to improve the stability and increase the circulation half-life of polyplexes, liposomes, and other types of vectors. For example, when conjugated to PEI, PEG prevented the aggregation of PEI-plasmid DNA complexes in fetal bovine serum-enhanced media resulting in complexes that could circulate long enough for observed localization in the brain.[74] When encapsulated in PEGylated liposomes, PEI-oligonucleotide complexes were able to circulate substantially longer and had plasma concentrations significantly higher than naked complexes after 60 minutes.[75] By any route of administration, protecting delivery vehicles with a shielding agent minimizes aggregation and premature sequestration and can increase the distribution of the nucleic acids to desired cells.

1.2 Targeting the CNS and Neuronal Cells

Nevertheless, prolonged stability and circulation is not sufficient for substantial nucleic acid delivery to the brain and spinal cord because the nervous system is protected by barriers that

grossly prevent the access of therapeutics. Cells of the CNS can potentially be accessed through several contact points including: (1) the blood system, (2) the cerebral spinal fluid (CSF) in the ventricles or lumbar space, (3) intraparenchymal fluid in the extracellular space, or (4) nerve endings that extend outside of the nervous system. The nervous system is sequestered behind a barrier system composed of vascular tight junctions and glial elements that ensheath the blood supply producing a blood-brain and blood-spinal cord barrier (BBB or BSCB, respectively). Each of these compartments represent a potential entry point as well as unique challenges for neuronal targeting. Vehicles for systemic delivery must utilize a mechanism that will facilitate penetration and uptake across the BBB or BSCB. Within the brain, paracellular flow of neuro-active cytokines is controlled by pulsation of the blood vessels that mechanically drives a peristaltic movement of extracellular fluid. Gene delivery vehicles administered into the ventricles need to bind to cells of interest before being washed out of the CNS. At the periphery, a vehicle that promotes uptake at nerve termini and retrograde transport must be able to target a neuron for transfection and promote travel along the neuronal cytoskeleleton into the CNS. Consequently, the advent and development of targeting ligands has greatly enhanced the capacity of non-viral vectors to deliver genes into the CNS.

Drug delivery vehicles have been modified with targeting agents such as peptides, antibodies, proteins, and sugars to specifically home therapeutics to desired tissues and cell types. For systemic administration, active targeting is important in directing the accumulation of vehicles at the brain endothelium. One commonly used brain-targeting molecule is transferrin, a glycoprotein that binds to iron. The transferrin receptor is expressed on the brain endothelium and the binding of transferrin-decorated nucleic acid delivery vehicles to these receptors allows for accumulation right outside the brain.[76]

Vehicles administered directly into brain by intraventricular or intraparenchymal methods can also benefit from active targeting by focusing the delivery of nucleic acids to pertinent cells. For example, to more specifically transfect neural progenitor cells, Tet1, a peptide that specifically binds to neuronal cells, was conjugated to PEI complexes.[77] This Tet1-PEI polymer led to a significantly improved transfection of neural progenitors by targeted complexes over untargeted complexes. Thus, targeting moieties can help deliver nucleic acids to cells and tissues of interest while minimizing non-specific delivery. In addition, targeting ligands can improve the intracellular delivery of nucleic acids since many targeting ligands are endocytosed by cells after binding to its

receptor. Decorated macromolecules such as polyplexes and liposomes show enhanced uptake in cells compared to their non-targeted counterparts.

Chapter 2. Systemic Delivery

Intravenous administration is one of the most common routes of administration for macromolecule therapeutics and has the advantage of rapid distribution and high bioavailability. However, systemic circulation presents a major challenge for nucleic acid delivery. Naked DNA has poor stability and is rapidly broken down by nucleases, sequestered by the liver, and cleared from circulation with a plasma half-life of mere minutes.[78,79] To prevent premature degradation and prolong circulation, nucleic acids have been complexed with PEGylated cationic materials, such as polymers and liposomes, which act to shield the polyplex and facilitate compact packaging and protection. Targeting ligands conjugated to the synthetic vectors can facilitate recognition of brain endothelium. However, transport into the brain requires crossing the BBB, a tight network of endothelial cells that restricts entry into the brain parenchyma.[50] The brain endothelium has a high expression of efflux pumps and transporter proteins that exclude nearly 100% of large-molecule therapeutics and more than 98% of all small-molecule drugs.[49,57] Recent *in vivo* investigations have focused on transportation across the BBB and temporarily disrupting the BBB after systemic administration.

2.1 Transport Across the Blood-Brain Barrier

Strategic selection of brain targeting ligands can result in both recognition of the brain endothelium and facilitated transcytosis across the BBB. This process, called receptor-mediated transcytosis, has been demonstrated with cationic proteins and is believed to be carried out by clathrin-coated pits or caveolae.[80] After these materials bind to the luminal surface of the brain endothelial cells, vesicular transcytosis is mediated by different proteins and the high concentration of mitochondria in endothelial cells to cause exocytosis at the abluminal surface.

The transferrin receptor is frequently targeted for BBB transcytosis. After binding, the carrier protein, transferrin receptor, internalizes the transferrin-iron complex at the apical side of the brain endothelium and eventually exocytosis it at the opposite basal surface. Since transferrin receptor is expressed on the blood-brain barrier and transcytoses transferrin, it can be utilized as an uptake pathway into the brain by nucleic acid vehicles functionalized with transferrin. In one example, polyamidoamine (PAMAM) dendrimers were decorated with transferrin by a PEG linker and showed a ~2-fold higher brain uptake and gene transfer compared to PEGylated dendrimers

alone.[76] In another example, transferrin antibodies was used to decorate liposomes that housed plasmid DNA and this system was able to show a 10-fold greater β-glucuronidase enzyme activity in murine brains deficient of the protein.[81]

Another BBB transcytosis moiety is the rabies viral glycoprotein (RVG) peptide, a 29-amino acid peptide which binds to nicotinic acetylcholine receptors. Modifying the peptide sequence to include nine arginines on the C-terminus allows for complexation with nucleic acids.[82] Upon systemic intravenous administration, these complexes were able to transvascularly deliver siRNA to the brain through clathrin- and caveolae-mediated endocytosis by endothelial cells, which lead to extended lives of encephalitic mice. The RVG peptide can also modulate the accumulation of larger vehicles and has delivered macro-structures such as PAMAM dendrimers,[83] liposomes,[84] chitosan nanoparticles,[85] and exosomes[86] across the blood-brain barrier and into the brain parenchyma. Other targeting agents have included: angiopep, a peptide that binds to low-density lipoprotein receptor-related protein-1;[87] lactoferrin, an iron-binding protein of the transferrin family;[88,89] leptin, a peptide that binds to leptin receptor in different parts of the brain;[90] and chlorotoxin, a scorpion-derived venom that is a specific marker for gliomas.[91] Collectively, these targeting agents have shown to facilitate the accumulation of PEGylated PAMAM dendrimers, lysine dendrimers, and liposomes in the brain.

2.2 Blood-Brain Barrier Disruption

Other methods of systemic nucleic acid delivery focus on temporarily disrupting the BBB to enhance the diffusion of vehicles into the brain. Small molecules, such as mannitol, have been shown to temporarily open the BBB and allow the penetration of larger molecules into the brain parenchyma. Hypertonic solutions of these molecules is believed to widen tight junctions by shrinking vascular endothelial cells.[92] Consequently, the co-administration of mannitol with RVG-decorated PEI was able to significantly enhance the distribution of complexes throughout the brain when compared to carriers alone.[93]

More recently microbubbles, or gas-filled microspheres, have been coupled with ultrasound as a method to temporarily disrupt the blood-brain barrier.[61,94,95] This process, called sonoporation, creates micropores, permeabilizes cell membranes, and breaks up tight junctions as microbubbles act as local enhancers of the ultrasound acoustic energy and cavitate causing local shear flow, microstreams, and microjets.[61,96,97] These BBB openings are large enough to allow for

the permeation of macromolecules into the brain such as immunoglobulin G and 70 kDa dextran.[98–102] The safety of microbubble-mediated BBB disruption has been evaluated in rats and macaque monkeys with limited to no damage to brain tissue and no behavioral or visual deficits.[59,103] Microbubble-mediated disruption of the BBB has been used to increase anti-Huntingtin siRNA delivery into the murine brain to and shown to reduce Huntingtin protein levels in animal disease models.[65] In another example, DNA can be complexed with cationic polymer-decorated microbubbles to prevent premature degradation. In this manner, microbubble and DNA complexes were used to markedly enhance the expression of brain-derived neurotrophic factor and enhanced green fluorescence protein in murine brains.[63,104]

In some cases, such as brain gliomas and traumatic brain injury, there is a natural disruption of the BBB. In small rat brain tumors, there is no BBB permeability; however, as the tumor grows and neovascularization occurs, ultrastructural defects in the capillary vessels arise causing a stark disruption in the tumor.[105] This leaky BBB vasculature can be exploited by gene delivery vehicles as a facile method of CNS entry and can greatly complement receptor-mediated transcytosis. PEGylated nanoparticles and liposomes decorated with receptor-mediated transcytosis ligands were able to accumulate in gliomas after systemic administration and delay tumor growth.[70,106]

Chapter 3. Cerebrospinal Fluid Injection

The CSF is produced by the choroid plexus deep in the ventricles and drains along paravenous circulation. The CNS is unique in that it does not have a traditional lymph system and waste material and metabolites drain from the extracellular space to the CSF. While non-viral gene delivery into CSF-filled spaces is not as facile as intravenous administration, it does have the advantages of avoiding systemic circulation and placing therapeutics in close proximity to the brain parenchyma. In addition, there are excellent access points that are used routinely in the clinic including a lumbar puncture or intraventricular cannulas. Substances directly injected into the CSF circumvent the BBB and distribute in the brain depending on size and charge. The ependymal barriers in ventricles are comprised of the choroid plexus cells and in the sub-arachnoid space, the arachnoid barrier cells of glia and pial vessels.[107] For intraventricular delivery, large molecular weight proteins are not free to diffuse into the brain parenchyma due to the choroid plexus epithelium, which lines the cavities of the ventricles and the cranial and spinal sub-arachnoid space and secretes cerebrospinal fluid.[52,53] While the ependymal barrier is not as stringent as the BBB, access and penetration into the brain parenchyma is still difficult due to the low diffusion and the constant movement of CSF fluid through the CNS and back into the bloodstream.[54] While ventricular access of therapeutics to the brain is restricted, delivery to the sub-arachnoid space often results in widespread brain delivery of small molecular weight proteins.[108]

3.1 Overcoming Nucleic Acid Delivery Barriers

While the ependymal cell layer acts as a barrier, nucleic acid therapeutics intraventricularly injected are still able to have some efficacy likely due to the direct sampling of neural stem cells into the CSF and some penetration into the parenchyma. After intraventricular injection, PEI and DNA complexes have been shown to transfect neural progenitor cells;[109] while PEI complexes decorated with Tet1, a peptide that specifically binds to neuronal cells, bound better to neural progenitor cells and showed an improved transfection of neural progenitors over untargeted complexes.[77] Other carrier structures such as liposomes and silica nanoparticles have also been used as nucleic acid delivery vehicles. Cationic liposomes and organically modified silica nanoparticles were used to successfully deliver siRNA and plasmid DNA to neuronal cells *in vivo*, respectively.[110,111] Peptide-decorated micelles filled with dexamethasone, a glucocorticoid that

facilitates transport to the nucleus, were able to significantly reduce infarct size after middle cerebral artery occlusion by gene delivery.

Recently, multifunctional gene delivery vehicles have been synthesized with the aim of overcoming many of the barriers to gene delivery such as premature unpackaging, endosomal escape, and DNA release. A statistical copolymer of *N*-(2-hydroxypropyl)methacrylate (HPMA), oligo-*L*-lysine, and melittin was developed for gene delivery after intraventricular injection.[41] The HPMA monomers were for stability, the lysines were developed for DNA condensation and packaging, and the melittin, a membrane-lytic peptide developed from honey bee venom, was included to enhance endosomal escape after vesicular uptake. This polymer efficiently condensed DNA into stable particles to form polyplexes and increased brain transfection about 35-fold compared to melittin-free analogs. Another polymer designed for *in vivo* gene delivery utilized a double-headed reversible addition-fragmentation chain transfer agent and a ring-opening polymerization initiator to create two different polymer segmentsthat contribute to different aspects of gene delivery.[47] This copolymer, PCL-SS-p[(GMA-TEPA)-*s*-OEGMA], consisted of a block of poly(ε-caprolactone) (PCL) connected by a reducible disulfide to a statistical copolymer of tetraethylenepentamine (TEPA)-decorated poly(glycidyl methacrylate) (GMA) and oligo(ethylene glycol) monomethyl ether methacrylate (OEGMA). The TEPA amine groups bind to and condense nucleic acids to form polyplexes while the hydrophobic PCL and hydrophilic OEGMA provide extracellular stability. After polyplex internalization, the amine groups contribute to endosomal escape by pH buffering and the internal disulfide bond can be reduced by cytosolic glutathione facilitating polyplex destabilization and nucleic acid release. These polyplexes were shown to have diameters less than 200 nm, transfected HeLa cells more efficiently than PEI *in vitro*, and delivered luciferase genes to the brain more efficiently than its individual components. To improve transfection further, the amines of this polymer were guanidinylated and investigated *in vivo*. The delocalized charge of guanidinium groups is attributed to stronger interaction with DNA than amines and greater cell internalization by interacting with cell surface phosphates and sulfates.[112,113] While guanidinium groups show improved transfection *in vitro*, they did not translate to augmented transfection *in vivo* likely due to premature unpackaging as guanidinium groups have a predilection for sulfates of heparan sulfate proteoglycans over nucleic acid phosphate groups.[114]

Cerebrospinal fluid injections into other areas of the central nervous system have also been employed for the administration of nucleic acid carriers. After injection into the cisterna magma of rats, liposomes delivered luciferase plasmid throughout the brain that was still detectable seven to ten days later.[115] Interestingly, when the same system was directly injected into the parenchyma, luciferase expression was not as distributed. A micelle system of PEG-aspartic acid polymer was able to provide sustained protein expression with minimal immunogenicity.[116] Nucleic acid administration into the lumbar subarachnoid space has also been accomplished with a variety of delivery vehicles. Poly(lactic-co-glycolic acid) microparticles containing plasmid DNA that encodes IL-10 were able to relieve neuropathic pain in rats for greater than 74 days.[117] PEI complexes decorated with a peptide from nerve growth factor were able to more specifically transfect dorsal root ganglia.[118] By creating Tat decorated-PEI complexes with magnetic iron beads, researchers were able use magnetic fields to direct the movement of DNA complexes into remote areas away from the injection site in rat spinal cords.[119]

TABLE 3.1 PROPERTIES OF EFFECTIVE NUCLEIC ACID DELIVERY VEHICLES

3.2 Choroid Plexus Epithelium Disruption

In a similar fashion to BBB disruption, the choroid plexus epithelium may be transiently disrupted by microbubbles and ultrasound to allow for the enhanced penetration of materials into the brain parenchyma from the CSF fluid. Custom microbubbles were prepared and did not aggregate with aforementioned PCL-SS-p[(GMA-TEPA)-*s*-OEGMA] polyplexes.[120] In *in vitro* transwell assays, these microbubbles were able to sonoporate immortalized choroid plexus monolayers to allow for the enhanced flow through of 5 kDa PEG and 70 kDa dextran. Upon *in vivo* administration into murine ventricles, the microbubbles and ultrasound were able to significantly increase polyplex transfection of cells with luciferase compared to polyplexes alone or polyplexes and microbubbles without ultrasound. Temporary microbubble-mediated disruption of the choroid plexus epithelium seems like a viable strategy to enhance the penetration of polyplexes and may garner more research in the future.

Chapter 4. Intraparenchymal Injection

Intraparenchymal injection is the most direct access to discrete anatomy and cells of the brain and spinal cord. However, there are several critical challenges notwithstanding the inherent risk of an invasive CNS injection. Injection alone can create a reactive gliosis that may limit the transport of a therapeutic or exacerbate the disease. The use of small caliber pipettes and methods for convection enhanced delivery can mitigate some of these concerns and allow targeted delivery of relatively large volumes without harm. Once in the parenchyma, therapeutics have variable degrees of diffusion and clearance. Clearance is regulated by the lymphatic system which is comprised of the glia cells that ensheath the venous system of the brain which is localized primarily near the dural surfaces. In general, small molecular weight substances are diffuse readily and are cleared in minutes. Larger molecular weight substances may either lack significant diffusion or be cleared over a course of hours.

4.1 Bolus Injection

While the location of intraparenchymal injections into the brain can vary, the same type of nucleic acid delivery vehicles is still utilized. PEI decorated with 2 kDa PEG chains resulted in improved gene delivery after intrathecal administration into the lumber spinal cord subarachnoid space compared to PEI.[121] Reducible arginine-PAMAM dendrimers were able to knockdown genes after injection into the cortex.[122] Reversibly conjugated siRNA to liposomes was able to efficiently silence genes in oligodendrocytes after administration into the corpus callosum.[123] Targeting agents have also been used to enhance the nucleic acid delivery vehicles. PEGylated PEI was targeted with folate, which binds to folate receptor often overexpressed on cancer cells, and liposomes were targeted with transferrin to improve the delivery of plasmids and siRNA after injection into the right striatum.[124,125]

4.2 Sustained Delivery

The compact and tortuous morphology of the brain parenchyma severely limits the diffusion of nucleic acid delivery vehicles away from the administration site. To overcome this, sustained delivery is utilized to constantly introduce more vehicles and increase the diffusion throughout the

brain. In one example, an osmotic pump was able to continually inject siRNA and liposome complexes into the frontal lobe to knockdown the resistance of gliomas to therapy.[126] This treatment significantly sensitized tumors to the chemotherapeutic agents and extended the survival of mice.

Like the osmotic pump, convection-enhanced delivery is administered intraparenchymally and used to continually introduce therapeutics. A cannula is typically inserted stereotaxically into a designated spot in the brain and a therapeutic fluid is continuously injected under positive pressure.[127] The administration of siRNA by convection-enhanced delivery was able to silence genes in oligodendrocytes[128] and silence huntingtin gene in a widespread manner across the brain.[129] When a cell-penetrating peptide, TAT, was attached to liposomes, gene transfection increased *in vivo*; however, expression was restricted to the vicinity of the infusion catheter.[130] When comparing positively and negatively charged liposomes, anionic liposomes were better able to spread throughout the brain parenchyma with similar transfection levels.[131]

Chapter 5. Retrograde Transport

While there have been substantial advances in brain-targeted delivery to treat diseases that affect specific parts of the brain like Alzheimer's Disease,[82,132,133] few therapeutic options are available for degenerative diseases that affect motor neurons because many of the potential genes and small interfering RNA drugs show limited diffusion and penetration to motor neurons deep in the CNS parenchyma.[134,135] For decades, classes of viruses have been known to infect neuronal projections in the periphery and undergo retrograde axonal transport into the brain and spinal cord.[136,137] Thus, several lab have begun to systematically mutate adeno-associated vectors in order to expand their clinical application and increase delivery into the CNS,[138,139] Innovative strategies have been adopted to utilize retrograde axonal transport to deliver biologics into the spinal cord.[140–142] As a result, these viruses have been engineered and shown to be effective for remote gene transfer into the CNS after intramuscular injection to induce neurotrophic factor expression in animal models of neurodegenerative disease.[66,143–146]

Recently, small targeting agents have been used to direct the trafficking of cargo into the CNS after peripheral administration. Tetanus toxin subunit-C (TTC), an atoxic fragment of tetanus toxin that contains the ganglioside-binding site, is able to mediate uptake at both pre- and post-synaptic at nerve termini to allow retrograde transport passage of TTC within neurons.[147,148] Consequently, these trans-synaptic properties of TTC have been exploited as a fusion protein to enable delivery into the spinal cord after TTC uptake at peripheral nerve termini.[149–151] While the TTC fusion-proteins were shown to increase delivery into the spinal cord, these studies were not able to discern a therapeutic benefit, which may suggest that that TTC-fusions do not escape the endosome after uptake and remain sequestered in the vescicle that mediated uptake. More recently, a targeted axonal import peptide (TAxI) was identified by *in vivo* phage display. The TAxI peptide was able to mediate uptake and delivery of an active Cre recombinase into the nucleus of spinal cord motor neurons after hindlimb intramuscular injection.[152] These data suggest that small peptides are not only able to mediate synaptic uptake at nerve termini and retrograde transport within neurons, but they allow for functional protein cargo delivery via the neuron. While there have yet to be any reports of synthetic, retrograde nucleic acid delivery into the CNS, the discovery of targeting ligands that mediate uptake by neurons in the periphery, transport within neurons to

the CNS, and release of active cargo into the cytoplasm has the potential of opening a whole new delivery route for non-viral technologies to target motor neurons for gene delivery.

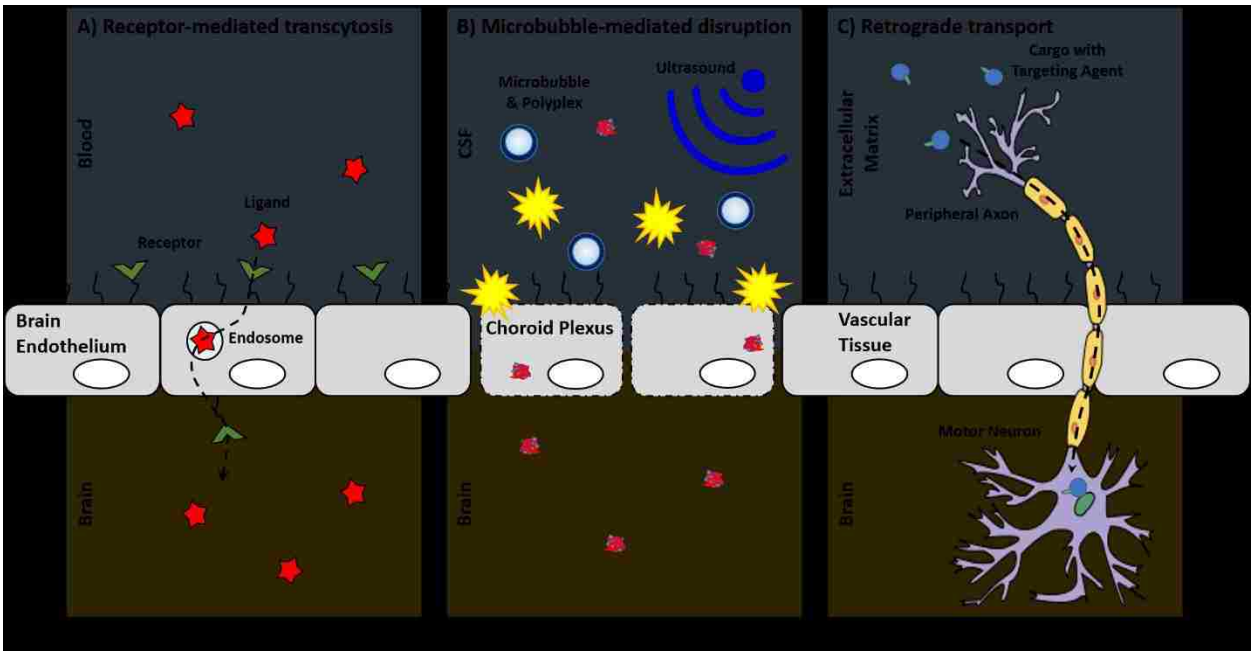

Figure 5.1 Mechanisms of entering the CNS. (A) With receptor-mediated endocytosis, the binding of a ligand to its receptor on the brain endothelium facilitates cellular endocytosis, vesicular trafficking, and eventually exocytosis on the contralateral side into the brain. **(B)** Microbubble-mediated disruption of the choroid plexus epithelium breaks tight junctions and creates micropores, allowing for the enhanced penetration of polyplexes into the brain. **(C)** New targeting ligands allow for uptake by peripheral neurons and the retrograde transport of cargo along axons to cell bodies in the CNS.

Chapter 6. Conclusion

While viral vectors are still the main type of vehicles used in clinical trials, non-viral vectors are gaining traction due to their potential safety advantages, greater customization, ease of manufacturing, and ability to deliver all nucleic acid varieties. The ability of viral vectors to permanently alter the genome and activate the immune system make non-viral vectors more compelling for clinical trials. However, the lower efficacy and transfection levels by synthetic vectors hinder their wide clinical use. For any application, nucleic acid delivery vehicles face cellular obstacles such as recognition by pertinent cells, internalization into cells, escaping the lysosomal degradation pathway, and unpackaging the nucleic acids in the cell cytosol. Delivery into the CNS presents an even greater challenge due to the supracellular blood-brain barrier and blood-spinal cord barrier. An apropos administration route must be chosen to maximize therapeutics at the treatment site (*i.e.* direct injections); however, caution must be heeded in avoiding unnecessary damage to healthy tissues by direct administration into the CNS (*i.e.* intravenous and peripheral administration). Each route of administration has its advantages and disadvantages, as well as local barriers, as previously discussed. Fortunately, the advances in vehicular design, materials, and synthesis described above have allowed for specific engineering of gene delivery vehicles to overcome these challenges and step closer to the transfection efficiency of viruses. Improvements such as nucleic acid shielding and targeting have lessened premature degradation and increased the localization of cargo in the CNS. Advances in crossing the blood-brain barrier and sustained delivery directly into the brain allow for improved gene transfection and a step closer to clinical application. Meanwhile, new techniques such as microbubble-mediated sonoporation and small molecule-mediated retrograde transport allow the permeation of otherwise excluded vehicles into the brain and spinal cord. All of these examples can serve as guidelines and inspiration for the next generation of synthetic gene delivery vectors. With these improvements, we anticipate that synthetic delivery systems will be applied more successfully for nucleic acid therapies in animal models of CNS disease and will make significant progress toward clinical evaluation in the upcoming years.

Chapter 7. Acknowledgments

This work was supported by NIH 2R01NS064404. JKYT was supported by NSF GRFP (2011128558); Binhan Pham was supported by Mary Gates Undergraduate Research Fellowship.

References

6. Mattson, M. P. & Magnus, T. Ageing and neuronal vulnerability. *Nat. Rev. Neurosci.* **7,** 278–294 (2006).

25. Dodge, J. C. *et al.* AAV4-mediated expression of IGF-1 and VEGF within cellular components of the ventricular system improves survival outcome in familial ALS mice. *Mol. Ther.* **18,** 2075–84 (2010).

28. Masserdotti, G. *et al.* Transcriptional Mechanisms of Proneural Factors and REST in Regulating Neuronal Reprogramming of Astrocytes. *Cell Stem Cell* 74–88 (2015). doi:10.1016/j.stem.2015.05.014

29. Matsuoka, N. *et al.* Adenovirus-mediated gene transfer of fibroblast growth factor-2 increases BrdU-positive cells after forebrain ischemia in gerbils. *Stroke.* **34,** 1519–25 (2003).

30. Zhang, Y., Pak, C., Han, Y. & Ahlenius, H. Rapid single-step induction of functional neurons from human pluripotent stem cells. *Neuron* **78,** 785–798 (2013).

39. Pack, D. W., Hoffman, A. S., Pun, S. & Stayton, P. S. Design and development of polymers for gene delivery. *Nat. Rev. Drug Discov.* **4,** 581–93 (2005).

41. Schellinger, J. G. *et al.* Melittin-grafted HPMA-oligolysine based copolymers for gene delivery. *Biomaterials* **34,** 2318–26 (2013).

45. Al-Dosari, M. S. & Gao, X. Nonviral gene delivery: principle, limitations, and recent progress. *AAPS J.* **11,** 671–81 (2009).

46. Kwon, E. J., Liong, S. & Pun, S. H. A truncated HGP peptide sequence that retains endosomolytic activity and improves gene delivery efficiencies. *Mol. Pharm.* **7,** 1260–5 (2010).

47. Wei, H. *et al.* Dual responsive, stabilized nanoparticles for efficient in vivo plasmid delivery. *Angew. Chem. Int. Ed. Engl.* **52,** 5377–81 (2013).

49. Begley, D. Understanding and circumventing the blood-brain barrier. *Acta Paediatr.* **443,** 83–91 (2003).

50. Gabathuler, R. Development of new peptide vectors for the transport of therapeutic across the blood-brain barrier. *Ther. Deliv.* **1,** 571–586 (2010).

54. Pardridge, W. M. Drug transport in brain via the cerebrospinal fluid. *Fluids Barriers CNS* **8,** 7 (2011).

59. McDannold, N., Arvanitis, C. D., Vykhodtseva, N. & Livingstone, M. S. Temporary disruption of the blood-brain barrier by use of ultrasound and microbubbles: safety and efficacy evaluation in rhesus macaques. *Cancer Res.* **72,** 3652–63 (2012).

61. Panje, C. M., Wang, D. S. & Willmann, J. K. Ultrasound and microbubble-mediated gene delivery in cancer: progress and perspectives. *Invest. Radiol.* **48,** 755–69 (2013).

63. Huang, Q. *et al.* Targeted gene delivery to the mouse brain by MRI-guided focused ultrasound-induced blood-brain barrier disruption. *Exp. Neurol.* **233,** 350–356 (2012).

64. Sugiura, S. *et al.* Adenovirus-mediated gene transfer of heparin-binding epidermal growth factor-like growth factor enhances neurogenesis and angiogenesis after focal cerebral ischemia in rats. *Stroke.* **36,** 859–64 (2005).

65. Burgess, A., Huang, Y., Querbes, W., Sah, D. W. & Hynynen, K. Focused ultrasound for targeted delivery of siRNA and efficient knockdown of Htt expression. *J. Control. Release* **163,** 125–129 (2012).

66. Kaspar, B. K., Lladó, J., Sherkat, N., Rothstein, J. D. & Gage, F. H. Retrograde viral delivery of IGF-1 prolongs survival in a mouse ALS model. *Science* **301,** 839–42 (2003).

67. Wang, H. *et al.* Therapeutic gene silencing delivered by a chemically modified small interfering RNA against mutant SOD1 slows amyotrophic lateral sclerosis progression. *J. Biol. Chem.* **283,** 15845–15852 (2008).

68. Morille, M., Passirani, C., Vonarbourg, A., Clavreul, A. & Benoit, J. P. Progress in developing cationic vectors for non-viral systemic gene therapy against cancer. *Biomaterials* **29,** 3477–3496 (2008).

69. Laga, R., Carlisle, R., Tangney, M., Ulbrich, K. & Seymour, L. W. Polymer coatings for delivery of nucleic acid therapeutics. *J. Control. Release* **161,** 537–53 (2012).

70. Lu, W., Sun, Q., Wan, J., She, Z. & Jiang, X. G. Cationic albumin-conjugated pegylated nanoparticles allow gene delivery into brain tumors via intravenous administration. *Cancer Res.* **66,** 11878–11887 (2006).

71. Immordino, L., Dosio, F. & Cattel, L. Stealth liposomes: review of the basic science, rationale, and clinical applications,. *Int. J. Nanomedicine* **1,** 297–315 (2006).

72. Pombo García, K. *et al.* Zwitterionic-coated 'stealth' nanoparticles for biomedical applications: recent advances in countering biomolecular corona formation and uptake by the mononuclear phagocyte system. *Small* **10,** 2516–29 (2014).

73. Schöttler, S. *et al.* Protein adsorption is required for stealth effect of poly(ethylene glycol)- and poly(phosphoester)-coated nanocarriers. *Nat. Nanotechnol.* 1–6 (2016).

doi:10.1038/nnano.2015.330

74. Son, S. *et al.* RVG peptide tethered bioreducible polyethylenimine for gene delivery to brain. *J. Control. Release* **155,** 18–25 (2011).

75. Ko, Y. T., Bhattacharya, R. & Bickel, U. Liposome encapsulated polyethylenimine/ODN polyplexes for brain targeting. *J. Control. Release* **133,** 230–7 (2009).

76. Huang, R.-Q. *et al.* Efficient gene delivery targeted to the brain using a transferrin-conjugated polyethyleneglycol-modified polyamidoamine dendrimer. *FASEB J.* **21,** 1117–1125 (2007).

77. Kwon, E. J. *et al.* Targeted nonviral delivery vehicles to neural progenitor cells in the mouse subventricular zone. *Biomaterials* **31,** 2417–2424 (2010).

78. Emlen, W. & Mannik, M. Effect of DNA size and strandedness on the in vivo clearance and organ localization of DNA. *Clin. Exp. Immunol.* **56,** 185–92 (1984).

79. Kawabata, K., Takakura, Y. & Hashida, M. The Fate of Plasmid DNA After Intravenous Injection in Mice: Involvement of Scavenger Receptors in Its Hepatic Uptake. *Pharm. Res.* **12,** 825–830 (1995).

80. Hervé, F., Ghinea, N. & Scherrmann, J.-M. CNS delivery via adsorptive transcytosis. *AAPS J.* **10,** 455–472 (2008).

81. Zhang, Y., Wang, Y., Boado, R. J. & Pardridge, W. M. Lysosomal enzyme replacement of the brain with intravenous non-viral gene transfer. *Pharm. Res.* **25,** 400–406 (2008).

82. Kumar, P. *et al.* Transvascular delivery of small interfering RNA to the central nervous system. *Nature* **448,** 39–43 (2007).

83. Liu, Y. *et al.* Brain-targeting gene delivery and cellular internalization mechanisms for modified rabies virus glycoprotein RVG29 nanoparticles. *Biomaterials* **30,** 4195–4202 (2009).

84. Pulford, B. *et al.* Liposome-siRNA-peptide complexes cross the blood-brain barrier and significantly decrease PrPC on neuronal cells and PrPRES in infected cell cultures. *PLoS One* **5,** 1–13 (2010).

85. Gao, Y. *et al.* RVG-peptide-linked trimethylated chitosan for delivery of siRNA to the brain. *Biomacromolecules* **15,** 1010–1018 (2014).

86. Alvarez-Erviti, L. *et al.* Delivery of siRNA to the mouse brain by systemic injection of targeted exosomes. *Nat. Biotechnol.* **29,** 341–5 (2011).

87. Ke, W. *et al.* Gene delivery targeted to the brain using an Angiopep-conjugated polyethyleneglycol-modified polyamidoamine dendrimer. *Biomaterials* **30,** 6976–6985 (2009).

88. Huang, R. *et al.* Lactoferrin-modified nanoparticles could mediate efficient gene delivery to the brain in vivo. *Brain Res. Bull.* **81,** 600–604 (2010).

89. Huang, R., Ke, W., Liu, Y., Jiang, C. & Pei, Y. The use of lactoferrin as a ligand for targeting the polyamidoamine-based gene delivery system to the brain. *Biomaterials* **29,** 238–246 (2008).

90. Liu, Y. *et al.* A leptin derived 30-amino-acid peptide modified pegylated poly-l-lysine dendrigraft for brain targeted gene delivery. *Biomaterials* **31,** 5246–5257 (2010).

91. Costa, P. M. *et al.* Tumor-targeted Chlorotoxin-coupled Nanoparticles for Nucleic Acid Delivery to Glioblastoma Cells: A Promising System for Glioblastoma Treatment. *Mol. Ther. Nucleic Acids* **2,** e100 (2013).

92. Rapoport, S. I. Advances in osmotic opening of the blood-brain barrier to enhance CNS chemotherapy. *Expert Opin. Investig. Drugs* **10,** 1809–18 (2001).

93. Hwang, D. W. *et al.* A brain-targeted rabies virus glycoprotein-disulfide linked PEI nanocarrier for delivery of neurogenic microRNA. *Biomaterials* **32,** 4968–4975 (2011).

94. Rychak, J. J. & Klibanov, A. L. Nucleic acid delivery with microbubbles and ultrasound. *Adv. Drug Deliv. Rev.* **72,** 82–93 (2014).

95. Meairs, S. & Alonso, A. Ultrasound, microbubbles and the blood-brain barrier. *Prog. Biophys. Mol. Biol.* **93,** 354–62 (2007).

96. Greenleaf, W. & Bolander, M. Artificial cavitation nuclei significantly enhance acoustically induced cell transfection. *Ultrasound Med. …* **24,** 587–595 (1998).

97. Zhou, Y., Yang, K., Cui, J., Ye, J. & Deng, C. Controlled permeation of cell membrane by single bubble acoustic cavitation. *J. Control. Release* **157,** 103–111 (2012).

98. Choi, J. J., Pernot, M., Small, S. a & Konofagou, E. E. Noninvasive, transcranial and localized opening of the blood-brain barrier using focused ultrasound in mice. *Ultrasound Med. Biol.* **33,** 95–104 (2007).

99. Choi, J. J., Wang, S., Tung, Y.-S., Morrison, B. & Konofagou, E. E. Molecules of various pharmacologically-relevant sizes can cross the ultrasound-induced blood-brain barrier opening in vivo. *Ultrasound Med. Biol.* **36,** 58–67 (2010).

100. Choi, J. J. *et al.* Noninvasive and localized blood-brain barrier disruption using focused ultrasound can be achieved at short pulse lengths and low pulse repetition frequencies. *J. Cereb. Blood Flow Metab.* **31,** 725–37 (2011).

101. Xie, F. *et al.* Effects of transcranial ultrasound and intravenous microbubbles on blood brain barrier permeability in a large animal model. *Ultrasound Med. Biol.* **34,** 2028–34 (2008).

102. Sheikov, N., McDannold, N., Vykhodtseva, N., Jolesz, F. & Hynynen, K. Cellular mechanisms of the blood-brain barrier opening induced by ultrasound in presence of microbubbles. *Ultrasound Med. Biol.* **30,** 979–89 (2004).

103. Kobus, T., Vykhodtseva, N., Pilatou, M., Zhang, Y. & McDannold, N. Safety Validation of Repeated Blood–Brain Barrier Disruption Using Focused Ultrasound. *Ultrasound Med. Biol.* **42,** 481–492 (2015).

104. Huang, Q. *et al.* Effective Gene Transfer into Central Nervous System Following Ultrasound-Microbubbles-Induced Opening of the Blood-Brain Barrier. *Ultrasound Med. Biol.* **38,** 1234–1243 (2012).

105. Yamada, K. *et al.* Quantitative autoradiographic measurements of blood-brain barrier permeability in the rat glioma model. *J. Neurosurg.* **57,** 394–8 (1982).

106. Yue, P. *et al.* OX26/CTX-conjugated PEGylated liposome as a dual-targeting gene delivery system for brain glioma. *Mol. Cancer* **13,** 191 (2014).

107. Abbott, N. J., Rönnbäck, L. & Hansson, E. Astrocyte-endothelial interactions at the blood-brain barrier. *Nat. Rev. Neurosci.* **7,** 41–53 (2006).

108. Iliff, J. J. *et al.* A paravascular pathway facilitates CSF flow through the brain parenchyma and the clearance of interstitial solutes, including amyloid β. *Sci. Transl. Med.* **4,** 147ra111 (2012).

109. Lemkine, G. F. *et al.* Preferential transfection of adult mouse neural stem cells and their immediate progeny in vivo with polyethylenimine. *Mol. Cell. Neurosci.* **19,** 165–174 (2002).

110. Zou, S., Scarfo, K., Nantz, M. H. & Hecker, J. G. Lipid-mediated delivery of RNA is more efficient than delivery of DNA in non-dividing cells. *Int. J. Pharm.* **389,** 232–243 (2010).

111. Bharali, D. J. *et al.* Organically modified silica nanoparticles: a nonviral vector for in vivo gene delivery and expression in the brain. *Proc. Natl. Acad. Sci. U. S. A.* **102,** 11539–44 (2005).

112. Wehling, K. *et al.* Specficificity of DNA-basic polypeptide interactions. Influence of neutral residues incorporated into polylysine and polyarginine. *Nucleic Acids Res.* **2,** 799–807 (1975).

113. Cheng, Q. *et al.* The effect of guanidinylation of PEGylated poly(2-aminoethyl methacrylate) on the systemic delivery of siRNA. *Biomaterials* **34,** 3120–3131 (2013).

114. Choi, J. L. *et al.* Guanidinylated block copolymers for gene transfer : A comparison with amine-based materials for in vitro and in vivo gene transfer ef fi ciency. *Biomaterials* **54,** 87–96 (2015).

115. Hauck, E. S., Zou, S., Scarfo, K., Nantz, M. H. & Hecker, J. G. Whole animal in vivo imaging after transient, nonviral gene delivery to the rat central nervous system. *Mol. Ther.* **16,** 1857–1864 (2008).

116. Uchida, S. *et al.* In Vivo Messenger RNA Introduction into the Central Nervous System Using Polyplex Nanomicelle. *PLoS One* **8,** (2013).

117. Soderquist, R. *et al.* Release of Plasmid DNA-encoding IL-10 from PLGA Microparticles Facilitates Long-term Reversal of Neuropathic Pain Following a Single Intrathecal Administration. *Pharm. Res.* **27,** 841–854 (2007).

118. Zeng, J., Wang, X. & Wang, S. Self-assembled ternary complexes of plasmid DNA, low molecular weight polyethylenimine and targeting peptide for nonviral gene delivery into neurons. *Biomaterials* **28,** 1443–1451 (2007).

119. Song, H. P. *et al.* Gene transfer using self-assembled ternary complexes of cationic magnetic nanoparticles, plasmid DNA and cell-penetrating tat peptide. *Biomaterials* **31,** 769–778 (2010).

120. Tan, J.-K. Y. *et al.* Microbubbles and ultrasound increase intraventricular polyplex gene transfer to the brain. *J. Control. Release* **231,** 86–93 (2016).

121. Tang, G. P. *et al.* Polyethylene glycol modified polyethylenimine for improved CNS gene transfer: Effects of PEGylation extent. *Biomaterials* **24,** 2351–2362 (2003).

122. Kim, I. D. *et al.* Neuroprotection by biodegradable PAMAM ester (e-PAM-R)-mediated HMGB1 siRNA delivery in primary cortical cultures and in the postischemic brain. *J. Control. Release* **142,** 422–430 (2010).

123. Chen, Q. *et al.* Lipophilic siRNAs mediate efficient gene silencing in oligodendrocytes with direct CNS delivery. *J. Control. Release* **144,** 227–232 (2010).

124. Liang, B. *et al.* The use of folate-PEG-grafted-hybranched-PEI nonviral vector for the inhibition of glioma growth in the rat. *Biomaterials* **30,** 4014–4020 (2009).

125. Cardoso, A. L. C. *et al.* Tf-lipoplexes for neuronal siRNA delivery: A promising system to mediate gene silencing in the CNS. *J. Control. Release* **132,** 113–123 (2008).

126. Kato, T. *et al.* Efficient delivery of liposome-mediated MGMT-siRNA reinforces the cytotoxity of temozolomide in GBM-initiating cells. *Gene Ther.* **17,** 1363–1371 (2010).

127. Allard, E., Passirani, C. & Benoit, J.-P. Convection-enhanced delivery of nanocarriers for the treatment of brain tumors. *Biomaterials* **30,** 2302–2318 (2009).

128. Querbes, W. *et al.* Direct CNS delivery of siRNA mediates robust silencing in oligodendrocytes. *Oligonucleotides* **19,** 23–29 (2009).

129. Stiles, D. K. *et al.* Widespread suppression of huntingtin with convection-enhanced delivery of siRNA. *Exp. Neurol.* **233,** 463–471 (2012).

130. MacKay, J. A. *et al.* HIV TAT peptide modifies the distribution of DNA nanolipoparticles following convection-enhanced delivery. *Mol. Ther.* **16,** 893–900 (2008).

131. Kenny, G. D. *et al.* Multifunctional receptor-targeted nanocomplexes for the delivery of therapeutic nucleic acids to the Brain. *Biomaterials* **34,** 9190–9200 (2013).

132. Spencer, B. J. & Verma, I. M. Targeted delivery of proteins across the blood-brain barrier. *Proc. Natl. Acad. Sci. U. S. A.* **104,** 7594–7599 (2007).

133. Yu, Y. J. *et al.* Boosting brain uptake of a therapeutic antibody by reducing its affinity for a transcytosis target. *Sci. Transl. Med.* **3,** 84ra44 (2011).

134. Monani, U. R. Spinal muscular atrophy: A deficiency in a ubiquitous protein; a motor neuron-specific disease. *Neuron* **48,** 885–896 (2005).

135. Mitchell, J. D. & Borasio, G. D. Amyotrophic lateral sclerosis. *Lancet* **369,** 2031–41 (2007).

136. Lavail, J. H. & Lavail, M. M. Retrograde Axonal Transport in the Central Nervous System. *Science (80-.).* **176,** 1416–1417 (1972).

137. Salinas, S., Schiavo, G. & Kremer, E. J. A hitchhiker's guide to the nervous system: the complex journey of viruses and toxins. *Nat. Rev. Microbiol.* **8,** 645–655 (2010).

138. Maheshri, N., Koerber, J. T., Kaspar, B. K. & Schaffer, D. V. Directed evolution of adeno-associated virus yields enhanced gene delivery vectors. *Nat. Biotechnol.* **24,** 198–204 (2006).

139. Kotterman, M. A. & Schaffer, D. V. Engineering adeno-associated viruses for clinical

gene therapy. *Nat. Rev. Genet.* **15,** 445–51 (2014).

140. Snyder, B. R. *et al.* Comparison of Adeno-Associated Viral Vector Serotypes for Spinal Cord and Motor Neuron Gene Delivery. *Hum. Gene Ther.* **22,** 1129–1135 (2011).

141. Hollis II, E. R. *et al.* Efficient Retrograde Neuronal Transduction Utilizing Self-complementary AAV1. *Mol. Ther.* **16,** 296–301 (2008).

142. Xu, J., Ma, C., Bass, C. & Terwilliger, E. F. A combination of mutations enhances the neurotropism of AAV-2. *Virology* **341,** 203–214 (2005).

143. Azzouz, M., Ralph, G. & Storkebaum, E. VEGF delivery with retrogradely transported lentivector prolongs survival in a mouse ALS model. *Nature* **429,** 413–417 (2004).

144. Hirano, M. *et al.* Highly Efficient Retrograde Gene Transfer into Motor Neurons by a Lentiviral Vector Pseudotyped with Fusion Glycoprotein. *PLoS One* **8,** 1–8 (2013).

145. Petruska, J. C. *et al.* To Motoneurons in Adult Rats. **32,** 997–1005 (2011).

146. Benkhelifa-Ziyyat, S. *et al.* Intramuscular scAAV9-SMN injection mediates widespread gene delivery to the spinal cord and decreases disease severity in SMA mice. *Mol. Ther.* **21,** 282–90 (2013).

147. Price, D., Griffin, J., Young, A., Peck, K. & Stocks, A. Tetanus toxin: direct evidence for retrograde intraaxonal transport. *Science (80-.).* **188,** 945–947 (1975).

148. Schwab, M. E., Suda, K. & Thoenen, H. Selective retrograde synaptic transer of a protein, tetanus toxin, subsequent to its retrotransport. *J. Cell Biol.* **82,** 798–810 (1979).

149. Li, J. *et al.* Insect GDNF:TTC fusion protein improves delivery of GDNF to mouse CNS. *Biochem. Biophys. Res. Commun.* **390,** 947–951 (2009).

150. Francis, J. W. *et al.* A survival motor neuron:tetanus toxin fragment C fusion protein for the targeted delivery of SMN protein to neurons. *Brain Res.* **995,** 84–96 (2004).

151. Chian, R.-J. J. *et al.* IGF-1:tetanus toxin fragment C fusion protein improves delivery of IGF-1 to spinal cord but fails to prolong survival of ALS mice. *Brain Res.* **1287,** 1–19 (2009).

152. Sellers, D. L. *et al.* Targeted Axonal Import (TAxI) peptide delivers functional proteins into the spinal cord after peripheral administration. *PNAS* 1–6 (2016). doi:10.1073/pnas.1515526113

Part 3: Synthetic Polymers for Gene Delivery to the Brain

In developing effective polymeric gene delivery vehicles, there is a balance between high gene transfer efficiency and cytotoxicity that needs to be considered. This section focuses on lowing the toxicity and improving the transfection efficiency of gene delivery vehicles.

Chapter 1. Reducible, Dibromomaleimide-linked Polymers for Gene Delivery

James-Kevin Y. Tan, Jennifer L. Choi, Hua Wei, Joan G. Schellinger, Suzie H. Pun

This work has resulted in a publication: Tan, *et al*. *Biomater. Sci*. (2015) **3**:112-120.

Synopsis:

Polycations have been successfully used as gene transfer vehicles both *in vitro* and *in vivo*; however, their cytotoxicity has been associated with increasing molecular weight. Polymers that can be rapidly degraded after internalization are typically better tolerated by mammalian cells compared to their non-degradable counterparts. Here, we report the use of a dibromomaleimide-alkyne (DBM-alkyne) linking agent to reversibly bridge cationic polymer segments for gene delivery and to provide site-specific functionalization by azide-alkyne cycloaddition chemistry. A panel of reducible and non-reducible, statistical copolymers of (2-dimethylamino) ethyl methacrylate (DMAEMA) and oligo(ethylene glycol) methyl ether methacrylate (OEGMA) were synthesized and evaluated. When complexed with plasmid DNA, the reducible and non-reducible polymers had comparable DNA condensation properties, sizes, and transfection efficiencies. When comparing cytotoxicity, the DBM-linked, reducible polymers were significantly less toxic than the non-reducible polymers. To demonstrate polymer functionalization by click chemistry, the DBM-linked polymers were tagged with an azide-fluorophore and were used to monitor cellular uptake. Overall, this polymer system introduces the use of a reversible linker, DBM-alkyne, to the area of gene delivery and allows for facile, orthogonal, and site-specific functionalization of gene delivery vehicles.

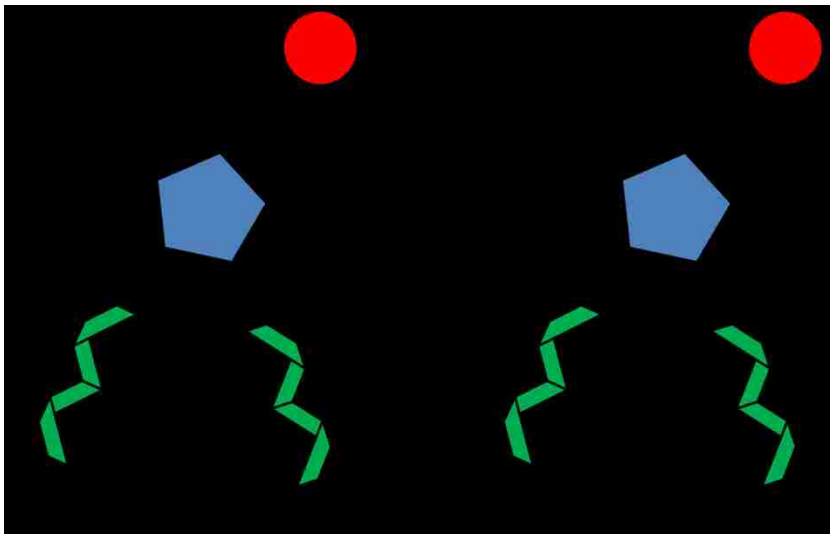

1.1 INTRODUCTION

Gene-based drugs typically require a carrier to facilitate delivery into cell nuclei, where they are transcribed and later translated into proteins that can elicit a therapeutic effect. While virally-derived carriers have been the preferred vectors in clinical trials, a number of safety concerns have arisen due to their ability to alter the genome (retrovirus and lentivirus) and activate the immune system.[26,39,153] While non-viral vectors generally have lower transfection efficiencies compared to viral vectors, they offer potential safety advantages. A class of materials that is highly investigated for non-viral gene transfer is cationic polymers, which condense DNA through electrostatic interactions, protect cargo from early elimination, and can be readily functionalized with molecular targeting agents.[45,154–156] One of the most effective and commonly used cationic polymers is polyethylenimine (PEI); however, it is non-degradable and has a high density of positive amino groups that contribute to its cytotoxicity.[157] *In vivo*, PEI aggregates and accumulates in the lungs and liver upon systemic administration due to strong electrostatic interactions with cell membranes, proteins, and the extracellular matrix.[45,155] Several other cationic materials such as poly[*L*-lysine],[41,42] chitosan,[158–160] poly[(*N*-2-hydroxypropyl) methacrylamide] (pHPMA),[161–163] and poly[(2-dimethylamino) ethyl methacrylate] (pDMAEMA)[164–167] have also been investigated and are able to achieve transfection efficiencies comparable to that of PEI but with the advantage of improved cell viability. Nevertheless, cationic polymers such as pDMAEMA still have inherent cytotoxicity due to their non-degradable nature.[167,168] To ameliorate these effects, degradable linkages have been incorporated into cationic polymers so they can dissociate into smaller, less toxic fragments.[39,167,169,170] Two commonly used chemistries for synthesizing degradable polymers are reducible disulfide bonds and hydrolyzable ester bonds.[167,168,171] Several degradable polymers containing ethylene imine units have been reported with comparable gene delivery efficiency to that of PEI but with reduced cytotoxicity.[43,161,169,172]

Bromomaleimide-functional groups have recently been developed for their ability to reversibly react with thiols. For example, dibromomaleimide (DBM) has two bromines that can be substituted with free thiols to form two thioether bonds.[173] Upon the addition of an excess of thiols, the thioether bonds can be readily cleaved to regenerate the original, thiolated product. Since the cell cytoplasm contains reducing agents such as glutathione, intracellular bromomaleimide-linked conjugates can potentially be cleaved *in vivo*. In fact, these thioether bonds have been shown to be

cleaved within 1 hour in the cytoplasm of mammalian cells.[174] Another advantage of DBM is that it has a third point of attachment off the maleimide group. This has allowed for a very site-specific and quantity-controlled conjugation of various moieties ranging from fluorophores to polymers.[173–175]

Herein, we describe synthesis of cleavable gene delivery vehicles that utilize DBM as a reversible bridging agent for cationic polymer segments as well as a moiety for site-specific functionalization. A panel of reducible, statistical copolymers of DMAEMA and oligo(ethylene glycol) methyl ether methacrylate (OEGMA) were synthesized by reacting thiol-terminated polymers with a DBM-alkyne derivative. Polymer fragmentation in reducing environments was confirmed. While polymer reducibility did not significantly affect gene transfer ability, the reducible polymers were better tolerated by mammalian cells than their non-reducible analogs. We further demonstrated site-specific modification of polymers by click conjugation of an azide-functionalized fluorophore to the alkyne site. Fluorophore-labeled polymers were used to monitor polyplex uptake by flow cytometry. Overall, the DBM-alkyne derivative offers a facile way to reversibly connect different polymers for gene delivery while the alkyne allows for the site-specific functionalization of polymers.

1.2 Materials and Methods

1.2.1 *Materials*

All chemicals were purchased from Sigma-Aldrich (St. Louis, MO). Cell culture reagents were purchased from Cellgro/Mediatech (Fisher Scientific, Pittsburgh PA). The pCMV-Luc2 plasmid was isolated using the Qiagen Plasmid Giga Kit (Hilden, Germany). The bicinchoninic acid (BCA) protein quantification assay kit was purchased from Thermo Fischer Scientific (Waltham, MA) while the luciferase expression quantification kit and MTS assay were obtained from Promega (Madison, WI).

1.2.2 *Polymer synthesis and characterization*

1.2.2.1 Synthesis of dibromomaleimide-alkyne

Dibromomaleic anhydride was synthesized as previously reported (Supporting Information).[176] Propargylamine (0.1 mL, 1.6 mmol), dibromomaleic anhydride (0.6 g, 2.2 mmol), and 34 mL of glacial acetic acid were added to a reaction vessel and refluxed at 120 °C for 5 hours with stirring. Afterwards, the reaction vessel was cooled to room temperature and the glacial acetic acid was azeotropically removed with toluene under reduced pressure. The crude DBM-alkyne was dissolved in DCM and isolated by silica gel column (10:0.5 hexane:ethyl acetate) to yield the product as an off-white powder (0.38 g, 82%). The product identity and purity was confirmed by GC-MS on a Hewlett-Packard (Palo Alto, CA) 5971A GC-MSD.

1.2.2.2 ATRP copolymerization of DMAEMA and OEGMA

A double-headed atom-transfer radical polymerization (ATRP) initiator with an internal disulfide bond was prepared by N,N′-dicyclohexylcarbodiimide coupling between 2-hydroxyethyl disulfide and 2-bromo-2-methylpropionic acid (Supporting Information). Reducible p(DMAEMA-*s*-OEGMA) containing an internal disulfide bond was synthesized by ATRP using the double-headed ATRP initiator and CuCl/bpy as the catalyst. Polymers of three different sizes were synthesized by changing the monomer ratio; these polymers were called Low Molecular Weight (MW) (~15k), Medium MW (~20k), and High MW (~40k). Briefly, double-headed ATRP initiator (0.27 g, 0.06 mmol), DMAEMA (1.5 mmol, 3.0 mmol, or 6 mmol), OEGMA (0.3 mmol, 0.6 mmol, or 1.2 mmol), and bpy (37.48 mg, 0.24 mmol) were dissolved in isopropanol to a final monomer concentration of 2 M. The solution was sparged for 15 min with Ar. CuCl (11.88 mg, 0.12 mmol) was added and the solution continued to sparge for 3 minutes before immersing the flask in an oil bath preheated to 40 °C. After 6 hours, the flask was taken out and vented to quench the reaction. The solution underwent exhaustive dialysis for 3 days to remove the copper catalyst and subsequently lyophilized to yield a slightly opaque solid gel. Non-reducible p(DMAEMA-*s*-

OEGMA) analogs were similarly synthesized with an ethyl α-bromoisobutyrate initiator (8.80 μL, 0.06 mmol), DMAEMA (3 mmol, 6.0 mmol, or 12.0 mmol), OEGMA (0.6 mmol, 1.2 mmol, or 2.4 mmol), bpy (18.74 mg, 0.12 mmol), and CuCl (5.94 mg, 0.06 mmol). ^{1}H NMR in $CDCl_3$ was used to determine the ratio of DMAEMA to OEGMA by comparing the ester methylene peaks of DMAEMA and OEGMA (3.9-4.2 ppm) to the methoxy peak of OEGMA (3.3-3.4 ppm). To determine molecular weight and polydispersity (PDI), aqueous SEC-MALLS was performed in 1:1 methanol:300 mM acetate buffer pH 4.4 on a Shodex (Kawasaki, Japan) SB-804 HQ column connected to a Shimadzu (Kyoto, Japan) LC-20AD liquid chromatography pump and Wyatt (Sana Barbara, CA) MiniDawn Treos and Optilab rEX system. Number and weight average molecular weight (M_n and M_w) and d*n*/d*c* values were calculated using ASTRA software (Wyatt).

1.2.2.3 p(DMAEMA-s-OEGMA) substitution to DBM-alkyne

Reducible p(DMAEMA-*s*-OEGMA) (5.0 μmol) and *tris*(2-carboxyethyl)phosphine (TCEP) (0.7 mg, 5.5 μmol) were dissolved in 3:1 (v/v) DMF:0.05 mM PBS to a final concentration of 0.02 M. The solution was stirred for 30 minutes before the addition of DBM-alkyne (1.5 mg, 5.0 μmol). After 2 hours of stirring, the solution was dialyzed to remove DMF and salts and subsequently lyophilized to yield an orange solid gel. Polymers were characterized by aqueous SEC as mentioned previously.

1.2.2.4 Glutathione reduction assay

DBM-substituted and non-reducible p(DMAEMA-*s*-OEGMA) were dissolved in a cytoplasmic mimic buffer (20 mM HEPES, 100 mM KCl, 1 mM $MgCl_2$, 1 mM EDTA, and 1 mM glutathione, pH 7.4) to a final concentration of 0.1 mM. After 2 hours of stirring, aqueous SEC-MALLS was performed as mentioned previously.

1.2.2.5 Fluorophore cycloaddition to DBM-alkyne

DBM-substituted polymer (0.34 μmol), *N*,*N*,*N′*,*N″*,*N″*-pentamethyldiethylenetriamine (0.34 μmol), and azide-tetramethylrhodamine (0.34 μmol) were dissolved in 2 mL of DMF. The solution was sparged with Ar for 3 minutes, Cu(I)Br (0.34 μmol) was added, and then sparged for an additional 2 minutes. The vessel was placed in an oil bath at 60 °C for 24 hours. Afterwards, the solution was precipitated twice into ether, dialyzed, and lyophilized.

1.2.3 *Polyplex characterization*

1.2.3.1 Polyplex formation

The pCMV-Luc2 plasmid was diluted in double distilled H_2O (ddH_2O) to a concentration of 0.1 mg/mL and mixed with an equal volume of polymer (in ddH_2O) at the desired amine to phosphate (N/P) ratio. The required amount of polymer was calculated by determining the polymer mass to charge ratio and taking into account that 1 μg of DNA contains 3 nmol of phosphate. After mixing, the polyplexes were allowed to form for 10 min at room temperature.

1.2.3.2 DNA complexation by agarose gel retardation

The ability of the cationic polymers to bind with DNA was assessed by a gel retardation assay. The polyplexes (1 μg DNA, 20 μL solution, various N/P ratios) with 10% (v/v) BlueJuice™ gel loading buffer (Invitrogen, Carlsbad, CA) were loaded onto a 1% agarose gel containing TAE buffer (40 mM Tris-acetate, 1 mM EDTA) and 5 mg/mL ethidium bromide. The gel was electrophoresed at 100 V for 40 min. The plasmid DNA was then visualized using a Kodak (Rochester, NY) UV transilluminator (laser-excited fluorescence gel scanner).

1.2.3.3 Polyplex sizing and surface charge analysis

Polyplexes were formed at the same concentration as previously stated but at half the volume. Briefly, polyplexes (0.5 μg DNA, 10 μL solution, N/P = 5 and 10) were mixed with either 90 μL of ddH_2O or PBS. A Brookhaven Instruments Corporation (Holtsville, NY) ZetaPLUS instrument was used to determine the

particle size by dynamic light scattering (DLS) and surface charge by zeta potential measurements.

1.2.3.4 Polyplex unpackaging

The pCMV-Luc2 plasmid was mixed with the bis-intercalating dye YOYO-1 iodide (Invitrogen, Carlsbad, CA) at a dye to base pair ratio of 1:100 and incubated at room temperature for 1 hour. Polyplexes were prepared at an N/P = 10 by complexing YOYO-labeled plasmid with reducible and non-reducible polymers as previously mentioned. Polyplexes were pre-treated with 1 mM glutathione for 8 hours and then treated with 5 μg/mL heparin sulfate for 1 hour. The fluorescence (ex: 491 nm, ex: 509 nm) of each well was normalized to its respective DNA only control.

1.2.4 In vitro *studies*

1.2.4.1 Luciferase plasmid transfection

Human epithelial adenocarcinoma cells (HeLa) were seeded in 10% FBS and 1% AbAm antibiotic supplemented MEM culture medium into a 24-well plate at a density of 3.0×10^4 cells per well. Cells were placed in a 37 °C, 5% CO_2, humidified incubator for 16 hours prior to transfection (60% confluency at time of polymer addition). Polyplexes were formed as previously described at N/P = 5 and 10 using 1 μg of pCMV-Luc2 plasmid DNA in 20 μL of total volume. Polyplexes were incubated with cells in OptiMEM™ or complete media for 4 hours; afterwards, polyplexes were washed off and replaced with fresh complete media. After an additional 44 hours, cells were lysed and analyzed by a luciferase quantification expression kit and BCA assay for total protein content. Protein content was used to normalize luciferase expression as well as quantify cell population viability.

1.2.4.2 IC_{50} study

HeLa cells were seeded at 5.0×10^3 cells per well in a 96-well plate as mentioned above. Non-reducible and reducible, DBM-substituted polymers at various

concentrations were incubated with the cells in serum for 4 hours and were subsequently replaced with fresh serum media. After an additional 44 hours, an MTS assay was conducted to assess cell viability. Half maximal inhibitory concentration (IC_{50}) was calculated with Graphpad (La Jolla, CA) using a non-linear regression fit with variable slope.

1.2.4.3 Flow cytometry uptake study

HeLa cells were plated as described above at a density of 7.5×10^4 cells per well. Polyplexes of non-functionalized and fluorophore-functionalized polymer were formed with DNA at N/P ratios = 5 and 10 in OptiMEM™ as described above. Fluorophore only, polymer polyplexes, polymer polyplexes with free fluorophore, and fluorophore-polymer polyplexes were incubated with cells for 1 hour. Cells were then washed with PBS and CellScrub™ before analysis with a MACSQuant (Miltenyi, Bergisch Gladbach, Germany) flow cytometer. Analysis was performed with FlowJo analysis software (Tree Star, Ashland, Oregon).

1.2.5 *Statistical analysis*

All statistical analyses were performed using a two-tailed Student's t-test with unequal variance.

1.3 Results and Discussion

1.3.1 *Polymer synthesis and characterization*

Three cationic, reducible polymers were synthesized by substituting a DBM-alkyne molecule with thiolated copolymers of DMAEMA and OEGMA (**Figure 1.1a**).

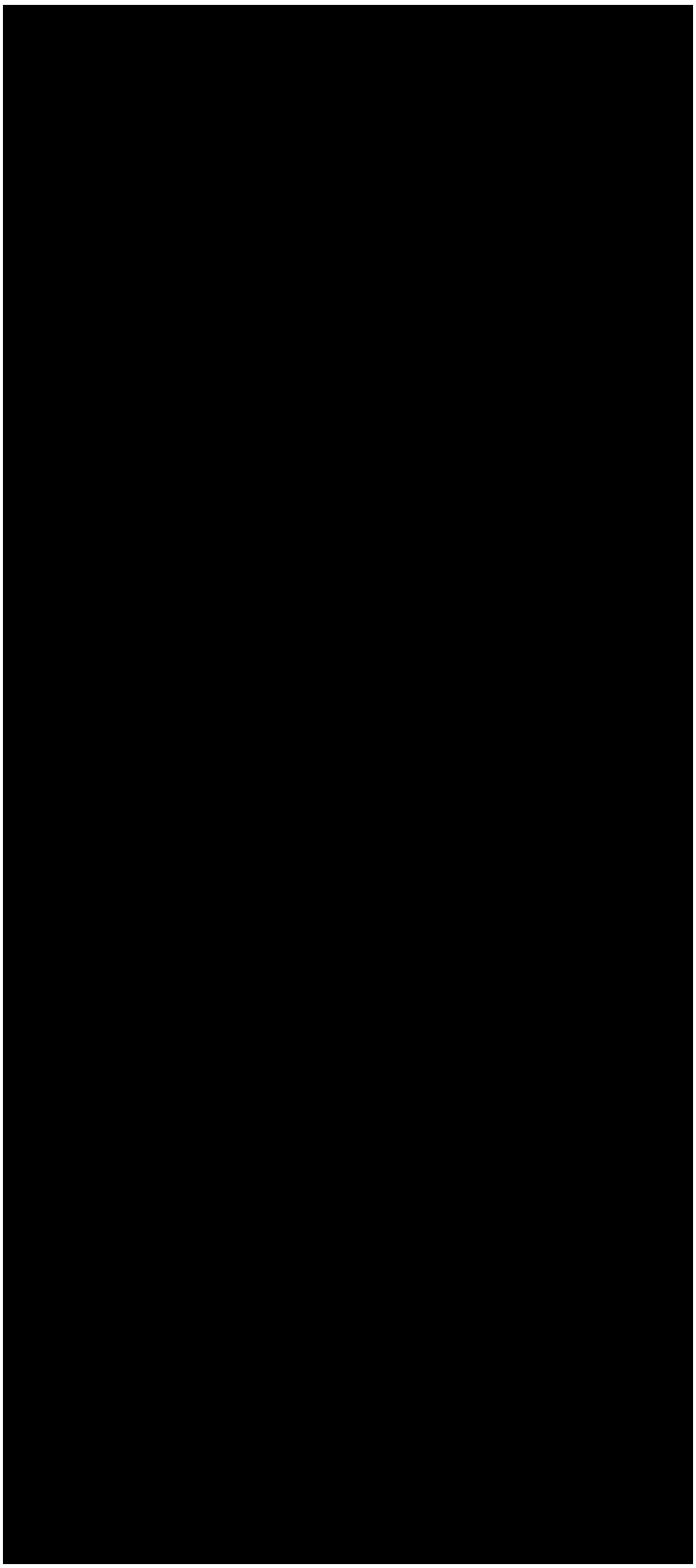

Figure 1.1 (a) Synthesis of fluorophore-functionalized, DBM-substituted p(DMAEMA-*s*-OEGMA); **(b)** Synthesis of non-reducible p(DMAEMA-*s*-OEGMA).

DBM-alkyne was synthesized as previously reported (**Figure S1.1** & **Figure S1.2**).[173] A double-headed ATRP initiator with an internal disulfide was prepared by N,N′-dicyclohexylcarbodiimide coupling between 2-hydroxyethyl disulfide and 2-bromo-2-methylpropionic acid (**Figure S1.3**). The double-headed initiator was used to prepare statistical copolymers of DMAEMA and OEGMA with low (~10 kDa), medium (~20 kDa), and high (~40 kDa) target molecular weights (**Table 1.1**).

TABLE 1.1 CHARACTERIZATION OF VARIOUS DMAEMA AND OEGMA STATISTICAL COPOLYMERS

The DMAEMA monomer provides cationic charge for DNA condensation while the OEGMA affords colloidal stability as reported previously for similar systems.[167,168,177] The resulting p(DMAEMA-*s*-OEGMA) materials possessed near-target molecular weights and compositions close to monomer feed ratios (5:1 DMAEMA to OEGMA) (**Figure S1.4**). These parent p(DMAEMA-*s*-OEGMA) polymers were reduced with TCEP to generate thiol-terminated fragments that were substituted onto DBM-alkyne. Under SEC-MALLS analysis, TCEP reduction caused a delayed elution compared to the elution of the parent polymers due to the reduction of the disulfide bond and decreased molecular weight (**Figure 1.2**).

Figure 1.2 SEC traces of **(a)** low, **(b)** medium, and **(c)** high molecular weight parent, reduced, and DBM-substituted DMAEMA and OEGMA copolymers. Parent polymers were reduced with TCEP (right-shifted trace) and resulting thiolated polymer fragments were substituted to DBM-alkyne (overlapping trace with parent polymer).

DBM-alkyne was added to the thiolated polymers in the presence of TCEP to prevent disulfide formation and to yield the DBM-substituted polymers. The SEC traces of the DBM-substituted polymers were shifted back to the earlier elution times, as expected for the increased molecular weight due to polymer substitution (**Figure 1.2** and **Table 1.1**). The reaction was rapid and highly efficient as only equimolar amounts of parent polymer and DBM-alkyne were needed. Excess TCEP ensured the complete reduction of parent p(DMAEMA-*s*-OEGMA) and did not reduce the newly formed thioether bonds. Furthermore, the substituted polymers showed a new increase in UV absorbance and exhibited fluorescent properties [data not shown]. These findings are consistent with reports of other substituted dibromomaleimides.[173,175,176,178] As non-reducible controls, polymers of similar molecular weights were polymerized with a conventional ATRP initiator, α-bromoisobutyrate (**Figure 1.1b**). The non-reducible polymers had molecular weights similar to those of the substituted polymers and monomer incorporations close to the initial feed ratio (5:1 DMAEMA to OEGMA) (**Table 1.1** and **Figure S1.4**).

Larger molecular weight pDMAEMA has been correlated with higher cytotoxicity.[179] Unlike the slow hydrolysis rate of DMAEMA esters,[168] the DBM-substituted polymers should be more rapidly reduced after intracellular uptake of the polyplexes in order to facilitate cargo release and reduce cytotoxicity. To demonstrate polymer reduction under physiological conditions, DBM-substituted polymers were incubated in a cytoplasmic mimic buffer[173] containing 1 mM glutathione reducing agent for 2 hours and analyzed by SEC (**Figure 1.3a**).

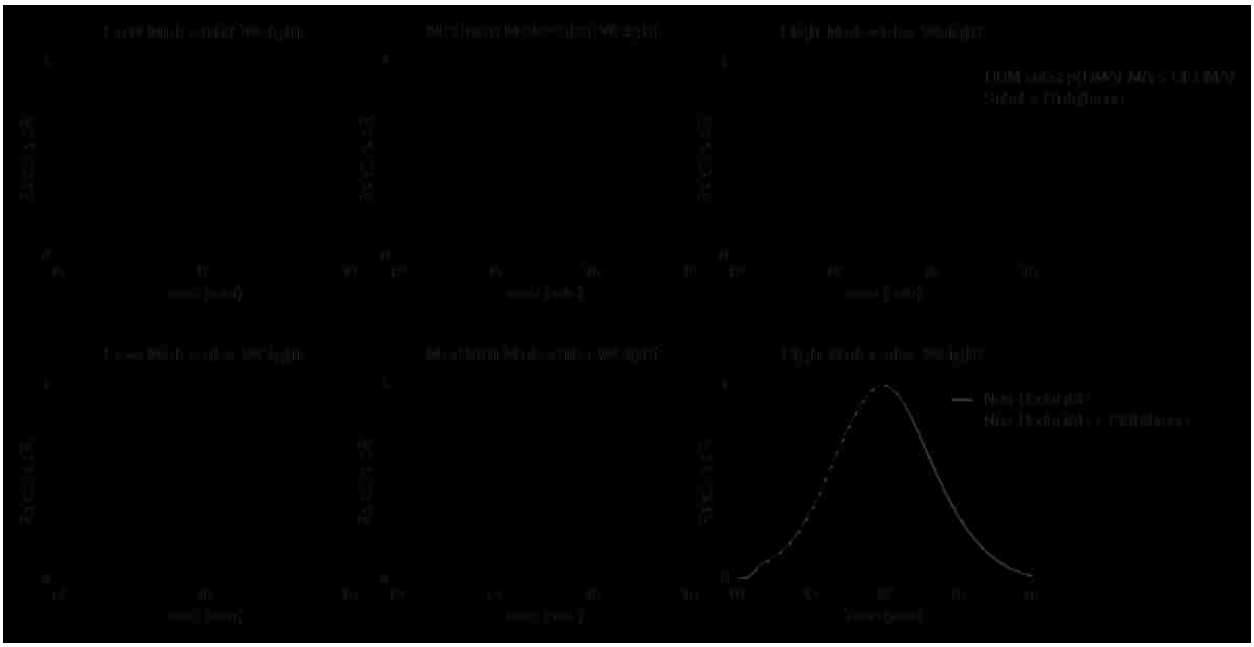

Figure 1.3 SEC traces **(a)** DBM-substituted and **(b)** non-reducible DMAEMA and OEGMA copolymers with glutathione. The copolymers were incubated in a cell cytoplasm mimic buffer containing 20 mM HEPES, 100 mM KCl, 1 mM $MgCl_2$, and 1 mM glutathione, pH 7.4. Incubation with glutathione reduced the DBM-substituted polymers and caused a rightward peak shift, signifying a decrease in MW.

Substituted polymers with glutathione had a delayed elution compared to the peak of the DBM-substituted polymers, demonstrating that the thioether bonds in the copolymer were cleaved by glutathione. The reducibility of this polymer system is consistent with other DBM systems and suggests that the material can be cleaved in the reducing environment of the cell cytoplasm.[173,174,180] Non-reducible polymers were also incubated with glutathione and analyzed by SEC (**Figure 1.3b**). No peak shift was seen in the SEC traces for the non-reducible polymers.

1.3.2 *Characterization of polyplexes*

Polyplexes were formed by mixing the polymers with plasmid DNA at various amine to phosphate (N/P) ratios. The ability of the polyplexes to complex DNA was assessed by a gel retardation assay (**Figure S1.5**). Complete complexation of DNA was observed starting at an N/P = 2 for reducible and non-reducible copolymers, suggesting that DBM-alkyne and the reducible thioethers did not affect DNA

condensation. Polyplexes formed at N/P = 5 and 10 were characterized by DLS in either ddH_2O or PBS containing physiological salt concentrations (**Figure 1.4**).

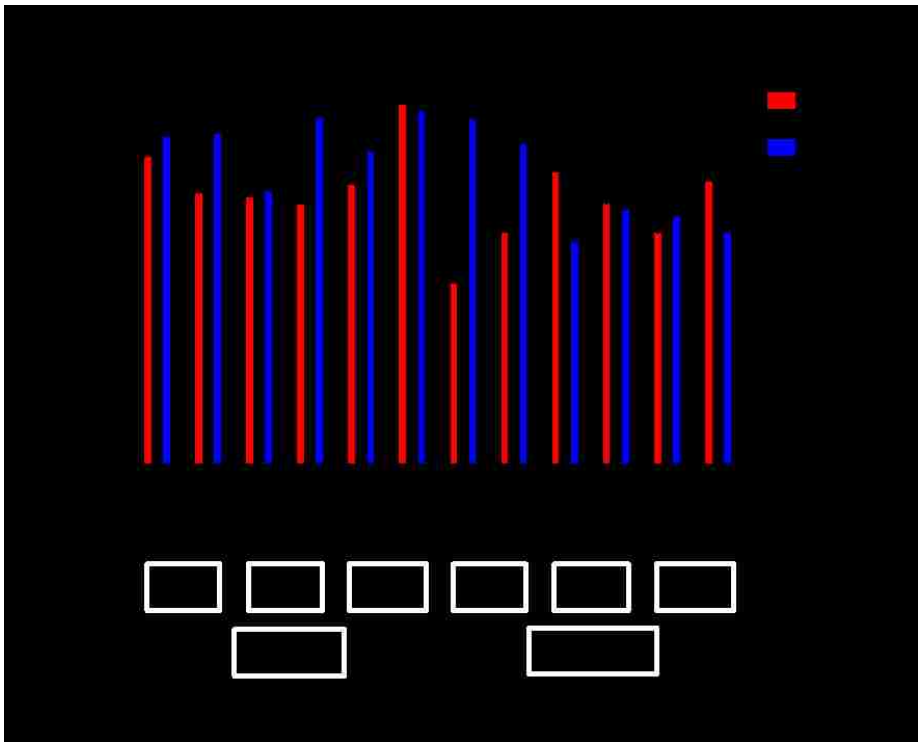

Figure 1.4 Average diameter of reducible and non-reducible polymer polyplexes measured by DLS. Polyplexes were formed in water and allowed to form for 10 minutes. Afterwards, polyplexes were diluted with water or 150 mM PBS and measured by DLS. Data is presented as mean + SD, n = 3.

In water, reducible polyplexes showed comparable polyplex size (150-225 nm) to non-reducible polyplexes (175-260 nm), suggesting that DBM-alkyne and the reducible thioethers did not affect polyplex formation and size. In physiological salt concentrations, relatively good stability is observed as particles remained the same size or only slightly increased in size. Homopolymers of DMAEMA tend to form large complexes and aggregates with DNA (~1 μm); thus, the incorporation of OEGMA was able to stabilize polyplexes in physiological salt concentrations.[164,166] The uncharged, hydrophilic properties of OEGMA provided steric hindrance and an extra hydration layer that conferred increased stabilization as reported for other DMAEMA and OEGMA copolymers.[164–166,181,182] Zeta potential measurements (**Figure S1.6**) indicate that the net surface charges for both reducible and non-

reducible copolymers at N/P = 5 and 10 are all positive (~20-40 mV in water, ~5-20 mV in PBS). A positive charge is necessary for polyplex-mediated gene delivery since the excess positive charge interacts with the negatively charged cell membrane for enhanced uptake and gene delivery.[183]

Polyplex unpackaging in non-reducible and reducible conditions was assessed by incubating YOYO-1-labeled DNA polyplexes with heparin sulfate and glutathione (**Figure S1.7**). In condensed complexes, the YOYO-1 fluorescence is self-quenching; however, as the polyplex unpackages, the fluorescence is recovered. When comparing the heparin only versus heparin and glutathione conditions, the reducible medium MW and high MW polyplexes unpackaged more after exposure to a reducing environment. These results suggest that cleavable thioether bonds of the reducible, DBM-linked polymers were able to mediate greater DNA unpackaging in the presence of glutathione.

1.3.3 In vitro *transfection and cytotoxicity*

To investigate the effect of cleavable linkages on transfection efficiency, polymers were complexed with the luciferase reporter plasmid at N/P = 5 and 10 and exposed to HeLa cells. Branched polyethylenimine (bPEI, 25k) at an N/P = 5 was used as a standard for comparison. Transfection efficiency of both reducible and non-reducible polymers improved with increasing molecular weight as seen with other DMAEMA and OEGMA copolymers and other cationic systems (**Figure 1.5a**).[182]

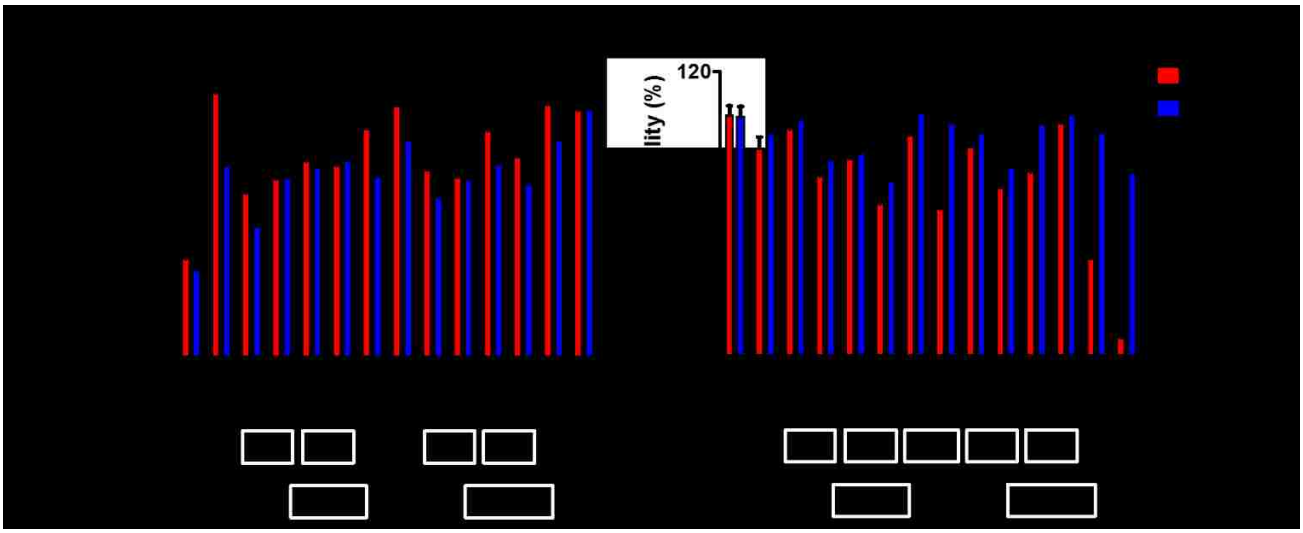

Figure 1.5 (a) Luciferase plasmid transfection efficiency and **(b)** cytotoxicity of reducible DBM-alkyne and non-reducible low, medium, and high MW polyplexes at N/P ratios = 5 and 10. Naked DNA and bPEI (25 kDa) controls are included for comparison. Data is presented as mean + SD, n = 4. Statistically significant ($P < 0.05$) differences are indicated with a (*).

The transfection efficiencies of the polyplexes were comparable with only 5 of the 12 reducible and analogous non-reducible polyplex sets showing statistically significant differences in transfection efficiency ($P < 0.05$), as marked by an (*) in **Figure 1.5a**. The reducible polymers had higher transfection efficiency for two of the statistically significant sets while the non-reducible polymers had higher transfection efficiency for the other three statistically significant sets. This suggests that polymer reducibility did not greatly affect transfection efficiency.

The cytotoxicity of the polymers was assessed by measuring the total protein content in cell lysates after transfection as compared to untreated cells (**Figure 1.5b**). Larger molecular weight copolymers were more cytotoxic than smaller copolymers as is reported for other systems.[157] Overall, the reducible, DBM-substituted polymers had higher cell viabilities than their non-reducible counterparts in both OptiMEM™ and serum. Seven of the 12 analogous polymer sets showed statistically significant ($P < 0.05$) differences in cytotoxicity, as marked with an (*). The reducible polymers had better viability for six of the statistically significant sets, suggesting that the reducible polyplexes were less cytotoxic than the non-reducible polyplexes. The reducible nature of the DBM-substituted polyplexes allowed the

large size of positive charge to more readily disassemble into smaller, less toxic pieces as reported for other reducible systems.[43,167,169]

1.3.4 *IC_{50} Study*

While the reducible polyplexes were less toxic than the non-reducible polyplexes, there is a lack of direct measurement of polymer toxicity without DNA. An MTS assay with HeLa cells was conducted to determine half maximal inhibitory concentration (IC_{50}) values of polymers alone without DNA (**Table 1.2**).

TABLE 1.2 IC_{50} VALUES FOR THE REDUCIBLE AND NON-REDUCIBLE DMAEMA AND OEGMA COPOLYMERS BASED ON [DMAEMA]

The IC_{50} values were based on DMAEMA monomer concentration to account for differences in molecular weight, amount of DMAEMA incorporation, and because the cytotoxicity of the polymers is heavily based on the cationic charge. The reducible polymers had higher IC_{50} values than their non-reducible counterparts, consistent with the lower toxicity seen with reducible polyplexes in **Figure 1.5b**. Statistically significant ($P < 0.05$) differences are marked with an (*). The IC_{50} decreased with increasing molecular weight which is also consistent with the trend that larger molecular weight polymers are less tolerated by cells.[157]

Cleavage of the reducible high and medium MW polymers results in polymers similar in size to the non-reducible medium and low MW polymers, respectively. Therefore, similar IC_{50} values might be expected for these pairs of polymers; however, the IC_{50} value of the reducible polymer is lower in each case. The higher cytotoxicity from the reducible polymer compared to the lower molecular non-reducible polymer may be due to the kinetics and location of the dithiomaleimide

reduction. The expected location for reduction of DBM-substituted polymers is in the cytoplasm and another 2 hours is needed for complete reduction of thioether bonds once inside the cell cytoplasm.[174] In addition, there is a higher concentration of reduced polymer than the non-reducible polymer since the reduction of each DBM-substituted polymer yields two polymers. Nonetheless, the reducible polymers are less toxic than their non-reducible counterparts. Together with the glutathione reduction study (**Figure 1.3**), these results suggest that the DBM-substituted polymers are better tolerated by mammalian cells compared to their non-reducible counterparts due to fragmentation triggered after cellular internalization.

1.3.5 *Polyplex Uptake by Flow Cytometry*

The reducible, DBM-substituted polymers may be easily modified at the alkyne functional group by using azide-alkyne cycloaddition. Most cationic polymers are functionalized by reaction with their primary amines; however, this can be undesirable in gene transfer applications since amine reactions may interfere with nucleic acid packaging. Therefore, the DBM-alkyne provides a location for site-specific functionalization without affecting polymer charge. As a proof-of-concept, we functionalized the DBM-substituted polymers with azide-modified rhodamine fluorophores and used flow cytometry to monitor cellular uptake of the fluorescently-labeled polyplexes. Fluorophore alone, un-functionalized polyplexes, un-functionalized polyplexes with free fluorophore, and fluorophore-functionalized polyplexes were incubated with cells and polymer uptake was analyzed by flow cytometry (**Figure 1.6**).

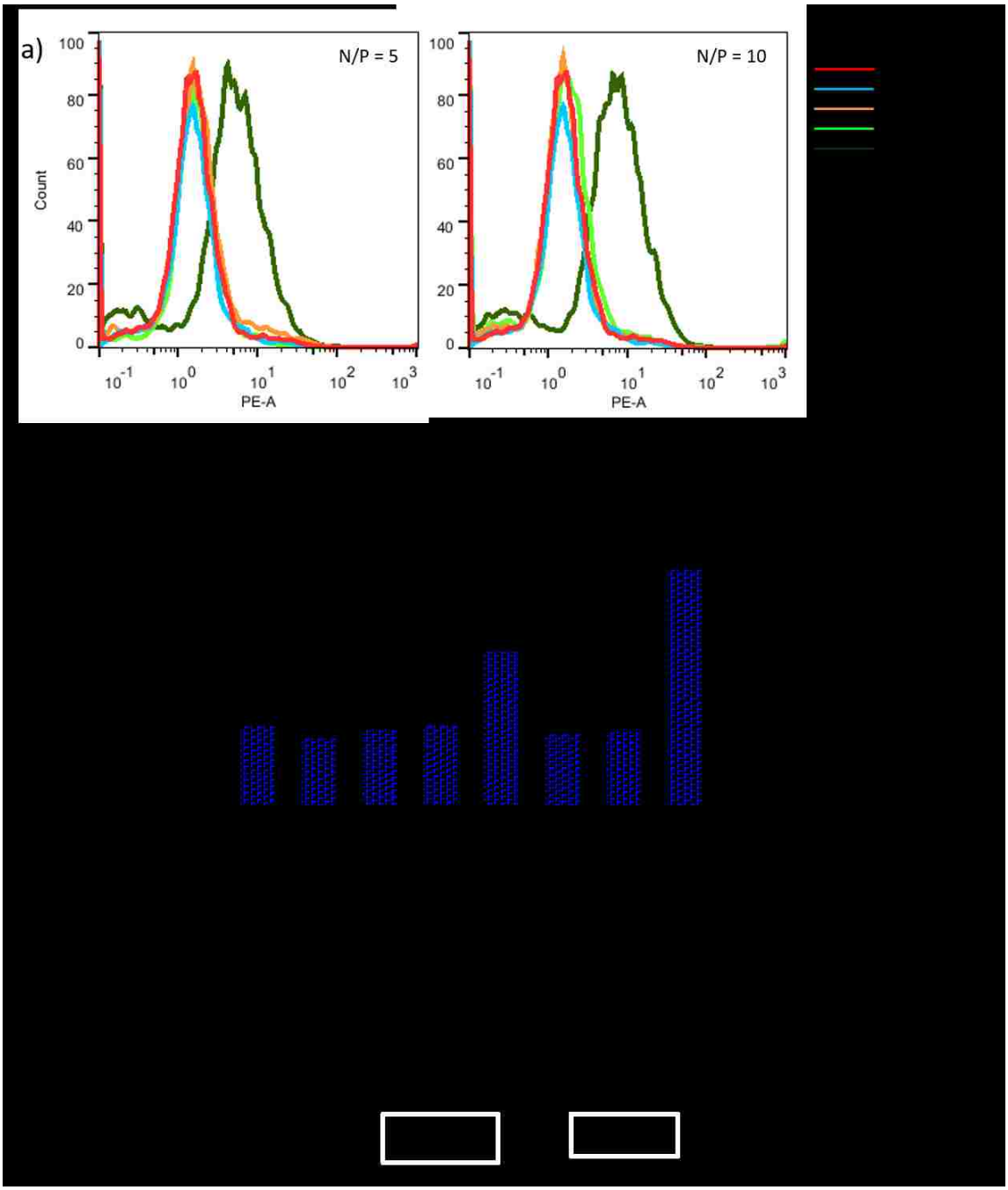

Figure 1.6 (a) Histograms representing the data and **(b)** average fluorescence as assessed by flow cytometry. Uptake of fluorophore, non-functionalized polyplexes, polyplexes plus free fluorophore, and fluorophore-functionalized polyplexes was monitored in HeLa cells. Data is presented as mean + SD, n = 4. Statistically significant ($P < 0.05$) differences are indicated with a (*).

Statistically significant ($P < 0.05$) differences are marked with an (*). Cells treated with fluorophore-labelled polyplexes exhibited the highest levels of mean

fluorescence intensity compared to the fluorophore only, polymer only, and polyplex with free fluorophore groups. Thus, the fluorophore-labelled polymers were able to monitor the uptake of the polyplexes.

In addition to imaging agents, these DBM-linked conjugates can be functionalized with other moieties such as peptides and antibodies. The DBM-alkyne derivative provides a site-specific and quantity-controlled method of conjugation that is less promiscuous than other conjugation methods such as amine chemistry. Another possible application is to use the alkyne handle to immobilize polymers or polyplexes to azide-functionalized surfaces. Polymers or drug carriers can then be easily released from surfaces by a reducing agent such as glutathione.

1.4 CONCLUSION

A panel of reducible and non-reducible DMAEMA and OEGMA copolymers was synthesized by ATRP. The double-headed polymers were reduced and substituted onto a DBM-alkyne derivative. All polymers condensed plasmid DNA and were stable in water and physiological salt concentrations. The reducibility afforded by DBM did not have a significant effect on transfection efficiency; however, it did confer much reduced cytotoxicity since the polymer can dissociate in the reducing environment of the cell cytoplasm. In addition to lowering cytotoxicity, DBM-alkyne provided a site-specific and quantity-controlled place of attachment. A fluorophore was clicked onto the DBM-linked polymers and these polyplexes were able to monitor cell uptake. The site-specific and quantity-controlled functionalization of DBM may allow for more controlled conjugation of biomolecules such as peptides and antibodies.

1.5 ACKNOWLEDGMENTS

This work was supported by NIH 2R01 NS064404. JKYT is supported by an NSF Graduate Research Fellowship (2011128558). We would also like to thank David S. Chu for his expertise and guidance and Binhan Pham for his assistance.

1.6 SUPPORTING INFORMATION

1.6.1 *Synthesis of dibromomaleic anhydride (3,4-dibromofuran-2,5-dione)*

Briefly, maleic anhydride (0.4 g, 4.1 mmol), aluminum (III) chloride (8.2 mg, 0.06 mmol), and bromine (0.42 mL, 8.2 mmol) were added to a pressure tube and heated at 120 °C for 16 hours. The tube was cooled and 20 mL of ethyl acetate was added. The solution was filtered and the solvent was azeotropically removed with chloroform under reduced pressure. The crude solution was re-dissolved in 20 mL of chloroform, washed twice with 20 mL of water, and dried with anhydrous sodium sulfate. The solution was filtered and the solvent was removed to yield a white powder (0.69 g, 64%). The product was analyzed by GC-MS on a Hewlett-Packard (Palo Alto, CA) 5971A GC-MSD.

δ_C (500 MHz; $CDCl_3$): 158.70 (2 C), 131.54 (2 C)

m/z: 258 (19%), 256 (M^+, 37), 254 (19), 214 (13), 212 (26), 210 (13), 186 (9), 184 (18), 182 (9), 133 (98), 131 (100); fragmentation follows bromine pattern

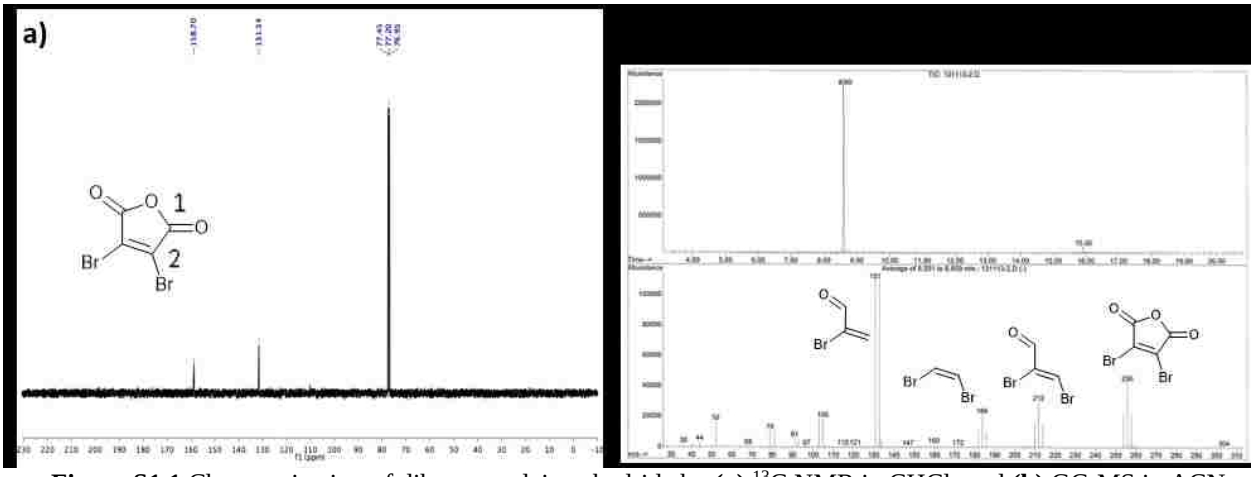

Figure S1.1 Characterization of dibromomaleic anhydride by **(a)** ^{13}C NMR in $CHCl_3$ and **(b)** GC-MS in ACN.

1.6.2 *Synthesis of dibromomaleimide-alkyne (3,4-dibromo-1-(prop-2-ynyl)-1H-pyrrole-2,5-dione)*

m/z: 295 (9%), 293 (M^+, 18), 291 (9), 186 (95), 184 (100), 133 (51), 131 (52); fragmentation follows bromine pattern

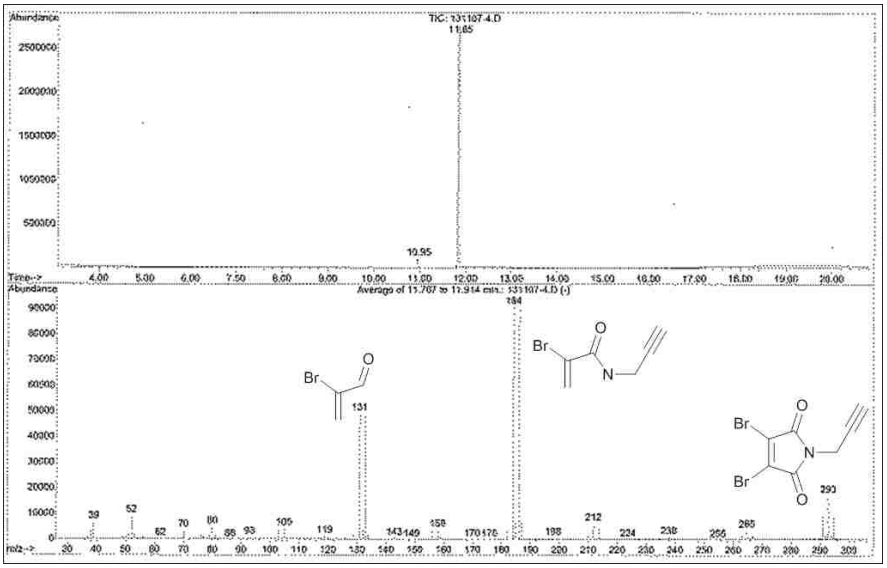

Figure S1.2 Characterization of dibromomaleimide-alkyne by GC-MS in ACN.

1.6.3 *Synthesis of double-headed ATRP initiator*

2-hydroxyethyl disulfide (330 µL, 2.7 mmol), *N*,*N*'-dicyclohexyl carbodiimide (DCC) (2.5 g, 11.9 mmol), and 4-dimethylaminopyridine (DMAP) (0.10 g, 1 mmol) were dissolved in 25 mL of DCM and added dropwise to 2-bromo-2-methylpropionic acid (1.8 g, 10.8 mmol) dissolved in 25 mL of DCM in an ice bath with stirring. After all of the solution was added, the ice bath was removed and the solution was stirred for 30 more minutes. Afterwards, the solution was vacuum filtered and removed under reduced pressure. The crude product was isolated by a silica gel column (1:7 ethyl acetate:hexane) to yield the product as a semi-crystalline gel. ^{1}H NMR of the product was recorded on a Bruker (Billerica, MA) AV-500 MHz instrument.

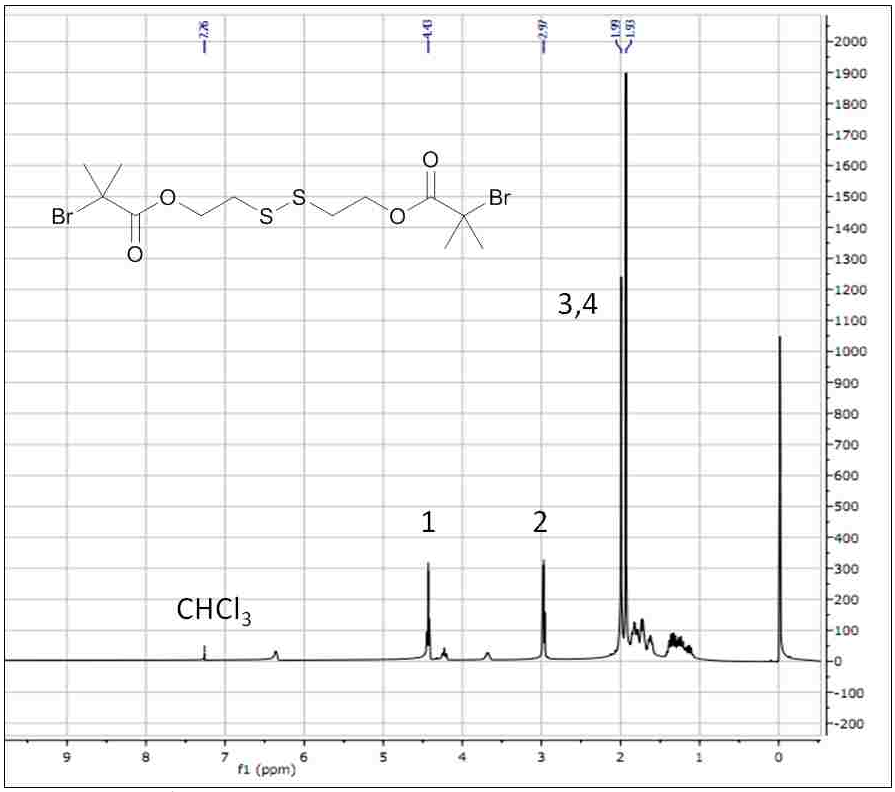

Figure S1.3 ^{1}H NMR characterization of double-headed ATRP initiator in $CDCl_3$.

1.6.4 *ATRP copolymerization of DMAEMA and OEGMA*

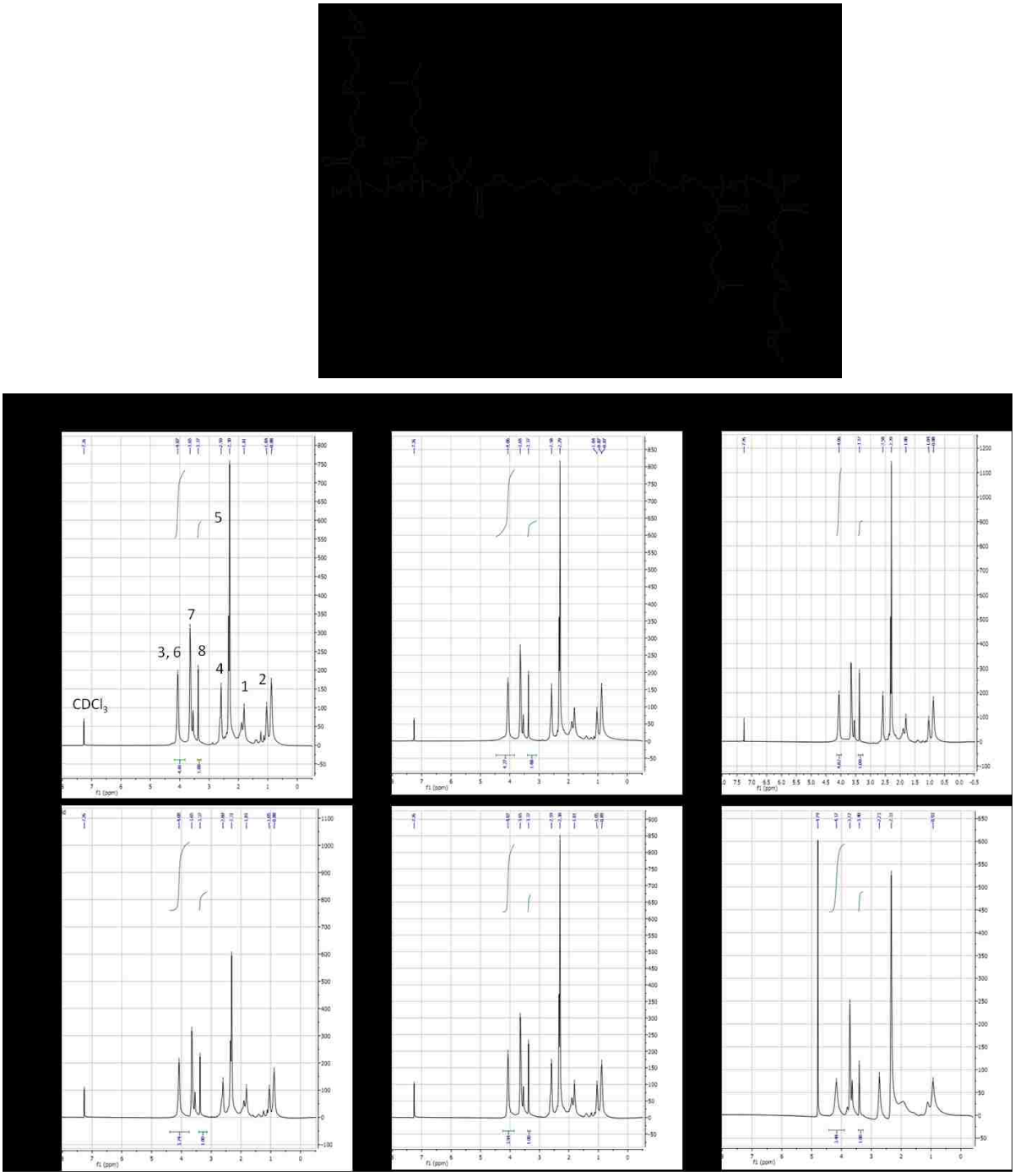

Figure S1.4 ^{1}H NMR characterization of reducible, double-headed and non-reducible DMAEMA and OEGMA copolymers in $CDCl_3$. The ratio of DMAEMA to OEGMA was determined by comparing the ester methylene peaks of DMAEMA and OEGMA (3.9-4.2 ppm, peaks 3 & 6, 2 H's each) to the methoxy peak of OEGMA (3.3-3.4 ppm, peak 8, 3 H's) and the following formula: $\frac{peak\ f}{peak\ b+\ d} = \frac{3x}{2x+2y}$, where "x" is the number of OEGMA units and "y" is the number of DMAEMA units.

1.6.5 *DNA condensation by agarose gel retardation*

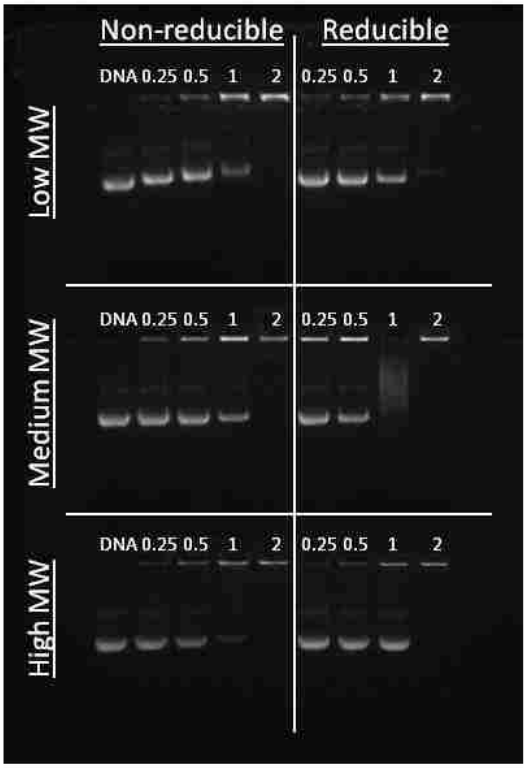

Figure S1.5 Gel retardation assay for all polyplexes formulated at N/P ratios of 0.25, 0.5, 1, and 2 as labeled above. A moving band indicates incomplete complexation while an unmoved band indicated complete complexation with DNA. All polymers are able to fully complex DNA at N/P = 2.

1.6.6 *Zeta potential of polyplexes*

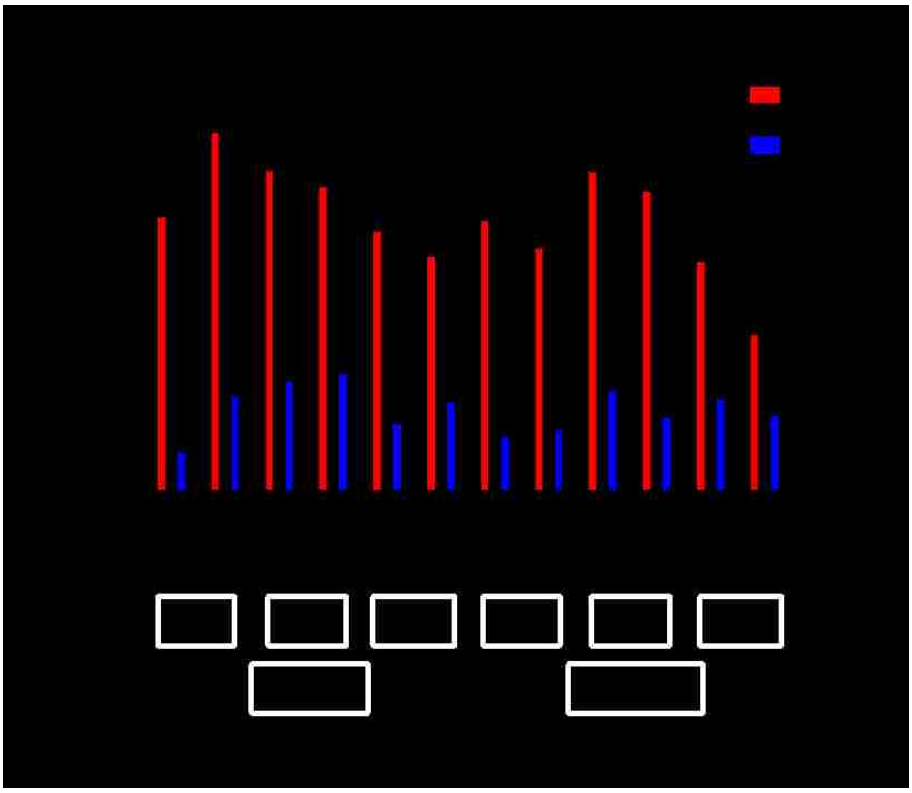

Figure S1.6 Zeta potential of polyplexes in water and 10 mM PBS. Data is presented as mean + SD, n = 3.

1.6.7 *Polyplex unpackaging*

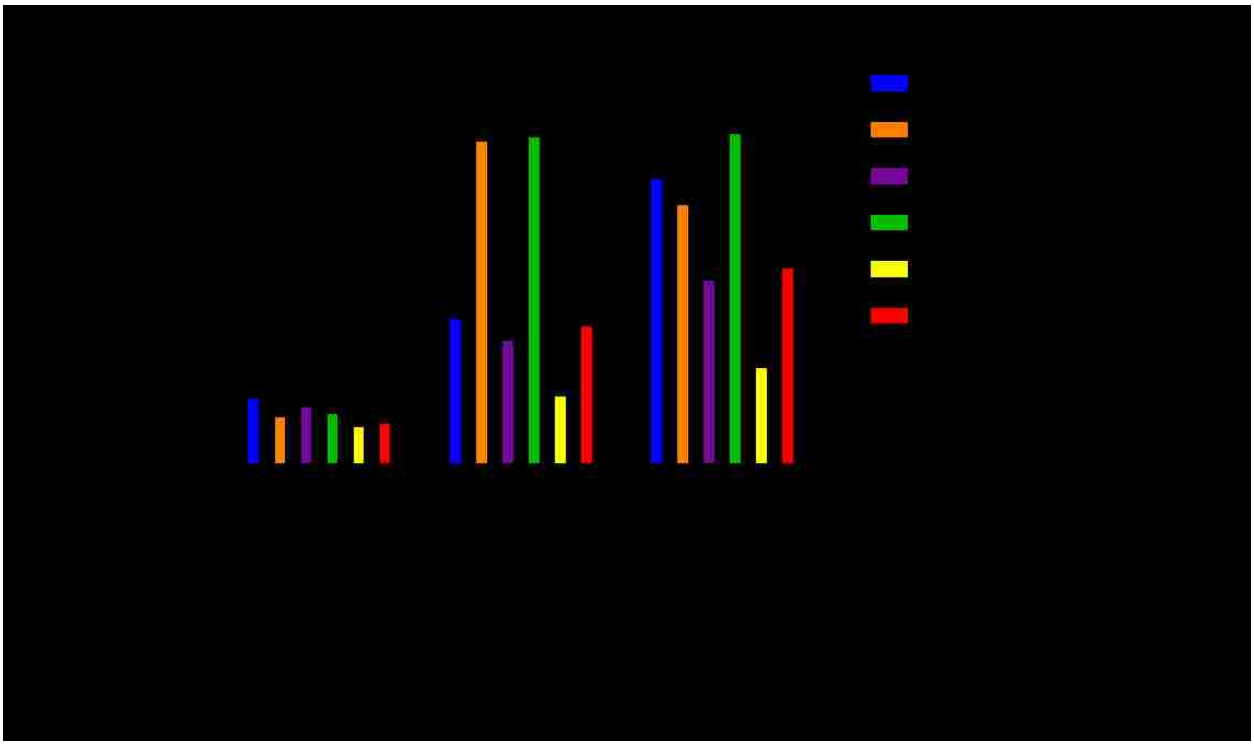

Figure S1.7 Polyplex unpackaging in heparin sulfate and glutathione. Data is presented as mean + SD, n = 3.

1.7 REFERENCES

25. Dodge, J. C. *et al.* AAV4-mediated expression of IGF-1 and VEGF within cellular components of the ventricular system improves survival outcome in familial ALS mice. *Mol. Ther.* **18,** 2075–84 (2010).

39. Pack, D. W., Hoffman, A. S., Pun, S. & Stayton, P. S. Design and development of polymers for gene delivery. *Nat. Rev. Drug Discov.* **4,** 581–93 (2005).

41. Schellinger, J. G. *et al.* Melittin-grafted HPMA-oligolysine based copolymers for gene delivery. *Biomaterials* **34,** 2318–26 (2013).

42. Chu, D. S. H., Schellinger, J. G., Bocek, M. J., Johnson, R. N. & Pun, S. H. Optimization of Tet1 ligand density in HPMA-co-oligolysine copolymers for targeted neuronal gene delivery. *Biomaterials* **34,** 9632–7 (2013).

43. Wei, H., Schellinger, J. G., Chu, D. S. H. & Pun, S. H. Neuron-targeted copolymers with sheddable shielding blocks synthesized using a reducible, RAFT-ATRP double-head agent. *J. Am. Chem. Soc.* **134,** 16554–7 (2012).

45. Al-Dosari, M. S. & Gao, X. Nonviral gene delivery: principle, limitations, and recent progress. *AAPS J.* **11,** 671–81 (2009).

153. Niidome, T. & Huang, L. Gene therapy progress and prospects: nonviral vectors. *Gene Ther.* **9,** 1647–52 (2002).

154. Abdallah, B., Hassan, A. & Benoist, C. A powerful nonviral vector for in vivo gene transfer into the adult mammalian brain: polyethylenimine. *Hum. Gene Ther.* **7,** 1947–1954 (1996).

155. Jäger, M., Schubert, S., Ochrimenko, S., Fischer, D. & Schubert, U. S. Branched and linear poly(ethylene imine)-based conjugates: synthetic modification, characterization, and application. *Chem. Soc. Rev.* **41,** 4755–67 (2012).

156. Lv, H., Zhang, S., Wang, B., Cui, S. & Yan, J. Toxicity of cationic lipids and cationic polymers in gene delivery. *J. Control. Release* **114,** 100–9 (2006).

157. Fischer, D., Li, Y., Ahlemeyer, B., Krieglstein, J. & Kissel, T. In vitro cytotoxicity testing of polycations: influence of polymer structure on cell viability and hemolysis. *Biomaterials* **24,** 1121–31 (2003).

158. Wong, K. *et al.* PEI-g-chitosan, a novel gene delivery system with transfection efficiency comparable to polyethylenimine in vitro and after liver administration in vivo. *Bioconjug. Chem.* **17,** 152–8 (2006).

159. Erbacher, P., Zou, S. & Bettinger, T. Chitosan-based vector/DNA complexes for gene delivery: biophysical characteristics and transfection ability. *Pharm. …* **15,** (1998).

160. Köping-Höggård, M. *et al.* Improved chitosan-mediated gene delivery based on easily dissociated chitosan polyplexes of highly defined chitosan oligomers. *Gene Ther.* **11,** 1441–52 (2004).

161. Wei, H., Pahang, J. a & Pun, S. H. Optimization of brush-like cationic copolymers for nonviral gene delivery. *Biomacromolecules* **14,** 275–84 (2013).

162. Chu, D. S. H., Johnson, R. N. & Pun, S. H. Cathepsin B-sensitive polymers for compartment-specific degradation and nucleic acid release. *J. Control. Release* **157,** 445–54 (2012).

163. Johnson, R. N. *et al.* Synthesis of Statistical Copolymers Containing Multiple Functional Peptides for Nucleic Acid Delivery. *Biomacromolecules* 3007–3013 (2010). doi:10.1021/bm100806h

164. Rungsardthong, U. *et al.* Copolymers of amine methacrylate with poly(ethylene glycol) as vectors for gene therapy. *J. Control. Release* **73,** 359–80 (2001).

165. Uzgün, S. *et al.* Characterization of tailor-made copolymers of oligo(ethylene glycol) methyl ether methacrylate and N,N-dimethylaminoethyl methacrylate as nonviral gene transfer agents: influence of macromolecular structure on gene vector particle properties and transfect. *Biomacromolecules* **11,** 39–50 (2010).

166. Deshpande, M. C. *et al.* The effect of poly(ethylene glycol) molecular architecture on cellular interaction and uptake of DNA complexes. *J. Control. Release* **97,** 143–56 (2004).

167. You, Y.-Z., Manickam, D. S., Zhou, Q.-H. & Oupický, D. Reducible poly(2-dimethylaminoethyl methacrylate): synthesis, cytotoxicity, and gene delivery activity. *J. Control. Release* **122,** 217–25 (2007).

168. Zhang, Y., Zheng, M., Kissel, T. & Agarwal, S. Design and biophysical characterization of bioresponsive degradable poly(dimethylaminoethyl methacrylate) based polymers for in vitro DNA transfection. *Biomacromolecules* **13,** 313–22 (2012).

169. Gosselin, M. a, Guo, W. & Lee, R. J. Efficient gene transfer using reversibly cross-linked low molecular weight polyethylenimine. *Bioconjug. Chem.* **12,** 989–94 (2001).

170. Christensen, L. V *et al.* Reducible poly(amido ethylenimine)s designed for triggered intracellular gene delivery. *Bioconjug. Chem.* **17,** 1233–40 (2006).

171. Burke, R. S. & Pun, S. H. Synthesis and characterization of biodegradable HPMA-oligolysine copolymers for improved gene delivery. *Bioconjug. Chem.* **21,** 140–50 (2010).

172. Peng, Q., Zhong, Z. & Zhuo, R. Disulfide cross-linked polyethylenimines (PEI) prepared via thiolation of low molecular weight PEI as highly efficient gene vectors. *Bioconjug. Chem.* **19,** 499–506 (2008).

173. Smith, M. E. B. *et al.* Protein modification, bioconjugation, and disulfide bridging using

bromomaleimides. *J. Am. Chem. Soc.* **132,** 1960–5 (2010).

174. Moody, P. *et al.* Bromomaleimide-linked bioconjugates are cleavable in mammalian cells. *Chembiochem* **13,** 39–41 (2012).

175. Cui, Y., Yan, Y., Chen, Y. & Wang, Z. Dibromomaleimide Derivative as an Efficient Polymer Coupling Agent for Building Topological Polymers. *Macromol. Chem. Phys.* **214,** 470–477 (2013).

176. Jones, M. W. *et al.* Polymeric dibromomaleimides as extremely efficient disulfide bridging bioconjugation and pegylation agents. *J. Am. Chem. Soc.* **134,** 1847–52 (2012).

177. van de Wetering, P., Cherng, J. Y., Talsma, H., Crommelin, D. J. & Hennink, W. E. 2-(Dimethylamino)ethyl methacrylate based (co)polymers as gene transfer agents. *J. Control. Release* **53,** 145–53 (1998).

178. Robin, M. P. *et al.* Conjugation-induced fluorescent labeling of proteins and polymers using dithiomaleimides. *J. Am. Chem. Soc.* **135,** 2875–8 (2013).

179. Layman, J. M., Ramirez, S. M., Green, M. D. & Long, T. E. Influence of polycation molecular weight on poly(2-dimethylaminoethyl methacrylate)-mediated DNA delivery in vitro. *Biomacromolecules* **10,** 1244–52 (2009).

180. Ryan, C. P. *et al.* Tunable reagents for multi-functional bioconjugation: reversible or permanent chemical modification of proteins and peptides by control of maleimide hydrolysis. *Chem. Commun. (Camb).* **47,** 5452–4 (2011).

181. Verbaan, F. J. *et al.* Steric stabilization of poly(2-(dimethylamino)ethyl methacrylate)-based polyplexes mediates prolonged circulation and tumor targeting in mice. *J. Gene Med.* **6,** 64–75 (2004).

182. Venkataraman, S. *et al.* The role of PEG architecture and molecular weight in the gene transfection performance of PEGylated poly(dimethylaminoethyl methacrylate) based cationic polymers. *Biomaterials* **32,** 2369–78 (2011).

183. Richard, J. P. *et al.* Cell-penetrating peptides. A reevaluation of the mechanism of cellular uptake. *J. Biol. Chem.* **278,** 585–90 (2003).

Chapter 2. Guanidinylated Block Copolymers for Gene Transfer: A Comparison with Amine-Based Materials for *In Vitro* and *In Vivo* Gene Transfer Efficiency

Jennifer L. Choi*, James-Kevin Y. Tan*, Drew L. Sellers, Hua Wei, Philip J. Horner, Suzie H. Pun

*These authors should be regarded as joint first authors.

This work has resulted in a publication: Choi & Tan, *et al*. *Biomaterials*. (2015) **54**:87-96.

Synopsis:

There is currently no cure for neuron loss in the brain, which can occur due to traumatic injury or neurodegenerative disease. One method proposed to enhance neurogenesis in the brain is gene transfer to neural progenitor cells. In this work, a guanidine-based copolymer was synthesized and compared to an amine-based copolymer analog previously shown to effectively deliver genes in the murine brain. The guanidine-based copolymer was more efficient at gene transfer to immortalized, cultured cell lines; however, the amine-based copolymer was more effective at gene transfer in the brain. DNA condensation studies revealed that the nucleic acid complexes formed with the guanidine-based copolymer were more susceptible to unpackaging in the presence of heparan sulfate proteoglycans compared to complexes formed with the amine-based copolymer. Therefore, polyplexes formed from the amine-based copolymer may be more resistant to destabilization by the heparan sulfate proteoglycans present in the stem cell niches of the brain.

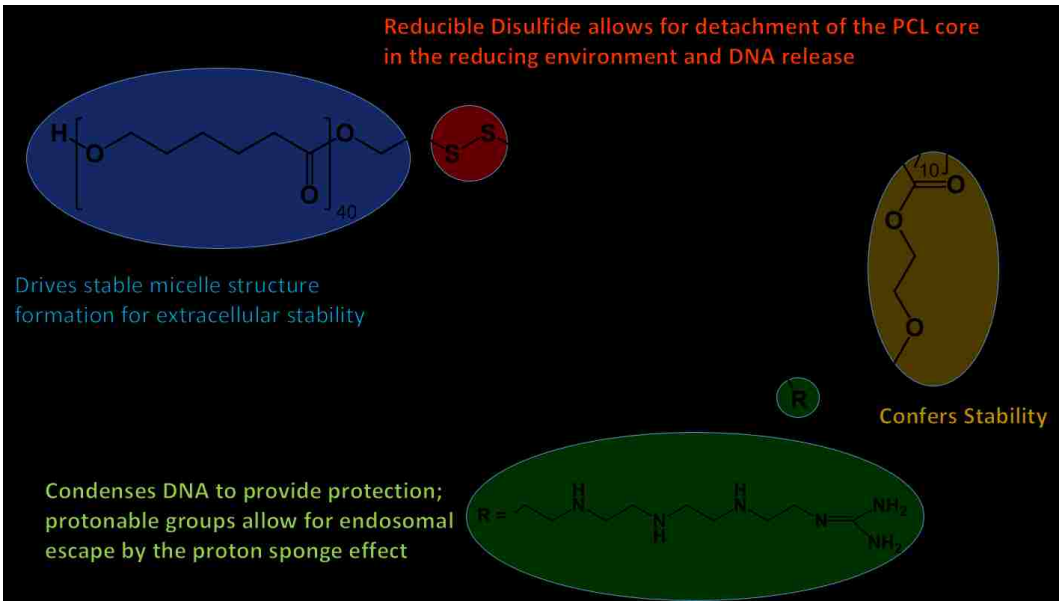

2.1 INTRODUCTION

Neural stem and progenitor cells (NSCs and NPCs) reside in two specialized niches in the adult mammalian brain: the subventricular zone (SVZ) of the lateral ventricles and the hippocampus.[1,184] These cells contribute to neurogenesis and have been shown in rodent models to respond to cortical injury by proliferating.[10,13,14] Progenitors can be diverted to participate in scar tissue formation, however; replacement of diseased neuronal populations is very limited. Despite their capacity to regenerate cells, neurogenic regions cannot fully counteract neuron death in progressive neurodegenerative disease or trauma. Gene transfer has been proposed as a method to both direct and enhance neurogenesis in the brain.[185,186] In order to realize the potential of this approach, effective nucleic acid transfer technologies to the central nervous system are needed. While non-viral vectors such as polymeric materials are preferred over viral vectors for their conceivable safety profiles and lower manufacturing cost, only a minority of clinical trials use this class of delivery modality due to their lower delivery efficiencies compared to viral vectors.[187,188]

Most polymers used for gene transfer are polycations comprised of monomers containing primary, secondary, or tertiary amines.[39] Several groups, however, have demonstrated that guanidinylated polycations outperform their amine-based analogs in transfection to cultured cells.[12,189–191] Guanidiniums are protonated at physiological pH and have electrons that are delocalized, resulting in resonance-stabilized charge spread around the three nitrogen atoms.[192,193] Polyarginines, which are cationic due to multiple guanidine groups, have been shown to bind with higher affinity to double-stranded DNA (dsDNA) than polylysines, which contain multiple primary amine groups.[112,194,195] The stronger DNA binding and the ability to interact with cell surface phosphates and sulfates to facilitate cell internalization are attributed to the efficient gene transfer capability of guanidine-containing polycations.[113]

Previously, our group designed a block-statistical copolymer comprised of a poly(ε-caprolactone) (PCL) block connected by a reducible disulfide to a statistical copolymer of tetraethylenepentamine (TEPA)-decorated poly(glycidyl methacrylate) (pGMA) monomers and oligo(ethylene glycol) monomethyl ether methacrylate (OEGMA) monomers.[47] This copolymer, PCL-SS-p[(GMA-TEPA)-*s*-OEGMA], complexes with nucleic acids to form polyplexes (cationic polymer/DNA particles) with diameters < 200 nm and was specifically designed to overcome many of the barriers to gene delivery. The hydrophilic OEGMA monomers and hydrophobic PCL

monomers provide extracellular stability by reducing salt-induced aggregation and premature unpackaging, respectively. Once internalized into a cell, the protonatable amines in TEPA facilitate endosomal escape via the proton sponge effect and the internal disulfide bond can be reduced by glutathione in the cytosol to detach the PCL core. After the disulfide is reduced, the remaining statistical polycation is less stable and can therefore release its DNA cargo. We further demonstrated that this polymer transfects cultured HeLa cells more efficiently than branched polyethylenimine (PEI, 25k) and mediates effective gene transfer in the brain of mice.[47]

We hypothesized that the transfection efficiency of PCL-SS-p[(GMA-TEPA)-*s*-OEGMA] could be further increased by guanidinylating the primary amines in TEPA. In this study, guanidinylated PCL-SS-p[(GMA-TEPA)-*s*-OEGMA] copolymers were synthesized and tested both *in vitro* and *in vivo* for gene transfer ability. The results of this study highlight discordance between *in vitro* and *in vivo* efficiency and illustrate the importance of *in vivo* evaluation of new polymeric gene transfer materials.

2.2 Materials and Methods

2.2.1 *Materials*

Reagents for polymer synthesis were purchased from Sigma-Aldrich (St. Louis, MO) unless otherwise noted. ε-Caprolactone (CL) was dried over CaH_2 and distilled under reduced pressure prior to use. Glycidyl methacrylate was purified by vacuum distillation before use. Oligo(ethylene glycol) monomethyl ether methacrylate (OEGMA, M_n= 300 g/mol and pendent EO units DP ~4.5) was purified by passing through a column filled with basic alumina to remove the inhibitor. Copper (I) chloride (CuCl) was washed with acetic acid and ethanol in turn to remove Cu^{2+}. All cell culture reagents were purchased from Cellgro/Mediatech (Fisher Scientific, Pittsburgh PA). Endotoxin-free plasmid pCMV-Luc2 (Photinuspyralis luciferase under control of the cytomegalovirus (CMV) enhancer/promoter) was produced with the Qiagen Plasmid GigaPrep kit (Qiagen, Hilden, Germany) according to the manufacturer's recommendations. The pmaxGFP® plasmid (green fluorescent protein from the copepod *Pontellina p.*) was purchased from Lonza. The bicinchoninic acid (BCA) protein quantification assay kit was purchased from

Thermo Fischer Scientific (Waltham, MA) while the luciferase expression quantification kit was obtained from Promega (Madison, WI).

2.2.2 *Cell lines*

HeLa cells, human cervical carcinoma cells (ATCC® CCL-2™), were maintained in minimum essential medium (MEM) supplemented with 10% fetal bovine serum (FBS) and antibiotics/antimyotics (AbAm) (100 IU of penicillin, 100 ug/mL of streptomycin, and 0.25 ug/mL of amphotericin B). Z310 cells were donated by Prof. Wei Zheng (Purdue) and cultured in Dulbecco's minimum essential medium (DMEM) supplemented with 10% heat-inactivated FBS, 10% penicillin/streptomycin, 40 μg/mL gentamicin, and 10 ng/mL nerve growth factor (NGF). Primary neural progenitor cells (NPCs) were maintained in DMEM/F12 supplemented with 2 mM L-glutamine, 1% N-2 supplement, 5 μg/mL heparin, and 20 ng/mL of both endothelial growth factor and NGF.

2.2.3 *Polymer synthesis*

2.2.3.1 Synthesis of PCL-SS-p[(GMA-TEPA)-st-OEGMA

The reducible 2-hydroxyethyl-2'-(bromoisobutyryl)ethyl disulfide double-head initiator (HO-SS-iBuBr) was prepared according to literature.[47] PCL-SS-p[(GMA-TEPA)-*s*-OEGMA] (denoted as "Base copolymer") was synthesized as reported previously.[47] Briefly, ring opening polymerization (ROP) of CL was performed using HO-SS-iBuBr as the initiator and $Sn(Oct)_2$ as the catalyst. Then, a one-pot atom transfer radical polymerization (ATRP) of GMA and OEGMA was performed using PCL_{40}-SS-iBuBr as the macroinitiator and CuCl/bpy as the catalyst. The copolymer composition was determined by ^{1}H NMR. Integration of the NMR resonances assigned to the PCL block at 2.35 ppm (characteristic to the first carbon next to the carbonyl carbon), GMA block at 4.32 ppm (characteristic of the ethylene adjacent to the epoxy group), and OEGMA block at 3.40 ppm (characteristic of the methyl group) were compared. The GMA monomers in the polymer were then reacted with excess TEPA. Complete conversion was confirmed by monitoring the disappearance of the epoxy group peaks (3.26 ppm,

2.87 pp.m, 2.66 p.m.) and appearance of TEPA amine groups (2.5 – 3.0 pp.m.) in ^{1}H NMR.

2.2.3.2 Synthesis of guanidinylated copolymer

The guanidinylated copolymer, denoted as "Guan copolymer", was synthesized by reacting Base copolymer with a 10-fold molar excess of *o*-methylisourea to primary amines in GMA-TEPA unit. Base copolymer was dissolved at 10 mg/mL in 1:1 (v/v) saturated $NaCO_3$ and ddH_2O and mixed with *o*-methylisourea dissolved in an equivalent amount of 1:1 (v/v) saturated $NaCO_3$ and ddH_2O in a round bottom flask with a stir bar and sealed with a septum. The solution was stirred at room temperature for 72 hours. After the reaction, the polymer was purified by dialysis (MW cutoff: 10,000 g/mol) against 4 L of distilled water, which was renewed 3 times per day over the course of 3 days, followed by lyophilization to yield a fluffy, white product. Polymer guanidinylation was confirmed spectroscopically by disappearance of primary amines (quantified by ninhydrin assay) and by appearance of guanidines assessed using a ligand-exchange assay developed by Weber.[196] For the ninhydrin assay, the Base copolymer was used to make a standard curve. To quantify the number of primary amines, the absorbance (420 nm) of polymer reacted with ninhydrin was read on a Tecan Infinite M1000 PRO microplate reader. To confirm guanidinylation, 0.2g of potassium hexacyanoferrate and 0.2g of sodium nitroferricyanide(III) dihydrate were dissolved in 4 mL of 1M NaOH and then mixed with 3 mL of aqueous Guan copolymer at 3 mg/mL. After 1.5 minutes, the absorbance at 498 nm was measured. *L*-arginine, which contains a guanidine group, was used as the standard and Base copolymer, while *o*-methylisourea, and aqueous sodium carbonate were used as the negative controls.

2.2.4 *Polyplex preparation and characterization*

2.2.4.1 Polyplex formulation

Stock solutions of copolymers were prepared at 5 mg/mL in ddH_2O and then acidified to pH = 6.4 using 1N HCl. The pCMV-Luc2 plasmid was diluted in

ddH_2O to a concentration of 0.1 mg/mL. Copolymer-DNA complexes (termed polyplexes) were formed by adding copolymer diluted in ddH_2O to an equal volume of diluted pCMV-Luc2 plasmid at the desired charge ratio (N/P), followed by incubation at room temperature for 10 minutes.

2.2.4.2 Gel retardation testing

Copolymer complexation of plasmid was assessed by a gel retardation or electrophoretic mobility shift assay. Polyplexes (1 μg of pCMV-Luc2, 20 μL solution) were formed at various N/P ratios with 10% (v/v) of 10X BlueJuice™ Gel Loading Buffer and loaded into a 1% agarose gel made with TAE buffer (40 mMTris-acetate, 1 mMEDTA) and 5 mg/mL ethidium bromide. The gel was electrophoresed at 100 V for 50 minutes. The gel was then imaged on a Kodak (Rochester, NY) UV transilluminator (laser-excited fluorescence gel scanner).

2.2.4.3 Size and surface charge analysis

The average hydrodynamic diameter and surface charge of polyplexes were determined using dynamic light scattering (DLS, Brookhaven Instruments Corp ZetaPALS) and zeta potential analysis (Malvern Zetasizer). Polyplexes (N/P = 15, 1 μg of pCMV-Luc2, 20 μL solution) were diluted with 80 μL of ddH_2O or 150 mM PBS (phosphate-buffered saline, pH 7.2). DLS was analyzed at room temperature using a wavelength of 659 nm and a detection angle of 90°. Measurements were taken over five 30-second intervals.

2.2.4.4 Polyplex unpackaging by heparin/heparan sulfate competition

The pCMV-Luc2 plasmid was mixed with the bis-intercalating dye YOYO-1 iodide (Invitrogen, Carlsbad, CA) at a dye to base pair ratio of 1:100 and incubated at room temperature for 1 hour. Polyplexes were prepared at an N/P = 15 by complexing YOYO-labeled plasmid with Base and Guan copolymers as previously mentioned. Polyplexes were treated with stated concentrations of heparin or heparan sulfate for 1 hour. The fluorescence (ex: 491 nm, ex: 509 nm) of each well was normalized to a DNA only control. To test polyplex unpackaging

by gel retardation, heparin (10 μg/mL) was added to polyplexes for 10 minutes and the gel was electrophoresed as previously mentioned.

2.2.5 In vitro *transfection and cytotoxicity analysis*

2.2.5.1 Evaluation in HeLa and Z310 immortalized cells

HeLa cells and Z310 cells were seeded in complete cell culture medium at a density of 30,000 cells/well in a 24-well plate. Cells were allowed to attach for 16 hours at 37 °C, 5% CO_2. Polyplexes were formed at different N/P ratios using 1 μg of pCMV-Luc2 in 20 μL total volume diluted in 180 μL of OptiMEM medium per well. The cells were washed once with PBS and then the polyplexes diluted in OptiMEM were added. The plates were incubated at 37 °C, 5% CO_2 for 4 hours. After 4 hours, the polyplex solutions were aspirated, the cells were washed with PBS, and complete media was added to each well. After an additional 44 hours at 37 °C, 5% CO_2, the wells were washed with PBS and 1X Reporter Lysis Buffer was added to each well. The plates were incubated at room temperature for 15 minutes, freeze-thawed, and then samples centrifuged at 15,000 *g* for 15 minutes at 4 °C to pellet the cell debris. The lysates were analyzed using a luciferase assay kit (Promega Corp.) according to the manufacturer's instructions. Luminescence intensity was measured on a Tecan Infinite M1000 PRO microplate reader with integration for 1 second. The total protein content in each well was measured by a BCA Protein Assay Kit (Thermo Scientific, Rockford, IL) to assess cell viability and to normalize luciferase expression. Each copolymer at each N/P ratio was tested with a sample size of (n) = 4 for both cell lines.

2.2.5.2 Transfection of primary NPCs

NPCs were plated at a density of 26,300 cells/cm^2 in growth media 24 hours prior to transfection. Polyplexes were prepared at an N/P ratio = 15 prior to dilution in NPC growth media with reduced heparin (1 μg/mL). After 4 hours of incubation with polyplexes at 37˚C, NPCs were rinsed with DMEM/F12 before an exchange to fresh growth media. After an additional 44 hours, cells were incubated with

reporter lysis buffer (Promega Corporation) for 15 minutes before storage at -80˚C until analysis. Luciferase activity in cell lysates was measured as described for Z310 and HeLa cell lysates.

2.2.5.3 Flow cytometry analysis of GFP plasmid transfection

HeLa cells were transfected with polyplexes formed with Base or Guan copolymers and pmaxGFP™ (Lonza) as previously mentioned. For analysis, cells were washed with PBS, trypsinized, and pelleted at 500 g for 5 min at 4°C. The pellet was resuspended in 0.3 mL propidium iodide (PI) solution (1 μg/mL in PBS), kept on ice, and analyzed using flow cytometry, MACSQuant Analyzer (Miltenyi Biotec Inc., Auburn, CA). Intact cells were identified using the forward and side scatter data. The resulting cell population was gated into GFP^+/PI^+, GFP^+/PI^-, GFP^-/PI^+ and GFP^-/PI^- based on the green fluorescence and PI intensity from the control samples and with proper compensation.

2.2.6 In vivo *polyplex delivery to murine brain*

2.2.6.1 Intraventricular injections

All animal procedures were completed using protocols approved by the Institutional Animal Care and Use Committee at the University of Washington. Polyplexes were prepared as described above in 5% glucose using 2.5 μg of DNA in 10 μL total volume at an N/P of 15. Adult female C57BL/6J mice (Jackson Laboratories) were anesthetized by an intraperitoneal injection of Avertin. A 1 mm diameter craniotomy was made on the right side of the skull using a dental drill and 10 μL of polyplex solution or DNA only (n = 5 or 6 per group) was stereotaxically injected at 1 mm lateral, 0.5 mm caudal to bregma, and 1.9 mm depth from the dura using a 33 gauge 10 μL Hamilton syringe. The injection was made over 2.5 minutes and the syringe was kept in place for 2 minutes after injection to prevent backflow.

2.2.6.2 Luciferase expression analysis

Brains were harvested from mice 48 hours post injection and separated into three sections: hindbrain, left hemisphere, and right hemisphere. Tissues were collected in 1X Reporter Lysis Buffer (Promega, Madison, WI) with 1X EDTA-free Roche's Complete Protease Inhibitor Cocktail (Roche, Nutley, NJ) and three freeze-thaw cycles were performed in liquid nitrogen. Tissues were mechanically homogenized and cell debris were pelleted at 15,000 *g* for 15 minute at 4 °C. The lysates were collected and 20 μL of each lysate was analyzed using a luciferase assay kit (Promega Corporation) according to the manufacturer's instructions. Luminescence intensity was measured on a Tecan Infinite M1000 PRO microplate reader with integration for 1 second. The total protein content in each well was measured by a BCA Protein Assay Kit (Thermo Scientific, Rockford, IL) to normalize luciferase expression by protein content.

2.2.6.3 Immunohistochemistry and confocal microscopy

Injections were done as described above using polyplexes formulated with pmaxGFP™ (Lonza). Two days post-injection, mice were euthanized with Avertin overdose and perfused intracardially with 0.9% saline followed by 4% paraformaldehyde in 0.1 M phosphate buffer. After perfusion and fixation, the brains were excised and equilibrated to 30% sucrose in phosphate buffer. Brains were embedded in OCT and sectioned into 40 um-thick coronal slices. For immunofluorescent labeling, slides were rinsed with PBS and blocked in PBS, 0.3% TritonX-100, 2% BSA for 1 hour. Primary antibodies (goat anti-Sox2, Santa Cruz Biotechnology; 1:250) were applied to the tissue sections in PBS, 0.3% TritonX-100, 2% BSA overnight at 4 °C. Sections were rinsed three times for 20 minutes in TBS, 0.1% Tween-20 and species appropriate secondary antibodies conjugated with fluorophore were incubated in PBS, 0.1% Tween-20, 2% donkey serum for 2 hours. Sections were, again, rinsed three times for 20 minutes in TBS-Tween, with the last rinse containing the nuclear marker, 4',6-diamidino-2-phenylindole (DAPI; 1:1000). Sections were then mounted onto glass slides, sealed and coverslipped with gelvatol, and imaged using a confocal microscope.

2.2.6.4 Stereology

To quantify the population of GFP-transfected cells, cells populations surrounding the ventricles was calculated via fractionator stereology (an unbiased sampling method) by Stereo Investigator (Microbrightfield, Inc.). A grid size of 150 x 150 µm and counting frame of 50 x 50 µm was used to assure unbiased sampling of a randomized grid in a 1 in 6 series of tissue sections to generate averaged populations for each animal. Measurements were limited to the SVZ by creating electronic templates of a 100 µm margin around the ventricle borders.

2.3 RESULTS

2.3.1 *Polymer synthesis and characterization*

The PCL-SS-p[GMA-*s*-OEGMA] copolymer was synthesized using a combination of ring opening polymerization and atom transfer radical polymerization (ATRP) as we previously described.[47] Polymer composition was determined by ^{1}H NMR spectroscopy to be PCL_{40}-SS-p[GMA_{60}-*s*-$OEGMA_{10}$]. The GMA monomers were then reacted with excess TEPA; ^{1}H NMR revealed complete disappearance of the GMA epoxy group resonances at 3.26 ppm, 2.87 ppm, and 2.66 ppm, and appearance of a broad peak characteristic of the amines in TEPA at 2.5-3.0 ppm, demonstrating complete reaction of GMA monomers. The molecular weight (MW) of the resulting polymer, PCL-SS-p[(GMA-TEPA)-*s*-OEGMA], called "Base copolymer", was calculated to be 27.0 kDa. The Base copolymer was guanidinylated by reaction with 10-fold excess of *o*-methylisourea to TEPA as described previously,[189,197] resulting in the polymer called "Guan copolymer" with MW ~ 29.0 kDa (**Figure 2.1**).

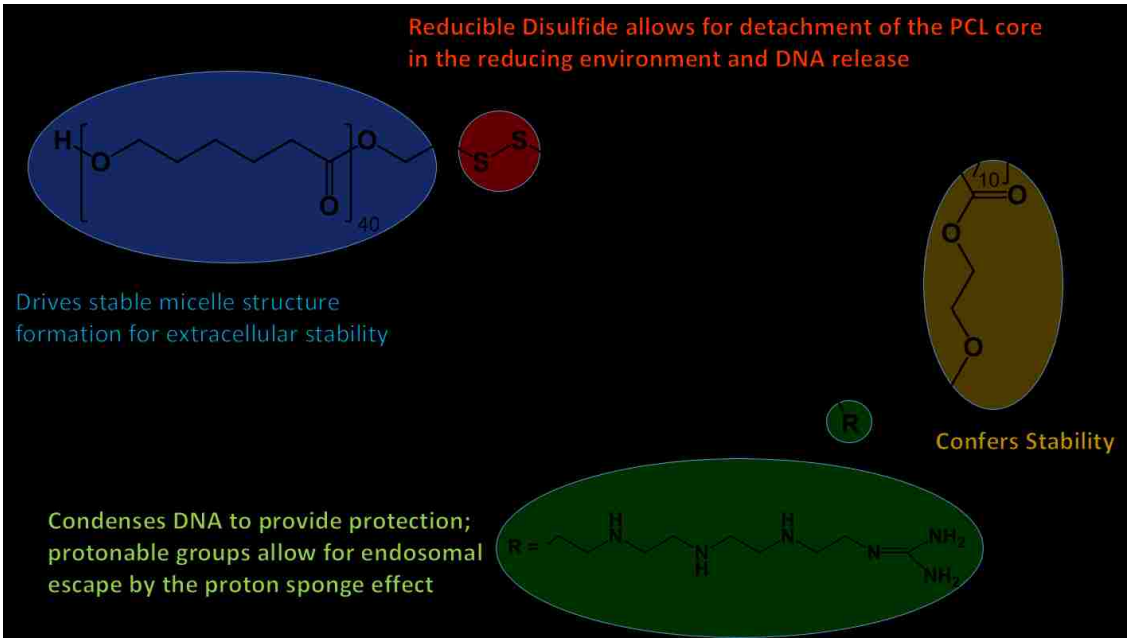

Figure 2.1 Guanidinylated copolymer. The block copolymer contains a polycaprolactone block (PCL, in blue), an internal disulfide bond (red), and a hydrophilic second block of pendant guanidines (green) for DNA binding and oligoethylene glycols (OEG, yellow) for stability.

Guanidinylation of 90% of the TEPA primary amines was confirmed by ninhydrin assay and conversion of primary amines to guanidine was further confirmed by a ligand-exchange guanidine assay developed by Weber.[196]

2.3.2 *Polyplex formulation*

Polyplexes were formed by adding polymer solutions to plasmid DNA at desired charge ratios. Gel electrophoresis showed that the Base copolymer and Guan copolymer complexed plasmid DNA at similar charge ratios (~N/P = 3, **Figure S2.1**). The surface charge and average hydrodynamic diameter of polyplexes formed with both polymers at an N/P (defined as molar TEPA to molar phosphate) ratio of 15 were determined by zeta potential and dynamic light scattering measurements, respectively (**Table 2.1**).

TABLE 2.1 PHYSIOCHEMICAL PROPERTIES OF BASE AND GUAN POLYPLEXES (N/P = 15)

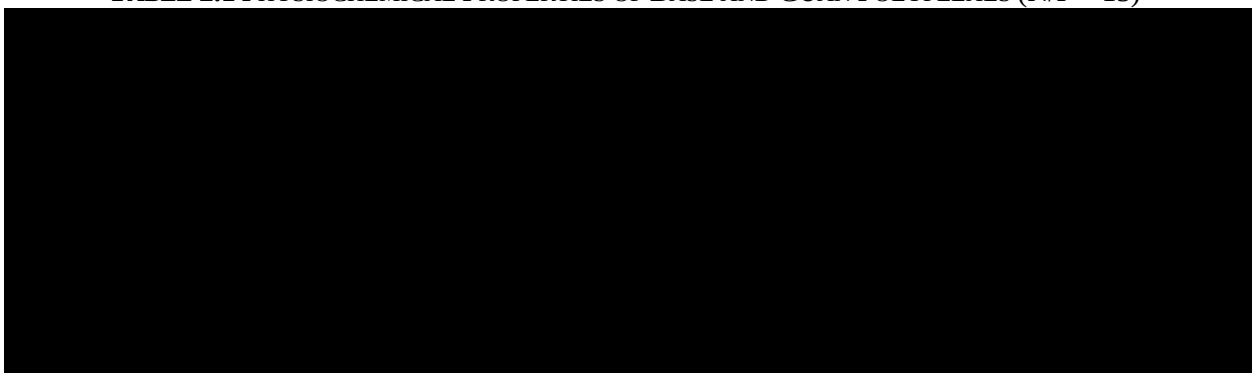

This charge ratio was selected because it was shown previously to be optimal for the Base copolymer.[47] The zeta potential of polyplexes formed with both Base and Guan copolymer were both positive (+23.5 – 41.6 mV) and their average sizes in water were comparable (160 nm). Particle size increased slightly in physiological salt concentrations (150 mM phosphate-buffered saline) to 226.4 ± 1.0 nm and 195.1 ± 4.4 nm for Base and Guan copolymer polyplexes, respectively.

2.3.3 *Transfection and cytotoxicity to cultured cells*

The luciferase plasmid was used as a reporter to track gene transfer efficiency with luciferase enzyme activity analyzed by light output. Polyplexes were prepared at N/P ratios of 10, 15, and 20 based on previous studies that showed N/P = 15 as an optimal formulation for the Base copolymer.[47] First, transfection efficiency and cytotoxicity to HeLa cervical carcinoma cells were evaluated as the immortalized cell line is a commonly used standard for evaluation of transfection. The Guan copolymer transfected HeLa cells more efficiently (8- to 32-fold increased luciferase activity) than Base copolymer at all three charge ratios tested (**Figure 2.2A**). Transfection increased with increasing charge ratio at the cost of cell survival. Trends of reduced cell viability (decreased by ~5-10%) were observed for the Guan copolymer compared to Base copolymer, but were not statistically significant (**Figure 2.2B**).

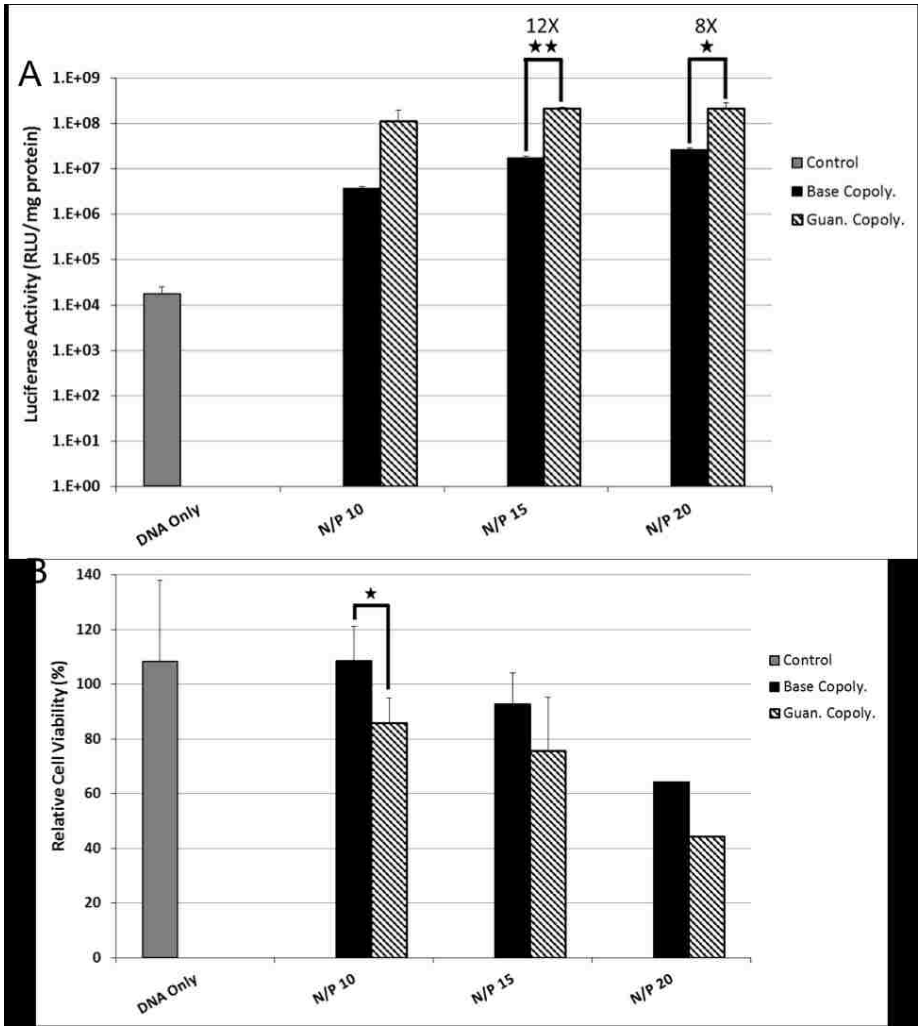

Figure 2.2 (A) Transfection efficiency of Base and Guan copolymer polyplexes at various N/P ratios in HeLa cells normalized to protein content. **(B)** Cytotoxicity of Base and Guan copolymer polyplexes at various N/P ratios to HeLa cells as determined by protein content. Data is presented as mean + SD. Statistically significant ($P < 0.02$) differences are indicated with a (★) and ($P < 0.002$) with (★★).

The luciferase reporter gene provides rapid information about total protein production from transgene delivery to a population of cells. To evaluate the percentage of transfected cells achieved using the Base versus Guan copolymer, the GFP plasmid was delivered using these polyplexes analysis by flow cytometry. Cells treated with polyplexes formed from the Guan copolymer had a higher percent GFP expression (GFP^+/PI^-) (3- to 5-fold increase) than cells treated with polyplexes from the Base copolymer at all charge ratios (**Figure 2.3A**). The Guan copolymer was more toxic to cells at high N/P ratios (**Figure 2.3B**).

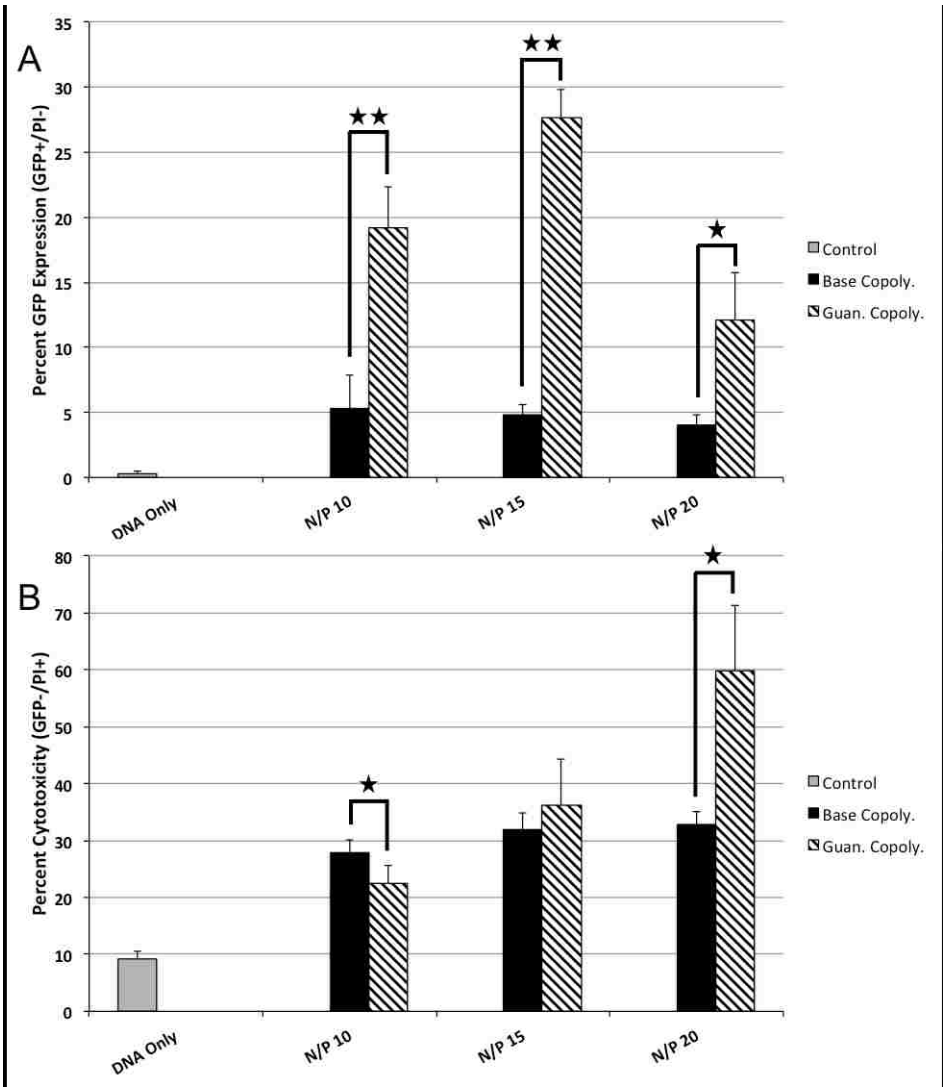

Figure 2.3 (A) Flow cytometry quantification of GFP plasmid transfection by Base and Guan copolymer polyplexes at various N/P ratios to HeLa cells. **(B)** Cytotoxicity of Base and Guan copolymer polyplexes at various N/P ratios in HeLa cells determined by PI+/– staining. Data is presented as mean + SD. Statistically significant ($P < 0.04$) differences are indicated with a (★) and ($P < 0.001$) with (★★).

For intraventricular gene delivery to the brain, polyplexes first encounter the ependymal cells of the choroid plexus layer before reaching the NSCs and NPCs in the SVZ. Therefore, transfection efficiency of the polyplexes to both an immortalized rodent choroid plexus cell line, Z310, and to primary murine neural progenitor cells (NPCs) was next determined. As observed with HeLa cells, the Guan copolymer transfected Z310 cells more efficiently than the Base copolymer at both

N/P = 10 and N/P = 15 (17-fold and 4-fold increase luciferase activity, respectively) (**Figure 2.4A**). No significant difference in luciferase activity was observed at N/P = 20, likely due to the increased toxicity from the Guan copolymer at this high charge ratio (**Figure 2.4B**).

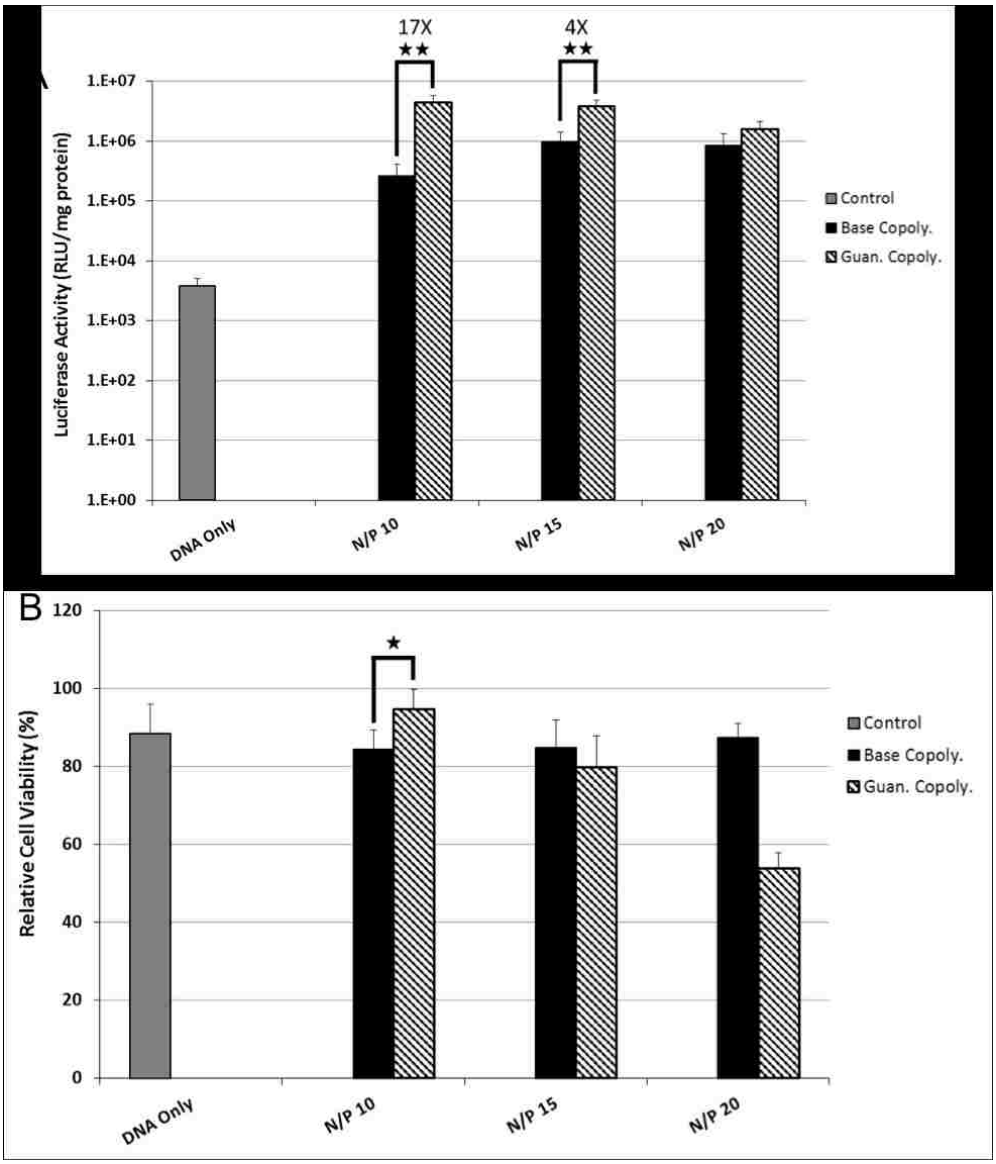

Figure 2.4 (A) Transfection efficiency of Base and Guan copolymer polyplexes at various N/P ratios in immortalized Z310 choroid plexus cells normalized to protein content. **(B)** Cytotoxicity of Base and Guan copolymer polyplexes at various N/P ratios to HeLa cells as determined by protein content. Data presented shown as mean + SD. Statistically significant ($P < 0.05$) differences are indicated with a (★) and ($P < 0.01$) with (★★).

Based on this data, polyplexes at N/P = 15 were tested for transfection to primary NPCs in growth media at 37˚C for 4 hours. In contrast to the results from the two epithelial cell lines, no increase in transfection efficiency was observed in NPCs by using Guan copolymer compared to Base copolymer (**Figure 2.5**). In addition, polyplexes formed using the Guan copolymer were more toxic to NPCs than polyplexes formed using Base copolymer.

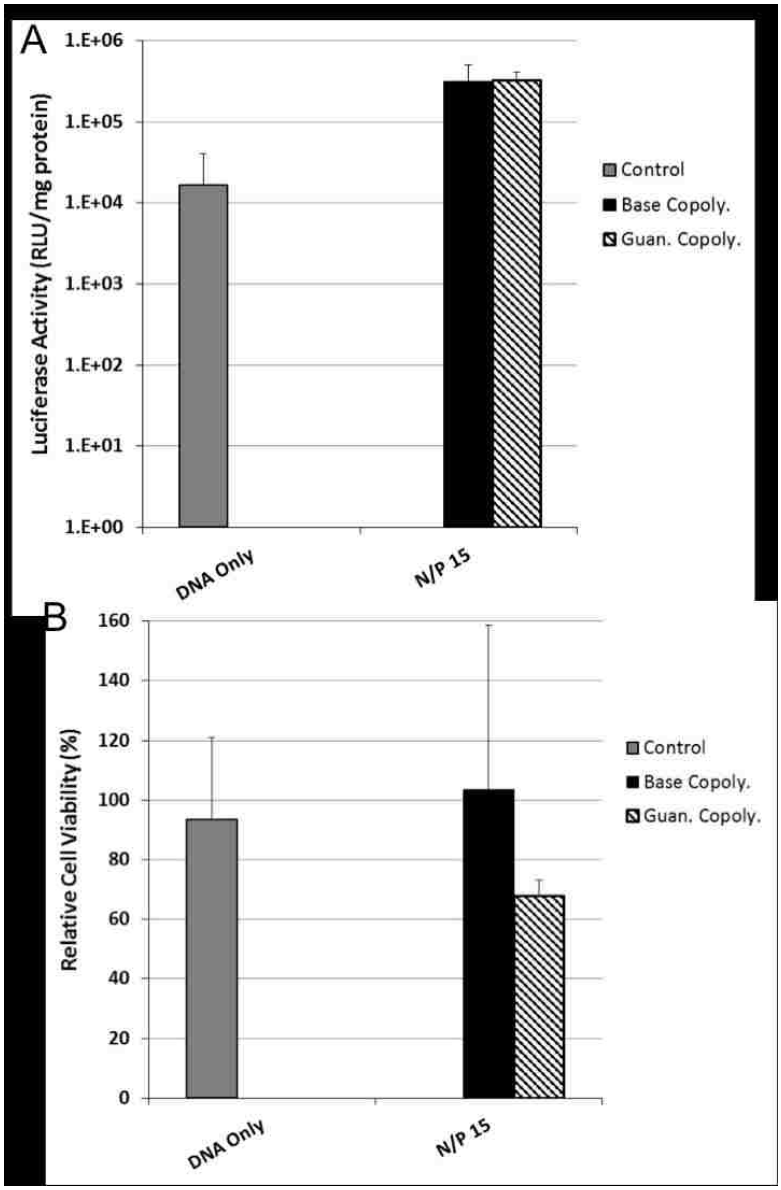

Figure 2.5 (A) Transfection efficiency of Base and Guan copolymer polyplexes at N/P = 15 in primary murine neural progenitor cells. **(B)** Cytotoxicity of Base and Guan copolymer polyplexes at N/P = 15 to primary murine neural progenitor cells as determined by protein content. Data presented shown as mean + SD.

2.3.4 *In vivo delivery via intraventricular injection to murine brain*

The N/P = 15 polyplexes were next tested for their ability to transfect cells in the murine SVZ. Polyplexes containing the luciferase plasmid were injected into the right lateral ventricle. Two days post injection, brain tissue was collected and separated into left hemisphere, right hemisphere, and hindbrain and then analyzed for luciferase expression. As observed previously, polyplexes formed with the Base copolymer transfected cells *in vivo*, resulting in luciferase activity ~10^4 relative light units (RLU)/mg protein in all three brain areas (**Figure 2.6**).

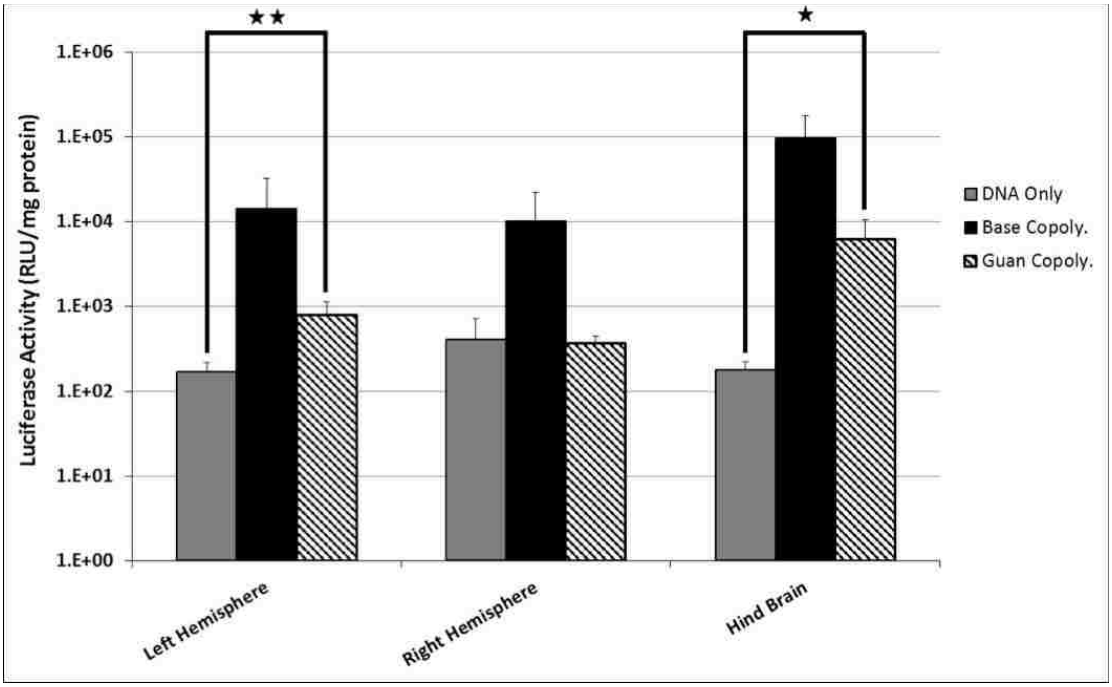

Figure 2.6 Luciferase expression in murine brain sections at 48 hrs post-intraventricular injection of polyplexes at N/P = 15. Data is presented as mean + SD, n = 6. Statistically significant ($P < 0.02$) differences are indicated with a (★) and ($P < 0.01$) with (★★).

Surprisingly, Guan copolymer polyplexes transfected cells less efficiently *in vivo* compared to Base copolymer polyplexes; luciferase activity was reduced by at least one order of magnitude in all sections of the brain. Statistically significant levels of

reporter gene expression over DNA delivery alone were measured in the left hemisphere and hindbrains.

To further confirm these results, Base copolymer and Guan copolymer polyplexes (N/P = 15) containing the EGFP gene were prepared and administered by intraventricular injection as described above. The distribution of transfected cells in the brain two days after injection was determined by confocal imaging of coronal brain tissue sections stained with the neural stem cell marker, Sox2 and a nuclear stain, DAPI (**Figure 2.7**). As seen with luciferase expression, transfected, GFP^+-expressing cells were reduced in number throughout the brain of Guan copolymer polyplex-treated mice. Brains injected with Base copolymer showed an abundance of the target cell population (GFP^+ (green), $Sox2^+$-cells (red)) within the injected ventricle (yellow arrows, **Figure 2.7A & Figure 2.7B**) and within the contra lateral hemisphere (yellow arrows, **Figure 2.7C**). Conversely, few $Sox2^+$-cells expressed GFP in brains injected with the Guan copolymer (**Figure 2.7D-F**). Importantly, Guan polymer treated brains had GFP expression primarily limited to the choroid and ependymal cells of the ventricle surface (Cyan arrow, **Figure 2.7E**).

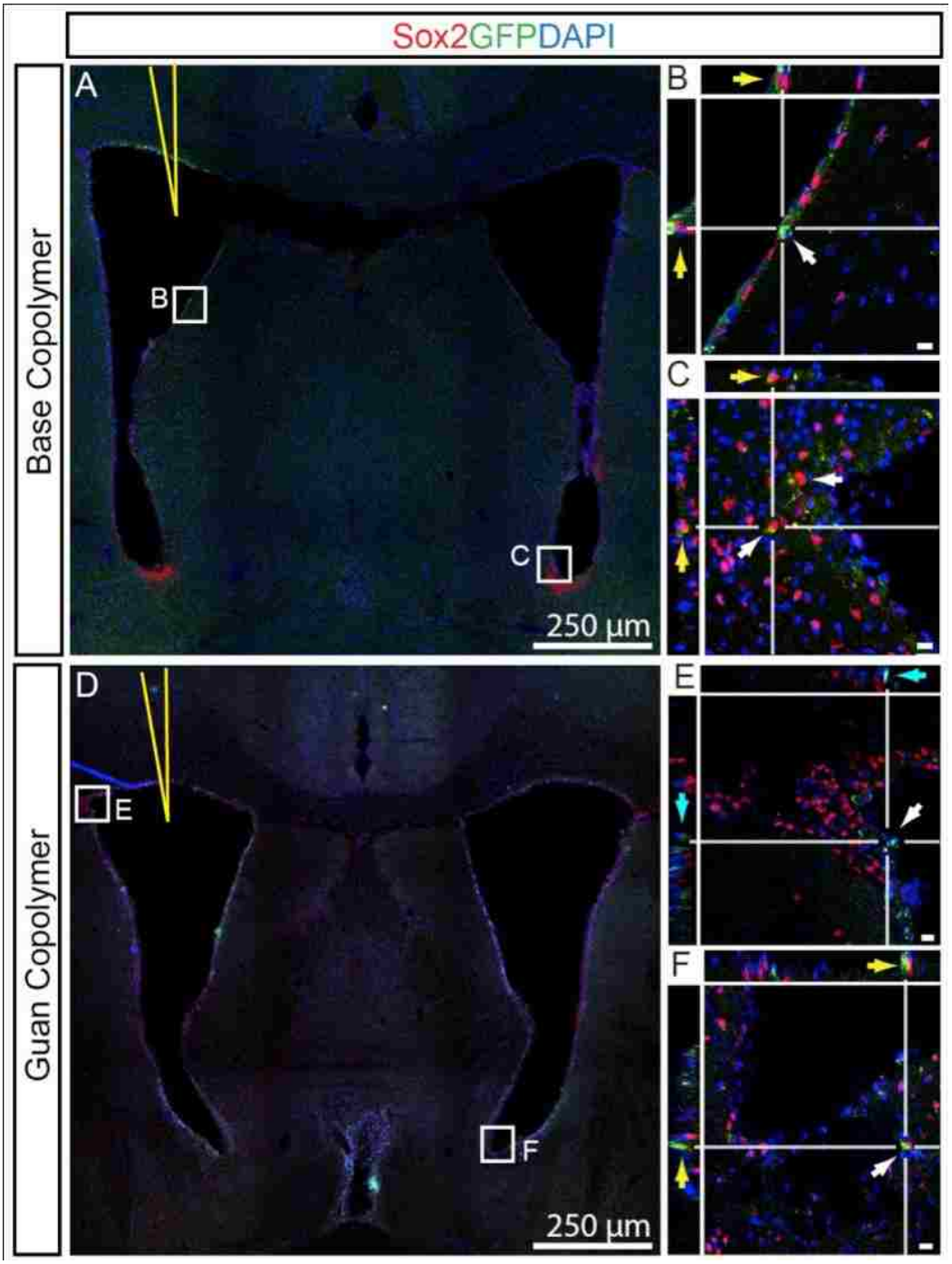

Figure 2.7 Confocal micrographs of GFP^+ cells 48 hrs after delivery of Base and Guan polyplexes containing GFP plasmid. Base Copolymer complexes into the lateral ventricle (yellow needle) showed Sox2-cells transfected within the ipsilateral margin (B, yellow arrows) as well as numerous cells at the contralateral ventricle margin (C). Brains injected with Guan copolymer polyplexes showed markedly fewer $Sox2^+$, GFP^+-cells at the ipsilateral (E, cyan arrow) and contralateral margin (F, yellow). Bar = 10 µm.

2.3.5 *Evaluation of polyplex stability in the presence of heparan sulfate*

We hypothesized that the reduced transfection efficiency of Guan copolymer polyplexes *in vivo* might be due to differences in extracellular stability of the two formulations. Therefore, the stability of polyplexes in the presence of anionic glycosaminoglycans, heparin and heparan sulfate (HS), was determined using a YOYO-1 fluorescence quenching assay. The YOYO-1 dye fluoresces when intercalated in DNA; this fluorescence is quenched when the plasmid DNA is condensed in polyplex form. The compaction state of YOYO-1-labeled polyplexes incubated with HS for 1 hr was monitored by fluorescence emission measurements (**Figure 2.8**).

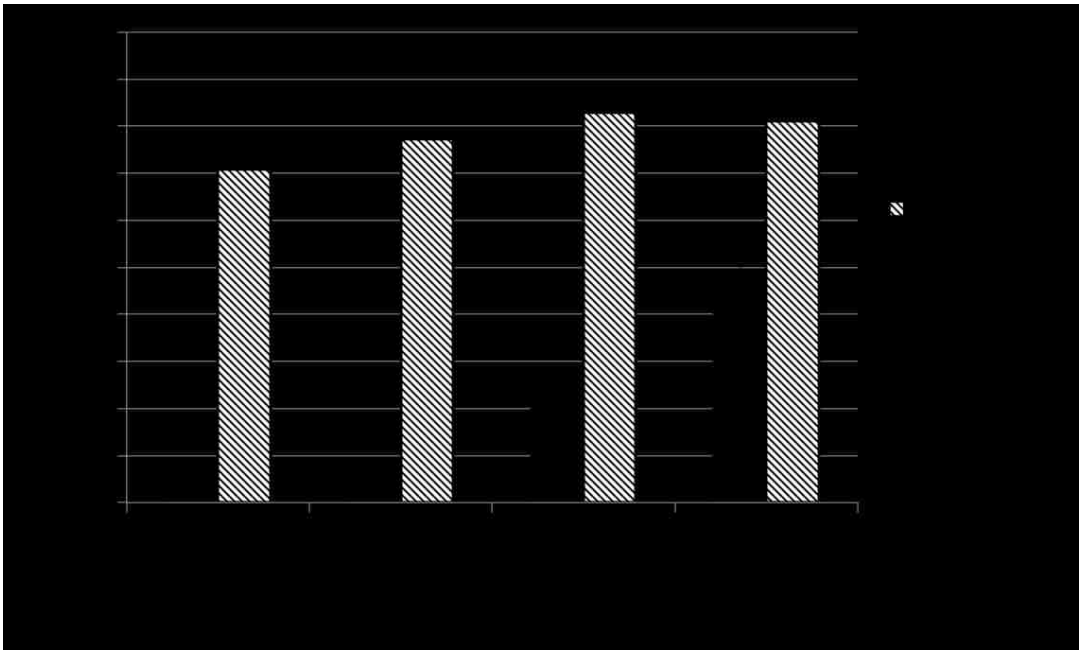

Figure 2.8 Polyplex unpackaging study with polyplexes (N/P = 15) treated with heparin or heparan sulfate for 1 hr as assessed by YOYO-1 fluorescence.

While Base copolymer polyplexes treated with 5 μg/mL heparin remained condensed, with similar levels of YOYO-1 fluorescence as untreated polyplexes, Guan copolymer polyplexes showed nearly complete unpackaging, evidenced by the recovery of YOYO-1 fluorescence. Increasing heparin concentration to 10 μg/mL increased unpackaging in both copolymer polyplexes but Base copolymer polyplexes

remained more condensed compared to Guan copolymer polyplexes. A similar result was obtained by competition with 10 μg/mL heparin in the gel retardation study of polyplexes (**Figure S2.1**). While the addition of heparin releases free plasmid from Guan polyplexes formed at N/P = 3, analogous polyplexes formed using Base copolymer remain stable in the presence of heparin. Thus, Base copolymer polyplexes are more resistant to competitive unpackaging by anionic glycosaminoglycans and proteoglycans compared to Guan copolymer polyplexes.

2.4 DISCUSSION

Peptides and polymers containing multiple guanidine groups, such as the TAT peptide from human immunodeficiency virus (HIV), have been shown to be effective materials for facilitating intracellular delivery to mammalian cells.[198,199] In addition, an arginine-conjugated dendrimer has been used to deliver nucleic acids to brain by direct injection and by intranasal administration.[122,200] In this work, we synthesized a guanidinylated analog of an efficient amine-based gene carrier that we previously developed.[47] Polyplexes formed from the two polymers were similar in physicochemical properties (**Table 2.1**), but consistent with several prior reports,[12,189–191] the guanidinylated materials transfected immortalized cultured cells with higher efficiency than the amine-based materials (**Figure 2.2-4**). Transfection efficiency to primary neural progenitor cells was comparable between the two polymers (**Figure 2.5**). However, when the polyplexes were injected intraventricularly to the murine brain, the amine-based polymers outperformed the guanidine-based polymers in gene transfer efficiency by over one order of magnitude (**Figure 2.6**).

The main type of cells transfected in the SVZ by intraventricular injection of polyplexes are NPCs due to their proliferative state and the strong preference of polyplexes to transfect dividing cells.[77] It was recently shown that the NPCs proliferate in niches directly in contact with fractones, extracellular matrix structures with branched fractal structures that are enriched in N-sulfate heparan sulfate (HS) proteoglycans, which bind and present the growth factor FGF-2 (fibroblast growth factor 2).[201,202] We previously showed that HS proteoglycans in the liver prematurely unpackage polyplexes.[40] Juhasz and Biemann's results with complexing oligoarginines with polyanionic biological molecules (such as oligonucleotides and proteoglycans) revealed that oligoarginines bind more strongly to sulfates than phosphates.[203] Therefore, we hypothesized that the guanidine-based polyplexes may be destabilized more by the SVZ fractones than lysine-based polyplexes. Indeed, several studies have compared the binding of the sulfates with either the guanidinium side chain of arginine or the amine side chain of lysine and found that greater affinity of sulfates to arginine.[204,205] Fromm and coworkers, for example, demonstrated tighter interaction of arginine versus lysine for heparin, with $K_{d(lys)}/K_{d(arg)}$ ~2.5, possibly due to stronger hydrogen bonding with guanidine, which can form parallel hydrogen bonds with sulfates, compared to lysine, which forms hydrogen bonds at 120°.

We tested this hypothesis by incubating polyplexes with both heparin and heparan sulfate, and monitoring unpackaging by a YOYO-1 dye-quenching assay (**Figure 2.8**). Guanidinylated polyplexes unpackaged readily in the presence of either heparin or heparan sulfate whereas amine-containing polyplexes resisted unpackaging under the experimental conditions. Similarly, Guan polyplexes were more destabilized by the presence of heparin than Base polyplexes as seen in the gel retardation electrophoresis (**Figure S2.1**). In addition, we found that neural progenitor cells could not be transfected with the guanidinylated polymer when heparin (used to bind FGF-2) is present in the media at 5 μg/mL (data not shown); instead, heparin had to be reduced to 1 μg/mL. Thus, the guanidine-based polyplexes are likely unpackaged to a greater extent *in vivo* compared to the amine-containing polyplexes due to stronger interactions with sulfated extracellular matrix components.

2.5 CONCLUSION

In this work, we compared the *in vitro* and *in vivo* gene transfer efficiency of an amine- and a guanidine-based polycation. While the guanidine-based polycation transfected cultured cells more efficiently, the amine-based polycation was more effective for *in vivo* gene transfer to the adult SVZ. Our data suggest that guanidinylated polyplexes may be more susceptible to premature, extracellular destabilization *in vivo* due to stronger affinity of the polymers for anionic proteoglycans encountered in the extracellular matrix. The molecular structure of the ventricular zone and the stem cell niche needs to be considered in the future design of materials for nucleic acid delivery to NPCs.

2.6 ACKNOWLEDGEMENTS

This work was supported by NIH 2R01NS064404; JKYT was supported by NSF GRFP (2011128558). We are grateful to Prof. Wei Zheng (Purdue University) for the generous donation of the Z310 cell line. We thank Prof. Patrick Stayton (University of Washington) for use of his ZetaPALS analyzer and Prof. Shaoyi Jiang (University of Washington) for use of his Malvern Zetasizer.

2.7 SUPPORTING INFORMATION

2.7.1 *Gel retardation of Base and Guan polyplexes*

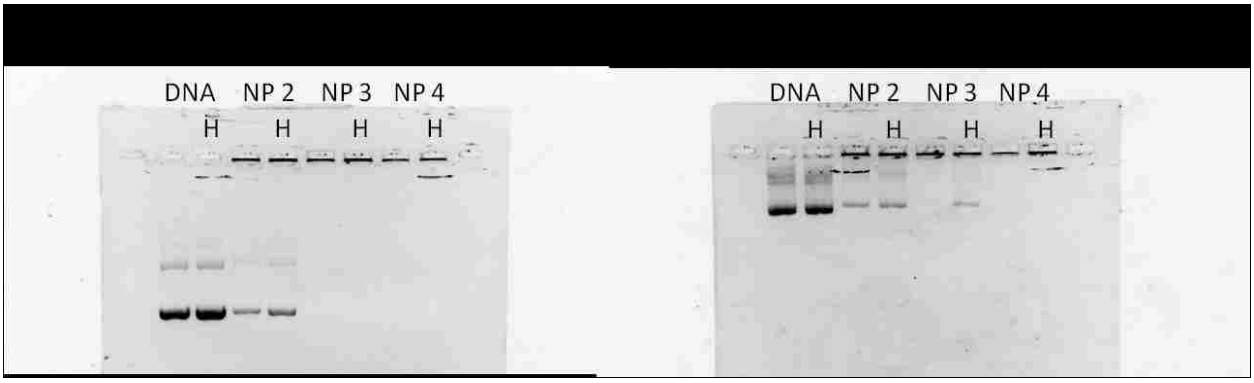

Figure S2.1 Gel retardation study of polyplexes. Base and Guan copolymers were complexes with plasmid DNA at various charge ratios, with and without heparin ("H"), and DNA condensation was analyzed by get electrophoresis.

2.8 REFERENCES

1. Gage, F. H. Mammalian Neural Stem Cells. *Science (80-.).* **287,** 1433–8 (2000).

10. Chirumamilla, S., Sun, D., Bullock, M. R. & Colello, R. J. Traumatic brain injury induced cell proliferation in the adult mammalian central nervous system. *J. Neurotrauma* **19,** 693–703 (2002).

12. Zhang, R., Zheng, N., Song, Z., Yin, L. & Cheng, J. The effect of side-chain functionality and hydrophobicity on the gene delivery capabilities of cationic helical polypeptides. *Biomaterials* **35,** 3443–3454 (2014).

13. Dash, P. K., Mach, S. a & Moore, a N. Enhanced neurogenesis in the rodent hippocampus following traumatic brain injury. *J. Neurosci. Res.* **63,** 313–319 (2001).

14. Ramaswamy, S., Goings, G. E., Soderstrom, K. E., Szele, F. G. & Kozlowski, D. a. Cellular proliferation and migration following a controlled cortical impact in the mouse. *Brain Res.* **1053,** 38–53 (2005).

39. Pack, D. W., Hoffman, A. S., Pun, S. & Stayton, P. S. Design and development of polymers for gene delivery. *Nat. Rev. Drug Discov.* **4,** 581–93 (2005).

40. Burke, R. S. & Pun, S. H. Extracellular barriers to in vivo PEI and PEGylated PEI polyplex-mediated gene delivery to the liver. *Bioconjug. Chem.* **19,** 693–704 (2008).

47. Wei, H. *et al.* Dual responsive, stabilized nanoparticles for efficient in vivo plasmid delivery. *Angew. Chem. Int. Ed. Engl.* **52,** 5377–81 (2013).

49. Begley, D. Understanding and circumventing the blood-brain barrier. *Acta Paediatr.* **443,** 83–91 (2003).

77. Kwon, E. J. *et al.* Targeted nonviral delivery vehicles to neural progenitor cells in the mouse subventricular zone. *Biomaterials* **31,** 2417–2424 (2010).

112. Wehling, K. *et al.* Specficificity of DNA-basic polypeptide interactions. Influence of neutral residues incorporated into polylysine and polyarginine. *Nucleic Acids Res.* **2,** 799–807 (1975).

113. Cheng, Q. *et al.* The effect of guanidinylation of PEGylated poly(2-aminoethyl methacrylate) on the systemic delivery of siRNA. *Biomaterials* **34,** 3120–3131 (2013).

164. Rungsardthong, U. *et al.* Copolymers of amine methacrylate with poly(ethylene glycol) as vectors for gene therapy. *J. Control. Release* **73,** 359–80 (2001).

165. Uzgün, S. *et al.* Characterization of tailor-made copolymers of oligo(ethylene glycol) methyl ether methacrylate and N,N-dimethylaminoethyl methacrylate as nonviral gene transfer agents: influence of macromolecular structure on gene vector particle properties and transfect. *Biomacromolecules* **11,** 39–50 (2010).

166. Deshpande, M. C. *et al.* The effect of poly(ethylene glycol) molecular architecture on cellular interaction and uptake of DNA complexes. *J. Control. Release* **97,** 143–56 (2004).

167. You, Y.-Z., Manickam, D. S., Zhou, Q.-H. & Oupický, D. Reducible poly(2-dimethylaminoethyl methacrylate): synthesis, cytotoxicity, and gene delivery activity. *J. Control. Release* **122,** 217–25 (2007).

168. Zhang, Y., Zheng, M., Kissel, T. & Agarwal, S. Design and biophysical characterization of bioresponsive degradable poly(dimethylaminoethyl methacrylate) based polymers for in vitro DNA transfection. *Biomacromolecules* **13,** 313–22 (2012).

169. Gosselin, M. a, Guo, W. & Lee, R. J. Efficient gene transfer using reversibly cross-linked low molecular weight polyethylenimine. *Bioconjug. Chem.* **12,** 989–94 (2001).

170. Christensen, L. V *et al.* Reducible poly(amido ethylenimine)s designed for triggered intracellular gene delivery. *Bioconjug. Chem.* **17,** 1233–40 (2006).

171. Burke, R. S. & Pun, S. H. Synthesis and characterization of biodegradable HPMA-oligolysine copolymers for improved gene delivery. *Bioconjug. Chem.* **21,** 140–50 (2010).

172. Peng, Q., Zhong, Z. & Zhuo, R. Disulfide cross-linked polyethylenimines (PEI) prepared via thiolation of low molecular weight PEI as highly efficient gene vectors. *Bioconjug. Chem.* **19,** 499–506 (2008).

173. Smith, M. E. B. *et al.* Protein modification, bioconjugation, and disulfide bridging using bromomaleimides. *J. Am. Chem. Soc.* **132,** 1960–5 (2010).

174. Moody, P. *et al.* Bromomaleimide-linked bioconjugates are cleavable in mammalian cells. *Chembiochem* **13,** 39–41 (2012).

175. Cui, Y., Yan, Y., Chen, Y. & Wang, Z. Dibromomaleimide Derivative as an Efficient Polymer Coupling Agent for Building Topological Polymers. *Macromol. Chem. Phys.* **214,** 470–477 (2013).

176. Jones, M. W. *et al.* Polymeric dibromomaleimides as extremely efficient disulfide bridging bioconjugation and pegylation agents. *J. Am. Chem. Soc.* **134,** 1847–52 (2012).

177. van de Wetering, P., Cherng, J. Y., Talsma, H., Crommelin, D. J. & Hennink, W. E. 2-(Dimethylamino)ethyl methacrylate based (co)polymers as gene transfer agents. *J. Control. Release* **53,** 145–53 (1998).

178. Robin, M. P. *et al.* Conjugation-induced fluorescent labeling of proteins and polymers using dithiomaleimides. *J. Am. Chem. Soc.* **135,** 2875–8 (2013).

179. Layman, J. M., Ramirez, S. M., Green, M. D. & Long, T. E. Influence of polycation molecular weight on poly(2-dimethylaminoethyl methacrylate)-mediated DNA delivery in vitro. *Biomacromolecules* **10,** 1244–52 (2009).

180. Ryan, C. P. *et al.* Tunable reagents for multi-functional bioconjugation: reversible or permanent chemical modification of proteins and peptides by control of maleimide hydrolysis. *Chem. Commun. (Camb).* **47,** 5452–4 (2011).

181. Verbaan, F. J. *et al.* Steric stabilization of poly(2-(dimethylamino)ethyl methacrylate)-based polyplexes mediates prolonged circulation and tumor targeting in mice. *J. Gene Med.* **6,** 64–75 (2004).

182. Venkataraman, S. *et al.* The role of PEG architecture and molecular weight in the gene transfection performance of PEGylated poly(dimethylaminoethyl methacrylate) based cationic polymers. *Biomaterials* **32,** 2369–78 (2011).

183. Richard, J. P. *et al.* Cell-penetrating peptides. A reevaluation of the mechanism of cellular uptake. *J. Biol. Chem.* **278,** 585–90 (2003).

184. Eriksson, P. S. *et al.* Neurogenesis in the adult human hippocampus. *Nat. Med.* **4,** 1313–1317 (1998).

185. Hallbergson, A. F., Gnatenco, C. & Peterson, D. a. Neurogenesis and brain injury: Managing a renewable resource for repair. *J. Clin. Invest.* **112,** 1128–1133 (2003).

186. Yoshimura, S. *et al.* FGF-2 regulation of neurogenesis in adult hippocampus after brain injury. *Proc. Natl. Acad. Sci. U. S. A.* **98,** 5874–5879 (2001).

187. Bergen, J. M., Park, I. K., Horner, P. J. & Pun, S. H. Nonviral approaches for neuronal delivery of nucleic acids. *Pharm. Res.* **25,** 983–998 (2008).

188. Davidson, B. L. & Breakefield, X. O. Viral vectors for gene delivery to the nervous system. *Nat. Rev. Neurosci.* **4,** 353–364 (2003).

189. Carlson, P. & Schellinger, J. Comparative study of guanidine-based and lysine-based brush copolymers for plasmid delivery. *Biomater. Sci.* 736–744 (2013). doi:10.1039/c3bm60079c

190. Choi, J. S. *et al.* Enhanced transfection efficiency of PAMAM dendrimer by surface modification with l-arginine. *J. Control. Release* **99,** 445–456 (2004).

191. Kim, T. Il, Ou, M., Lee, M. & Kim, S. W. Arginine-grafted bioreducible poly(disulfide amine) for gene delivery systems. *Biomaterials* **30,** 658–664 (2009).

192. Gund, P. Guanidine, trimethylenemethane, and 'Y-delocalization.' Can acyclic compounds have 'aromatic' stability? *J. Chem. Educ.* **49,** 100 (1972).

193. Schug, K. a & Lindner, W. Noncovalent binding between guanidinium and anionic groups: focus on biological- and synthetic-based arginine/guanidinium interactions with phosph[on]ate and sulf[on]ate residues. *Chem. Rev.* **105,** 67–114 (2005).

194. Mascotti, D. P. & Lohman, T. M. Thermodynamics of oligoarginines binding to RNA and

DNA. *Biochemistry* **36,** 7272–7279 (1997).

195. Standke, K. C. & Brunnert, H. The estimation of affinity constants for the binding of model peptides to DNA by equilibrium dialysis. *Nucleic Acids Res.* **2,** 1839–49 (1975).

196. Weber, C. J. The Determination of the Guanidine Bases in Urine. *J Biol Chem* **78,** 465–473 (1928).

197. Brancia, F. L., Oliver, S. G. & Gaskell, S. J. Improved matrix-assisted laser desorption/ionization mass spectrometric analysis of tryptic hydrolysates of proteins following guanidination of lysine-containing peptides. *Rapid Commun. Mass Spectrom.* **14,** 2070–2073 (2000).

198. Futaki, S. Membrane-permeable arginine-rich peptides and the translocation mechanisms. *Adv. Drug Deliv. Rev.* **57,** 547–558 (2005).

199. Wender, P. a., Galliher, W. C., Goun, E. a., Jones, L. R. & Pillow, T. H. The design of guanidinium-rich transporters and their internalization mechanisms. *Adv. Drug Deliv. Rev.* **60,** 452–472 (2008).

200. Kim, I.-D. *et al.* Intranasal Delivery of HMGB1 siRNA Confers Target Gene Knockdown and Robust Neuroprotection in the Postischemic Brain. *Mol. Ther.* **20,** 829–839 (2012).

201. Kerever, A. *et al.* Novel extracellular matrix structures in the neural stem cell niche capture the neurogenic factor fibroblast growth factor 2 from the extracellular milieu. *Stem Cells* **25,** 2146–2157 (2007).

202. Mercier, F. & Arikawa-Hirasawa, E. Heparan sulfate niche for cell proliferation in the adult brain. *Neurosci. Lett.* **510,** 67–72 (2012).

203. Juhasz, P. & Biemann, K. Mass spectrometric molecular-weight determination of highly acidic compounds of biological significance via their complexes with basic polypeptides. *Proc. Natl. Acad. Sci. U. S. A.* **91,** 4333–4337 (1994).

204. Fromm, J. R., Hileman, R. E., Caldwell, E. E., Weiler, J. M. & Linhardt, R. J. Differences in the interaction of heparin with arginine and lysine and the importance of these basic amino acids in the binding of heparin to acidic fibroblast growth factor. *Arch. Biochem. Biophys.* **323,** 279–87 (1995).

205. Wernersson, E. *et al.* Effect of association with sulfate on the electrophoretic mobility of polyarginine and polylysine. *J. Phys. Chem. B* **114,** 11934–11941 (2010).

Part 4: Microbubbles and Ultrasound for the Transient Disruption of the Choroid Plexus

Despite the development of effective gene delivery vehicles for neurological applications, these vectors are futile if they cannot reach the neural progenitor and stem cells in the brain. Recently, microbubbles and ultrasound have been developed to spatially and transiently open the blood-brain barrier and allow for the permeation of molecules into the brain that would otherwise be excluded by the blood-brain barrier. Here, we investigate the development of microbubbles and ultrasound to open the choroid plexus epithelium and increase the transfection of our gene delivery vehicles.

Chapter 1. Microbubbles and Ultrasound Increase Intraventricular Polyplex Gene Transfer to the Brain

James-Kevin Y. Tan, Binhan Pham, Yujin Zong, Camilo Perez, Don O. Maris, Ashton Hemphill, Carol Miao, Thomas J. Matula, Pierre D. Mourad, Hua Wei, Drew L. Sellers, Philip J. Horner, Suzie H. Pun

This work has resulted in a publication: Tan, *et al*. *Journal of Controlled Release*. (2016) **12** (20):2750-2758.

Synopsis:

Neurons in the brain can be damaged or lost from neurodegenerative disease, stroke, or traumatic injury. Although neurogenesis occurs in mammalian adult brains, the levels of natural neurogenesis are insufficient to restore function in these cases. Gene therapy has been pursued as a promising strategy to induce differentiation of neural progenitor cells into functional neurons. Non-viral vectors are a preferred method of gene transfer due to potential safety and manufacturing benefits but suffer from lower delivery efficiencies compared to viral vectors. Since the neural stem and progenitor cells reside in the subventricular zone of the brain, intraventricular injection has been used as an administration route for gene transfer to these cells. However, the choroid plexus epithelium remains an obstacle to delivery. Recently, transient disruption of the blood-brain barrier by microbubble-enhanced ultrasound has been used to successfully improve drug delivery to the brain after intravenous injection. In this work, we demonstrate that microbubble-enhanced ultrasound can similarly improve gene transfer to the subventricular zone after intraventricular injection. Microbubbles of different surface charges (neutral, slightly cationic, and cationic) were prepared, characterized by acoustic flow cytometry, and evaluated for their ability to increase the permeability of immortalized choroid plexus epithelium monolayers *in vitro*. Based on these results, slightly cationic microbubbles were evaluated for microbubble and ultrasound-mediated enhancement of non-viral gene transfer *in vivo*. When coupled with our previously reported gene delivery vehicles, the slightly cationic microbubbles significantly increased ultrasound-mediated transfection of the murine brain when compared to commercially available Definity® microbubbles. Temporary disruption of the choroid plexus by microbubble-enhanced ultrasound is therefore a viable way of enhancing gene delivery to the brain and merits further research.

Keywords: gene delivery, microbubble, polyplex, ultrasound, *in vivo*, choroid plexus epithelium

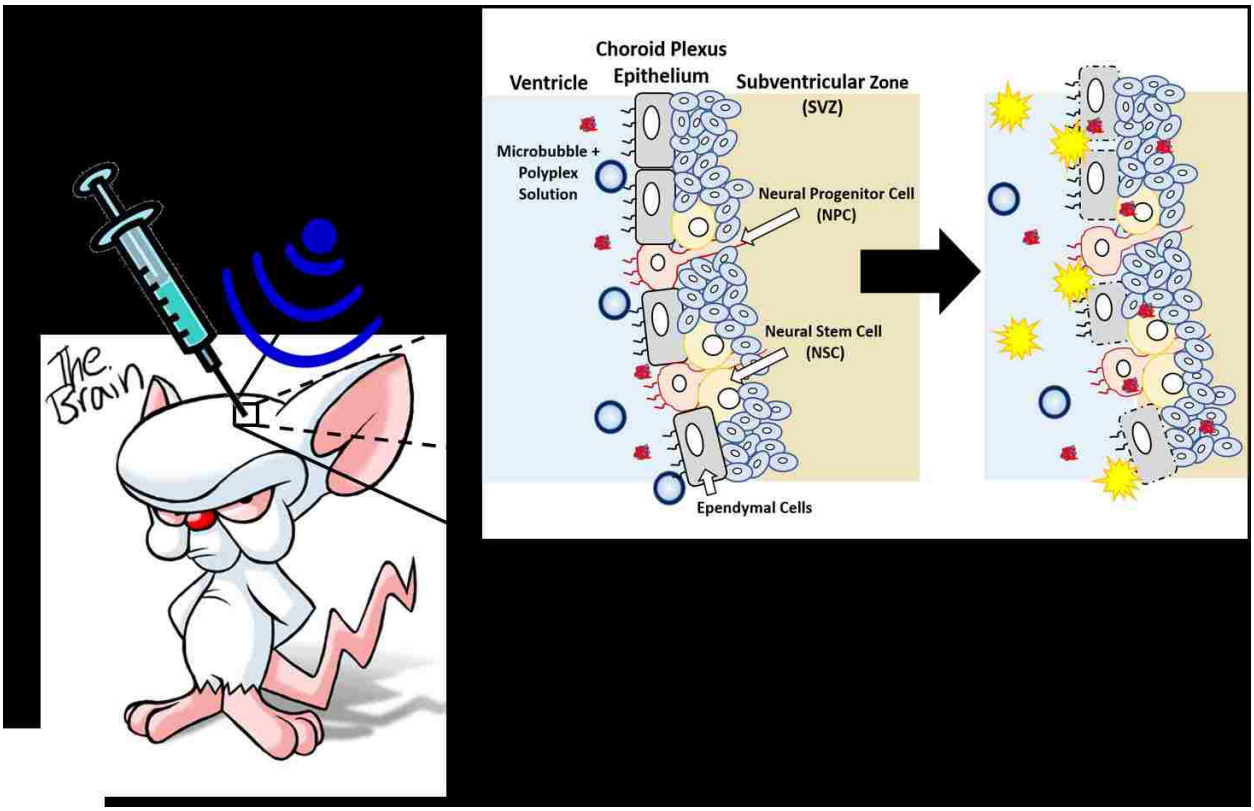
The Brain
Choroid Plexus
Epithelium
Ventricle
Subventricular Zone
(SVZ)
Microbubble +
Polyplex
Solution
Neural Progenitor Cell
(NPC)
Neural Stem Cell
(NSC)
Ependymal Cells

1.1 INTRODUCTION

Neurological diseases or injuries such as ischemic stroke can induce a natural neurogenesis response that includes proliferation of neural progenitor cells (NPCs) and neural stem cells (NSCs) in the subventricular zone (SVZ), angiogenesis, and migration of NPCs and NSCs toward the injury site, where they differentiate and mature.[3,15,16] However, only a limited fraction of these cells differentiate into functional, mature neurons.[4,5] Gene delivery strategies that encourage NPC and NSC differentiation into neurons can potentially improve the recovery of lost neuron populations and help restore function.[34] For example, the delivery of genes encoding for fibroblast growth factor-2, epidermal growth factor, insulin growth factor-1, and vascular endothelial growth factor have been shown to increase neuron regeneration after ischemic stroke or delay the progression of amyotrophic lateral sclerosis in mice, rats, and gerbils.[25,29,64,66] *In vivo* gene delivery to NPCs and NSCs in the stem cell niche of the brain is therefore a promising strategy to enhance neurogenesis and offers several advantages over protein delivery and stem cell transplant therapy such as a more sustained expression that localizes in a migrating cell population and a more straightforward clinical translation, respectively. Nevertheless, there still remains a significant need for effective methods for gene transfer to the NPC and NSC populations in the brain.

Previously, our group designed and synthesized a polymeric carrier that demonstrated successful gene transfer to the subventricular zone.[47] This copolymer, PCL-SS-p[(GMA-TEPA)-*s*-OEGMA], consists of a block of poly(ε-caprolactone) (PCL) connected by a reducible disulfide to a statistical copolymer of tetraethylenepentamine (TEPA)-decorated poly(glycidyl methacrylate) (GMA) and oligo(ethylene glycol) monomethyl ether methacrylate (OEGMA). The cationic TEPA groups of the polymer bind to and condense nucleic acids to form polyplexes while the hydrophobic PCL and hydrophilic OEGMA provide extracellular stability. After polyplex internalization, the TEPA groups contribute to endosomal escape by the proton sponge effect and the internal disulfide bond can be reduced by cytosolic glutathione facilitating polyplex destabilization and nucleic acid release. These PCL-SS-p[(GMA-TEPA)-*s*-OEGMA] polyplexes were shown to have diameters less than 200 nm and delivered nucleic acids to mouse brains *in vivo* after intraventricular injection.[47] However, gene transfer was limited to a few cell layers adjacent to the ventricular surface.[114]

Along the cavities of the ventricles lie the choroid plexus barrier, comprised of choroid plexus epithelium cells that secrete cerebrospinal fluid.[54,206] These ependymal cells are held together by tight junctions and prevent materials from entering the brain parenchyma after intraventricular injection.[52] For example, both small molecules such as 1,3-*bis*(2-chloroethyl-1-nitroso-urea) and macromolecules such as brain-derived neurotrophic factor have limited permeation through the choroid plexus and only 1% diffuse 1 mm into the barrier.[54] We therefore hypothesized that the ependymal cells of the choroid plexus epithelium act as a significant barrier to gene transfer in the subventricular zone after intraventricular injection.

To transiently disrupt cell barriers, microbubbles (MBs), or gas-filled microspheres, have been coupled with ultrasound (US) as a method to permeabilize cell membranes and break up tight junctions, thus allowing for enhanced penetration of materials.[61,94,95] This process, called sonoporation, creates micropores as MBs act as local enhancers of acoustic energy and cavitate causing local shear flow, microstreams, and microjets.[61,96,97] The micropores can be spatially and temporally controlled by varying the parameters and location of US. Intravenous injections of MBs with transcranial US have been applied to the CNS to temporarily disrupt the blood-brain barrier and allow for the permeation of macromolecules such as immunoglobulinG and 70 kDa dextran into the brain.[59,62,98–102,207] However, to our knowledge, sonoporation of the choroid plexus epithelium as a way to enhance permeation of materials into the brain parenchyma has yet to be reported.

Herein, we investigated MB-enhanced US as a method to increase gene transfer to the brain parenchyma after intraventricular injection. Custom, lipid-based MBs of neutral, slightly cationic, and cationic charge were formulated and compared to commercially available Definity® (Def) MBs. Neutral and slightly cationic MBs, but not Definity MBs, were able to increase the permeability of cell monolayers *in vitro*. Furthermore, co-delivery of slightly cationic MBs with polyplexes increased *in vivo* gene transfer to the brain. Sonoporation of the choroid plexus is a viable method to increase gene transfection after intraventricular injection. Further investigation may allow for the effective permeation of gene delivery vehicles through the choroid plexus into the SVZ to augment transfection of NPCs and NSCs and drive neuron differentiation and neurogenesis.

1.2 MATERIALS & METHODS

1.2.1 *Materials*

Lipids were purchased from Avanti Polar Lipids, Inc. (Alabaster, AL) and perfluorobutane (PFB) was purchased from Synquest Laboratories (Alachua, FL). Definity® MBs and a Vialmix® machine were purchased from Lantheus Medical Imaging (N. Billerica, MA); Optison® MBs were from GE Healthcare (Chicago, IL). The Z310 choroid plexus cell line was a generous gift from Dr. Wei Zheng at Purdue University. Tissue culture reagents and bicinchoninic acid (BCA) protein quantification assay kit were purchased from Thermo Fisher Scientific (Waltham, MA). The 70 kDa Texas Red-dextran was purchased from Life Technologies (Carlsbad, CA) while the 5 kDa FITC-PEG was purchased from NanoCS (New York, NY). The pCMV-Luc2 plasmid was isolated using the Qiagen Plasmid Giga Kit (Hilden, Germany) while the pmaxGFP™ was from Lonza (Walkersville, MD). The luciferase expression quantification kit and MTS assay was obtained from Promega (Madison, WI).

1.2.2 *MB formation and characterization*

Custom MBs of different surface charges were formulated by mixing a total of 1 mg of different chloroform-dissolved lipids in a 2 mL tube followed by overnight drying under vacuum. Neutral (Neu) MBs were formulated at a 9:1 molar ratio of 1,2-distearoyl-*sn*-glycero-3-phosphocholine (DSPC) and 1,2-distearoyl-*sn*-glycero-3-phosphoethanolamine-*N*-[methoxy(polyethylene glycol)2000] (DSPE-mPEG2000), Slightly cationic (SCat) MBs were formulated at a 9:1 molar ratio of DSPC and 1,2-distearoyl-*sn*-glycero-3-phosphoethanolamine-*N*-[amino(polyethylene glycol)2000] (DSPE-PEG2000-Amine), and cationic (Cat) MBs were formulated at a 9:2:1 molar ratio of DSPC, DSPE-PEG2000-Amine, and 1,2-distearoyl-3-trimethylammonium-propane (DSTAP). The lipid film was rehydrated in a 1 mL solution of 10:10:80 (v/v/v) glycerol:propylene glycol:water at 67 °C. The tube headspace was filled with PFB and amalgamated with a Vialmix® machine for 45 s. The MB suspension was processed by differential centrifugation to remove micelles/free lipids and to isolate

MBs with diameters less than 2 μm as previously described.[208] Definity® MBs were processed as per manufacturer's instructions. MB diameter and concentration were determined by a Beckman Coulter Multisizer 3 (Brea, CA). The zeta potential of the MBs was determined in 10 mM PBS pH 7.4 by a Malvern Zetasizer Nano ZS (Westborough, MA). Mechanical shell properties were characterized by a modified flow cytometer that had a piezoelectric ultrasound transducer coupled to the flow channel.[209–211] US was applied at 1 MHz and as the MBs flowed through the channel, instantaneous change in their size in response to acoustic energy was characterized by change in laser scattering signal that was detected by a photomultiplier tube. This data was fitted to previously reported MB models and the mechanical MB parameters were determined.[212]

1.2.3 *Synthesis of PCL-SS-p[(GMA-TEPA)-s-OEGMA]*

The reducible 2-hydroxyethyl-2'-(bromoisobutyryl)ethyl disulfide double-head initiator (HO-SS-iBuBr) and PCL-SS-p[(GMA-TEPA)-*s*-OEGMA] were synthesized as previously reported.[47] Briefly, ring-opening polymerization (ROP) of caprolactone was performed using HO-SS-iBuBr as the initiator and $Sn(Oct)_2$ as the catalyst. Then, a one-pot atom-transfer radical polymerization (ATRP) of GMA and OEGMA was performed using PCL_{40}-SS-iBuBr as the macroinitiator and CuCl/bpy as the catalyst. The copolymer composition and molecular weight were determined by ^{1}H NMR and gel permeation chromatography (GPC) using an Optilab-rEX and miniDAWN TREOS triple-angle static light scattering detector (Wyatt Technology, Santa Barbara CA). The GMA monomers in the polymer were reacted with excess TEPA in dimethylacetamide.

1.2.4 *Polyplex formation*

The pCMV-Luc2 plasmid was diluted in double-distilled H_2O (ddH2O) to a concentration of 0.1 mg/mL and mixed with an equal volume of polymer (in ddH_2O) at an amine-to-phosphate (N/P) ratio = 15. The required amount of polymer was calculated by determining the polymer mass-to-charge ratio and taking into account

that 1 μg of DNA contains 3 nmol of phosphate. After mixing, the polyplexes were allowed to form for 10 min at room temperature.

1.2.5 *MB stability*

MB stability was assessed by measuring the MB concentration over time with a Multisizer 3 relative to the initial MB concentration. In a similar manner, MB stability was assessed while in the presence of polyplexes at a ratio of 1.25×10^7 MBs/μg DNA.

1.2.6 *MB cytotoxicity*

Immortalized Z310 choroid plexus cells were cultured in 10% heat-inactivated FBS, 1% penicillin-streptomycin, 40 μg/mL gentamicin, and 10 ng/mL endothelial growth factor-supplemented DMEM culture medium as previously described.[213,214] MBs (1.25×10^7) were dispensed into each well of a 96-well plate with 10,000 adhered Z310 cells. The plate was covered with an adhesive plate seal film and inverted so that MBs would rise and be in contact with the cells. After 30 min in an incubator, an MTS assay was performed to assess cell viability.

1.2.7 *Polyplex stability with MBs*

The ability of polyplexes to remain complexed in the presence of MBs was assessed by a gel retardation assay. The polyplexes (1 μg DNA, 20 μL solution, N/P = 15) were incubated with 1.25×10^7 MBs/μg DNA for 10 min. Solutions were mixed with 10% (v/v) BlueJuice™ gel loading buffer (Invitrogen, Carlsbad, CA) and loaded onto a 1% agarose gel containing TAE buffer (40 mM tris-acetate, 1 mM EDTA) and 5 mg/mL ethidium bromide. The gel was electrophoresed at 100 V for 40 min. The plasmid DNA was then visualized using a Kodak (Rochester, NY) UV transilluminator (laser-excited fluorescence gel scanner).

1.2.8 *MB turbidity assay*

In a water bath, MBs were sonicated by a diagnostic Sonosite MicroMaxx® machine (Bothell, WA) with a P17 transducer (center frequency: 3 MHz, imaging modality: general, mechanical index: 0.8, phased array, pen mode, 4.7 cm depth). The turbidity

of the MB suspension was assessed by measuring the absorbance at 900 nm, relative to unsonicated MBs.

1.2.9 In vitro *Z310 permeability studies*

Z310 cells were seeded in Transwell® permeable supports at 10,000 cells/transwell and were allowed to grow in a 24-well plate for 3 days. Monolayer formation was verified by transepithelial electrical resistance measurements with an EVOM instrument (World Precision Instruments, Sarasota, FL). For permeability studies, transwells were washed, submerged, and inverted into an OptiMEM® bath. Underneath the bath, a P17 transducer was pointed upwards towards the transwell and was controlled by a SonoSite MicroMaxx® machine. MBs ($2.5x10^7$) were pipetted in the transwell space between the cells and the glass bath container and US was applied for 15 s. Afterwards, the transwell was removed from the bath, washed with OptiMEM®, and placed in a well plate. An OptiMEM® solution of 0.02 mM 5 kDa FITC-PEG and 0.02 mM 70 kDa Texas-Red dextran was added to each transwell. After 4 hour incubation, samples were taken from the bottom well plate and the fluorescence was measured (FITC ex: 492 nm, em: 518 nm; Texas Red: ex: 595 nm, em: 615 nm). Permeability was expressed as a percentage of the average control value. In addition, Z310 cells were analyzed by flow cytometry to measure fluorescence uptake. Z310 cells in transwells were treated with SCat MBs and US as mentioned above. The solution was replaced with 0.02 mM of 5 kDa FITC-PEG and placed in an incubator for 1 hr. The cells were washed, trypsinized, collected, and washed before flow cytometry analysis with a MACSQuant (Miltenyi, Bergisch Gladbach, Germany) flow cytometer. Analysis was performed with FlowJo analysis software (Tree Star, Ashland, Oregon).

1.2.10 In vivo *MB, US, and polyplex transfection*

All animal procedures were completed using protocols approved by the Institutional Animal Care and Use Committee at the University of Washington. Luciferase or GFP reporter polyplexes were prepared in 5% glucose using 2.5 μg of DNA in 10 μL total volume at an N/P = 15 as previously described.[48] Adult (8-9 weeks) female C57BL/6J

mice (Jackson Laboratories) were anesthetized by an intraperitoneal injection of Avertin. A 1 mm diameter craniotomy was made on the right side of the skull using a dental drill and 10 μL of polyplex or polyplex/MB suspension at 1.25×10^7 MBs/μg DNA (n = 6 or 9 per group) was stereotaxically injected at 1 mm lateral, 0.5 mm caudal to bregma, and 1.9 mm depth from the dura using a 33 gauge 10 μL Hamilton syringe. The injection was made over 2.5 minutes and the syringe was kept in place for 2 minutes after injection to prevent backflow. Afterwards, a P17 transducer was held to the mouse skull and US was applied for 1 min with a SonoSite MicroMaxx® machine.

1.2.11 *Luciferase expression analysis*

Brains were harvested from mice 48 hours post injection and separated into three sections: hindbrain, left brain, and right brain. Tissues were collected in 1X reporter lysis buffer (RLB, Promega Corp., Madison, WI) with 1X EDTA-free Roche's Complete Protease Inhibitor Cocktail (Roche, Nutley, NJ) and three freeze-thaw cycles were performed in liquid nitrogen. Tissues were mechanically homogenized and cell debris were pelleted at 15,000 *g* for 15 minute at 4 °C. The lysates were collected and analyzed by a luciferase assay kit (integration time = 1 s) and by the BCA assay to normalize luciferase expression by protein content.

1.2.12 *Immunohistochemistry and confocal microscopy*

Injections were done as described above using polyplexes formulated with pmaxGFP™. Two days post-injection, mice were euthanized with Avertin overdose and perfused intracardially with 0.9% saline followed by 4% paraformaldehyde in 0.1 M phosphate buffer. After perfusion and fixation, the brains were excised and equilibrated to 30% sucrose in phosphate buffer. Brains were embedded in OCT and sectioned into 40 um-thick coronal slices. For immunofluorescent labeling, slides were rinsed with PBS and blocked in PBS, 0.3% TritonX-100, 2% bovine serum albumin (BSA) for 1 hour. Primary antibodies (goat anti-Sox2, Santa Cruz Biotechnology; 1:250) were applied to the tissue sections in PBS, 0.3% TritonX-100, 2% BSA overnight at 4 °C. Sections were rinsed three times for 20 minutes in TBS,

0.1% Tween 20 and species appropriate secondary antibodies conjugated with fluorophore were incubated in PBS, 0.1% Tween 20, and 2% donkey serum for 2 hours. Sections were rinsed three times for 20 minutes in TBS-Tween, with the last rinse containing the nuclear marker, 4',6-diamidino-2-phenylindole (DAPI; 1:1000). Sections were then mounted onto glass slides, sealed and cover-slipped with gelvatol, and imaged using a confocal microscope.

1.2.13 *Statistical Analysis*

All statistical analyses were performed using a two-tailed Student's t-test with unequal variance.

1.3 RESULTS & DISCUSSION

MB-enhanced US has been used to disrupt the blood-brain barrier to facilitate the penetration of immunoglobulinG, dextrans, and viruses.[27,99,215,216] Herein, we focus on MB sonoporation to temporarily disrupt the choroid plexus barrier after intraventricular injection. Direct injection allows for close proximity to the neuron stem cell niche of the subventricular zone (SVZ) while keeping the BBB intact. In this paper, three custom MBs were developed, characterized, and evaluated *in vitro* and *in vivo* as a non-viral gene delivery system that combines physical and chemical delivery methods for gene transfer into the SVZ.

1.3.1 *Microbubble and polyplex characterization*

Three custom, lipid-based microbubble (MB) formulations with different surface charges, Neutral (Neu), Slightly Cationic (SCat), and Cationic (Cat), were prepared and compared to commercially available, neutrally charged Definity® (Def) MBs and negatively charged Optison® (Opt) MBs. Different surface charges of the custom MBs were obtained by varying the lipid compositions and the chemical termini of the lipids (**Table 1.1**).

TABLE 1.1 Lipid Composition of MBs

Neutral microbubbles were formulated with 90% DSPC and 10% DSPE-mPEG2000. The cationic charge in SCat MBs was obtained by replacing DSPE-mPEG with an amine-terminated PEG, DSPE-PEG-Amine. While most positively charged MBs are formulated by replacing 20% of the DSPC lipids with cationic DSTAP lipids; here, switching the end chemistry of the PEGylated lipid provided another way to change MB surface charge. A higher cationic surface charge with the Cat MBs was obtained by using both DSPE-PEG-Amine and cationic lipid DSTAP. The custom MBs were prepared from rehydrated lipid films with perfluorobutane using a Vialmix® amalgamator. All MBs, including the commercially available Def and Opt MBs, were similar in size (~1 μm) and concentration (~10^{10} MBs/mL) to MBs of other reports[217,218] with expected surface zeta potential values (**Table 1.2**).

TABLE 1.2 PHYSICAL CHARACTERIZATION OF MBS

The DNA condensing copolymer, PCL-SS-p[(GMA-TEPA)-*s*-OEGMA], was synthesized and formed polyplexes with DNA at N/P = 15 as previously described.[47] As an initial study, polyplexes were incubated with the different types of MBs to test for visible aggregation. No precipitation was observed upon addition of Neu, SCat, Cat, and Def MBs with cationic polyplexes. Conversely, mixing with the Opt MBs resulted in rapid aggregation and precipitation likely due to the strong electrostatic interactions between the anionic shell of the albumin-coated Opt MBs and the cationic polyplexes. Therefore, we decided to move forward with the other types of MBs and exclude Opt MBs from further investigation.

Next, the MBs were characterized by acoustic flow cytometry and MB modeling was utilized to determine the mechanical shell properties of the MBs[209–211] (**Figure 1.1**). An ultrasonic transducer was coupled to a conventional flow cytometer and MBs were sonicated as they pass through the laser interrogation region of the flow channel. In response to the acoustic energy, the MBs undergo an instantaneous change in size which was detected by a change in laser scattering. The radial dynamics were fitted to a Marmottant MB model to extract the shell elastic modulus (χ) and the shell dilatational viscosity (κ_S).

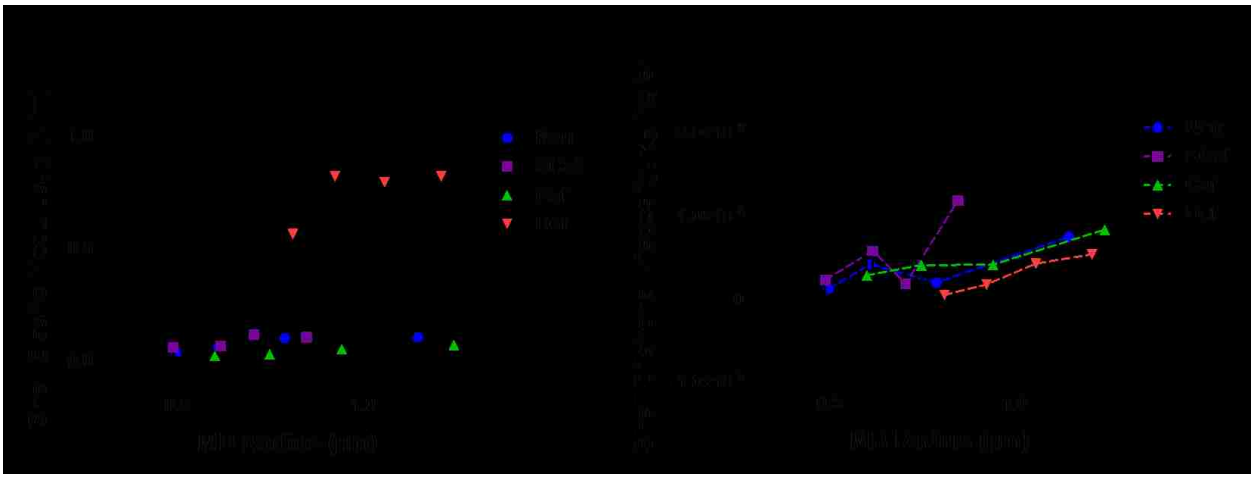

Figure 1.1 Acoustic characterization was performed with a modified flow cytometer to determine the shell mechanical properties: **(A)** shell elastic modulus and **(B)** shell dilatational viscosity. Data is presented as mean ± SD.

The shell elastic modulus, or the stiffness of the MB shell, was similar for all three custom MB formulations, ranging from around 0.05 to 0.10 N/m (**Figure 1.1A**). The elastic modulus was relatively independent of MB size as consistent with other lipid MBs like Def MBs.[209–211] In contrast, the Def MBs had an order of magnitude higher shell elastic modulus, suggesting a possible higher cavitation threshold.[219,220] The shell dilatational viscosity, or compressibility of the MB, increased as a function of MB size and ranged from 1.04×10^{-9} to 7.22×10^{-9}, 2.24×10^{-9} to 1.13×10^{-8}, 2.27×10^{-9} to 8.10×10^{-9}, and 4.53×10^{-10} to 5.34×10^{-9} kg/s for the Neu, SCat, Cat, and Def MBs, respectively (**Figure 1.1B**). This suggests that there is a size dependent and thus frequency dependent effect of the viscosity as consistent with other lipid-shelled bubbles.[210,212]

The stability of the MB formulations in solution was evaluated by measuring the MB concentration over time relative to initial concentration by a Multisizer 3 (**Figure 1.2A**). Microbubble concentrations decreased over the first 2 hours to nearly 50% of initial values, but then remained relatively stable over the time course of the experiment (300 min). In addition, the stability of the MB formulations in the presence of polyplexes was also evaluated (Figure S1.1). MBs in the presence of polyplexes had a similar rate of disappearance to MBs without any polyplexes. In addition, polyplex stability in the presence of MBs was tested by a gel retardation assay (Figure S1.2). The MBs did not affect polyplex stability and DNA remained complexed with polymer at N/P = 15.

MB cytotoxicity was assessed by incubating MBs with HeLa cells for 30 min and performing an MTS assay (**Figure S1.3**). The MBs exhibited minimal cytotoxicity as the relative cell viability across all MB types was greater than 95%.

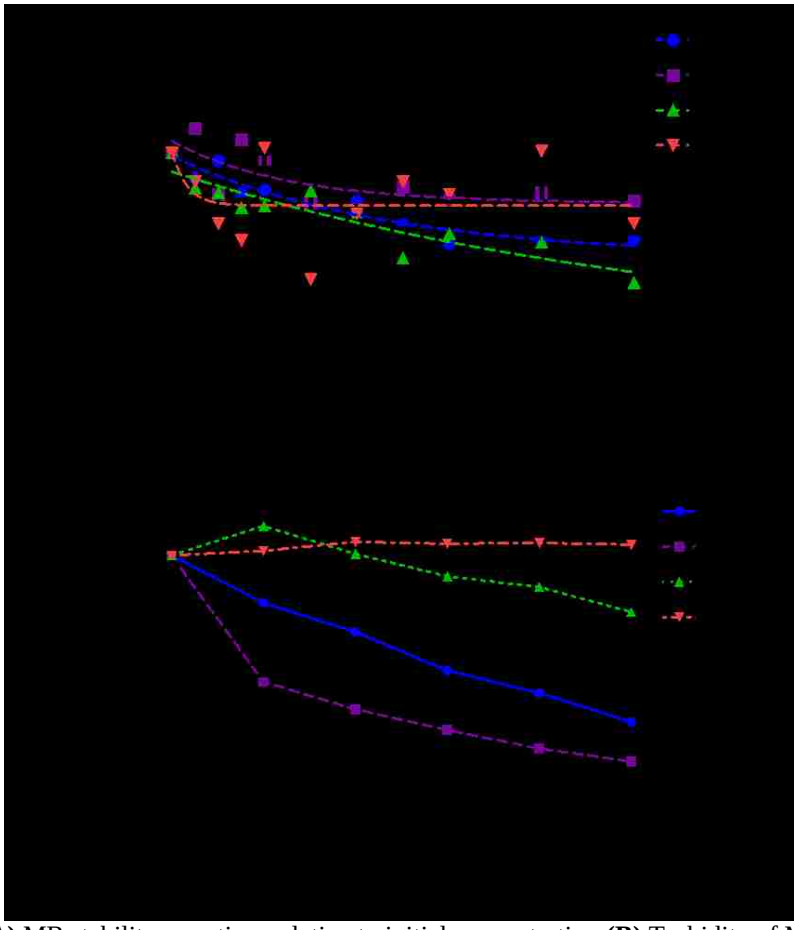

Figure 1.2 (A) MB stability over time relative to initial concentration **(B)** Turbidity of MB suspensions as measured by absorbance after US sonication. Data is presented as mean ± SD, n = 3.

Next, we monitored MB destruction in response to US from a diagnostic Sonosite Micromaxx® US machine. The Def MBs are more elastic than the custom MBs, which can lead to more dampening under US, thus raising the inertial cavitation threshold.[219,221] This was tested by sonicating the MBs and assessing MB intactness by measuring turbidity of the solution (**Figure 1.2B**). The SCat MBs easily cavitated as half of the initial MB absorbance was lost within 1 min of sonication and only about 20% remained after 5 min of sonication. The Neu MBs were a little more robust under these US conditions and about 40% of the MB absorbance remained after 5 min of sonication. The Cat and Def MBs did not cavitate as well under these US conditions. After 5 min of sonication, about 80% of the Cat MB absorbance remained while the absorbance of the Def MBs remained relatively unchanged over the 5 min of US sonication. The Def MBs seem to have a higher cavitation threshold under

these US conditions, consistent with the higher shell elastic modulus shown in **Figure 1.1A**.

1.3.2 In vitro *Z310 permeability studies*

The ability to sonoporate cell layers was assessed by monitoring choroid plexus monolayer permeability to hydrophilic tracer polymers of dextran (70 kDa) and PEG (5 kDa) (**Figure 1.3A**). Z310 choroid plexus epithelium cells were allowed to grow as monolayers in transwells as confirmed by transepithelial electrical resistance measurements (+25 **Ω** relative to blank transwells, data not shown). Microbubbles were then added to inverted cultures to allow for contact between floating MBs and cell layers and US from a Sonosite Micromaxx® applied for 15 sec with a P17 transducer. The transwells were then transferred back to culture chambers and tracers (70 kDa Texas-Red dextran and 5 kDa FITC-PEG) added to the top compartment. Permeability to tracers was determined after sonoporation by custom MBs or by commercially available Def MBs (**Figure 1.3B** and **Figure S1.4**).

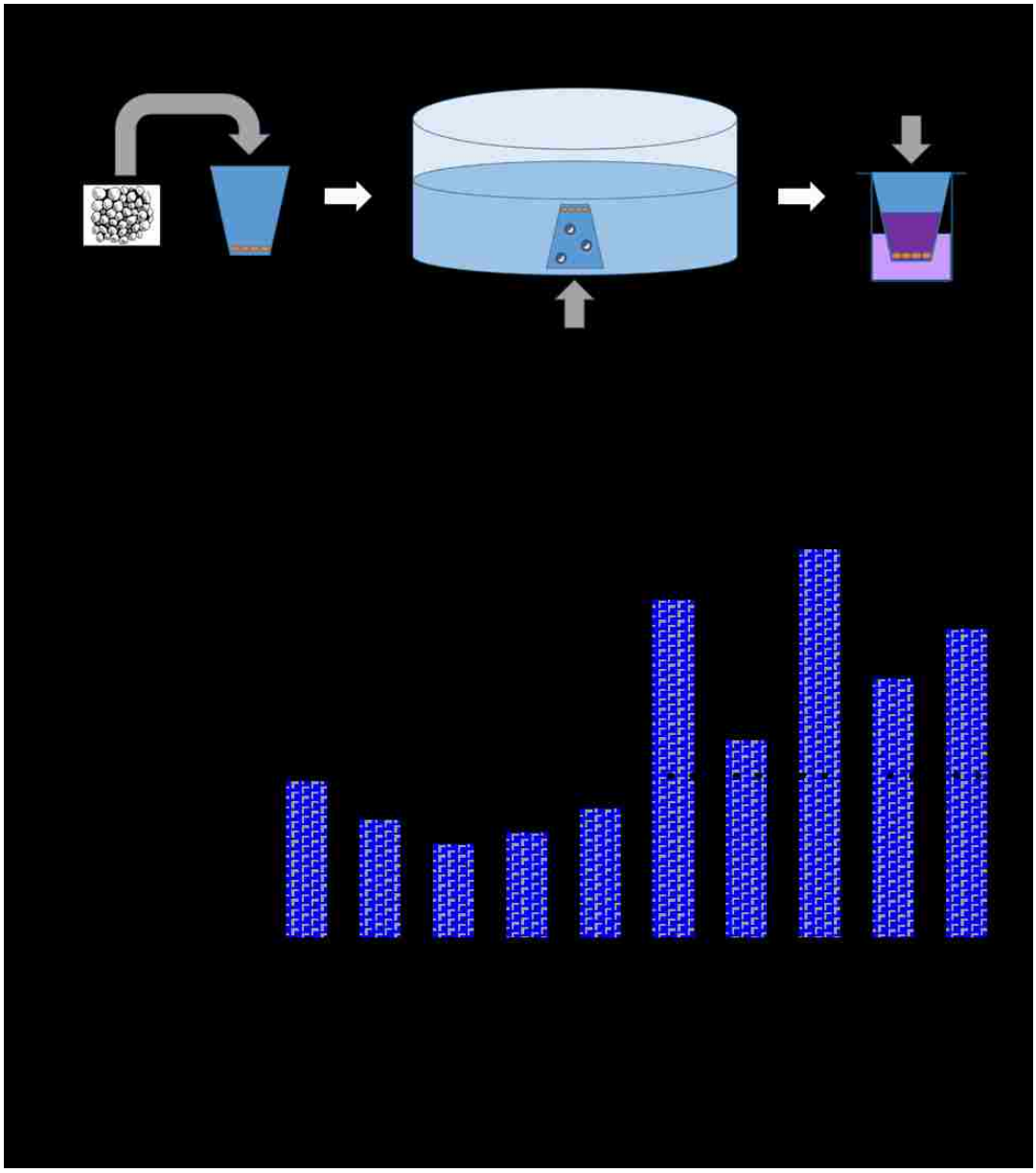

Figure 1.3 (A) Schematic of method to determine choroid plexus epithelium permeability to fluorescent polymers after MB sonoporation. Z310 choroid plexus cells were seeded in transwells and allowed to grow into a monolayer. The transwell was submerged in OptiMEM^{TM}, exposed to MBs and US, and filled with fluorescent dextran to determine leakage through to the bottom well. **(B)** Permeability of Z310 choroid plexus cell monolayers to 70 kDa Texas Red-dextran after sonoporation with MBs and US. Data is presented as mean + SD, n = 4. Statistically significant ($P < 0.05$) differences are indicated with a (*).

Monolayer permeability was unaffected by either US treatment alone or treatment with Def, Neu, or SCat MBs in the absence of ultrasound. A slight increase in permeability was observed with cationic MB treatment alone. Cationic lipids have

been shown to destabilize cell membranes and cause toxicity which may explain the slight increase in permeability without US.[156,222] With US, the Def MBs did not show an increase in sonoporation, possibly due to the higher inertial cavitation threshold afforded by the more elastic nature of the Def lipid shell and limited cavitation under these US conditions (**Figure 1.1A and Figure 1.2B**).[219,221] Conversely, the custom MBs were better able to undergo inertial cavitation, sonoporate Z310 monolayers, and increase Z310 monolayer permeability. When US was applied to the Neu or SCat MB groups, Z310 monolayer permeability doubled and was statistically significant ($P < 0.05$) when compared to Cells, US, or respective MB only groups (**Figure 1.3B** and **Figure S1.4**). More severe MB cavitation and collapse, as seen with the SCat and Neu MBs (**Figure 1.2B**), has been the most effective in generating membrane disruption and was linked to greater rates of membrane poration than when MBs undergo stable cavitation, coalescence, or translation.[223,224] In fact, greater US parameters such as frequency and pressure, which cause greater MB cavitation, are consistently linked to better delivery of macromolecules across in the blood-brain barrier in mice[98,100]. On the other hand, more subtle sonoporation, such as those at low pressures, are more closely linked to MBs interacting and "massaging" the cell membrane, causing increased endocytosis.[224,225] The ability of MBs to undergo inertial cavitation at these US conditions seem to be imperative in increasing the permeability of the Z310 monolayers.

The SCat MBs may have had the highest sonoporation and increase in permeability by being the most sensitive to cavitation under these US conditions (**Figure 1.2B**) and by closely interacting with negatively charged cell membranes by electrostatic interactions. Since the impact of MB cavitation rapidly reduces with increasing distance between the MB and cell membrane,[97] a higher sonoporation is achieved by minimizing the distance between the MB and the cell surface. This is consistent with the higher permeability seen after SCat MB sonoporation over Neu MB sonoporation. In addition, Z310 cells were analyzed by flow cytometry to measure fluorescence uptake. Treatment with SCat MBs, US, or SCat MBs + US did not increase FITC-PEG uptake relative to cells only under these experimental conditions (**Figure S1.5**). Since the SCat MBs showed the largest increase in

permeability and would interact more closely with cells by electrostatic interactions with anionic membranes, they were further evaluated *in vivo* and compared to commercially available Def MBs.

1.3.3 In vivo *transfection in mouse brain*

To determine if choroid plexus sonoporation would increase transfection in brains, polyplex and polyplex/MB formulations with the luciferase reporter gene were intraventricularly administered into murine right brains followed by 1 min of transcranial US applied with a Sonosite MicroMaxx® with a P17 transducer. Brains were harvested two days post-administration for analysis of transgene expression by bulk luciferase assay (**Figure 1.4**).

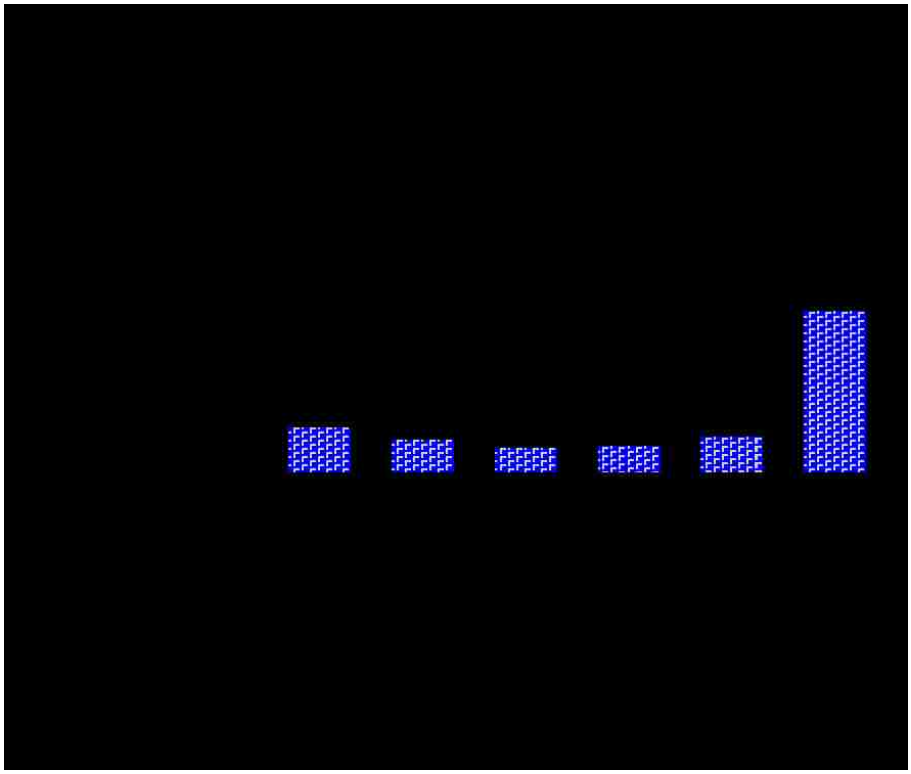

Figure 1.4 *In vivo* luciferase expression in the mouse right brain after treatment with polyplexes, MBs, and US. Data is presented as mean + SD, n = 6 or 9. Statistically significant ($P < 0.05$) differences are indicated with a (*).

Mice treated with polyplex alone resulted in luciferase activity ~10^4 relative light units (RLU)/mg protein in each part of the brain as consistent with our previous report.[47] Addition of either MBs or US separately to polyplexes did not significantly affect transfection efficiency. However, a 4.35-fold increase in luciferase expression was observed by a combination of polyplexes, SCat MBs, and US ($P < 0.05$). Increased permeability of the choroid plexus likely allowed enhanced penetration of the polyplexes and subsequently a higher transfection of cells in the SVZ area. This effect was not observed with Def MBs which is consistent with the low cavitation and sonoporation seen in the turbidity assay (**Figure 1.2B**) and in the *in vitro* permeability assay (**Figure 1.3B** and **Figure S1.4**). While current reports demonstrate the enhanced penetration of molecules like adenoviruses and dextrans across the BBB after US,[27,100,102] this study suggests that MB-enhanced US can increase the permeation of larger macromolecules such as polyplexes across the choroid plexus epithelium. In the hindbrain and left brain, the SCat and Def MBs with US had little to no effect on transfection as there was no statistically significant difference in luciferase activity among all the groups (**Figure S1.6**). This is consistent with other reports of BBB opening where enhanced permeation of molecules occurred only in the region of overlap between MB and US administration and molecules were not able to diffuse to the contralateral side.[27,102,226]

1.3.4 *Distribution of transfected cells in mouse brain*

To determine the types of cells transfected after intraventricular injection, polyplexes were formed with a green fluorescence protein (GFP) reporter plasmid and brain tissues were stained for the neural progenitor/stem cell marker, Sox2; intermediate filaments found in ependymal cells, vimentin; and nuclei (**Figure 1.5**).

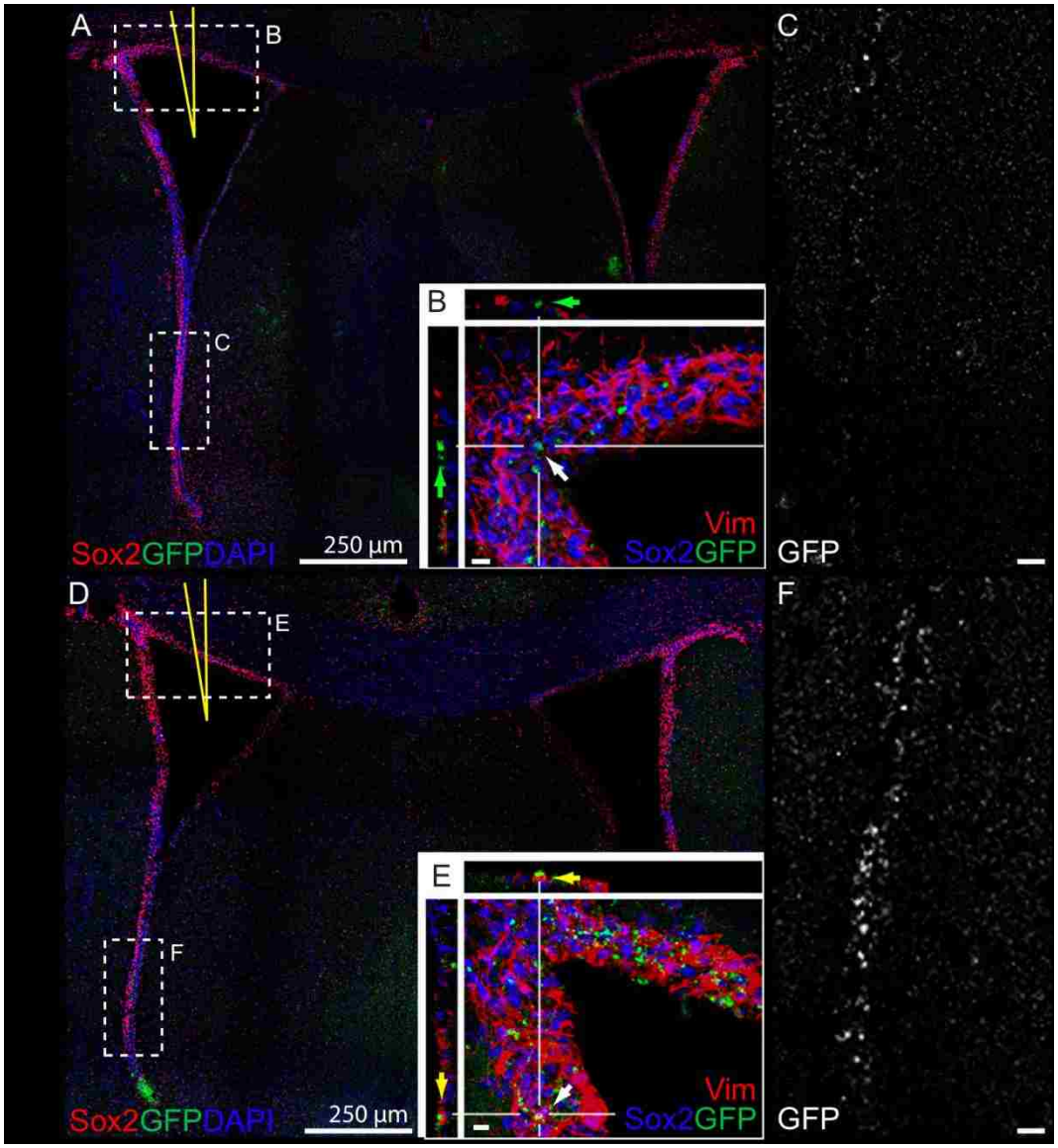

Figure 1.5 Confocal micrographs of cells expressing GFP after *in vivo* transfection with SCat MBs. Brains injected with polyplexes and SCat MBs in the lateral ventricle (**A**, yellow needle) showed a lesser number of transfected cells (GFP^+, Green) along the ependymal cells ($vimentin^+$, Red) of the dorsal aspects of the ventricle (**B**) than brains treated with SCat MBs and US (**D** & **E**). Along the ventral walls of the SVZ, more fluorescence is observed in the GFP channel images of brains treated with MBs and US (**F**) than in brains with MBs only (**C**). Small bar, 10 µm.

As seen with the luciferase expression (**Figure 1.4**), there were more transfected, GFP^+-expressing cells when polyplexes were combined with SCat MBs and US than without US. SCat MBs increased GFP expression at the dorsal surface of the ventricle walls (**Figure 1.5D** & **E**). MB sonoporation was able to increase transfection and

more GFP^+ cells are found throughout the layer of the SVZ (**Figure 1.5E**) than in the brains receiving MB treatment only (**Figure 1.5B**). In the ventricle walls, significantly more GFP expression is seen in brains treated with MBs and US as evidenced by the GFP channel pictures (**Figure 1.5C** & **F**). Even at the most ventral side, away from the injection site, there was more transfection and GFP expression upon the addition of US. In fact, propelling MBs toward the cell surface has been shown to cause pore formation and cause an influx of molecules into the cell.[225] Since US was applied to top of the skull towards the ventral side, it is likely that some of the MBs were propelled towards the ventral walls and caused permeation of cell membranes allowing for more polyplex uptake and increased transfection. Overall, the confocal images confirm the increased number of transfected cells after MB and US treatment and support the results in the luciferase analysis (**Figure 1.4**).

1.4 CONCLUSION

In this work, three MBs (Neu, SCat, and Cat) of different surface charge were formulated and compared to commercially available Def MBs. We investigated the ability of US-treated MBs to enhance the delivery of our previously-reported polyplexes into the SVZ to increase the transfection of NPCs, NSCs, and other cells. SCat MBs best sonoporated cultured choroid plexus monolayers and caused the greatest increase in permeability. These MBs and polyplexes were injected into the ventricles of mice and US was applied to sonoporate the choroid plexus barrier to the SVZ. The SCat MBs increased transfection *in vivo* better than the commercially available Def MBs or polyplexes alone. MB disruption of the choroid plexus epithelium is a viable strategy to enhance the penetration of polyplexes into the brain and merits further research.

1.5 ACKNOWLEDGMENTS

This work was supported by NIH 2R01NS064404 and Washington State Life Discover Fund (3292512). JKYT was supported by NSF GRFP (2011128558). We would like to thank: Dr. Joyce Wong for her consultation on microbubbles, Dr. Wei Zheng for providing the Z310 choroid plexus cells, Dr. Shaoyi Jiang for the use of his Zetasizer Nano ZS, Dr. Elaine Raines for the use of her EVOM instrument, and Chayanon Ngambenjawong and Nathaniel Coulson for their assistance with experiments.

1.6 SUPPLEMENTARY FIGURES

1.6.1 *MB stability in presence of polyplexes*

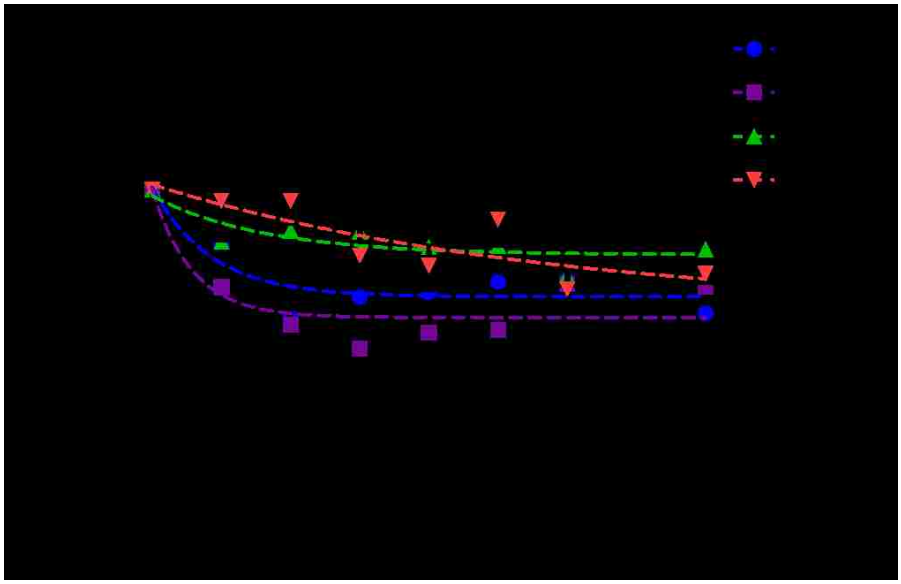

Figure S1.1 MB stability in the presence of polyplexes over time relative to initial concentration. Data is presented as mean ± SD, n = 3.

1.6.2 *Polyplex stability in presence of MBs*

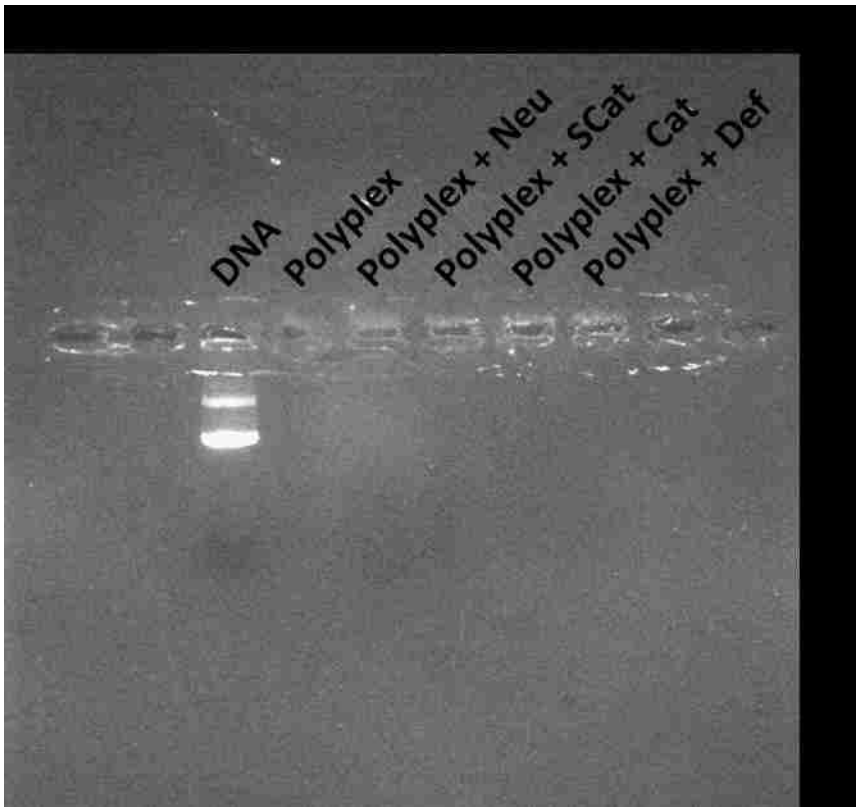

Figure S1.2 Gel retardation assay for polyplexes (N/P = 15) in the presence of Neu, SCat, Cat, and Def MBs. A moving band indicates incomplete complexation while an unmoved band indicates complete complexation with DNA.

1.6.3 *Cell viability in presence of MBs*

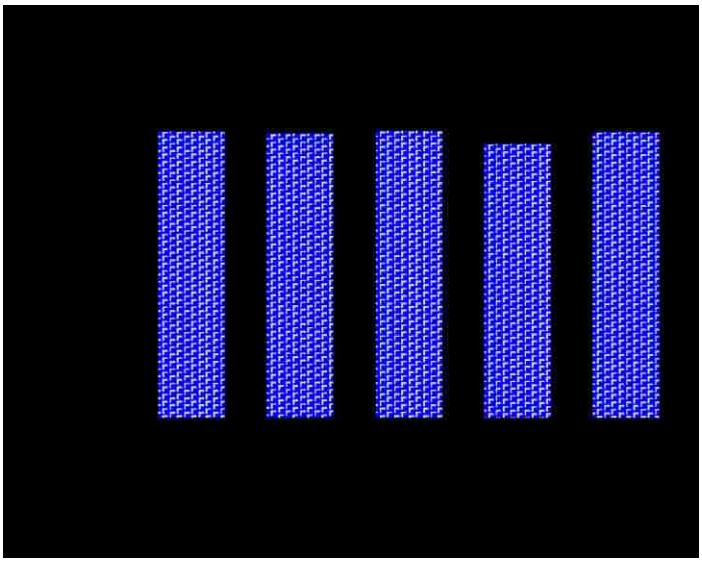

Figure S1.3 Relative cell viability of HeLa cells in the presence of Neu, SCat, Cat, and Def MBs.

1.6.4 *Permeability of Z310 choroid plexus monolayers to 5 kDa FITC-PEG*

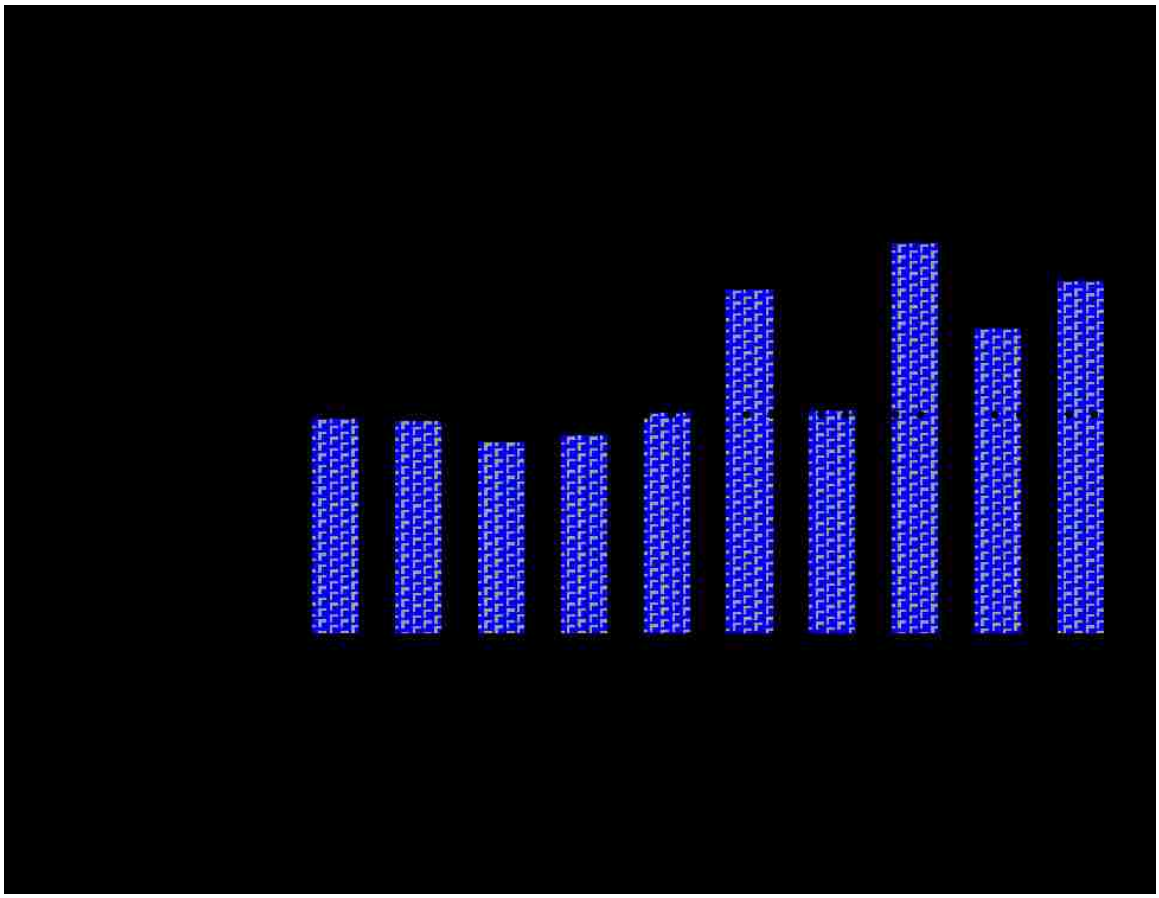

Figure S1.4 Permeability of Z310 choroid plexus cell monolayers to 5 kDa FITC-PEG after sonoporation with MBs and US. Data is presented as mean + SD, n = 4. Statistically significant ($P < 0.05$) differences are indicated with a (*)

1.6.5 *Fluorescence uptake after sonoporation*

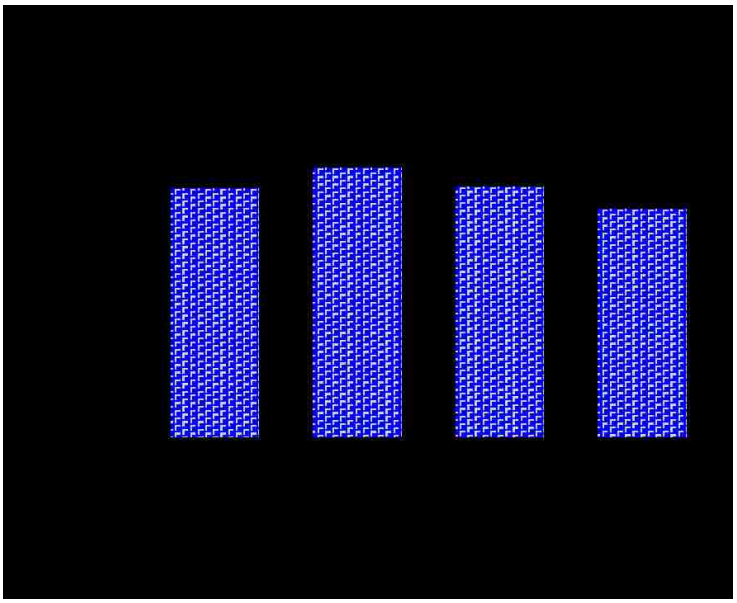

Figure S1.5 Relative median fluorescence intensity (MFI) of intracellular 5 kDa FITC-PEG in Z310 cells after transwell sonoporation by SCat MBs. Data is presented as mean + SD, n = 3.

1.6.6 In vivo *luciferase expression in the mouse hindbrain and left brain*

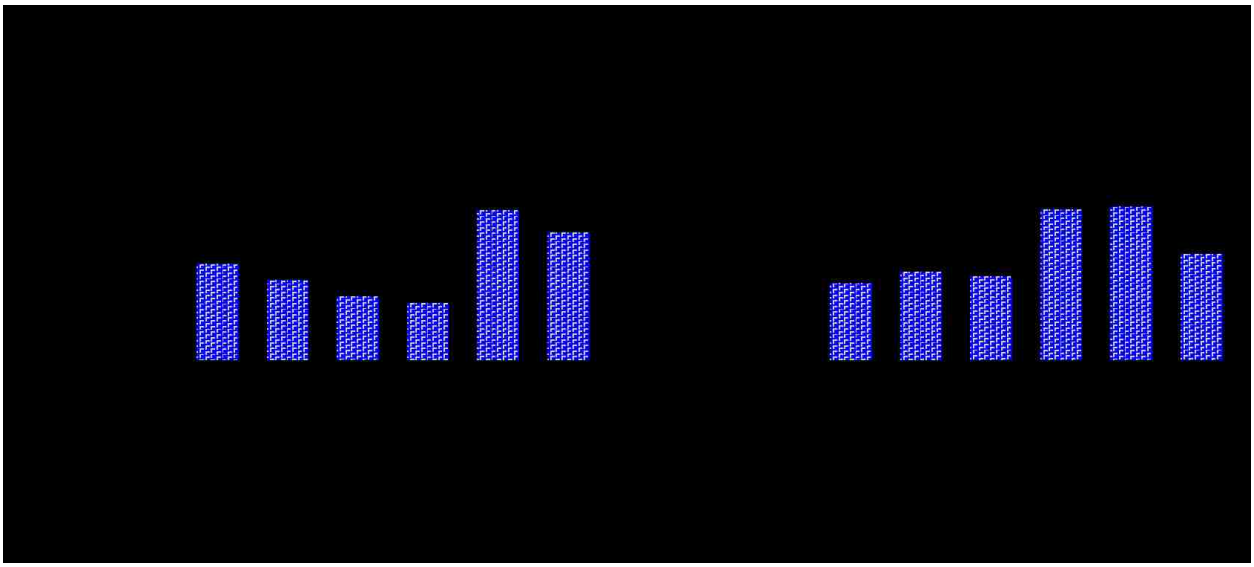

Figure S1.6 *In vivo* luciferase expression in mouse **(a)** hindbrain and **(b)** left brain after treatment with polyplexes, MBs, and US. Data is presented as mean + SD, n = 6 or 9.

1.7 REFERENCES

3. Sawada, M. & Sawamoto, K. Mechanisms of Neurogenesis in the Normal and Injured Adult Brain. *Keio J. Med.* **62,** 13–28 (2013).

4. Parent, J. M., Vexler, Z. S., Gong, C., Derugin, N. & Ferriero, D. M. Rat forebrain neurogenesis and striatal neuron replacement after focal stroke. *Ann. Neurol.* **52,** 802–13 (2002).

5. Arvidsson, A., Collin, T., Kirik, D., Kokaia, Z. & Lindvall, O. Neuronal replacement from endogenous precursors in the adult brain after stroke. *Nat. Med.* **8,** 963–70 (2002).

15. Saha, B., Peron, S., Murray, K., Jaber, M. & Gaillard, A. Cortical lesion stimulates adult subventricular zone neural progenitor cell proliferation and migration to the site of injury. *Stem Cell Res.* **11,** 965–77 (2013).

16. Zheng, W. *et al.* Neurogenesis in adult human brain after traumatic brain injury. *J. Neurotrauma* **30,** 1872–80 (2013).

25. Dodge, J. C. *et al.* AAV4-mediated expression of IGF-1 and VEGF within cellular components of the ventricular system improves survival outcome in familial ALS mice. *Mol. Ther.* **18,** 2075–84 (2010).

27. Weber-Adrian, D. *et al.* Gene delivery to the spinal cord using MRI-guided focused ultrasound. *Gene Ther.* 1–10 (2015). doi:10.1038/gt.2015.25

29. Matsuoka, N. *et al.* Adenovirus-mediated gene transfer of fibroblast growth factor-2 increases BrdU-positive cells after forebrain ischemia in gerbils. *Stroke.* **34,** 1519–25 (2003).

34. Goldman, S. Stem and progenitor cell-based therapy of the human central nervous system. *Nat. Biotechnol.* **23,** 862–71 (2005).

47. Wei, H. *et al.* Dual responsive, stabilized nanoparticles for efficient in vivo plasmid delivery. *Angew. Chem. Int. Ed. Engl.* **52,** 5377–81 (2013).

48. Tan, J.-K. Y., Choi, J. L., Wei, H., Schellinger, J. G. & Pun, S. H. Reducible, dibromomaleimide-linked polymers for gene delivery. *Biomater. Sci.* **3,** 112–120 (2015).

52. Mortazavi, M. M. *et al.* The choroid plexus: A comprehensive review of its history, anatomy, function, histology, embryology, and surgical considerations. *Child's Nerv. Syst.* **30,** 205–214 (2014).

54. Pardridge, W. M. Drug transport in brain via the cerebrospinal fluid. *Fluids Barriers CNS* **8,** 7 (2011).

59. McDannold, N., Arvanitis, C. D., Vykhodtseva, N. & Livingstone, M. S. Temporary disruption of the blood-brain barrier by use of ultrasound and microbubbles: safety and

efficacy evaluation in rhesus macaques. *Cancer Res.* **72,** 3652–63 (2012).

61. Panje, C. M., Wang, D. S. & Willmann, J. K. Ultrasound and microbubble-mediated gene delivery in cancer: progress and perspectives. *Invest. Radiol.* **48,** 755–69 (2013).

62. Meairs, S., Alonso, A., Fatar, M., Kern, R. & Hennerici, M. Microbubbles traversing the blood-brain barrier for imaging and therapy. *Med. Biol. Eng. Comput.* **47,** 839–49 (2009).

66. Kaspar, B. K., Lladó, J., Sherkat, N., Rothstein, J. D. & Gage, F. H. Retrograde viral delivery of IGF-1 prolongs survival in a mouse ALS model. *Science* **301,** 839–42 (2003).

94. Rychak, J. J. & Klibanov, A. L. Nucleic acid delivery with microbubbles and ultrasound. *Adv. Drug Deliv. Rev.* **72,** 82–93 (2014).

95. Meairs, S. & Alonso, A. Ultrasound, microbubbles and the blood-brain barrier. *Prog. Biophys. Mol. Biol.* **93,** 354–62 (2007).

96. Greenleaf, W. & Bolander, M. Artificial cavitation nuclei significantly enhance acoustically induced cell transfection. *Ultrasound Med. …* **24,** 587–595 (1998).

97. Zhou, Y., Yang, K., Cui, J., Ye, J. & Deng, C. Controlled permeation of cell membrane by single bubble acoustic cavitation. *J. Control. Release* **157,** 103–111 (2012).

98. Choi, J. J., Pernot, M., Small, S. a & Konofagou, E. E. Noninvasive, transcranial and localized opening of the blood-brain barrier using focused ultrasound in mice. *Ultrasound Med. Biol.* **33,** 95–104 (2007).

99. Choi, J. J., Wang, S., Tung, Y.-S., Morrison, B. & Konofagou, E. E. Molecules of various pharmacologically-relevant sizes can cross the ultrasound-induced blood-brain barrier opening in vivo. *Ultrasound Med. Biol.* **36,** 58–67 (2010).

100. Choi, J. J. *et al.* Noninvasive and localized blood-brain barrier disruption using focused ultrasound can be achieved at short pulse lengths and low pulse repetition frequencies. *J. Cereb. Blood Flow Metab.* **31,** 725–37 (2011).

101. Xie, F. *et al.* Effects of transcranial ultrasound and intravenous microbubbles on blood brain barrier permeability in a large animal model. *Ultrasound Med. Biol.* **34,** 2028–34 (2008).

102. Sheikov, N., McDannold, N., Vykhodtseva, N., Jolesz, F. & Hynynen, K. Cellular mechanisms of the blood-brain barrier opening induced by ultrasound in presence of microbubbles. *Ultrasound Med. Biol.* **30,** 979–89 (2004).

114. Choi, J. L. *et al.* Guanidinylated block copolymers for gene transfer : A comparison with amine-based materials for in vitro and in vivo gene transfer ef fi ciency. *Biomaterials* **54,** 87–96 (2015).

206. Chodobski, A. & Szmydynger-chodobska, J. Choroid plexus: target for polypeptides and

site of their synthesis. *Microsc. Res. Tech.* **52,** 65–82 (2001).

207. Wang, S., Samiotaki, G., Olumolade, O., Feshitan, J. a & Konofagou, E. E. Microbubble type and distribution dependence of focused ultrasound-induced blood-brain barrier opening. *Ultrasound Med. Biol.* **40,** 130–7 (2014).

208. Feshitan, J. a, Chen, C. C., Kwan, J. J. & Borden, M. a. Microbubble size isolation by differential centrifugation. *J. Colloid Interface Sci.* **329,** 316–24 (2009).

209. Matula, T. J., Swalwell, J., Tu, J., Cui, W. & Chen, W. Flow cytometry to characterize microbubbles. *2011 IEEE Int. Ultrason. Symp.* 156–159 (2011). doi:10.1109/ULTSYM.2011.0039

210. Tu, J. *et al.* Microbubble sizing and shell characterization using flow cytometry. *IEEE Trans. Ultrason. Ferroelectr. Freq. Control* **58,** 955–963 (2011).

211. Cavalieri, F. *et al.* Mechanical characterization of ultrasonically synthesized microbubble shells by flow cytometry and AFM. *ACS Appl. Mater. Interfaces* **5,** 10920–10925 (2013).

212. Doinikov, A. a., Haac, J. F. & Dayton, P. a. Modeling of nonlinear viscous stress in encapsulating shells of lipid-coated contrast agent microbubbles. *Ultrasonics* **49,** 269–275 (2009).

213. Zheng, W. & Zhao, Q. Establishment and characterization of an immortalized Z310 choroidal epithelial cell line from murine choroid plexus. *Brain Res.* **958,** 371–80 (2002).

214. Shi, L., Li, G., Wang, S. & Zheng, W. Use of Z310 cells as an in vitro blood–cerebrospinal fluid barrier model: Tight junction proteins and transport properties. *Toxicol. Vitr.* **22,** 190–199 (2008).

215. Wang, S., Olumolade, O. O., Sun, T., Samiotaki, G. & Konofagou, E. E. Noninvasive, neuron-specific gene therapy can be facilitated by focused ultrasound and recombinant adeno-associated virus. *Gene Ther.* **22,** 104–110 (2014).

216. Wu, S.-Y., Chen, C. C., Tung, Y.-S., Olumolade, O. O. & Konofagou, E. E. Effects of the Microbubble Shell Physicochemical Properties on Ultrasound-Mediated Drug Delivery to the Brain. *J. Control. Release* **212,** 30–40 (2015).

217. Wang, D. *et al.* Cationic versus neutral microbubbles for ultrasound-mediated gene delivery in cancer. *Radiology* **264,** 721–732 (2012).

218. Sun, R. R., Noble, M. L., Sun, S. S., Song, S. & Miao, C. H. Development of therapeutic microbubbles for enhancing ultrasound-mediated gene delivery. *J. Control. Release* **182,** 111–20 (2014).

219. Guo, X., Li, Q., Zhang, Z., Zhang, D. & Tu, J. Investigation on the inertial cavitation threshold and shell properties of commercialized ultrasound contrast agent microbubbles. *J. Acoust. Soc. Am.* **134,** 1622 (2013).

220. Dicker, S. *et al.* Influence of Shell Composition on the Resonance Frequency of Microbubble Contrast Agents. *Ultrasound Med. Biol.* **39,** 1292–1302 (2013).

221. Dicker, S., Mleczko, M., Schmitz, G. & Wrenn, S. P. Determination of microbubble cavitation threshold pressure as function of shell chemistry. *Bubble Sci. Eng. Technol.* **2,** 55–64 (2010).

222. Dass, C. R. Oligonucleotide delivery to tumours using macromolecular carriers. *Biotechnol. Appl. Biochem.* **40,** 113–122 (2004).

223. Fan, Z., Chen, D. & Deng, C. X. Improving ultrasound gene transfection efficiency by controlling ultrasound excitation of microbubbles. *J. Control. Release* **170,** 401–13 (2013).

224. Delalande, A., Leduc, C., Midoux, P., Postema, M. & Pichon, C. Efficient Gene Delivery by Sonoporation Is Associated with Microbubble Entry into Cells and the Clathrin-Dependent Endocytosis Pathway. *Ultrasound Med. Biol.* 1–14 (2015). doi:10.1016/j.ultrasmedbio.2015.03.010

225. Cock, I. De *et al.* Ultrasound and microbubble mediated drug delivery : Acoustic pressure as determinant for uptake via membrane pores or endocytosis. *J. Control. Release* **197,** 20–28 (2015).

226. Samiotaki, G., Acosta, C., Wang, S. & Konofagou, E. E. Enhanced delivery and bioactivity of the neurturin neurotrophic factor through focused ultrasound — mediated blood – brain barrier opening in vivo. *J. Cereb. Blood flow Metab.* 1–12 (2015). doi:10.1038/jcbfm.2014.236

Chapter 2. Sonoporation of the Choroid Plexus with Targeted Microbubbles and Ultrasound for Gene Transfer to the Brain

James-Kevin Y. Tan, Drew L. Sellers, Christina Keravnou, Ine de Cock, Yilong Cheng, Philip J. Horner, Suzie H. Pun

This chapter is in preparation for manuscript submission.

Synopsis:

Physiological barriers such as cell-cell junctions are necessary protective structures but also prevent the absorption and distribution of therapeutics. Microbubble-mediated ultrasound has shown to sonoporate, or transiently disrupt, cellular barriers by permeating cell membranes and opening tight junctions. Previously, we demonstrated that sonoporation of the choroid plexus epithelium, the lining of the brain ventricles, was a viable way to increase gene transfection to the brain after intraventricular injection. Herein, we aimed to further enhance transfection by using targeted microbubbles and ultrasound to transiently open the choroid plexus. By targeting microbubbles to the surface of the ependymal barrier, a greater sonoporation would occur due to a higher number of microbubbles at the surface and a shorter distance between microbubble cavitation and cells. TAT-decorated microbubbles were developed and were similar in size and concentration to untargeted slightly cationic microbubbles. Liposomal analogs of the targeted microbubbles better bound to cultured choroid plexus epithelium cells than untargeted microbubbles. *In vivo,* targeted microbubbles performed on par with untargeted microbubbles. Further characterization and studies to optimize the acoustics of the targeted microbubbles will be needed in order to accurately compare the two microbubbles.

Keywords: gene delivery, targeted microbubble, polyplex, ultrasound, *in vivo*, choroid plexus epithelium

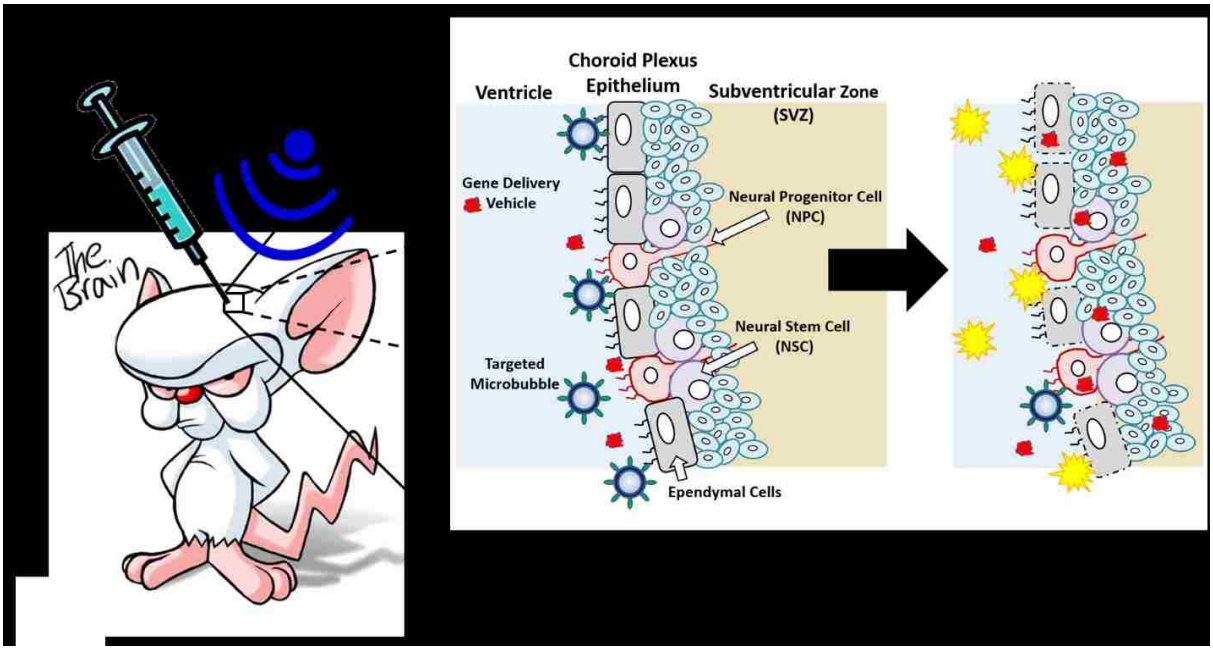
The Brain
Choroid Plexus
Epithelium
Ventricle
Subventricular Zone
(SVZ)
Gene Delivery
Vehicle
Neural Progenitor Cell
(NPC)
Neural Stem Cell
(NSC)
Targeted
Microbubble
Ependymal Cells

2.1 INTRODUCTION

A major problem in drug delivery is transporting cargo past the natural protective barriers of the human body. Whether it be the skin,[227] blood-brain barrier,[57] or the choroid plexus epithelium,[52,54] these hurdles significantly prevent the absorption and distribution of therapeutics to their target sites. Recently, microbubbles (MBs), or gas-filled microspheres, have been coupled with ultrasound (US) as a technique to transiently disrupt cellular barriers. With US, MBs can oscillate under the acoustic pressure differences and cavitate to permeabilize cell membranes, break up tight junctions, and enhance the penetration of materials into surrounding tissues in a process known as sonoporation.[61,94,95,97] Many groups have used MB-enhanced US as a way to transiently open the blood-brain barrier and deliver different materials in animals such as mice,[98–100,207,216,226,228] rats,[27,103,229,230] pigs,[101] and monkeys[59,60] with minimal safety concerns. Recently, we applied sonoporation to the choroid plexus, a barrier of ependymal cells that lines the cavities of the brain ventricles.[54,206] These ependymal cells are held together by tight junctions and prevent materials from entering the brain parenchyma after intraventricular injection.[52] When co-administered with our polymeric gene delivery vehicles, MB-mediated sonoporation was able to augment luciferase transfection by over 4-fold compared to vehicles alone.[120]

More advanced, targeted MBs decorated with various homing ligands such peptides, proteins, and antibodies have started to show improved localization and binding to tissues of interest.[231] Targeted MBs have the potential to augment sonoporation by increasing the number of MBs at the area of interest and by decreasing the distance between MB cavitation and the intended tissues. The use of targeting ligands has already shown to increase MB localization in expected areas which lead to enhanced contrast and improved diagnosis of angiogenesis, early atherosclerosis, intracardiac thrombus, and vulnerable plaques in different animal models.[231–234] Furthermore, being in close proximity to the cells of interest allows for a stronger sonoporation since the impact of MB cavitation is inversely proportional to the distance from the MB.[97] In fact, at 2-5 times lower acoustic pressures, targeted MBs bound to cells could induce the same levels of sonoporation as untargeted MBs at higher acoustic pressures.[235] In another example, targeted MBs that were bound to ischemic myocardium were able to significantly increase gene transfection over untargeted MBs.[236]

In this work, we sought to further improve gene transfer to the brain with a next-generation targeted MB coupled with a more advanced synthetic gene delivery vehicle, virus-inspired polymer for endosomal release (VIPER). This polymer is composed of a cationic block, poly(oligo(ethylene glycol) monomethyl ether methacrylate)-*co*-poly(2-(dimethylamino)ethyl methacrylate) (p(OEGMA-DMAEMA)), for nucleic acid condensation and a pH-sensitive block, poly(2-diisopropylaminoethyl methacrylate)-*co*-poly(pyridyl disulfide ethyl methacrylate) (p(DIPAMA-PDSEMA)), for triggered display of a membrane lytic peptide, melittin, in acidic conditions [paper submitted]. VIPER polyplexes, or polymer-DNA complexes, showed membrane-lytic activity only in the acidic conditions of the cell endosome and were able to efficiently mediate release into the cytoplasm. For targeting the choroid plexus epithelium, we decorated MBs with the non-discriminantly cell-binding peptide, TAT, since choroid plexus ependymal cells are the main cell type in the ventricles.[52,206] The TAT peptide is a cationic peptide derived from the transduction domain of HIV-1 and it tightly and rapidly interacts with cell membranes.[237,238] We hypothesized that co-administration of the polyplexes and targeted MBs into the brain ventricle would further increase sonoporation of the choroid plexus epithelium due to the greater number and close proximity of MBs at the ependymal surface, thus achieving higher transfection.

2.2 MATERIALS AND METHODS

2.2.1 *Materials*

Lipids were purchased from Avanti Polar Lipids, Inc. (Alabaster, AL) except for 1,2-distearoyl-*sn*-glycero-3-phosphoethanolamine-*N*-[azido(polyethylene glycol)5000] (DSPE-PEG5000-Azide) and 1,2-distearoyl-*sn*-glycero-3-phosphoethanolamine-*N*-[fluorescein(polyethylene glycol)5000] (DSPE-PEG5000-Fluorescein) which were from Nanocs (New York, NY). Perfluorobutane (PFB) was purchased from Synquest Laboratories (Alachua, FL) and a Vialmix® machine was from Lantheus Medical Imaging (N. Billerica, MA). TAT-dibenzocyclooctyne (TAT-DBCO: GRKKRRQRRRK-DBCO) was purchased from Elim Biopharmaceuticals (Hayward, CA). The Z310 choroid plexus cell line was a generous gift from Dr. Wei Zheng at Purdue University. Tissue culture reagents and bicinchoninic acid (BCA)

protein quantification assay kit were purchased from Thermo Fisher Scientific (Waltham, MA). The pCMV-Luc2 plasmid was isolated using the Qiagen Plasmid Giga Kit (Hilden, Germany) while the reporter lysis buffer and luciferase expression quantification kit were obtained from Promega (Madison, WI).

2.2.2 *TAT-lipid conjugation and characterization*

DSPE-PEG5000-Azide (10 mg, 1.72 μmol) and TAT-DBCO (5.39 mg, 2.06 μmol) were dissolved in DMSO (425 μL) in a tube and allowed to mix overnight at room temperature. DSPE-PEG5000-Azide and DSPE-PEG5000-TAT were analyzed by HPLC in a Kinetex C18 column (Phenomenex, Torrance, CA) on a 15-40% ACN gradient over 30 min.

2.2.3 *MB formation and physical characterization*

MBs were formulated by mixing a total of 1 mg of different chloroform-dissolved lipids in a 2 mL tube followed by overnight drying under vacuum. The untargeted, SCat MBs were formulated at a 9:1 molar ratio of 1,2-distearoyl-sn-glycero-3-phosphocholine (DSPC) and 1,2-distearoyl-*sn*-glycero-3-phosphoethanolamine-*N*-[amino(polyethylene glycol)5000] (DSPE-PEG5000-Amine). Targeted, TAT-slightly cationic (SCat) MBs were formulated at a 9:0.5:0.5 molar ratio of DSPC, DSPE-PEG5000-Amine, and DSPE-PEG5000-TAT. Lipid films were rehydrated in a 1 mL solution of 10:10:80 (v/v/v) glycerol:propylene glycol:water at 67 °C. The tube headspace was filled with PFB and amalgamated with a Vialmix® machine for 45 s. The MB suspension was processed by differential centrifugation to remove micelles/free lipids and to isolate MBs with diameters less than 2 μm as previously described.[208] MB diameter and concentration were determined by a Beckman Coulter Multisizer 3 (Brea, CA).

2.2.4 *MB acoustic characterization and cavitation*

Acoustic characterization of the MB response to US was carried out in a flow phantom setup as previously reported.[239] Briefly, freshly prepared MB solutions were continuously mixed in a beaker and peristaltically pumped into an 8-mm wall-less

tube in a tissue-mimicking flow phantom (Model 523A; ATS Laboratories Inc., Bridgeport, CT) at a flow rate of 200 mL/min. A C5-1 probe (curved linear array) or an L9-3 probe (linear array) attached to a Philips iU-22 diagnostic US scanner (Bothell, WA) was used to interrogate and image the MBs at different frequencies and mechanical indices (MIs) to identify MB cavitation. The frame rate was set at 1.0 Hz to ensure that the tube in the image plane was refreshed with new bubbles in every frame. Images were taken using a second harmonic amplitude.

2.2.5 *Polymer synthesis*

The VIPER polymer (p(OEGMA$_{11}$-DMAEMA$_{56}$)-*b*-p(DIPAMA$_{25}$-(PDSEMA-melittin)$_1$) was synthesized and characterized as previously reported [paper submitted]. Briefly, OEGMA and DMAEMA polymers were formed by RAFT polymerization with AIBN initiator and CPADB chain transfer agent (CTA). This polymer was used as a macro-CTA to polymerize DIPAMA and PDSEMA to form the block, statistical copolymer: p(OEGMA-DMAEMA)-*b*-p(DIPAMA-PDSEMA). The membrane lytic portion, melittin-cys peptide (GIGAVLKVLTTGLPALISWIKRKRQQC), was conjugated to the polymer by disulfide exchange reaction. The polymer was characterized by ^{1}H NMR, SEC, and UV absorbance.

2.2.6 *Polyplex formation*

The pCMV-Luc2 plasmid was diluted in double-distilled H_2O (ddH2O) to a concentration of 0.1 mg/mL and mixed with an equal volume of polymer (in ddH_2O) at an amine-to-phosphate (N/P) ratio = 15. The required amount of polymer was calculated by determining the polymer mass-to-charge ratio and taking into account that 1 μg of DNA contains 3 nmol of phosphate. After mixing, the polyplexes were allowed to form for 30 min at room temperature.

2.2.7 *Liposome binding to Z310 cells*

Immortalized Z310 choroid plexus cells were cultured in 10% heat-inactivated FBS, 1% penicillin–streptomycin, 40 μg/mL gentamicin, and 10 ng/mL endothelial growth

factor-supplemented DMEM culture medium as previously described.[213,214] Lipid films of the different MBs were prepared as described above except that 10% of the total amount of various DSPE-PEG5000 lipids were replaced with DSPE-PEG5000-Fluorescein to monitor binding. The films were dissolved in 1 mL solution of 10:10:80 (v/v/v) glycerol:propylene glycol:water at 67 °C to from liposomes and characterized by a Multisizer 3. Polyplexes (1 μg DNA) and liposomes (1.25×10^7 liposomes/μg DNA) in 1% (w/v) albumin in PBS were dispensed into each well of a 96-well plate with 10,000 adhered Z310 cells and allowed to bind to cells for 20 min. Subsequently, the wells were washed and the fluorescence was measured (ex: 495 nm, em: 515 nm).

2.2.8 *Transfection with insonified MBs and polyplexes*

Z310 were cultured as stated above and seeded into a 24-well plate at a density of 3.0×10^4 cells per well. Cells were placed in a 37 °C, 5% CO2, humidified incubator for 16 hours prior to transfection (~60% confluency at time of polymer addition). Polyplexes were formed as previously described at N/P = 15 using 0.5 μg of pCMV-Luc2 plasmid DNA in 20 μL of total volume. MBs (1.25×10^7 MBs/μg DNA) were added to the solution and brought to 200 μL with OptiMEM™. Solutions were sonicated in microcentrifuge tubes underwater for 1 min with either a 1 MHz transducer (custom built) or 3.5 MHz transducer (Olympus, Waltham, MA) connected to an RF power amplifier (Electronics & Innovation, Rochester, NY) and an AFG3102C function generator (Tektronix, Beaverton, OR). Solutions were then aliquoted into the well plate with Z310 cells and after 4 hrs, polyplexes were washed off and replaced with fresh complete media. After an additional 44 hours, cells were lysed and analyzed by a luciferase quantification expression kit and BCA assay for total protein content. Protein content was used to normalize luciferase expression as well as quantify cell population viability.

2.2.9 In vivo *US optimization for luciferase transfection*

All animal procedures were completed using protocols approved by the Institutional Animal Care and Use Committee at the University of Washington. Luciferase

reporter polyplexes were prepared in 5% glucose using 2.5 μg of DNA in 10 μL total volume at an N/P = 15 as previously described.[48] Adult (8-9 weeks) female C57BL/6J mice (Jackson Laboratories) were anesthetized by an intraperitoneal injection of Avertin. A 1 mm diameter craniotomy was made on the right side of the skull using a dental drill and 10 μL of polyplex or polyplex/MB suspension at 1.25×10^7 MBs/μg DNA was stereotaxically injected at 1 mm lateral, 0.5 mm caudal to bregma, and 1.9 mm depth from the dura using a 33 gauge 10 μL Hamilton syringe. The injection was made over 2.5 minutes and the syringe was kept in place for 2 minutes after injection to prevent backflow. Afterwards, either a previously described 1 MHz or 3.5 MHz transducer was held to the mouse skull and US was applied for 15 s, rested for 15 s, and repeated for a total of 2 min.

2.2.10 *Luciferase expression analysis*

Brains were harvested from mice 48 hours post injection and separated into three sections: hindbrain, left brain, and right brain. Tissues were collected in 1X reporter lysis buffer (RLB, Promega Corp., Madison, WI) with 1X EDTA-free Roche's Complete Protease Inhibitor Cocktail (Roche, Nutley, NJ) and three freeze-thaw cycles were performed in liquid nitrogen. Tissues were mechanically homogenized and cell debris were pelleted at 15,000 *g* for 15 min at 4 °C. The lysates were collected and analyzed by a luciferase assay kit (integration time = 1 s) and by the BCA assay to normalize luciferase expression by protein content.

2.2.11 *Statistical Analysis*

All statistical analyses were performed using a two-tailed Student's t-test with unequal variance.

2.3 RESULTS AND DISCUSSION

Previously, we investigated the application of MBs and US as a way to increase the permeation of our polyplex gene delivery vehicles through the choroid plexus epithelium into the subventricular zone after intraventricular brain injection. The MBs were able to increase the permeability of choroid plexus cell monolayers *in vitro* and well as increase the transfection of the murine brain *in vivo* by over 4-fold compared to polyplexes alone.[120] Herein, we aimed to develop the next-generation of MBs with a more specific and increased magnitude of disruption by targeting the MBs to the choroid plexus epithelium. We hypothesized a stronger sonoporation will be experienced due to the closer proximity and larger number of MBs at the ependymal barrier due to the active targeting of MBs.

2.3.1 *Microbubble and polyplex characterization*

Since the cellular barrier of interest lines the fluid cavity of the site of injection, the cationic peptide, TAT, was chosen as the targeting ligand due to its ability to rapidly and tightly bind to cell membranes.[237,238] TAT-DBCO peptide was reacted with DSPE-PEG5000-Azide lipid to first form a peptide-lipid conjugate that was used to form the targeted MBs. HPLC analysis confirmed the successful conjugation of the TAT peptide (**Figure S2.1**). To generate the targeted TAT-SCat MB, half of the DSPE-PEG5000-Amine lipids of the SCat MB formulation were replaced with DSPE-PEG5000-TAT lipids (**Table 2.1**).

TABLE 2.1 LIPID COMPOSITION OF MBS

MBs were prepared from rehydrated lipid films with perfluorobutane using a Vialmix® amalgamator. Both MBs were similar in size (~1 μm) and concentration (~10^{10} MBs/mL) to each other and to similar lipid MBs of other reports (**Table 2.2**).[217,218]

TABLE 2.2 PHYSICAL CHARACTERIZATION OF TARGETED AND UNTARGETED MBS

Next, the MBs were acoustically characterized by a Philips Medical Systems iU-22 diagnostic US scanner at two different frequencies, 1.7 and 3.1 MHz.

MBs in a flow phantom were visible at both frequencies and across a series of mechanical (MIs) as similar with other MBs (**Figure S2.2**).[239,240] In addition, MB destruction was quantified across the different US conditions (**Figure 2.1**). At 1.7 MHz, the TAT-SCat MBs were completely destroyed at an MI of 0.15 while the SCat MBs needed an MI of 0.3 for complete destruction. At 3.1 MHz, the TAT-SCat MBs were completely burst at an MI of around 0.35 while the SCat MBs completely cavitated at an MI of 0.15. While these results are preliminary, the addition of the TAT peptide to the surface of the MB does seem to change the acoustic properties of the MB shell. More studies will be done as confirmation and to further characterize the two MBs so that the optimal US settings can be narrowed down.

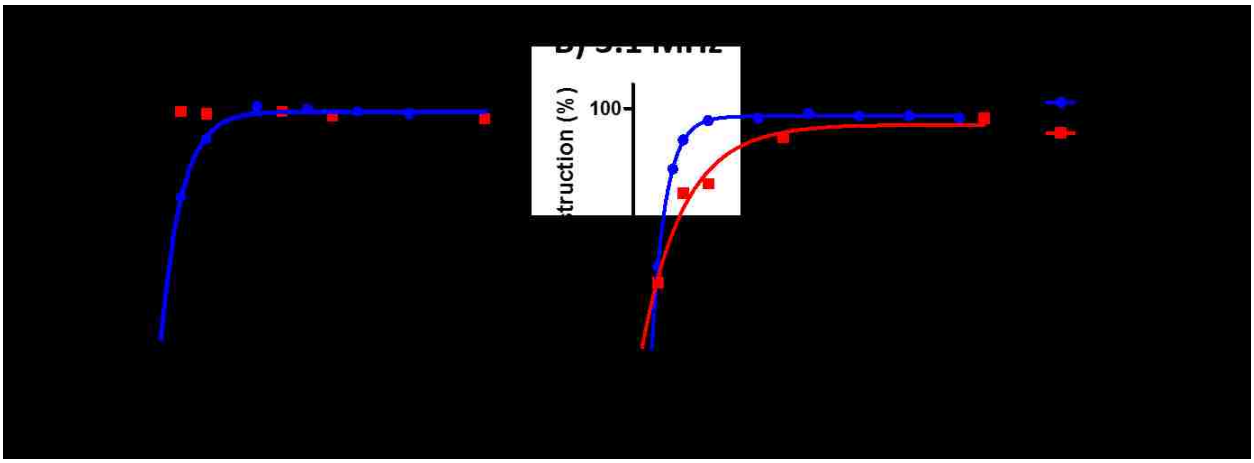

Figure 2.1 Percent destruction of untargeted SCat and targeted TAT-SCat MBs at different frequencies and mechanical indices (MI). Data is presented as mean.

The DNA condensing copolymer, VIPER, was synthesized and formed polyplexes with DNA at N/P = 15 as described previously [paper submitted]. To test the compatibility between the VIPER polyplexes and MBs, polyplexes were incubated with both MBs to check for visible aggregation. No precipitation was observed upon the addition of VIPER polyplexes to either untargeted SCat or targeted TAT-SCat MBs.

2.3.2 In vitro *studies*

To test if targeted MBs bound to ependymal cells, fluorescent liposomal analogs of the MB formulations were incubated with immortalized Z310 choroid

plexus cells (**Figure 2.2**). Liposomes, or unactivated MBs, were used as a facile way to test binding since MBs are gas-filled and float. TAT-SCat MBs bound 1.2 to almost 3 times better than untargeted SCat MBs to Z310 cells across the different numbers of MBs. While the untargeted SCat MBs did still bind to Z310 cells likely due to electrostatic interaction with negatively charged membranes, the targeted TAT-SCat MB binding was significantly greater ($P < 0.05$) than the SCat MBs due to the targeting and binding afforded by the TAT peptide.

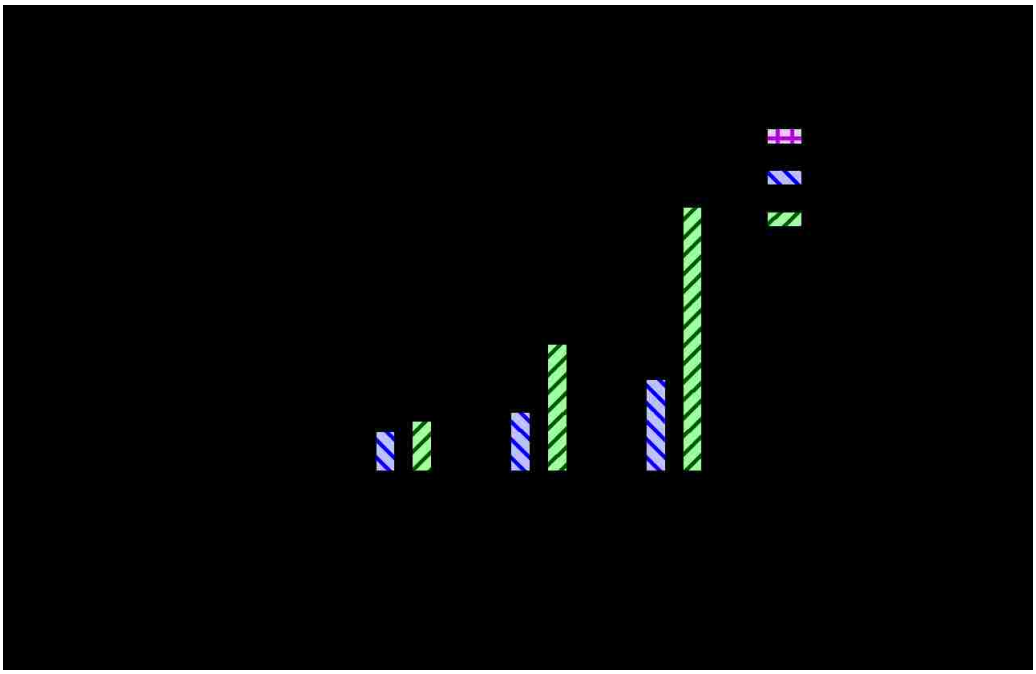

Figure 2.2 Binding of fluorescent liposomes analogous to the SCat and TAT-SCat MBs to cultured Z310 choroid plexus cells. Data is presented as mean + SD, n = 5. Statistically significant ($P < 0.05$) differences are indicated with a (*).

To ensure the polyplex gene delivery vehicles were stable in the presence of MB cavitation, solutions of VIPER polyplexes and SCat MBs were sonicated at various US settings and the resulting solutions were incubated with Z310 cells for transfection analysis (**Figure 2.3**). After SCat MB cavitation, VIPER polyplexes remained intact across all sonication frequencies and pressures as transfection levels were similar for VIPER polyplexes and MBs with and without US. Premature unpackaging or destruction of polyplexes by MB sonoporation was not a likely observation.

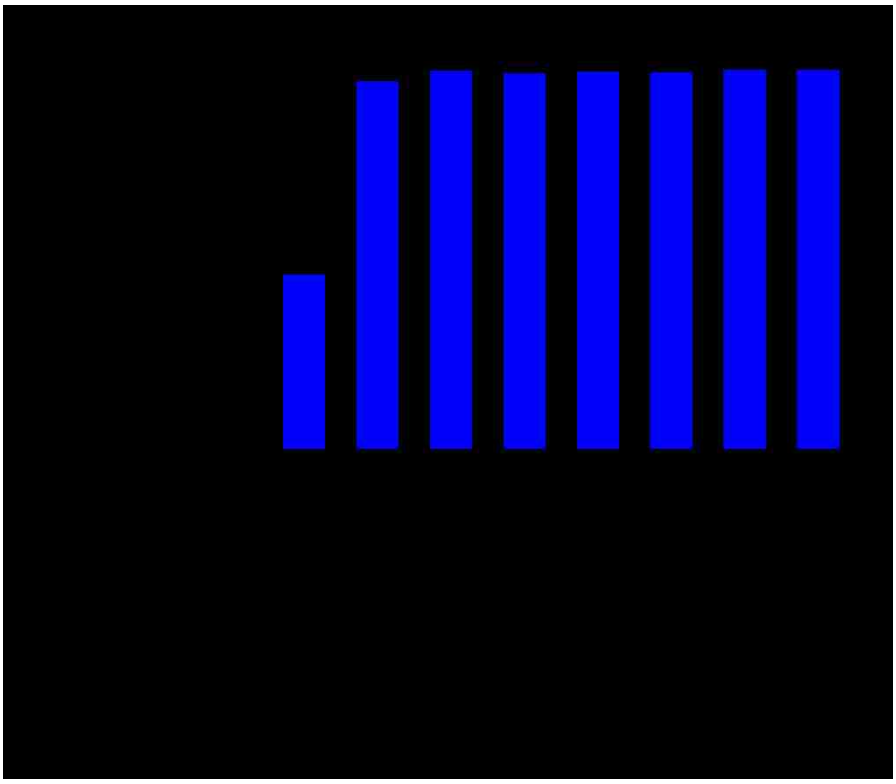

Figure 2.3 *In vitro* transfection of Z10 cells after sonication of VIPER polyplexes and SCat MBs. Data is presented as mean + SD, n = 3.

2.3.3 In vivo *transfection studies*

Next, the MBs were evaluated *in vivo* to determine if enhanced sonoporation of the choroid plexus with targeted MBs would further improve gene transfection. To determine the optimal US settings for gene transfer, VIPER polyplexes and SCat MBs were stereotaxically injected into the right brains of mice and different US conditions were applied to the top of the skull for a total of 1 min of sonication (**Figure 2.4**).

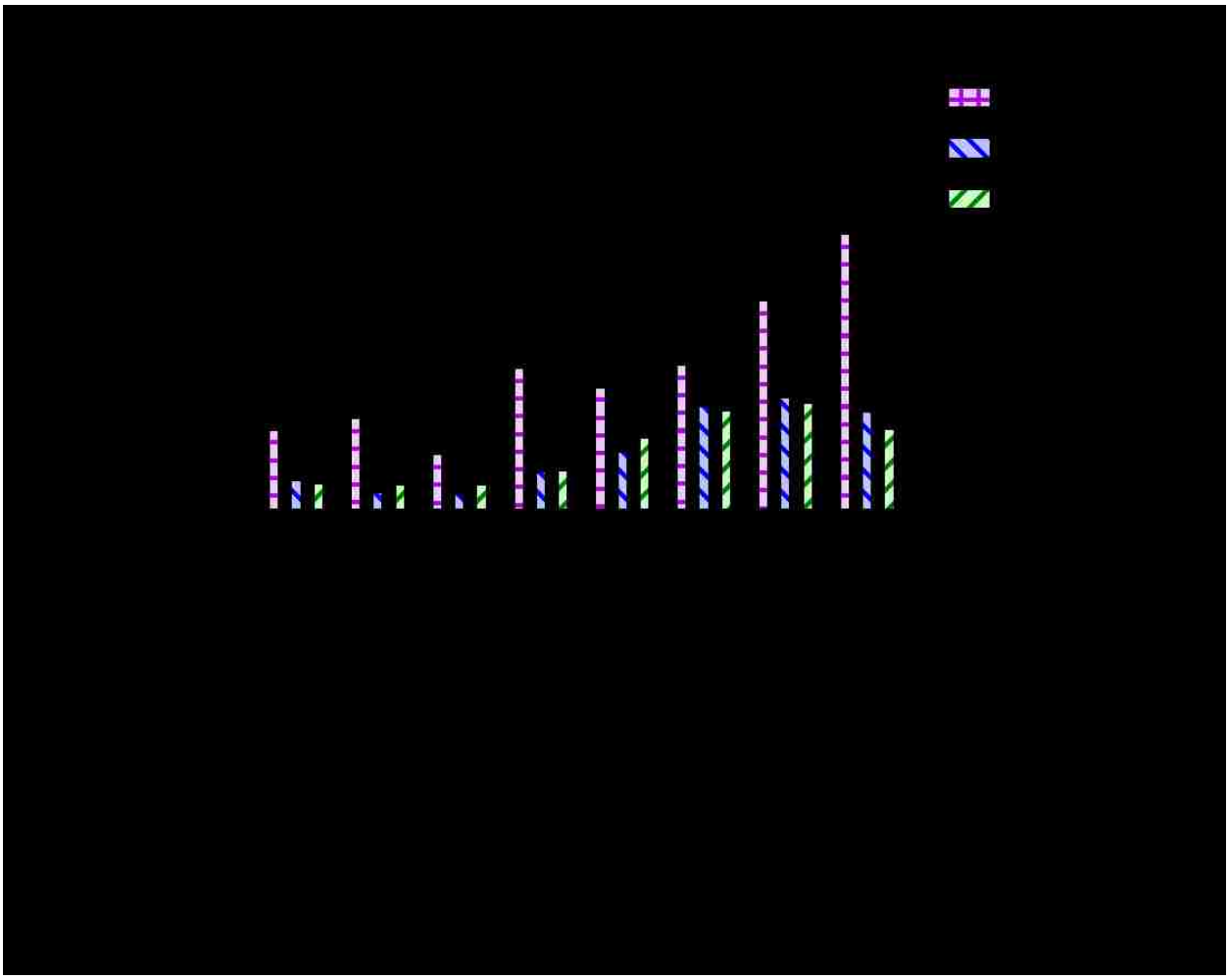

Figure 2.4 Luciferase expression in the mouse brain after treatment with VIPER polyplexes and untargeted SCat MBs under different US conditions. Data is presented as mean + SD, n = 3-9. Statistically significant ($P < 0.05$) differences are indicated with a (*).

Polyplex transfection levels were not affected by US alone. In general, luciferase expression scaled with increasing US frequency and amplitude. US at 3.5 MHz and 350 mV provided some of the highest levels of transfection in the mouse brain and was statistically significant ($P < 0.05$) compared to VIPER polyplexes with and without US. In fact, greater US parameters such as frequency and pressure, which cause stronger MB cavitation, are consistently linked to better delivery of macromolecules across in the blood–brain barrier in mice.[98,100] Conversely, subtler sonoporation, such as those at low pressures, are more closely linked to MBs interacting and lightly sonoporating the cell membrane, causing increased

endocytosis and less damage to cell membranes.[224,225] Since we are interested in using MB-mediated sonoporation as a way to break past the choroid plexus and not transfect it, the higher US setting of 3.5 MHz and 350 mV was selected as the optimal US settings. Interestingly, we were able to see significant increases in transfection in the left brain, the side contralateral to the injection site. Previously, we were unable to see significant increases on the contralateral side as similar to other reports.[27,102,120,226] More powerful, controlled US settings or a more stable gene delivery vehicle may explain these differences.

With the optimal US settings for the SCat MBs, a preliminary comparison of the untargeted and targeted MBs was conducted *in vivo* (**Figure 2.5**).

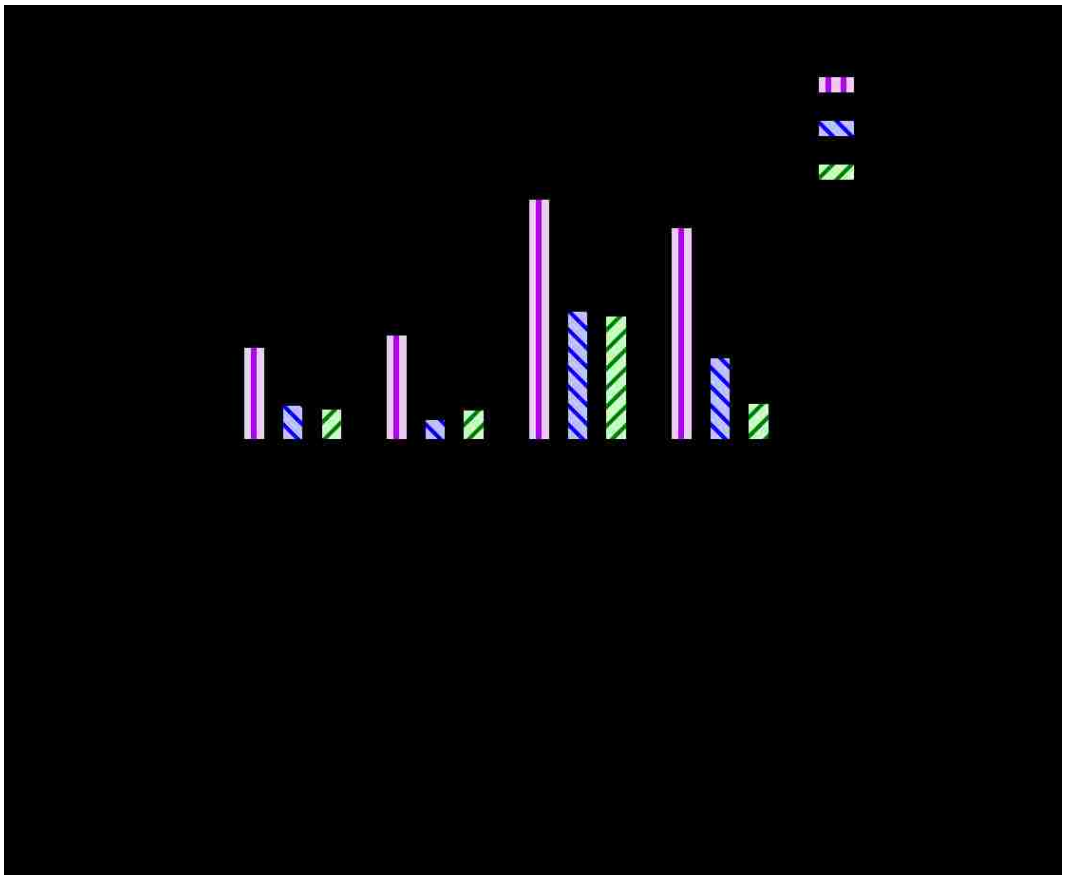

Figure 2.5 Luciferase expression in the mouse brain after treatment with VIPER polyplexes with untargeted SCat or targeted TAT-SCat MBs. Data is presented as mean + SD, n = 3-9.

Targeted TAT-SCat MBs were able to increase luciferase transfection better than polyplexes alone; however, they had transfection levels comparable to that of untargeted SCat MBs. Taken together with the MB destruction data (**Figure 2.1**), the US settings may not be optimal for the cavitation of TAT-SCat MBs. The addition of the TAT peptide does seem to alter the acoustic properties of the MBs and the *in vivo* US optimization was performed only for the untargeted SCat MBs (**Figure 2.4**). More US characterization of the MBs and possibly *in vivo* US optimization for the TAT-SCat MBs are needed. Another possible explanation is that the MBs do not bind well to ependymal cells *in vivo* despite binding well to Z310 choroid plexus cells *in vitro* (**Figure 2.2**). More studies will be needed to determine TAT-SCat MB binding in the mouse brain.

Another concern is that the TAT-SCat MBs are highly cationic and may not perform well as demonstrated in our previous formulation of Cationic (Cat) MBs.[120] While the TAT-SCat MB may be as cationic as the previous Cat MBs, there is still a difference in the shell dynamic between the two MBs. The Cat MB shell conformation does not seem to be ideal since there are a lot fewer Cat MBs made per a tube compared to the Neutral (Neu), SCat, and TAT-SCat MBs. In addition, the Cat MBs did not burst as easily as the Neu, SCat, and TAT-SCat MBs signifying there is an inherent difference in the MB shell properties. Perhaps the spread of the cationic lipids in the Cat MB is not ideal for this MB size. Even if the TAT-SCat MB is more cationic than the Cat MB, there is a difference in charge distribution around the MB. The charge of the TAT-SCat MB is mainly localized in and constrained to the TAT peptide which cannot spread out like each of the cationic lipids of the Cat MB. The targeted TAT-SCat and Cat MB are very different in terms of MB shell properties despite having similar surface charges.

Overall, more studies are needed to ensure that the TAT-SCat MBs are properly characterized and insonified. Once this is done, a proper comparison between the untargeted SCat and targeted TAT-SCat MBs can be conducted.

2.4 CONCLUSIONS

In this work, targeted MB sonoporation was investigated as a way to further increase the penetration of gene delivery vehicles past the choroid plexus barrier to augment gene transfer over untargeted MB sonoporation. Targeted, TAT peptide-decorated SCat MBs were created and had similar physical and acoustic properties to untargeted SCat MBs. Liposome analogs of the targeted MBs bound to cultured choroid plexus cells better than untargeted MBs. *In vivo*, the targeted TAT-SCat MBs performed on par with the untargeted SCat MBs. Further characterization of the TAT-SCat MBs is needed to accurately compare both MBs at their optimal US settings.

2.5 ACKNOWLEDGEMENTS

This work was supported by NIH 2R01NS064404; JKYT was supported by NSF GRFP (2011128558). We would like to thank Dr. Thomas J. Matula for the use of his Multiziser 3 and Dr. Wei Zheng for providing the Z310 choroid plexus cells.

2.6 SUPPLEMENTARY FIGURES

2.6.1 *HPLC of TAT-conjugated lipid*

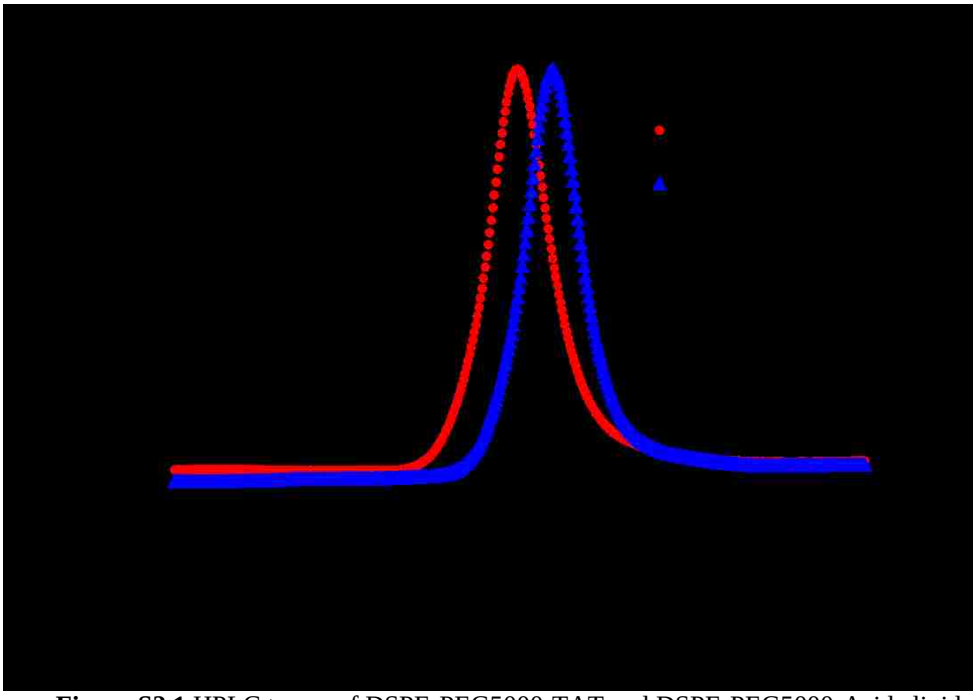

Figure S2.1 HPLC traces of DSPE-PEG5000-TAT and DSPE-PEG5000-Azide lipid.

2.6.2 *Acoustic MB characterization*

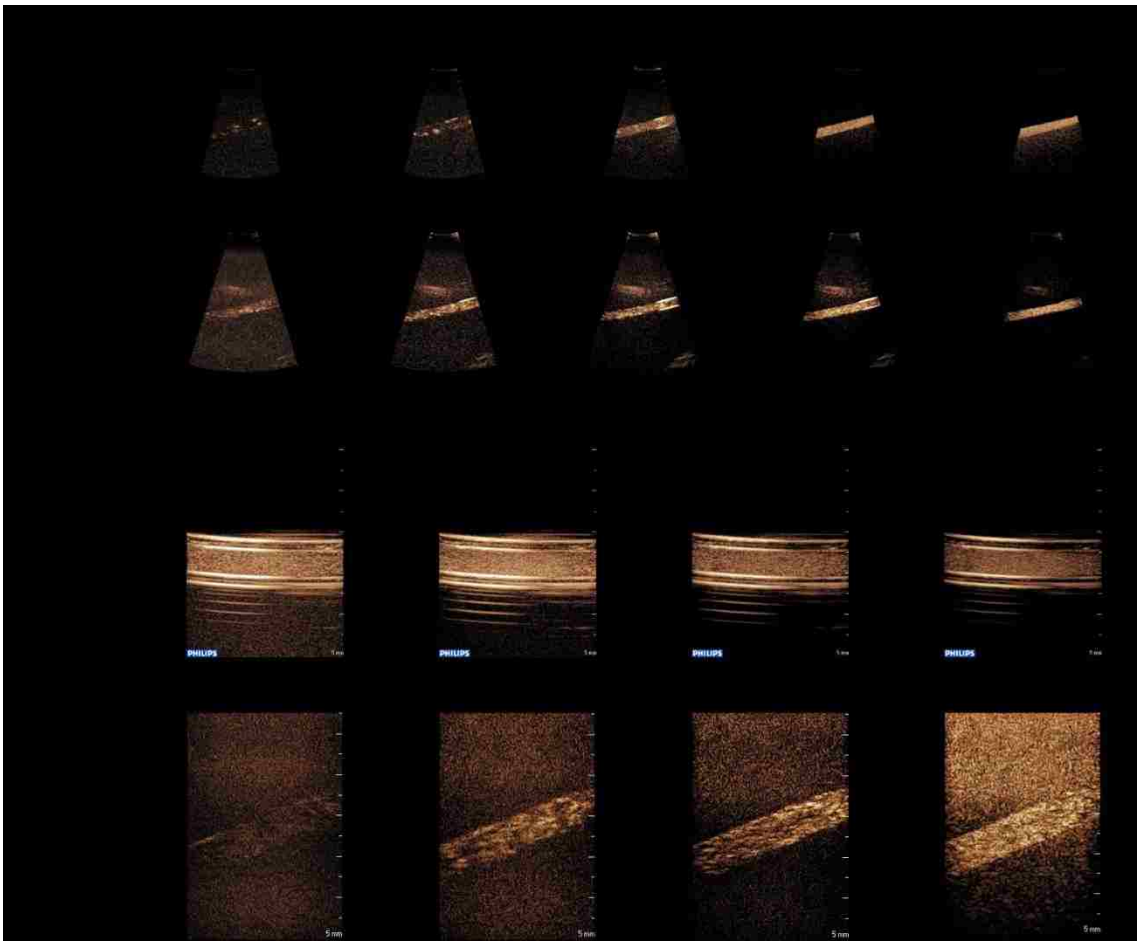

Figure S2.2 Flow phantom images of untargeted SCat and targeted TAT-SCat MBs at different US frequencies and mechanical indices (MIs).

2.7 REFERENCES

27. Weber-Adrian, D. *et al.* Gene delivery to the spinal cord using MRI-guided focused ultrasound. *Gene Ther.* 1–10 (2015). doi:10.1038/gt.2015.25

52. Mortazavi, M. M. *et al.* The choroid plexus: A comprehensive review of its history, anatomy, function, histology, embryology, and surgical considerations. *Child's Nerv. Syst.* **30,** 205–214 (2014).

54. Pardridge, W. M. Drug transport in brain via the cerebrospinal fluid. *Fluids Barriers CNS* **8,** 7 (2011).

57. Pardridge, W. The blood-brain barrier: bottleneck in brain drug development. *NeuroRx* **2,** 3–14 (2005).

59. McDannold, N., Arvanitis, C. D., Vykhodtseva, N. & Livingstone, M. S. Temporary disruption of the blood-brain barrier by use of ultrasound and microbubbles: safety and efficacy evaluation in rhesus macaques. *Cancer Res.* **72,** 3652–63 (2012).

60. Marquet, F. *et al.* Real-time, transcranial monitoring of safe blood-brain barrier opening in non-human primates. *PLoS One* **9,** e84310 (2014).

61. Panje, C. M., Wang, D. S. & Willmann, J. K. Ultrasound and microbubble-mediated gene delivery in cancer: progress and perspectives. *Invest. Radiol.* **48,** 755–69 (2013).

94. Rychak, J. J. & Klibanov, A. L. Nucleic acid delivery with microbubbles and ultrasound. *Adv. Drug Deliv. Rev.* **72,** 82–93 (2014).

95. Meairs, S. & Alonso, A. Ultrasound, microbubbles and the blood-brain barrier. *Prog. Biophys. Mol. Biol.* **93,** 354–62 (2007).

97. Zhou, Y., Yang, K., Cui, J., Ye, J. & Deng, C. Controlled permeation of cell membrane by single bubble acoustic cavitation. *J. Control. Release* **157,** 103–111 (2012).

98. Choi, J. J., Pernot, M., Small, S. a & Konofagou, E. E. Noninvasive, transcranial and localized opening of the blood-brain barrier using focused ultrasound in mice. *Ultrasound Med. Biol.* **33,** 95–104 (2007).

99. Choi, J. J., Wang, S., Tung, Y.-S., Morrison, B. & Konofagou, E. E. Molecules of various pharmacologically-relevant sizes can cross the ultrasound-induced blood-brain barrier opening in vivo. *Ultrasound Med. Biol.* **36,** 58–67 (2010).

100. Choi, J. J. *et al.* Noninvasive and localized blood-brain barrier disruption using focused ultrasound can be achieved at short pulse lengths and low pulse repetition frequencies. *J. Cereb. Blood Flow Metab.* **31,** 725–37 (2011).

101. Xie, F. *et al.* Effects of transcranial ultrasound and intravenous microbubbles on blood brain barrier permeability in a large animal model. *Ultrasound Med. Biol.* **34,** 2028–34

(2008).

102. Sheikov, N., McDannold, N., Vykhodtseva, N., Jolesz, F. & Hynynen, K. Cellular mechanisms of the blood-brain barrier opening induced by ultrasound in presence of microbubbles. *Ultrasound Med. Biol.* **30,** 979–89 (2004).

120. Tan, J.-K. Y. *et al.* Microbubbles and ultrasound increase intraventricular polyplex gene transfer to the brain. *J. Control. Release* **231,** 86–93 (2016).

206. Chodobski, A. & Szmydynger-chodobska, J. Choroid plexus: target for polypeptides and site of their synthesis. *Microsc. Res. Tech.* **52,** 65–82 (2001).

207. Wang, S., Samiotaki, G., Olumolade, O., Feshitan, J. a & Konofagou, E. E. Microbubble type and distribution dependence of focused ultrasound-induced blood-brain barrier opening. *Ultrasound Med. Biol.* **40,** 130–7 (2014).

208. Feshitan, J. a, Chen, C. C., Kwan, J. J. & Borden, M. a. Microbubble size isolation by differential centrifugation. *J. Colloid Interface Sci.* **329,** 316–24 (2009).

213. Zheng, W. & Zhao, Q. Establishment and characterization of an immortalized Z310 choroidal epithelial cell line from murine choroid plexus. *Brain Res.* **958,** 371–80 (2002).

214. Shi, L., Li, G., Wang, S. & Zheng, W. Use of Z310 cells as an in vitro blood–cerebrospinal fluid barrier model: Tight junction proteins and transport properties. *Toxicol. Vitr.* **22,** 190–199 (2008).

216. Wu, S.-Y., Chen, C. C., Tung, Y.-S., Olumolade, O. O. & Konofagou, E. E. Effects of the Microbubble Shell Physicochemical Properties on Ultrasound-Mediated Drug Delivery to the Brain. *J. Control. Release* **212,** 30–40 (2015).

217. Wang, D. *et al.* Cationic versus neutral microbubbles for ultrasound-mediated gene delivery in cancer. *Radiology* **264,** 721–732 (2012).

218. Sun, R. R., Noble, M. L., Sun, S. S., Song, S. & Miao, C. H. Development of therapeutic microbubbles for enhancing ultrasound-mediated gene delivery. *J. Control. Release* **182,** 111–20 (2014).

224. Delalande, A., Leduc, C., Midoux, P., Postema, M. & Pichon, C. Efficient Gene Delivery by Sonoporation Is Associated with Microbubble Entry into Cells and the Clathrin-Dependent Endocytosis Pathway. *Ultrasound Med. Biol.* 1–14 (2015). doi:10.1016/j.ultrasmedbio.2015.03.010

225. Cock, I. De *et al.* Ultrasound and microbubble mediated drug delivery : Acoustic pressure as determinant for uptake via membrane pores or endocytosis. *J. Control. Release* **197,** 20–28 (2015).

226. Samiotaki, G., Acosta, C., Wang, S. & Konofagou, E. E. Enhanced delivery and bioactivity of the neurturin neurotrophic factor through focused ultrasound — mediated

blood – brain barrier opening in vivo. *J. Cereb. Blood flow Metab.* 1–12 (2015). doi:10.1038/jcbfm.2014.236

227. Kumar, S. *et al.* Peptides as skin penetration enhancers: Mechanisms of action. *J. Control. Release* **199,** 168–178 (2015).

228. Lin, C.-Y. *et al.* Non-invasive, Neuron-Specific Gene Therapy by Focused Ultrasound-Induced Blood-Brain Barrier Opening in Parkinson's Disease Mouse Model. *J. Control. Release* **235,** 72–81 (2016).

229. Shi, L. & Palacio-Mancheno, P. Quantification of transient increase of the blood–brain barrier permeability to macromolecules by optimized focused ultrasound combined with microbubbles. *Int. J. …* 4437–4448 (2014).

230. Marty, B. *et al.* Dynamic study of blood–brain barrier closure after its disruption using ultrasound: a quantitative analysis. *J. Cereb. Blood Flow Metab.* **32,** 1948–1958 (2012).

231. Lanza, G. M. & Wickline, S. A. Targeted Ultrasonic Contrast Agents for Molecular Imaging and Therapy. *Curr. Probl. Cardiol.* 625–653 (2003). doi:10.1016/j.cpccardiol.2003.11.001

232. Willmann, J. K. *et al.* Targeted Contrast-Enhanced Ultrasound Imaging of Tumor Angiogenesis with Contrast Microbubbles Conjugated to Integrin-Binding Knottin Peptides. *J Nucl Med* **51,** 433–440 (2010).

233. Stieger, S. M. *et al.* Imaging of angiogenesis using Cadence contrast pulse sequencing and targeted contrast agents. *Contrast Media Mol. Imaging* **3,** 9–18 (2008).

234. Zhang, H. *et al.* Ultrasound molecular imaging of tumor angiogenesis with a neuropilin-1-targeted microbubble. *Biomaterials* **56,** 104–113 (2015).

235. Kooiman, K., Foppen-Harteveld, M., Der Steen, A. F. W. Van & De Jong, N. Sonoporation of endothelial cells by vibrating targeted microbubbles. *J. Control. Release* **154,** 35–41 (2011).

236. Yan, P. *et al.* The use of MMP2 antibody-conjugated cationic microbubble to target the ischemic myocardium, enhance Timp3 gene transfection and improve cardiac function. *Biomaterials* **35,** 1063–73 (2014).

237. Bayer, P. *et al.* Structural studies of HIV-1 tat protein. *J. Mol. Biol.* **247,** 529–535 (1995).

238. Xiong, X.-B., Uludağ, H. & Lavasanifar, A. Virus-mimetic polymeric micelles for targeted siRNA delivery. *Biomaterials* **31,** 5886–93 (2010).

239. Keravnou, C., Mannaris, C. & Averkiou, M. Accurate measurement of microbubble response to ultrasound with a diagnostic ultrasound scanner. *IEEE Trans. Ultrason. Ferroelectr. Freq. Control* **62,** 176–184 (2015).

240. Mannaris, C. & Averkiou, M. A. Investigation of Microbubble Response to Long Pulses Used in Ultrasound-Enhanced Drug Delivery. *Ultrasound Med. Biol.* **38,** 681–691 (2012).

Part 5: Future Projects

This section focuses on future works and potential projects.

Chapter 1. Completion of Targeted Microbubble Sonoporation of the Choroid Plexus and Other Improvements to Maximize Gene Delivery

1.1 Background and Significance

In Part 4, Chapter 2, we investigated the ability of targeted TAT-decorated slightly cationic microbubbles (TAT-SCat MBs) to further sonoporate the choroid plexus epithelium in order to enhance gene transfection over the use of untargeted SCat MBs. Unfortunately, the TAT-SCat MBs produced similar levels of transfection as the SCat MBs *in vivo*. Acoustic characterization suggests that the addition of the TAT peptide to the MB changes the lipid shell properties. Further characterization of the MBs and optimization of the targeted TAT-SCat MBs will enable an adequate comparison between the untargeted and targeted MBs.

1.2 Aim 1: Further Characterization & Evaluation of Microbubbles

TAT-SCat MBs can be formed and acoustically characterized by imaging across different ultrasound (US) frequencies and mechanical indices (MIs). Previous characterization of the TAT-Scat MBs were a little inconclusive and differed slightly from the SCat MBs; thus, repeated studies are needed to confirm the results and determine the optimal US settings for TAT-SCat MB cavitation. In addition, both MBs will be insonified with a higher US frequency (~5 MHz). Both MBs tend to lie on the small range of MB diameters and MB theories suggest that higher US frequencies are their optimal setting. The *in vivo* data also show a trend for better gene transfection with higher frequency and this US parameter may be the largest contributor to sonoporating the choroid plexus. Other MB formulations would be of interest in testing such as: 2 kDa PEG-shelled MBs with 5 kDa PEG targeting ligands and MBs with larger diameters. While 5 kDa PEG shells are more stable,[241] 2 kDa PEG shells may be able to sonoporate tissues more easily at lower acoustic pressures and better permeabilize membranes. There is not much literature on the acoustic differences between MBs of different PEG shell lengths and it may be worth further investigating. MBs of larger diameters would oscillate more than smaller MBs and can cause significantly more sonoporation upon inertial cavitation. Nevertheless, too much damage could cause fatalities when

disrupting the choroid plexus. Some of the mice in our studies already have a hard time recovering; thus, there is a limit to how much damage can be afforded before death. Another acoustic characterization experiment would be to measure the forces generated from MB cavitation under different US conditions. This may tell us which kind of disruption we are getting from the MBs and may serve as a way to screen the US settings before going *in vivo*.

1.3 Aim 2: *In Vivo* Optimization of MB System

After the most promising formulations of MBs and US settings are realized through acoustic analysis, the US settings can be optimized *in vivo* for maximum transfection efficiency in the mouse brain. MBs can be injected into the right brains of mice and different US frequencies and amplitudes can be applied based on the earlier acoustic findings. Other experimental parameters such as sonication time and number of MBs can be titrated to find the optimum level of success. The US settings producing the highest levels of transfection for each MB type will be used to compare the 2 MBs against each other.

1.4 Aim 3: Head-to-Head Comparison of Targeted and Untargeted MBs

The optimal US settings for each MB found in Aim 2 can be used to sonicate the targeted and untargeted MBs in mouse brains. Targeted MBs are expected to cause the more sonoporation over untargeted MBs because of a greater number of MBs next to the choroid plexus and the closer proximity to cells. This would lead to a higher level of gene delivery vehicle permeation into the brain parenchyma and higher levels of transfection. Transfection levels may still be comparable between the two different MBs. Decreasing the number of MBs or finding a better targeting ligand may help see a difference between the two MBs. Immunohistochemistry staining can be done to determine the types and distribution of cells that are transfected.

Chapter 2. Microbubble-Mediated Polymer Scission

2.1 Background and Significance

Recently, polymers have been shown to dissociate and depolymerize into their monomeric units under ultrasound (US).[242,243] However, severely high frequencies around 20 kHz are needed to provide enough strain to split the polymer backbone to initiate rapid depolymerization. In addition, the polymer dissociation was demonstrated in organic solutions at low temperatures (-15 ºC to 15 ºC). These conditions are not suitable for applications of the polymers in humans as high-level frequency poorly permeates tissue and the administration of polymers to humans in organic solvents at low temperatures is not feasible. Cavitation of microbubbles (MBs) under US may serve as a way to translate this technology form the benchtop to patients. MB bursting may provide enough shear force to cause nearby polymer scission at much lower US frequencies that are capable of being transmitted in human tissues. In addition, the anchoring the polymers to MBs may provide a way of directly breaking up polymers during cavitation and this technology can be applied to a variety of applications.

2.2 Aim 1: Test Microbubble-Mediated Polymer Scission

As a quick test, spiropyran polymers incubated with MBs can be insonified at a frequency known to cause MB inertial cavitation. Depolymerization of the polymer can be monitored by the emergence of fluorescence by polymer dissociation. This would serve as a proof-of-principle and would be a novel way to combine polymer depolymerization with MB acoustics at lower US settings. If this does not work, the MB concentration can be increased so that cavitation is closer to the polymer strands or higher magnitude US can be applied to cause rapid and forceful cavitation. If none of these conditions cause depolymerization, anchoring the polymer shell may be the only way to generate enough forces for polymer scission.

2.3 Aim 2: Development of Polymer-Tethered Microbubbles

Directly anchoring the polymers to the MB shell may provide more strain to break the polymer backbone since the polymer would be pulled apart each time the MB expands under negative US pressure. The greatest strain on the polymer would likely be when the MB expands so far that it

later implodes. Spiropyran polymers will be synthesized with either thiol or azide functionalization incorporated into the backbone. Slightly cationic (SCat) MBs (2 kDa PEG) will be formed and decorated with either a thiol reactive species or alkyne functionalization by incorporating either 1,2-dipalmitoyl-*sn*-glycero-3-phosphoethanolamine-*N*-[3-(2-pyridyldithio)propionate] or 1,2-dipalmitoyl-*sn*-glycero-3-phosphoethanolamine-*N*-[4-(p-maleimidophenyl)butyramide] for thiol addition or 1,2-dipalmitoyl-*sn*-glycero-3-phosphoethanolamine-*N*-(5-hexynoyl) for azide-alkyne cycloaddition. The newly formed MBs can be reacted with the polymers and then undergo differential centrifugation to isolate 1-2 μm MBs and remove unreacted polymer. A semi-dilute reaction volume should be used so there is a predilection for intra-MB conjugation rather than inter-MB crosslinking. However, the reaction needs to move quickly to minimize the loss of MBs over time. Purging may be done with perfluorobutane rather than argon or nitrogen as this will help keep MBs intact. Polymer-conjugated MBs can then be insonified with US and polymer scission can be monitored by the emergence of fluorescence. Optimization of the reaction conditions and the number of incorporated functional groups into the polymers and MBs will probably be needed. As an alternative, the polymer-lipid conjugate can be synthesized before making the MBs; however, this is likely to result in crosslinking of MBs and an uneven distribution of products.

2.4 Application of Polymer-Microbubble System

After the demonstration of polymer break-up by MBs and US, the system can be applied to areas such as cancer and blood homeostasis. One of the major problems after a cancer therapeutic reaches tumors is penetration into the tumor. Different research group already use MB-mediated US as a way to image and deliver therapeutics to tumors.[232,244] Drug-loaded, polymer-tethered MBs can be used to break up the tumor endothelial layer by US sonoporation. In addition, the MB cavitation can dissociate the polymer into smaller pieces and release the drug so that it can better permeate the tumor microenvironment. In addition, the junction opener protein 4 (JO-4) can be incorporated into the polymer or system to further enhance tumor penetration. Recently, PolySTAT, a synthetic hemostatic polymer, was developed as a way to stop bleeding and strengthen clots.[245] Currently there is no method to quickly reverse the incorporation on PolySTAT in fibrin networks. Incorporating fibin-binding peptides on a polymer-tethered MB may allow for the rapid breakdown on polymer and fibrin cross-linking under US. When intraveneously

administered, this system should still be able to stabilize and strengthen clots due to the fibrin-binding polymer. It may even perform better than PolySTAT alone due to the larger size of the polymer-MB system and higher crosslinking potential. If an unwanted clot is formed, US can be applied to cavitate the MBs and cause polymer scission and monomer dispersion, thus rapidly weakening the clot.

Chapter 3. Collagen-Crosslinking Polymers for Wrinkle Reduction

3.1 Background and Significance

With a large aging population and increased desire to retain youthful appearances, the anti-wrinkle industry continues to rapidly grow from the $43 billion estimation in the US alone in 2012.[246] One of the primary causes of wrinkle formation is less collagen in the skin.[247–249] Aged skin has increased collagen degradation and decreased collagen production. A variety of collagen fillers derived from humans, pigs, and cows have been used as dermal fillers. For example, glutaraldehyde crosslinked bovine collagen fillers, Zyderm® and Zyplast®, have been used but still suffer from a short 2-4 month duration due to degradation by collagenases.[250] Thus, a slow-degradable, synthetic polymer that is able to crosslink natural collagen may be able to plump up tissue while preventing the degradation of collagen.

3.2 Aim 1: Development of Collagen-Crosslinking Polymer

Just like PolySTAT, the hemostatic polymer, this collagen-crosslinking polymer can be comprised of (hydroxyethyl)methacrylate (HEMA) and *N*-hydroxysuccinimide methacrylate (NHSMA) for biocompatibility and conjugation to collagen-binding peptides.[245] For the peptide, there are two possible candidates: one also from the Caravan group and another from the Meijer group. The Caravan group identified a collagen I-binding peptide by phage display and further improved its binding by affinity maturation to yield cyclic GQWHCTTRFPHHYCLYBip-$CONH_2$ with a micromolar dissociation constant.[251,252] The Meijer group identified another collagen I-binding peptide by phage display, H(Dnp)VWMQAPGGG, which showed a nanomolar dissociation constant when presented as a pentamer.[253] These peptides can be conjugated to the HEMA-based polymer by NHS chemistry. A panel of different sized polymers with various amounts of peptide incorporation can be evaluated for collagen binding.

3.3 Aim 2: Evaluation of Collagen-Crosslinking Polymer

Polymers synthesized in Aim 1 will be evaluated in their ability to bind to collagen and prevent degradation by collagenases. Binding to type 1 human collagen can be determined as previously described.[252] Collagenases can be added after polymer incorporation into collagen to determine

which polymer best prevents collagen degradation. Through these studies, we will elucidate which polymer size, peptide sequence, and amount of peptide incorporation best bulks up collagen and prevents degradation. Lastly, *in vivo* efficacy studies will be conducted to assess wrinkle smoothening and histologic responses.[254]

References

1. Gage, F. H. Mammalian Neural Stem Cells. *Science (80-.).* **287,** 1433–8 (2000).

2. Emsley, J. G., Mitchell, B. D., Kempermann, G. & Macklis, J. D. Adult neurogenesis and repair of the adult CNS with neural progenitors, precursors, and stem cells. *Prog. Neurobiol.* **75,** 321–341 (2005).

3. Sawada, M. & Sawamoto, K. Mechanisms of Neurogenesis in the Normal and Injured Adult Brain. *Keio J. Med.* **62,** 13–28 (2013).

4. Parent, J. M., Vexler, Z. S., Gong, C., Derugin, N. & Ferriero, D. M. Rat forebrain neurogenesis and striatal neuron replacement after focal stroke. *Ann. Neurol.* **52,** 802–13 (2002).

5. Arvidsson, A., Collin, T., Kirik, D., Kokaia, Z. & Lindvall, O. Neuronal replacement from endogenous precursors in the adult brain after stroke. *Nat. Med.* **8,** 963–70 (2002).

6. Mattson, M. P. & Magnus, T. Ageing and neuronal vulnerability. *Nat. Rev. Neurosci.* **7,** 278–294 (2006).

7. Geraerts, M., Krylyshkina, O., Debyser, Z. & Baekelandt, V. Concise review: therapeutic strategies for Parkinson disease based on the modulation of adult neurogenesis. *Stem Cells* **25,** 263–270 (2007).

8. Shihabuddin, L. S., Palmer, T. D. & Gage, F. H. The search for neural progenitor cells: Prospects for the therapy of neurodegenerative disease. *Mol. Med. Today* **5,** 474–480 (1999).

9. Kim, M., Lee, S.-T., Chu, K. & Kim, S. U. Stem cell-based cell therapy for Huntington disease: a review. *Neuropathology* **28,** 1–9 (2008).

10. Chirumamilla, S., Sun, D., Bullock, M. R. & Colello, R. J. Traumatic brain injury induced cell proliferation in the adult mammalian central nervous system. *J. Neurotrauma* **19,** 693–703 (2002).

11. Ghajar, J. Traumatic brain injury. *Lancet* **356,** 923–929 (2000).

12. Zhang, R., Zheng, N., Song, Z., Yin, L. & Cheng, J. The effect of side-chain functionality and hydrophobicity on the gene delivery capabilities of cationic helical polypeptides. *Biomaterials* **35,** 3443–3454 (2014).

13. Dash, P. K., Mach, S. a & Moore, a N. Enhanced neurogenesis in the rodent hippocampus following traumatic brain injury. *J. Neurosci. Res.* **63,** 313–319 (2001).

14. Ramaswamy, S., Goings, G. E., Soderstrom, K. E., Szele, F. G. & Kozlowski, D. a. Cellular proliferation and migration following a controlled cortical impact in the mouse.

Brain Res. **1053,** 38–53 (2005).

15. Saha, B., Peron, S., Murray, K., Jaber, M. & Gaillard, A. Cortical lesion stimulates adult subventricular zone neural progenitor cell proliferation and migration to the site of injury. *Stem Cell Res.* **11,** 965–77 (2013).

16. Zheng, W. *et al.* Neurogenesis in adult human brain after traumatic brain injury. *J. Neurotrauma* **30,** 1872–80 (2013).

17. Wiltrout, C., Lang, B., Yan, Y., Dempsey, R. J. & Vemuganti, R. Repairing brain after stroke: A review on post-ischemic neurogenesis. *Neurochem. Int.* **50,** 1028–1041 (2007).

18. Lim, D. a. *et al.* Noggin antagonizes BMP signaling to create a niche for adult neurogenesis. *Neuron* **28,** 713–726 (2000).

19. Jin, K. *et al.* Vascular endothelial growth factor (VEGF) stimulates neurogenesis in vitro and in vivo. *Proc. Natl. Acad. Sci. U. S. A.* **99,** 11946–11950 (2002).

20. Zigova, T., Pencea, V., Wiegand, S. J. & Luskin, M. B. Intracentricular Administration of BDNF Increases the Number of Newly Generated Neurons in the Adult Olfactory Bulb. *Mol. Cell. Neurosci.* **245,** 234–245 (1998).

21. Gritti, A., Cova, L., Parati, E. a., Galli, R. & Vescovi, A. L. Basic fibroblast growth factor supports the proliferation of epidermal growth factor-generated neuronal precursor cells of the adult mouse CNS. *Neurosci. Lett.* **185,** 151–154 (1995).

22. Whittemore, S. R., Morassutti, D. J., Walters, W. M., Liu, R. H. & Magnuson, D. S. Mitogen and substrate differentially affect the lineage restriction of adult rat subventricular zone neural precursor cell populations. *Exp. Cell Res.* **252,** 75–95 (1999).

23. Arsenijevic, Y. & Weiss, S. Insulin-like growth factor-I is a differentiation factor for postmitotic CNS stem cell-derived neuronal precursors: distinct actions from those of brain-derived neurotrophic factor. *J. Neurosci.* **18,** 2118–2128 (1998).

24. Traynor, B. J. *et al.* Neuroprotective agents for clinical trials in ALS: a systematic assessment. *Neurology* **67,** 20–7 (2006).

25. Dodge, J. C. *et al.* AAV4-mediated expression of IGF-1 and VEGF within cellular components of the ventricular system improves survival outcome in familial ALS mice. *Mol. Ther.* **18,** 2075–84 (2010).

26. Thomas, C. E., Ehrhardt, A. & Kay, M. a. Progress and problems with the use of viral vectors for gene therapy. *Nat. Rev. Genet.* **4,** 346–58 (2003).

27. Weber-Adrian, D. *et al.* Gene delivery to the spinal cord using MRI-guided focused ultrasound. *Gene Ther.* 1–10 (2015). doi:10.1038/gt.2015.25

28. Masserdotti, G. *et al.* Transcriptional Mechanisms of Proneural Factors and REST in

Regulating Neuronal Reprogramming of Astrocytes. *Cell Stem Cell* 74–88 (2015). doi:10.1016/j.stem.2015.05.014

29. Matsuoka, N. *et al.* Adenovirus-mediated gene transfer of fibroblast growth factor-2 increases BrdU-positive cells after forebrain ischemia in gerbils. *Stroke.* **34,** 1519–25 (2003).

30. Zhang, Y., Pak, C., Han, Y. & Ahlenius, H. Rapid single-step induction of functional neurons from human pluripotent stem cells. *Neuron* **78,** 785–798 (2013).

31. Jin, K. *et al.* Neurogenesis and aging: FGF-2 and HB-EGF restore neurogenesis in hippocampus and subventricular zone of aged mice. *Aging Cell* **2,** 175–83 (2003).

32. Tabar, V. & Studer, L. Pluripotent stem cells in regenerative medicine: challenges and recent progress. *Nat. Rev. Genet.* **15,** 82–92 (2014).

33. Suhonen, J. O., Peterson, D. a, Ray, J. & Gage, F. H. Differentiation of adult hippocampus-derived progenitors into olfactory neurons in vivo. *Nature* **383,** 624–627 (1996).

34. Goldman, S. Stem and progenitor cell-based therapy of the human central nervous system. *Nat. Biotechnol.* **23,** 862–71 (2005).

35. Lindvall, O., Kokaia, Z. & Martinez-Serrano, A. Stem cell therapy for human neurodegenerative disorders-how to make it work. *Nat. Med.* **10 Suppl,** S42–S50 (2004).

36. Rossi, F. & Cattaneo, E. Opinion: neural stem cell therapy for neurological diseases: dreams and reality. *Nat. Rev. Neurosci.* **3,** 401–409 (2002).

37. Chu, D. S. H. *et al.* Application of living free radical polymerization for nucleic acid delivery. *Acc. Chem. Res.* **45,** 1089–99 (2012).

38. Moad, G., Rizzardo, E. & Thang, S. H. Living Radical Polymerization by the RAFT Process. *Aust. J. Chem.* **58,** 379 (2005).

39. Pack, D. W., Hoffman, A. S., Pun, S. & Stayton, P. S. Design and development of polymers for gene delivery. *Nat. Rev. Drug Discov.* **4,** 581–93 (2005).

40. Burke, R. S. & Pun, S. H. Extracellular barriers to in vivo PEI and PEGylated PEI polyplex-mediated gene delivery to the liver. *Bioconjug. Chem.* **19,** 693–704 (2008).

41. Schellinger, J. G. *et al.* Melittin-grafted HPMA-oligolysine based copolymers for gene delivery. *Biomaterials* **34,** 2318–26 (2013).

42. Chu, D. S. H., Schellinger, J. G., Bocek, M. J., Johnson, R. N. & Pun, S. H. Optimization of Tet1 ligand density in HPMA-co-oligolysine copolymers for targeted neuronal gene delivery. *Biomaterials* **34,** 9632–7 (2013).

43. Wei, H., Schellinger, J. G., Chu, D. S. H. & Pun, S. H. Neuron-targeted copolymers with sheddable shielding blocks synthesized using a reducible, RAFT-ATRP double-head agent. *J. Am. Chem. Soc.* **134,** 16554–7 (2012).

44. ur Rehman, Z., Hoekstra, D. & Zuhorn, I. S. Mechanism of polyplex- and lipoplex-mediated delivery of nucleic acids: real-time visualization of transient membrane destabilization without endosomal lysis. *ACS Nano* **7,** 3767–77 (2013).

45. Al-Dosari, M. S. & Gao, X. Nonviral gene delivery: principle, limitations, and recent progress. *AAPS J.* **11,** 671–81 (2009).

46. Kwon, E. J., Liong, S. & Pun, S. H. A truncated HGP peptide sequence that retains endosomolytic activity and improves gene delivery efficiencies. *Mol. Pharm.* **7,** 1260–5 (2010).

47. Wei, H. *et al.* Dual responsive, stabilized nanoparticles for efficient in vivo plasmid delivery. *Angew. Chem. Int. Ed. Engl.* **52,** 5377–81 (2013).

48. Tan, J.-K. Y., Choi, J. L., Wei, H., Schellinger, J. G. & Pun, S. H. Reducible, dibromomaleimide-linked polymers for gene delivery. *Biomater. Sci.* **3,** 112–120 (2015).

49. Begley, D. Understanding and circumventing the blood-brain barrier. *Acta Paediatr.* **443,** 83–91 (2003).

50. Gabathuler, R. Development of new peptide vectors for the transport of therapeutic across the blood-brain barrier. *Ther. Deliv.* **1,** 571–586 (2010).

51. Abbott, N. J. Blood-brain barrier structure and function and the challenges for CNS drug delivery. *J. Inherit. Metab. Dis.* **36,** 437–449 (2013).

52. Mortazavi, M. M. *et al.* The choroid plexus: A comprehensive review of its history, anatomy, function, histology, embryology, and surgical considerations. *Child's Nerv. Syst.* **30,** 205–214 (2014).

53. Dohrmann, G. J. The choroid plexus: a historical review. *Brain Res.* **18,** 197–218 (1970).

54. Pardridge, W. M. Drug transport in brain via the cerebrospinal fluid. *Fluids Barriers CNS* **8,** 7 (2011).

55. Begley, D. J. Delivery of therapeutic agents to the central nervous system: the problems and the possibilities. *Pharmacol. Ther.* **104,** 29–45 (2004).

56. Witt, K. a & Davis, T. P. CNS drug delivery: opioid peptides and the blood-brain barrier. *AAPS J.* **8,** E76–88 (2006).

57. Pardridge, W. The blood-brain barrier: bottleneck in brain drug development. *NeuroRx* **2,** 3–14 (2005).

58. Aryal, M., Arvanitis, C. D., Alexander, P. M. & McDannold, N. Ultrasound-mediated blood–brain barrier disruption for targeted drug delivery in the central nervous system. *Adv. Drug Deliv. Rev.* (2014). doi:10.1016/j.addr.2014.01.008

59. McDannold, N., Arvanitis, C. D., Vykhodtseva, N. & Livingstone, M. S. Temporary disruption of the blood-brain barrier by use of ultrasound and microbubbles: safety and efficacy evaluation in rhesus macaques. *Cancer Res.* **72,** 3652–63 (2012).

60. Marquet, F. *et al.* Real-time, transcranial monitoring of safe blood-brain barrier opening in non-human primates. *PLoS One* **9,** e84310 (2014).

61. Panje, C. M., Wang, D. S. & Willmann, J. K. Ultrasound and microbubble-mediated gene delivery in cancer: progress and perspectives. *Invest. Radiol.* **48,** 755–69 (2013).

62. Meairs, S., Alonso, A., Fatar, M., Kern, R. & Hennerici, M. Microbubbles traversing the blood-brain barrier for imaging and therapy. *Med. Biol. Eng. Comput.* **47,** 839–49 (2009).

63. Huang, Q. *et al.* Targeted gene delivery to the mouse brain by MRI-guided focused ultrasound-induced blood-brain barrier disruption. *Exp. Neurol.* **233,** 350–356 (2012).

64. Sugiura, S. *et al.* Adenovirus-mediated gene transfer of heparin-binding epidermal growth factor-like growth factor enhances neurogenesis and angiogenesis after focal cerebral ischemia in rats. *Stroke.* **36,** 859–64 (2005).

65. Burgess, A., Huang, Y., Querbes, W., Sah, D. W. & Hynynen, K. Focused ultrasound for targeted delivery of siRNA and efficient knockdown of Htt expression. *J. Control. Release* **163,** 125–129 (2012).

66. Kaspar, B. K., Lladó, J., Sherkat, N., Rothstein, J. D. & Gage, F. H. Retrograde viral delivery of IGF-1 prolongs survival in a mouse ALS model. *Science* **301,** 839–42 (2003).

67. Wang, H. *et al.* Therapeutic gene silencing delivered by a chemically modified small interfering RNA against mutant SOD1 slows amyotrophic lateral sclerosis progression. *J. Biol. Chem.* **283,** 15845–15852 (2008).

68. Morille, M., Passirani, C., Vonarbourg, A., Clavreul, A. & Benoit, J. P. Progress in developing cationic vectors for non-viral systemic gene therapy against cancer. *Biomaterials* **29,** 3477–3496 (2008).

69. Laga, R., Carlisle, R., Tangney, M., Ulbrich, K. & Seymour, L. W. Polymer coatings for delivery of nucleic acid therapeutics. *J. Control. Release* **161,** 537–53 (2012).

70. Lu, W., Sun, Q., Wan, J., She, Z. & Jiang, X. G. Cationic albumin-conjugated pegylated nanoparticles allow gene delivery into brain tumors via intravenous administration. *Cancer Res.* **66,** 11878–11887 (2006).

71. Immordino, L., Dosio, F. & Cattel, L. Stealth liposomes: review of the basic science, rationale, and clinical applications,. *Int. J. Nanomedicine* **1,** 297–315 (2006).

72. Pombo García, K. *et al.* Zwitterionic-coated 'stealth' nanoparticles for biomedical applications: recent advances in countering biomolecular corona formation and uptake by the mononuclear phagocyte system. *Small* **10,** 2516–29 (2014).

73. Schöttler, S. *et al.* Protein adsorption is required for stealth effect of poly(ethylene glycol)- and poly(phosphoester)-coated nanocarriers. *Nat. Nanotechnol.* 1–6 (2016). doi:10.1038/nnano.2015.330

74. Son, S. *et al.* RVG peptide tethered bioreducible polyethylenimine for gene delivery to brain. *J. Control. Release* **155,** 18–25 (2011).

75. Ko, Y. T., Bhattacharya, R. & Bickel, U. Liposome encapsulated polyethylenimine/ODN polyplexes for brain targeting. *J. Control. Release* **133,** 230–7 (2009).

76. Huang, R.-Q. *et al.* Efficient gene delivery targeted to the brain using a transferrin-conjugated polyethyleneglycol-modified polyamidoamine dendrimer. *FASEB J.* **21,** 1117–1125 (2007).

77. Kwon, E. J. *et al.* Targeted nonviral delivery vehicles to neural progenitor cells in the mouse subventricular zone. *Biomaterials* **31,** 2417–2424 (2010).

78. Emlen, W. & Mannik, M. Effect of DNA size and strandedness on the in vivo clearance and organ localization of DNA. *Clin. Exp. Immunol.* **56,** 185–92 (1984).

79. Kawabata, K., Takakura, Y. & Hashida, M. The Fate of Plasmid DNA After Intravenous Injection in Mice: Involvement of Scavenger Receptors in Its Hepatic Uptake. *Pharm. Res.* **12,** 825–830 (1995).

80. Hervé, F., Ghinea, N. & Scherrmann, J.-M. CNS delivery via adsorptive transcytosis. *AAPS J.* **10,** 455–472 (2008).

81. Zhang, Y., Wang, Y., Boado, R. J. & Pardridge, W. M. Lysosomal enzyme replacement of the brain with intravenous non-viral gene transfer. *Pharm. Res.* **25,** 400–406 (2008).

82. Kumar, P. *et al.* Transvascular delivery of small interfering RNA to the central nervous system. *Nature* **448,** 39–43 (2007).

83. Liu, Y. *et al.* Brain-targeting gene delivery and cellular internalization mechanisms for modified rabies virus glycoprotein RVG29 nanoparticles. *Biomaterials* **30,** 4195–4202 (2009).

84. Pulford, B. *et al.* Liposome-siRNA-peptide complexes cross the blood-brain barrier and significantly decrease PrPC on neuronal cells and PrPRES in infected cell cultures. *PLoS One* **5,** 1–13 (2010).

85. Gao, Y. *et al.* RVG-peptide-linked trimethylated chitosan for delivery of siRNA to the brain. *Biomacromolecules* **15,** 1010–1018 (2014).

86. Alvarez-Erviti, L. *et al.* Delivery of siRNA to the mouse brain by systemic injection of targeted exosomes. *Nat. Biotechnol.* **29,** 341–5 (2011).

87. Ke, W. *et al.* Gene delivery targeted to the brain using an Angiopep-conjugated polyethyleneglycol-modified polyamidoamine dendrimer. *Biomaterials* **30,** 6976–6985 (2009).

88. Huang, R. *et al.* Lactoferrin-modified nanoparticles could mediate efficient gene delivery to the brain in vivo. *Brain Res. Bull.* **81,** 600–604 (2010).

89. Huang, R., Ke, W., Liu, Y., Jiang, C. & Pei, Y. The use of lactoferrin as a ligand for targeting the polyamidoamine-based gene delivery system to the brain. *Biomaterials* **29,** 238–246 (2008).

90. Liu, Y. *et al.* A leptin derived 30-amino-acid peptide modified pegylated poly-l-lysine dendrigraft for brain targeted gene delivery. *Biomaterials* **31,** 5246–5257 (2010).

91. Costa, P. M. *et al.* Tumor-targeted Chlorotoxin-coupled Nanoparticles for Nucleic Acid Delivery to Glioblastoma Cells: A Promising System for Glioblastoma Treatment. *Mol. Ther. Nucleic Acids* **2,** e100 (2013).

92. Rapoport, S. I. Advances in osmotic opening of the blood-brain barrier to enhance CNS chemotherapy. *Expert Opin. Investig. Drugs* **10,** 1809–18 (2001).

93. Hwang, D. W. *et al.* A brain-targeted rabies virus glycoprotein-disulfide linked PEI nanocarrier for delivery of neurogenic microRNA. *Biomaterials* **32,** 4968–4975 (2011).

94. Rychak, J. J. & Klibanov, A. L. Nucleic acid delivery with microbubbles and ultrasound. *Adv. Drug Deliv. Rev.* **72,** 82–93 (2014).

95. Meairs, S. & Alonso, A. Ultrasound, microbubbles and the blood-brain barrier. *Prog. Biophys. Mol. Biol.* **93,** 354–62 (2007).

96. Greenleaf, W. & Bolander, M. Artificial cavitation nuclei significantly enhance acoustically induced cell transfection. *Ultrasound Med. …* **24,** 587–595 (1998).

97. Zhou, Y., Yang, K., Cui, J., Ye, J. & Deng, C. Controlled permeation of cell membrane by single bubble acoustic cavitation. *J. Control. Release* **157,** 103–111 (2012).

98. Choi, J. J., Pernot, M., Small, S. a & Konofagou, E. E. Noninvasive, transcranial and localized opening of the blood-brain barrier using focused ultrasound in mice. *Ultrasound Med. Biol.* **33,** 95–104 (2007).

99. Choi, J. J., Wang, S., Tung, Y.-S., Morrison, B. & Konofagou, E. E. Molecules of various pharmacologically-relevant sizes can cross the ultrasound-induced blood-brain barrier opening in vivo. *Ultrasound Med. Biol.* **36,** 58–67 (2010).

100. Choi, J. J. *et al.* Noninvasive and localized blood-brain barrier disruption using focused

ultrasound can be achieved at short pulse lengths and low pulse repetition frequencies. *J. Cereb. Blood Flow Metab.* **31,** 725–37 (2011).

101. Xie, F. *et al.* Effects of transcranial ultrasound and intravenous microbubbles on blood brain barrier permeability in a large animal model. *Ultrasound Med. Biol.* **34,** 2028–34 (2008).

102. Sheikov, N., McDannold, N., Vykhodtseva, N., Jolesz, F. & Hynynen, K. Cellular mechanisms of the blood-brain barrier opening induced by ultrasound in presence of microbubbles. *Ultrasound Med. Biol.* **30,** 979–89 (2004).

103. Kobus, T., Vykhodtseva, N., Pilatou, M., Zhang, Y. & McDannold, N. Safety Validation of Repeated Blood–Brain Barrier Disruption Using Focused Ultrasound. *Ultrasound Med. Biol.* **42,** 481–492 (2015).

104. Huang, Q. *et al.* Effective Gene Transfer into Central Nervous System Following Ultrasound-Microbubbles-Induced Opening of the Blood-Brain Barrier. *Ultrasound Med. Biol.* **38,** 1234–1243 (2012).

105. Yamada, K. *et al.* Quantitative autoradiographic measurements of blood-brain barrier permeability in the rat glioma model. *J. Neurosurg.* **57,** 394–8 (1982).

106. Yue, P. *et al.* OX26/CTX-conjugated PEGylated liposome as a dual-targeting gene delivery system for brain glioma. *Mol. Cancer* **13,** 191 (2014).

107. Abbott, N. J., Rönnbäck, L. & Hansson, E. Astrocyte-endothelial interactions at the blood-brain barrier. *Nat. Rev. Neurosci.* **7,** 41–53 (2006).

108. Iliff, J. J. *et al.* A paravascular pathway facilitates CSF flow through the brain parenchyma and the clearance of interstitial solutes, including amyloid β. *Sci. Transl. Med.* **4,** 147ra111 (2012).

109. Lemkine, G. F. *et al.* Preferential transfection of adult mouse neural stem cells and their immediate progeny in vivo with polyethylenimine. *Mol. Cell. Neurosci.* **19,** 165–174 (2002).

110. Zou, S., Scarfo, K., Nantz, M. H. & Hecker, J. G. Lipid-mediated delivery of RNA is more efficient than delivery of DNA in non-dividing cells. *Int. J. Pharm.* **389,** 232–243 (2010).

111. Bharali, D. J. *et al.* Organically modified silica nanoparticles: a nonviral vector for in vivo gene delivery and expression in the brain. *Proc. Natl. Acad. Sci. U. S. A.* **102,** 11539–44 (2005).

112. Wehling, K. *et al.* Specficificity of DNA-basic polypeptide interactions. Influence of neutral residues incorporated into polylysine and polyarginine. *Nucleic Acids Res.* **2,** 799–807 (1975).

113. Cheng, Q. *et al.* The effect of guanidinylation of PEGylated poly(2-aminoethyl methacrylate) on the systemic delivery of siRNA. *Biomaterials* **34,** 3120–3131 (2013).

114. Choi, J. L. *et al.* Guanidinylated block copolymers for gene transfer : A comparison with amine-based materials for in vitro and in vivo gene transfer ef fi ciency. *Biomaterials* **54,** 87–96 (2015).

115. Hauck, E. S., Zou, S., Scarfo, K., Nantz, M. H. & Hecker, J. G. Whole animal in vivo imaging after transient, nonviral gene delivery to the rat central nervous system. *Mol. Ther.* **16,** 1857–1864 (2008).

116. Uchida, S. *et al.* In Vivo Messenger RNA Introduction into the Central Nervous System Using Polyplex Nanomicelle. *PLoS One* **8,** (2013).

117. Soderquist, R. *et al.* Release of Plasmid DNA-encoding IL-10 from PLGA Microparticles Facilitates Long-term Reversal of Neuropathic Pain Following a Single Intrathecal Administration. *Pharm. Res.* **27,** 841–854 (2007).

118. Zeng, J., Wang, X. & Wang, S. Self-assembled ternary complexes of plasmid DNA, low molecular weight polyethylenimine and targeting peptide for nonviral gene delivery into neurons. *Biomaterials* **28,** 1443–1451 (2007).

119. Song, H. P. *et al.* Gene transfer using self-assembled ternary complexes of cationic magnetic nanoparticles, plasmid DNA and cell-penetrating tat peptide. *Biomaterials* **31,** 769–778 (2010).

120. Tan, J.-K. Y. *et al.* Microbubbles and ultrasound increase intraventricular polyplex gene transfer to the brain. *J. Control. Release* **231,** 86–93 (2016).

121. Tang, G. P. *et al.* Polyethylene glycol modified polyethylenimine for improved CNS gene transfer: Effects of PEGylation extent. *Biomaterials* **24,** 2351–2362 (2003).

122. Kim, I. D. *et al.* Neuroprotection by biodegradable PAMAM ester (e-PAM-R)-mediated HMGB1 siRNA delivery in primary cortical cultures and in the postischemic brain. *J. Control. Release* **142,** 422–430 (2010).

123. Chen, Q. *et al.* Lipophilic siRNAs mediate efficient gene silencing in oligodendrocytes with direct CNS delivery. *J. Control. Release* **144,** 227–232 (2010).

124. Liang, B. *et al.* The use of folate-PEG-grafted-hybranched-PEI nonviral vector for the inhibition of glioma growth in the rat. *Biomaterials* **30,** 4014–4020 (2009).

125. Cardoso, A. L. C. *et al.* Tf-lipoplexes for neuronal siRNA delivery: A promising system to mediate gene silencing in the CNS. *J. Control. Release* **132,** 113–123 (2008).

126. Kato, T. *et al.* Efficient delivery of liposome-mediated MGMT-siRNA reinforces the cytotoxity of temozolomide in GBM-initiating cells. *Gene Ther.* **17,** 1363–1371 (2010).

127. Allard, E., Passirani, C. & Benoit, J.-P. Convection-enhanced delivery of nanocarriers for the treatment of brain tumors. *Biomaterials* **30,** 2302–2318 (2009).

128. Querbes, W. *et al.* Direct CNS delivery of siRNA mediates robust silencing in oligodendrocytes. *Oligonucleotides* **19,** 23–29 (2009).

129. Stiles, D. K. *et al.* Widespread suppression of huntingtin with convection-enhanced delivery of siRNA. *Exp. Neurol.* **233,** 463–471 (2012).

130. MacKay, J. A. *et al.* HIV TAT peptide modifies the distribution of DNA nanolipoparticles following convection-enhanced delivery. *Mol. Ther.* **16,** 893–900 (2008).

131. Kenny, G. D. *et al.* Multifunctional receptor-targeted nanocomplexes for the delivery of therapeutic nucleic acids to the Brain. *Biomaterials* **34,** 9190–9200 (2013).

132. Spencer, B. J. & Verma, I. M. Targeted delivery of proteins across the blood-brain barrier. *Proc. Natl. Acad. Sci. U. S. A.* **104,** 7594–7599 (2007).

133. Yu, Y. J. *et al.* Boosting brain uptake of a therapeutic antibody by reducing its affinity for a transcytosis target. *Sci. Transl. Med.* **3,** 84ra44 (2011).

134. Monani, U. R. Spinal muscular atrophy: A deficiency in a ubiquitous protein; a motor neuron-specific disease. *Neuron* **48,** 885–896 (2005).

135. Mitchell, J. D. & Borasio, G. D. Amyotrophic lateral sclerosis. *Lancet* **369,** 2031–41 (2007).

136. Lavail, J. H. & Lavail, M. M. Retrograde Axonal Transport in the Central Nervous System. *Science (80-.).* **176,** 1416–1417 (1972).

137. Salinas, S., Schiavo, G. & Kremer, E. J. A hitchhiker's guide to the nervous system: the complex journey of viruses and toxins. *Nat. Rev. Microbiol.* **8,** 645–655 (2010).

138. Maheshri, N., Koerber, J. T., Kaspar, B. K. & Schaffer, D. V. Directed evolution of adeno-associated virus yields enhanced gene delivery vectors. *Nat. Biotechnol.* **24,** 198–204 (2006).

139. Kotterman, M. A. & Schaffer, D. V. Engineering adeno-associated viruses for clinical gene therapy. *Nat. Rev. Genet.* **15,** 445–51 (2014).

140. Snyder, B. R. *et al.* Comparison of Adeno-Associated Viral Vector Serotypes for Spinal Cord and Motor Neuron Gene Delivery. *Hum. Gene Ther.* **22,** 1129–1135 (2011).

141. Hollis II, E. R. *et al.* Efficient Retrograde Neuronal Transduction Utilizing Self-complementary AAV1. *Mol. Ther.* **16,** 296–301 (2008).

142. Xu, J., Ma, C., Bass, C. & Terwilliger, E. F. A combination of mutations enhances the neurotropism of AAV-2. *Virology* **341,** 203–214 (2005).

143. Azzouz, M., Ralph, G. & Storkebaum, E. VEGF delivery with retrogradely transported lentivector prolongs survival in a mouse ALS model. *Nature* **429,** 413–417 (2004).

144. Hirano, M. *et al.* Highly Efficient Retrograde Gene Transfer into Motor Neurons by a Lentiviral Vector Pseudotyped with Fusion Glycoprotein. *PLoS One* **8,** 1–8 (2013).

145. Petruska, J. C. *et al.* To Motoneurons in Adult Rats. **32,** 997–1005 (2011).

146. Benkhelifa-Ziyyat, S. *et al.* Intramuscular scAAV9-SMN injection mediates widespread gene delivery to the spinal cord and decreases disease severity in SMA mice. *Mol. Ther.* **21,** 282–90 (2013).

147. Price, D., Griffin, J., Young, A., Peck, K. & Stocks, A. Tetanus toxin: direct evidence for retrograde intraaxonal transport. *Science (80-.).* **188,** 945–947 (1975).

148. Schwab, M. E., Suda, K. & Thoenen, H. Selective retrograde synaptic transer of a protein, tetanus toxin, subsequent to its retrotransport. *J. Cell Biol.* **82,** 798–810 (1979).

149. Li, J. *et al.* Insect GDNF:TTC fusion protein improves delivery of GDNF to mouse CNS. *Biochem. Biophys. Res. Commun.* **390,** 947–951 (2009).

150. Francis, J. W. *et al.* A survival motor neuron:tetanus toxin fragment C fusion protein for the targeted delivery of SMN protein to neurons. *Brain Res.* **995,** 84–96 (2004).

151. Chian, R.-J. J. *et al.* IGF-1:tetanus toxin fragment C fusion protein improves delivery of IGF-1 to spinal cord but fails to prolong survival of ALS mice. *Brain Res.* **1287,** 1–19 (2009).

152. Sellers, D. L. *et al.* Targeted Axonal Import (TAxI) peptide delivers functional proteins into the spinal cord after peripheral administration. *PNAS* 1–6 (2016). doi:10.1073/pnas.1515526113

153. Niidome, T. & Huang, L. Gene therapy progress and prospects: nonviral vectors. *Gene Ther.* **9,** 1647–52 (2002).

154. Abdallah, B., Hassan, A. & Benoist, C. A powerful nonviral vector for in vivo gene transfer into the adult mammalian brain: polyethylenimine. *Hum. Gene Ther.* **7,** 1947–1954 (1996).

155. Jäger, M., Schubert, S., Ochrimenko, S., Fischer, D. & Schubert, U. S. Branched and linear poly(ethylene imine)-based conjugates: synthetic modification, characterization, and application. *Chem. Soc. Rev.* **41,** 4755–67 (2012).

156. Lv, H., Zhang, S., Wang, B., Cui, S. & Yan, J. Toxicity of cationic lipids and cationic polymers in gene delivery. *J. Control. Release* **114,** 100–9 (2006).

157. Fischer, D., Li, Y., Ahlemeyer, B., Krieglstein, J. & Kissel, T. In vitro cytotoxicity testing of polycations: influence of polymer structure on cell viability and hemolysis.

Biomaterials **24,** 1121–31 (2003).

158. Wong, K. *et al.* PEI-g-chitosan, a novel gene delivery system with transfection efficiency comparable to polyethylenimine in vitro and after liver administration in vivo. *Bioconjug. Chem.* **17,** 152–8 (2006).

159. Erbacher, P., Zou, S. & Bettinger, T. Chitosan-based vector/DNA complexes for gene delivery: biophysical characteristics and transfection ability. *Pharm. …* **15,** (1998).

160. Köping-Höggård, M. *et al.* Improved chitosan-mediated gene delivery based on easily dissociated chitosan polyplexes of highly defined chitosan oligomers. *Gene Ther.* **11,** 1441–52 (2004).

161. Wei, H., Pahang, J. a & Pun, S. H. Optimization of brush-like cationic copolymers for nonviral gene delivery. *Biomacromolecules* **14,** 275–84 (2013).

162. Chu, D. S. H., Johnson, R. N. & Pun, S. H. Cathepsin B-sensitive polymers for compartment-specific degradation and nucleic acid release. *J. Control. Release* **157,** 445–54 (2012).

163. Johnson, R. N. *et al.* Synthesis of Statistical Copolymers Containing Multiple Functional Peptides for Nucleic Acid Delivery. *Biomacromolecules* 3007–3013 (2010). doi:10.1021/bm100806h

164. Rungsardthong, U. *et al.* Copolymers of amine methacrylate with poly(ethylene glycol) as vectors for gene therapy. *J. Control. Release* **73,** 359–80 (2001).

165. Uzgün, S. *et al.* Characterization of tailor-made copolymers of oligo(ethylene glycol) methyl ether methacrylate and N,N-dimethylaminoethyl methacrylate as nonviral gene transfer agents: influence of macromolecular structure on gene vector particle properties and transfect. *Biomacromolecules* **11,** 39–50 (2010).

166. Deshpande, M. C. *et al.* The effect of poly(ethylene glycol) molecular architecture on cellular interaction and uptake of DNA complexes. *J. Control. Release* **97,** 143–56 (2004).

167. You, Y.-Z., Manickam, D. S., Zhou, Q.-H. & Oupický, D. Reducible poly(2-dimethylaminoethyl methacrylate): synthesis, cytotoxicity, and gene delivery activity. *J. Control. Release* **122,** 217–25 (2007).

168. Zhang, Y., Zheng, M., Kissel, T. & Agarwal, S. Design and biophysical characterization of bioresponsive degradable poly(dimethylaminoethyl methacrylate) based polymers for in vitro DNA transfection. *Biomacromolecules* **13,** 313–22 (2012).

169. Gosselin, M. a, Guo, W. & Lee, R. J. Efficient gene transfer using reversibly cross-linked low molecular weight polyethylenimine. *Bioconjug. Chem.* **12,** 989–94 (2001).

170. Christensen, L. V *et al.* Reducible poly(amido ethylenimine)s designed for triggered intracellular gene delivery. *Bioconjug. Chem.* **17,** 1233–40 (2006).

171. Burke, R. S. & Pun, S. H. Synthesis and characterization of biodegradable HPMA-oligolysine copolymers for improved gene delivery. *Bioconjug. Chem.* **21,** 140–50 (2010).

172. Peng, Q., Zhong, Z. & Zhuo, R. Disulfide cross-linked polyethylenimines (PEI) prepared via thiolation of low molecular weight PEI as highly efficient gene vectors. *Bioconjug. Chem.* **19,** 499–506 (2008).

173. Smith, M. E. B. *et al.* Protein modification, bioconjugation, and disulfide bridging using bromomaleimides. *J. Am. Chem. Soc.* **132,** 1960–5 (2010).

174. Moody, P. *et al.* Bromomaleimide-linked bioconjugates are cleavable in mammalian cells. *Chembiochem* **13,** 39–41 (2012).

175. Cui, Y., Yan, Y., Chen, Y. & Wang, Z. Dibromomaleimide Derivative as an Efficient Polymer Coupling Agent for Building Topological Polymers. *Macromol. Chem. Phys.* **214,** 470–477 (2013).

176. Jones, M. W. *et al.* Polymeric dibromomaleimides as extremely efficient disulfide bridging bioconjugation and pegylation agents. *J. Am. Chem. Soc.* **134,** 1847–52 (2012).

177. van de Wetering, P., Cherng, J. Y., Talsma, H., Crommelin, D. J. & Hennink, W. E. 2-(Dimethylamino)ethyl methacrylate based (co)polymers as gene transfer agents. *J. Control. Release* **53,** 145–53 (1998).

178. Robin, M. P. *et al.* Conjugation-induced fluorescent labeling of proteins and polymers using dithiomaleimides. *J. Am. Chem. Soc.* **135,** 2875–8 (2013).

179. Layman, J. M., Ramirez, S. M., Green, M. D. & Long, T. E. Influence of polycation molecular weight on poly(2-dimethylaminoethyl methacrylate)-mediated DNA delivery in vitro. *Biomacromolecules* **10,** 1244–52 (2009).

180. Ryan, C. P. *et al.* Tunable reagents for multi-functional bioconjugation: reversible or permanent chemical modification of proteins and peptides by control of maleimide hydrolysis. *Chem. Commun. (Camb).* **47,** 5452–4 (2011).

181. Verbaan, F. J. *et al.* Steric stabilization of poly(2-(dimethylamino)ethyl methacrylate)-based polyplexes mediates prolonged circulation and tumor targeting in mice. *J. Gene Med.* **6,** 64–75 (2004).

182. Venkataraman, S. *et al.* The role of PEG architecture and molecular weight in the gene transfection performance of PEGylated poly(dimethylaminoethyl methacrylate) based cationic polymers. *Biomaterials* **32,** 2369–78 (2011).

183. Richard, J. P. *et al.* Cell-penetrating peptides. A reevaluation of the mechanism of cellular uptake. *J. Biol. Chem.* **278,** 585–90 (2003).

184. Eriksson, P. S. *et al.* Neurogenesis in the adult human hippocampus. *Nat. Med.* **4,** 1313–1317 (1998).

185. Hallbergson, A. F., Gnatenco, C. & Peterson, D. a. Neurogenesis and brain injury: Managing a renewable resource for repair. *J. Clin. Invest.* **112,** 1128–1133 (2003).

186. Yoshimura, S. *et al.* FGF-2 regulation of neurogenesis in adult hippocampus after brain injury. *Proc. Natl. Acad. Sci. U. S. A.* **98,** 5874–5879 (2001).

187. Bergen, J. M., Park, I. K., Horner, P. J. & Pun, S. H. Nonviral approaches for neuronal delivery of nucleic acids. *Pharm. Res.* **25,** 983–998 (2008).

188. Davidson, B. L. & Breakefield, X. O. Viral vectors for gene delivery to the nervous system. *Nat. Rev. Neurosci.* **4,** 353–364 (2003).

189. Carlson, P. & Schellinger, J. Comparative study of guanidine-based and lysine-based brush copolymers for plasmid delivery. *Biomater. Sci.* 736–744 (2013). doi:10.1039/c3bm60079c

190. Choi, J. S. *et al.* Enhanced transfection efficiency of PAMAM dendrimer by surface modification with l-arginine. *J. Control. Release* **99,** 445–456 (2004).

191. Kim, T. Il, Ou, M., Lee, M. & Kim, S. W. Arginine-grafted bioreducible poly(disulfide amine) for gene delivery systems. *Biomaterials* **30,** 658–664 (2009).

192. Gund, P. Guanidine, trimethylenemethane, and 'Y-delocalization.' Can acyclic compounds have 'aromatic' stability? *J. Chem. Educ.* **49,** 100 (1972).

193. Schug, K. a & Lindner, W. Noncovalent binding between guanidinium and anionic groups: focus on biological- and synthetic-based arginine/guanidinium interactions with phosph[on]ate and sulf[on]ate residues. *Chem. Rev.* **105,** 67–114 (2005).

194. Mascotti, D. P. & Lohman, T. M. Thermodynamics of oligoarginines binding to RNA and DNA. *Biochemistry* **36,** 7272–7279 (1997).

195. Standke, K. C. & Brunnert, H. The estimation of affinity constants for the binding of model peptides to DNA by equilibrium dialysis. *Nucleic Acids Res.* **2,** 1839–49 (1975).

196. Weber, C. J. The Determination of the Guanidine Bases in Urine. *J Biol Chem* **78,** 465–473 (1928).

197. Brancia, F. L., Oliver, S. G. & Gaskell, S. J. Improved matrix-assisted laser desorption/ionization mass spectrometric analysis of tryptic hydrolysates of proteins following guanidination of lysine-containing peptides. *Rapid Commun. Mass Spectrom.* **14,** 2070–2073 (2000).

198. Futaki, S. Membrane-permeable arginine-rich peptides and the translocation mechanisms. *Adv. Drug Deliv. Rev.* **57,** 547–558 (2005).

199. Wender, P. a., Galliher, W. C., Goun, E. a., Jones, L. R. & Pillow, T. H. The design of guanidinium-rich transporters and their internalization mechanisms. *Adv. Drug Deliv. Rev.*

60, 452–472 (2008).

200. Kim, I.-D. *et al.* Intranasal Delivery of HMGB1 siRNA Confers Target Gene Knockdown and Robust Neuroprotection in the Postischemic Brain. *Mol. Ther.* **20,** 829–839 (2012).

201. Kerever, A. *et al.* Novel extracellular matrix structures in the neural stem cell niche capture the neurogenic factor fibroblast growth factor 2 from the extracellular milieu. *Stem Cells* **25,** 2146–2157 (2007).

202. Mercier, F. & Arikawa-Hirasawa, E. Heparan sulfate niche for cell proliferation in the adult brain. *Neurosci. Lett.* **510,** 67–72 (2012).

203. Juhasz, P. & Biemann, K. Mass spectrometric molecular-weight determination of highly acidic compounds of biological significance via their complexes with basic polypeptides. *Proc. Natl. Acad. Sci. U. S. A.* **91,** 4333–4337 (1994).

204. Fromm, J. R., Hileman, R. E., Caldwell, E. E., Weiler, J. M. & Linhardt, R. J. Differences in the interaction of heparin with arginine and lysine and the importance of these basic amino acids in the binding of heparin to acidic fibroblast growth factor. *Arch. Biochem. Biophys.* **323,** 279–87 (1995).

205. Wernersson, E. *et al.* Effect of association with sulfate on the electrophoretic mobility of polyarginine and polylysine. *J. Phys. Chem. B* **114,** 11934–11941 (2010).

206. Chodobski, A. & Szmydynger-chodobska, J. Choroid plexus: target for polypeptides and site of their synthesis. *Microsc. Res. Tech.* **52,** 65–82 (2001).

207. Wang, S., Samiotaki, G., Olumolade, O., Feshitan, J. a & Konofagou, E. E. Microbubble type and distribution dependence of focused ultrasound-induced blood-brain barrier opening. *Ultrasound Med. Biol.* **40,** 130–7 (2014).

208. Feshitan, J. a, Chen, C. C., Kwan, J. J. & Borden, M. a. Microbubble size isolation by differential centrifugation. *J. Colloid Interface Sci.* **329,** 316–24 (2009).

209. Matula, T. J., Swalwell, J., Tu, J., Cui, W. & Chen, W. Flow cytometry to characterize microbubbles. *2011 IEEE Int. Ultrason. Symp.* 156–159 (2011). doi:10.1109/ULTSYM.2011.0039

210. Tu, J. *et al.* Microbubble sizing and shell characterization using flow cytometry. *IEEE Trans. Ultrason. Ferroelectr. Freq. Control* **58,** 955–963 (2011).

211. Cavalieri, F. *et al.* Mechanical characterization of ultrasonically synthesized microbubble shells by flow cytometry and AFM. *ACS Appl. Mater. Interfaces* **5,** 10920–10925 (2013).

212. Doinikov, A. a., Haac, J. F. & Dayton, P. a. Modeling of nonlinear viscous stress in encapsulating shells of lipid-coated contrast agent microbubbles. *Ultrasonics* **49,** 269–275 (2009).

213. Zheng, W. & Zhao, Q. Establishment and characterization of an immortalized Z310 choroidal epithelial cell line from murine choroid plexus. *Brain Res.* **958,** 371–80 (2002).

214. Shi, L., Li, G., Wang, S. & Zheng, W. Use of Z310 cells as an in vitro blood–cerebrospinal fluid barrier model: Tight junction proteins and transport properties. *Toxicol. Vitr.* **22,** 190–199 (2008).

215. Wang, S., Olumolade, O. O., Sun, T., Samiotaki, G. & Konofagou, E. E. Noninvasive, neuron-specific gene therapy can be facilitated by focused ultrasound and recombinant adeno-associated virus. *Gene Ther.* **22,** 104–110 (2014).

216. Wu, S.-Y., Chen, C. C., Tung, Y.-S., Olumolade, O. O. & Konofagou, E. E. Effects of the Microbubble Shell Physicochemical Properties on Ultrasound-Mediated Drug Delivery to the Brain. *J. Control. Release* **212,** 30–40 (2015).

217. Wang, D. *et al.* Cationic versus neutral microbubbles for ultrasound-mediated gene delivery in cancer. *Radiology* **264,** 721–732 (2012).

218. Sun, R. R., Noble, M. L., Sun, S. S., Song, S. & Miao, C. H. Development of therapeutic microbubbles for enhancing ultrasound-mediated gene delivery. *J. Control. Release* **182,** 111–20 (2014).

219. Guo, X., Li, Q., Zhang, Z., Zhang, D. & Tu, J. Investigation on the inertial cavitation threshold and shell properties of commercialized ultrasound contrast agent microbubbles. *J. Acoust. Soc. Am.* **134,** 1622 (2013).

220. Dicker, S. *et al.* Influence of Shell Composition on the Resonance Frequency of Microbubble Contrast Agents. *Ultrasound Med. Biol.* **39,** 1292–1302 (2013).

221. Dicker, S., Mleczko, M., Schmitz, G. & Wrenn, S. P. Determination of microbubble cavitation threshold pressure as function of shell chemistry. *Bubble Sci. Eng. Technol.* **2,** 55–64 (2010).

222. Dass, C. R. Oligonucleotide delivery to tumours using macromolecular carriers. *Biotechnol. Appl. Biochem.* **40,** 113–122 (2004).

223. Fan, Z., Chen, D. & Deng, C. X. Improving ultrasound gene transfection efficiency by controlling ultrasound excitation of microbubbles. *J. Control. Release* **170,** 401–13 (2013).

224. Delalande, A., Leduc, C., Midoux, P., Postema, M. & Pichon, C. Efficient Gene Delivery by Sonoporation Is Associated with Microbubble Entry into Cells and the Clathrin-Dependent Endocytosis Pathway. *Ultrasound Med. Biol.* 1–14 (2015). doi:10.1016/j.ultrasmedbio.2015.03.010

225. Cock, I. De *et al.* Ultrasound and microbubble mediated drug delivery : Acoustic pressure as determinant for uptake via membrane pores or endocytosis. *J. Control. Release* **197,** 20–28 (2015).

226. Samiotaki, G., Acosta, C., Wang, S. & Konofagou, E. E. Enhanced delivery and bioactivity of the neurturin neurotrophic factor through focused ultrasound — mediated blood – brain barrier opening in vivo. *J. Cereb. Blood flow Metab.* 1–12 (2015). doi:10.1038/jcbfm.2014.236

227. Kumar, S. *et al.* Peptides as skin penetration enhancers: Mechanisms of action. *J. Control. Release* **199,** 168–178 (2015).

228. Lin, C.-Y. *et al.* Non-invasive, Neuron-Specific Gene Therapy by Focused Ultrasound-Induced Blood-Brain Barrier Opening in Parkinson's Disease Mouse Model. *J. Control. Release* **235,** 72–81 (2016).

229. Shi, L. & Palacio-Mancheno, P. Quantification of transient increase of the blood–brain barrier permeability to macromolecules by optimized focused ultrasound combined with microbubbles. *Int. J. …* 4437–4448 (2014).

230. Marty, B. *et al.* Dynamic study of blood–brain barrier closure after its disruption using ultrasound: a quantitative analysis. *J. Cereb. Blood Flow Metab.* **32,** 1948–1958 (2012).

231. Lanza, G. M. & Wickline, S. A. Targeted Ultrasonic Contrast Agents for Molecular Imaging and Therapy. *Curr. Probl. Cardiol.* 625–653 (2003). doi:10.1016/j.cpccardiol.2003.11.001

232. Willmann, J. K. *et al.* Targeted Contrast-Enhanced Ultrasound Imaging of Tumor Angiogenesis with Contrast Microbubbles Conjugated to Integrin-Binding Knottin Peptides. *J Nucl Med* **51,** 433–440 (2010).

233. Stieger, S. M. *et al.* Imaging of angiogenesis using Cadence contrast pulse sequencing and targeted contrast agents. *Contrast Media Mol. Imaging* **3,** 9–18 (2008).

234. Zhang, H. *et al.* Ultrasound molecular imaging of tumor angiogenesis with a neuropilin-1-targeted microbubble. *Biomaterials* **56,** 104–113 (2015).

235. Kooiman, K., Foppen-Harteveld, M., Der Steen, A. F. W. Van & De Jong, N. Sonoporation of endothelial cells by vibrating targeted microbubbles. *J. Control. Release* **154,** 35–41 (2011).

236. Yan, P. *et al.* The use of MMP2 antibody-conjugated cationic microbubble to target the ischemic myocardium, enhance Timp3 gene transfection and improve cardiac function. *Biomaterials* **35,** 1063–73 (2014).

237. Bayer, P. *et al.* Structural studies of HIV-1 tat protein. *J. Mol. Biol.* **247,** 529–535 (1995).

238. Xiong, X.-B., Uludağ, H. & Lavasanifar, A. Virus-mimetic polymeric micelles for targeted siRNA delivery. *Biomaterials* **31,** 5886–93 (2010).

239. Keravnou, C., Mannaris, C. & Averkiou, M. Accurate measurement of microbubble response to ultrasound with a diagnostic ultrasound scanner. *IEEE Trans. Ultrason.*

Ferroelectr. Freq. Control **62,** 176–184 (2015).

240. Mannaris, C. & Averkiou, M. A. Investigation of Microbubble Response to Long Pulses Used in Ultrasound-Enhanced Drug Delivery. *Ultrasound Med. Biol.* **38,** 681–691 (2012).

241. Park, Y. *et al.* Tunable diacetylene polymerized shell microbubbles as ultrasound contrast agents. *Langmuir* **28,** 3766–72 (2012).

242. Diesendruck, C. E. *et al.* Mechanically triggered heterolytic unzipping of a low-ceiling-temperature polymer. *Nat. Chem.* **6,** 623–8 (2014).

243. Peterson, G. I. & Boydston, A. J. Kinetic analysis of mechanochemical chain scission of linear poly(phthalaldehyde). *Macromol Rapid Commun* **35,** 1611–1614 (2014).

244. Liu, H.-L., Fan, C.-H., Ting, C.-Y. & Yeh, C.-K. Combining Microbubbles and Ultrasound for Drug Delivery to Brain Tumors: Current Progress and Overview. *Theranostics* **4,** 432–444 (2014).

245. Chan, L. W. *et al.* A synthetic fibrin cross-linking polymer for modulating clot properties and inducing hemostasis. *Sci. Transl. Med.* **7,** 1–11 (online) (2015).

246. Neill, U. S. Skin care in the aging female: myths and truths. *J. Clin. Invest.* **122,** 473–477 (2012).

247. Farage, M. a, Miller, K. W., Elsner, P. & Maibach, H. I. Characteristics of the Aging Skin. *Adv. wound care* **2,** 5–10 (2013).

248. Inge, C. Growth factors, peptides and stem cells: Their use in current skincare. *Prof. Beauty* (2013).

249. Malerich, S. & Berson, D. Next generation cosmeceuticals: the latest in peptides, growth factors, cytokines, and stem cells. *Dermatol. Clin.* **32,** 13–21 (2014).

250. Goldberg, D. J. Breakthroughs in US dermal fillers for facial soft-tissue augmentation. *J. Cosmet. Laser Ther.* **11,** 240–247 (2009).

251. Caravan, P. *et al.* Collagen-targeted MRI contrast agent for molecular imaging of fibrosis. *Angew. Chemie - Int. Ed.* **46,** 8171–8173 (2007).

252. Caravan, P. *et al.* A lysine walk to high relaxivity collagen-targeted MRI contrast agents. *Chem. Commun.* 430–432 (2009). doi:Doi 10.1039/B819098d

253. Helms, B. A. *et al.* High-affinity peptide-based collagen targeting using synthetic phage mimics: From phage display to dendrimer display. *J. Am. Chem. Soc.* **131,** 11683–11685 (2009).

254. KLIGMAN, A. M. & ARMSTRONG, R. C. Histologic Response to Intradermal Zyderm and Zyplast (Glutaraldehyde Cross-Linked) Collagen in Humans. *J. Dermatol. Surg.*

Oncol. **12,** 351–357 (1986).

Part 6: Protocols

Chapter 1. Dibromomaleimide Synthesis

TABLE 1.1 REAGENTS FOR DIBROMOMALEIMIDE SYNTHESIS

Reagent	MW (g/mol)	Mass (mg)	mmol	Equiv	Density (g/mL)	Volume (mL)
Maleic Anhydride	98.06	400	4.08	1		
Br_2	159.81	1302.45	8.15	2	3.119	0.421
AlCl3	133.34	8.16	0.0612	0.15		

1. Weigh out maleic anhydride and $AlCl_3$ and add to a pressure tube with a stirbar.
2. Double nitrile glove! In fume hood! First release pressure in the Br_2 bottle by inserting a needle. Attach a second needs to the Ar line with low flow and insert into the bottle. With a bent metal needle and glass syringe, carefully withdraw about 0.5 mL Br_2. Then pull in air into the syringe. While holding the plunger with one hand, carefully pull the syringe out of the Br_2 bottle with the other hand. Add Br_2 to the pressure tube and screw on the cap tightly. Pull out both needles carefully.
3. Clean out the syringe and needle with methanol. Disconnect all the pieces and let it air dry in the fume hood.
4. Let the solution stir for a few minutes at room temperature.
5. Lower the pressure tube into an oil bath at 120 °C and let it stir overnight (about 16 hours). Make sure the hood is cleared out and be ready to close the fume hood quickly if need be. Watch the reaction vessel for the first 15 minutes for any problems. The solution should boil.
6. After heating overnight, raise the pressure tube out of the hot oil and let it cool to room temperature. Wipe off oil from the outside of the tube.
7. Prepare an ice bath to later cool the tube. This will help relieve the pressure that has built up overnight. Place the tube in the ice bath and let it cool.
8. After some time, put on double nitrile gloves, lower the hood sash to protect yourself, and open the tube slowly. It may release fumes as it is opened.
9. Dispense 20 mL of ethyl acetate. Dissolve the crude DBM in aliquots of ethyl acetate and transfer it to a new flask.
10. Vacuum filter the solution to remove any precipitates.
11. Transfer the filtrate to a round bottom flask and rotovap it dry.
12. Redissolve the precipitate in 20 mL of chloroform.

13. Azeotropically remove all the ethyl acetate by adding more chloroform and rotovap. Repeat once more.
14. Perform an extraction twice with 20 mL of water. Collect the organic layer.
15. To the organic layer, add anhydrous sodium sulfate to dry the solution. Let it sit for 5 minutes.
16. Vacuum filter and rotovap.
17. Characterize by NMR and GC-MS.

Chapter 2. Synthesis of Dibromomaleimide-Alkyne

TABLE 2.1 REAGENTS FOR DIBROMOMALEIMIDE-ALKYNE SYNTHESIS

Reagent	MW (g/mol)	Mass (mg)	mmol	Equiv	Density (g/mL)	Volume (mL)
Propargylamine	55.08	85.92	1.56	1	0.86 g/mL	0.09991
DBM	255.85	558.8	2.18	1.4		
Glacial Acetic Acid	60.05	8.16	0.0612	0.15	1.049	34

1. Obtain propargylamine with a syringe and needle and add it to a reaction vessel with a stir bar.
2. In an ice bath, add glacial acetic dropwise and let it neutralize for a few minutes.
3. Add DBM to the vessel.
4. Set up the condenser with water running in at the bottom and water running out at the top. Wrap copper wire around the tubing to make sure it is secure.
5. Heat the reaction solution for 5 hours at 120 °C while stirring.
6. After the reaction is complete, raise the reaction vessel to let it cool.
7. Remove the condenser and stir bar.
8. Add toluene and azeotropically remove the glacial acetic acid under reduced pressure.
9. Prepare a flash column to purify DBM-alkyne with 10:0.5 hexane:ethyl acetate.
    a. For 100-300 mg use a 30 mm diameter column; for 400-600 mg scale use a 40 mm column.
    b. Make sure the column is dry. Run methanol, acetone, and thenair to dry it.
    c. If there is no frit, first put a cotton ball and then just enough sand to cover the hole.
    d. Create a silica slurry and pack a column about 6 inches in height.
    e. Dissolve crude DBM-alkyne in little amount of DCM. Just add enough to dissolve.
    f. Let solvent drip to right above the column bed.
    g. Transfer crude solution dropwise to the top of the column. Wash the side of the column with DCM to wash down any splashes.
    h. Lower the solvent level to just above the column bed.
    i. Pour a thin layer of dry silica above the sample.
    j. Add about an inch of sand.
    k. Add solvent and start running the column.

l. Collect about 30-50 mL as the void volume

10. Start collecting eluents in tubes.
11. Perform TLC to check for the appearance of the product.
12. Collect the fractions that have the product and rotovap dry.

Chapter 3. Microbubble Formation

List of Lipids

- DSPC (790.15 g/mol): 1,2-distearoyl-*sn*-glycero-3-phosphocholine (25 mg/mL)
- DSPE-MPEG(2000) (2805.497 g/mol): 1,2-distearoyl-*sn*-glycero-3-phosphoethanolamine-*N*-[methoxy(polyethylene glycol)2000] (ammonium salt) (25 mg/mL)
- DSPE-MPEG(5000) (5801.071 g/mol): 1,2-distearoyl-*sn*-glycero-3-phosphoethanolamine-*N*-[methoxy(polyethylene glycol)5000] (ammonium salt) (25 mg/mL)
- DSPE-PEG2000 Amine (2790.52 g/mol): 1,2-distearoyl-*sn*-glycero-3-phosphoethanolamine-*N*-[amino(polyethylene glycol)2000] (ammonium salt) (25 mg/mL)
- DSPE-PEG5000 Amine (5786.07 g/mol): 1,2-distearoyl-*sn*-glycero-3-phosphoethanolamine-*N*-[amino(polyethylene glycol)5000] (ammonium salt) (25 mg/mL)
- DSPE-PEG5000 Azide (5812.07 g/mol): 1,2-distearoyl-*sn*-glycero-3-phosphoethanolamine-*N*-[azido(polyethylene glycol)5000] (ammonium salt)
- DSPE-PEG5000 TAT (7651.07 g/mol): 1,2-distearoyl-*sn*-glycero-3-phosphoethanolamine-*N*-[TAT(polyethylene glycol)5000] (ammonium salt) (32 mg/mL)
- DSPE-PEG5000 scELLR (8421.07 g/mol): 1,2-distearoyl-*sn*-glycero-3-phosphoethanolamine-*N*-[scELLR(polyethylene glycol)5000] (ammonium salt) (34.67 mg/mL)
- DSPE-PEG5000 Fluorescein (6176.41 g/mol): 1,2-distearoyl-*sn*-glycero-3-phosphoethanolamine-*N*-[fluorescein(polyethylene glycol)5000] (ammonium salt) (25 mg/mL) (495/515 nm)
- DSTAP (702.58 g/mol): 1,2-distearoyl-3-trimethylammonium -propane (chloride salt) (25 mg/mL)

Microbubble Formulations

- Neutral MBs
    - 9 DSPC : 1 DSPE-MPEG2000/5000
    - 9 DSPC : 0.5 DSPE-MPEG5000 : 0.5 DSPE-PEG5000-TAT/scELLR
- Slightly Cationic MBs
    - 9 DSPC : 1 DSPE-PEG2000 Amine

- 9 DSPC : 0.5 DSPE-PEG5000 Amine : 0.5 DSPE-PEG5000-TAT/scELLR

— Cationic MBs

- 7 DSPC : 2 DSTAP : 1 DSPE-PEG2000 Amine
- 7 DSPC : 2 DSTAP : 0.5 DSPE-PEG5000 Amine : 0.5 DSPE-PEG5000-TAT/scELLR

TABLE 3.1 LIPID COMPOSITION OF 2 KDA PEG UNTARGETED MICROBUBBLES

	DSPC	DSTAP	DSPE-MPEG2k	DSPE-2k Amine
Neu, 2k	28.68 µL		11.32 µL	
SCat, 2k	28.73 µL			11.27 µL
Cat, 2k	22.75 µL	5.79 µL		11.50 µL

TABLE 3.2 LIPID COMPOSITION OF 5 KDA PEG UNTARGETED AND TARGETED MICROBUBBLES

	DSPC	DSTAP	DSPE-MPEG5k	DSPE-5k Amine	DSPE-5k TAT	DSPE-5k scELLR
Neu, 5k	22.03 µL		17.96 µL			
Neu-TAT, 5k	22.03 µL		8.98 µL		9.25 µL	
Neu-scELLR, 5k	22.03 µL		8.98 µL			9.4 µL
SCat, 5k	22.06 µL			17.95 µL		
SCat-TAT, 5k	22.06 µL			8.98 µL	9.27 µL	
SCat-scELLR, 5k	22.06 µL			8.98 µL		9.42 µL
Cat, 5k	17.40 µL	4.40 µL		18.20 µL		
Cat-TAT, 5k	17.40 µL	4.40 µL		9.1 µL	9.4 µL	
Cat-scELLR, 5k	17.40 µL	4.40 µL		9.1 µL		9.55 µL

TABLE 3.3 LIPID COMPOSITION OF FLUORESCENT 5 KDA PEG UNTARGETED AND TARGETED MICROBUBBLES

	DSPC	DSTAP	DSPE-MPEG5k	DSPE-5k Amine	DSPE-5k FITC	DSPE-5k TAT	DSPE-5k scELLR
Neu, 5k	22.03 µL		16.16 µL		1.8 µL		
Neu-TAT, 5k	22.03 µL		7.18 µL		1.8 µL	9.25 µL	
Neu-scELLR, 5k	22.03 µL		7.18 µL		1.8 µL		9.4 µL
SCat, 5k	22.06 µL			16.15 µL	1.8 µL		
SCat-TAT, 5k	22.06 µL			7.18 µL	1.8 µL	9.27 µL	
SCat-scELLR, 5k	22.06 µL			7.18 µL	1.8 µL		9.42 µL
Cat, 5k	17.40 µL	4.40 µL		16.38 µL	1.82 µL		
Cat-TAT, 5k	17.40 µL	4.40 µL		7.28 µL	1.82 µL	9.4 µL	
Cat-scELLR, 5k	17.40 µL	4.40 µL		7.28 µL	1.82 µL		9.55 µL

Lipid Film Preparation

1. Aliquot lipids in a 2 mL centrifuge tube according to the tables above.
2. Let the tubes dry overnight in a vacuum desiccator.
3. Once dry, store the tubes in a -20 °C freezer.

MB Formation

1. 1 day before: Dissolve lipids in 1 mL 10% (v/v) glycerol/10% (v/v) propelyne glycol (GP) solution, heat at 73 °C.
2. Check that the lipids dissolved by pipetting with 1 mL pipette and by inverting the tube.
3. Sparge and purge the tube, 1 min each with a 25G5/8 needle. Close the tube.
4. Cut off the tab that connects the lid to the tube and parafilm it closed with a thin strip.
5. Activate the MBs for 45 s with the Vialmix® machine.
6. Transfer the MB solution to a 15 mL tube.
7. Rinse the centrifuge tube with 2 mL of GP solution and add it to 15 mL tube.
8. Spin the tube for 10 min 300 rcf at 12° C with a brake speed of 5. The infranatant will have lipids and vesicles while the cake will contain MBs.
9. With a 25G1½ needle connected to a 5 mL syringe, take out 2 mL from the bottom of the 15 mL tube and do not disturb the cake. Add 2 mL of GP solution.
10. Repeat Step 9 once more.
11. Spin the tube for 1 min at 70 rcf. The infranatant will contain MBs < 6 μm while the cake will contain MBs > 6 μm. With an 18G1½ needle, take out 2 mL from the bottom of the tube. Pull the needle out of the tube and take in some air. Invert the syringe and screw off the needle. Slowly dispense the MB solution into a new 15 mL tube.
12. Spin the tube for 1 min at 160 rcf. The infranatant will contain MBs < 4 μm while the cake will contain MBs > 4 μm. With an 18G1½ needle, take out 2 mL from the bottom of the tube. Pull the needle out of the tube and take in some air. Invert the syringe and screw off the needle. Slowly dispense the MB solution into a new 15 mL tube.
13. Spin the tube for 1 min at 270 rcf. The infranatant will contain MBs 1-2 μm while the cake will contain MBs ~3 μm. With an 18G1½ needle, take out 2 mL from the bottom of the tube. Pull the needle out of the tube and take in some air. Invert the syringe and screw off the needle. Slowly dispense the MB solution into a new 15 mL tube.

14. Spin the tube for 10 min at 300 rcf to concentrate the MBs. With a 25G1½ needle connected to a 5 mL syringe, slowly and carefully take out the clear solution at the bottom of the syringe and try to avoid the milky MB solution. For a very concentrated MB solution, leave only about 200 µL of MBs left in the tube.
15. Use a Multisizer 3 to determine the diameter and concentration of the MBs.

VITA

James-Kevin Tan was born and raised in Orange County, California. He was a National Science Foundation Graduate Research Fellowship Program recipient during his time at the University of Washington. When not working in lab or contemplating his life choices, he was eating his feelings or undergoing retail therapy. Before that, he studied bioengineering at University of California, Los Angeles.